DETERMINANTS OF TRANSCRIPTIONAL REGULATION OF TRANSPORT AND OXIDATIVE PROCESSES IN HUMAN MODEL SYSTEMS

Thesis submitted in accordance with requirements of the University of Liverpool for the degree of Doctor of Philosophy

Beth Williamson

September 2013

This thesis is the results of my own work. The material contained within the thesis has not been presented, either wholly or in part, for any other degree or qualification.

Beth Williamson

This research was carried out in the

Liverpool HIV Pharmacology Group

Department of Molecular and Clinical Pharmacology

University of Liverpool

UK

Table of Contents

Acknowledgements

I wish to express my sincere appreciation to those who have assisted me during my PhD. Throughout this programme of study; I have received guidance, support and encouragement from many people. I firstly offer thanks and gratitude to Prof. Andrew Owen for his direction, support and patience. He has listened and tutored me throughout this stressful but rewarding process. I would like to thank Prof. David Back for his advice, help and assistance. In addition, I recognise the encouragement, wise words, time and effort Dr. Matt and Dr. Audrey Soars have invested into my PhD. I also thank Dr. Marco Siccardi for his support, insight and coffee.

Thank you to Post doctorate colleagues Neill, Phil and Lee for their understanding and advice. Fellow PhD students, James, Paul, Adeniyi and Christina, thank you for putting up with my stress and sharing an office with me. And, many thanks to Dee, for her help and support. Thank you to Bhav for being a friendly face and helping me keep calm when things did not always go as planned. You have been a great help meeting me for lunch when I needed an escape from the laboratory.

I would like to convey my heartfelt thanks to my family, Mum, Dad, Meg, Emily and Alice who have supported me throughout my study. They have allowed me time to complete my work and have been patient when dealing with stressful stages. They have reminded me to persist with my work to show that the effort has all been worth it.

Abbreviations

$1\alpha,25\text{-}(OH)_2D_3$	1α,25-dihydroxyvitamin D_3
µg	Microgram(s)
µl	Microliter(s)
µM	Micromolar
aa	Amino acid
ABC	ATP-binding cassette transporter
ADME	Absorption, distribution, metabolism, elimination
ADR	Adverse drug reaction
AhR	Aryl hydrocarbon receptor
ATP	Adenosine triphosphate
ATTC	American type tissue culture
AUC	Area Under the Curve
BCS	Biopharmaceutics Classification System
BDDCS	Biopharmaceutics Drug Disposition Classification System
BSA	Bovine serum albumin
bp	Base pairs
cAMP	Cyclic adenosine monophosphate
CAR	Constitutive Androstane Receptor
°C	Degree Celsius
cDNA	Complementary deoxyribonucleic acid
CHRM	Cryopreserved hepatocyte recovery medium
CL	Clearance
Cl_{int}	Intrinsic clearance
C_{max}	Maximum concentrations
C(t)	Comparative threshold
CTE	C-terminal extension
C_{trough}	Trough concentrations
CYP	Cytochrome P450
DBD	DNA binding domain
ddH_20	Double deionised water
DDI	Drug-drug interaction

DEX	Dexamethasone
DMSO	Dimethyl sulfoxide
dNTP	Deoxy nucleoside triphosphate
DNA	Deoxyribonucleic acid
DR	Direct repeat
dsDNA	Double stranded deoxy ribonucleic acid
E3S	Estrone-3-sulfate
ECL	Enhanced chemiluminescence
EMA	European Medicines Agency
FBS	Fetal bovine serum
FDA	Food and drug administration
f	Bioavailability
g	Gram(s)
Gadd45β	Growth arrest and DNA damage inducible 45 β
GST	Glutathione–S-transferase
h	Hour(s)
HAT	Histone acetylase
HBSS	Hanks balanced salt solution
HEPES	4-(2-hydroxyethyl)-1-piperazineethanesulfonic acid
HIV	Human immunodeficiency virus
HNF1	Hepatocyte nuclear factor 1
HNF4α	Hepatocyte nuclear factor 4α
HPLC	High Performance Liquid Chromatography
HRE	Hormone response element
HRP	Horseradish peroxidase
Hsp	Heat shock protein
IQR	Inter quartile range
IR	Inverted repeat
ITC	International Transporter Consortium
ka	Absorption rate constant
kb	Kilobases
kDa	KiloDalton

K_{el}	Elimination rate constant
kg	Kilograms
K_i	Inhibitory constant
K_m	Michaelis constant
kV	KiloVolts
L	Liter(s)
LBD	Ligand binding domain
Log_{10}	Logarithm to the base 10
LLQ	Lower Limit of Quantification
LOD	Lower Limit of Detection
LPV	Lopinavir
LTR	Long terminal repeats
Lucif	Luciferase
m/z	Mass to charge ratio
M	Molar
mCi	Millicurie
MDZ	Midazolam
MEC	Minimum effective concentrations
MED	Mitogen subunit complex
mg	Milligram(s)
$MgCl_2$	Magnesium chloride
min	Minute(s)
MAPK	Mitogen-activated protein kinase
ml	Millilitre(s)
mM	Millimolar
mRNA	Messenger ribonucleic acid
MTB	*Mycobacterium* tuberculosis
n	Number of observations
NCE	New chemical entity
NCOA	Nuclear receptor co-activator
NCOR	Nuclear corepressor
NFDM	Non fat dried milk

NF-κB	Nuclear factor kappa-light-chain-enhancer of activated B cells
ng	Nanogram(s)
nm	Nanometer(s)
nM	Nanomolar
NR	Nuclear receptor
NTC	Non transfected control
NTCO	Non transfected control optiMEM buffer
OCT	Organic Cation Transporter
PB	Phenobarbital
PBPK	Physiologically based pharmacokinetic
PCR	Polymerase chain reaction
PD	Pharmacodynamic
PDA	Photodiode Array Detector
PG	Pharmacogenetics
pH	$-\log_{10}$ hydrogen ion concentration
PGC1α	Peroxisome proliferator activated receptor γ co-activator 1α
PK	Pharmacokinetic
pmol	Picomole
PPAR	Peroxisome proliferator-activated receptors
PTEN	Phosphatase and tensin homolog
PTM	Post translational modification
PXR	Pregnane X receptor
QC	Quality control
qPCR	Quantitative polymerase chain reaction
R^2	Correlation coefficient
RNA	Ribonucleic acid
RAR	Retinoid activated receptor
RBT	Rifabutin
RIF	Rifampicin
RMM	RNA recognition motif
RPT	Rifapentine
RSD	Relative standard deviation

RT	Reverse Transcriptase
rtPCR	Real time polymerase chain reaction
RTV	Ritonavir
RXR	Retinoic acid receptor
s	Second(s)
SD	Standard Deviation
SE	Standard error
SLC	Solute carrier transporter
SLCO	Solute carrier organic anion transporter
SNP	Single nucleotide polymorphism
SPE	Solid phase extraction
STD	Standard
SULT	Sulfotransferase
$t_{1/2}$	Half-life
TDM	Therapeutic drug monitoring
TGFβ	Transforming growth factor beta
T-TBS	Tween-tris buffered saline
UGT	UDP-glucuronosyltransferase
UTR	Untranslated region
UV	Ultraviolet
Vd	Volume of distribution
VDR	Vitamin D receptor
V_{max}	Maximum Velocity
vs	Versus
WHO	World Health Organisation
WST-1	4-[3-(4-iodophenyl)-2-(4-nitrophenyl)-2H-5-tetrazolio]-1,3-benzene disulfonate

Publications

Dissecting the relative contribution of OATP1B1 – mediated uptake of Xenobiotics into human hepatocytes using siRNA (Xenobiotica e-pub March 2013)

***In Vitro* Induction of Influx and efflux transporters and cytochrome P450 3A4 in human hepatocytes by Rifampicin, Rifabutin and Rifapentine** (Antimicrobial Agents and Chemotherapy e-pub September 2013)

Communications

March 2013: Conference on Retroviruses and Opportunistic Infections (Atlanta, USA)

In Vitro Induction of Influx and Efflux Transporters and Cytochrome P450 3A4 in Human Hepatocytes by Rifampicin, Rifabutin and Rifapentine. *Young Investigator Award. Poster Presentation*

September 2012: Drug Metabolism Discussion Group (Loughborough, UK)

Determinants of transcriptional regulation of cytochrome P450 enzyme activity in hepatoma cell lines and primary human hepatocytes. *Poster Presentation and Oral Communication.*

March 2012: Hepatocyte Expert Programme (Paisley, Scotland)

Dissecting the relative contribution of OATP1B1 – mediated uptake of Xenobiotics into human hepatocytes using siRNA. *Oral Presentation*.

June 2011: International Conference on Cytochrome P450 (Manchester, UK)

The use of siRNA to dissect the relative contribution of OATP1B1 to human hepatic uptake of xenobiotics. *Poster Presentation.*

Abstract

Initial predictions of drug response and drug-drug interactions (DDIs) are made following high-throughput *in vitro* screening. Such assays are indispensible in the pharmaceutical industry to determine the metabolism, transport and pharmacokinetics of new chemical entities. However, they often fail when extrapolated to *in vivo* response due to unsuitable pharmacokinetic or pharmacodynamic prediction. The primary aim of this thesis was to investigate and understand the differences in the expression profiles of drug disposition genes, between transformed hepatic cell lines and primary human hepatocytes. Primary human hepatocytes were also analysed to determine uptake contribution, induction and genotype of key drug disposition-relevant genes.

The loss of hepatic phenotype in HepG2 and Huh7 cells is partly due to the altered expression of transcriptional regulators including; chaperones, co-chaperones, co-activators and co-repressors. Indeed, Chapter 2 of this thesis shows lower levels of the *Gadd45β* and *PGC1α* gene expression in HepG2 cells corresponds to a deficient expression and activity of cytochrome P450 3A4 (CYP3A4), with the levels reducing further as cell passage increases, in comparison to primary human hepatocytes. HepG2 cells were transfected with a novel complex transfection of Gadd45β and PGC1α with the aim to improve CYP3A4 activity in Chapter 3. CYP3A4 activity was improved by 54% and induction response was enhanced in comparison to control cells with no off-target effects.

Over the last decade it has become apparent that transporters can play a significant role in the disposition of many drugs. Organic anion transporting polypeptide (OATP) transporters have received considerable recent attention since they mediate sodium-independent uptake of a broad array of xenobiotics. A method to determine the specific contribution of OATP1B1 in the hepatic uptake was successfully optimised and applied for 5 therapeutic drugs in Chapter 4. Future application of this strategy is likely to have broad importance in determining relative contribution that individual transporters play in drug disposition.

To prevent accumulation and toxicity of xenobiotics, biotransformation and transport of foreign compounds occurs. However, these processes can be altered by induction or inhibition mechanisms. Rifampicin is a first line drug in tuberculosis (TB) treatment but it is a potent inducer of CYPs and transporters. DDIs during TB treatment are common but the induction potential of different rifamycins has not been comprehensively ranked. Chapter 5 investigated the induction potential of rifampicin, rifapentine and rifabutin. Rifampicin significantly induced CYP3A4, ABCB1, OATP1B1 and ABCC2 in primary human hepatocytes. Induction by rifabutin was observed for CYP3A4, OATP1B3 whilst rifapentine only significantly induced OATP1B1. This work serves as a basis for further study into the extent to which rifamycins induce key metabolism and transporter genes.

Nuclear receptors (NR) regulate the expression of CYPs and drug transporters influencing pharmacokinetics. PXR and VDR have been found to synergistically increase *CYP3A4* expression and activity in intestinal cell lines. This effect has been observed *in vivo* with seasonal variations apparent for CYP3A4 substrates. In Chapter 6, novel associations between vitamin D receptor polymorphisms and expression of it and its target genes involved in drug disposition were shown in D2 intestinal biopsies.

This thesis reports generation of model systems and their application to enable many questions to be answered relating to pharmacokinetics and DDIs. The thesis forms a solid platform from which to further investigate these issues in future studies.

CHAPTER 1

General Introduction

1.0 Introduction

For a drug to be effective at its site of action, adequate concentrations must reach the systemic circulation, following oral administration. Intestinal absorption, drug transport, and phase I metabolism in the liver, are considered to be the primary factors influencing the systemic bioavailability of xenobiotics (1). Cytochrome P450 (CYPs) metabolism enzymes (2), ATP-binding cassette (ABC) efflux proteins (3) and organic anion transporting polypeptides (OATPs), are abundantly expressed in the liver and intestine, and regulate the pharmacokinetics (PKs) of many drugs (4). These fundamental proteins are regulated by nuclear receptor (NR) transcription factors, which are subsequently induced or inhibited by endogenous compounds and xenobiotics. The complex and overlapping mechanisms involved contribute to inter-individual variability in responses observed in the clinic.

PK, is the science of how the body breaks down an active drug into metabolites or more simply, the effect the body has on a drug (5). Understanding the PK of a drug is crucial to identify potential adverse drug effects (ADRs) or drug-drug interactions (DDIs), but requires accurate *in vitro/in vivo* correlations to ensure strength in predictions (6). Drug absorption, distribution, metabolism and elimination (ADME) can be estimated and accurate doses of drug prescribed by applying mathematical models (7). In 2010, the American Food and Drug Administration (FDA) noted over 900,000 hospital admissions caused by DDIs or ADRs (8).

1.1 Pharmacokinetics

1.1.1 ADME

To clearly define ADME, the velocity at which a reaction occurs (rate of reaction) must be determined (9). Assuming clearance of a drug (A) from the body is directly proportional to its concentration remaining in the body, the rate of reaction is described as first-order (5):

$$\frac{\delta A}{\delta T} = -kA$$

Equation 1.1 First order rate of reaction (k = rate constant first order)

If the concentration of a drug is increased the clearance will increase accordingly. First order rates of reaction are used to describe the ADME of most therapeutically administered drugs, but not all follow this pattern. Clearance of phenytoin (antiepileptic) and aspirin (analgesic) are independent of concentrations administered (10, 11). This rate of reaction is described as zero order rate of reaction (5). For example, the clearance of drug (A) occurs at a constant rate:

$$\frac{\delta A}{\delta T} = -k^0$$

Equation 1.2 Zero order rate of reaction (k^0 = rate constant zero order)

During an overdose, a first order drug can change to a zero order process due to limiting factors such as, saturation of metabolism enzymes, co-factors or drug transporters (12).

1.1.2 Pharmacokinetic models

Animal models or primary cell assays used to study drug metabolism aim to define the effects that will be observed by the parent drug and/or the metabolites formed in humans (13). Fundamental parameters that are correlated to drug action include: concentration of the drug at its site of action and the duration this remains above the effective concentration (5). However, measuring the drug concentration at its site of action is difficult (e.g. practicality of access to tissue, number of tissue samples required and ethical constraints) and, plasma drug concentrations are frequently used as a surrogate (14). Understanding the PK of a drug is vital to determine the optimum dose and dosing frequency of a drug, and is of particular importance for drugs with a narrow therapeutic range (e.g. warfarin) (15). Figure 1.1 highlights some specific factors that may influence drug PK.

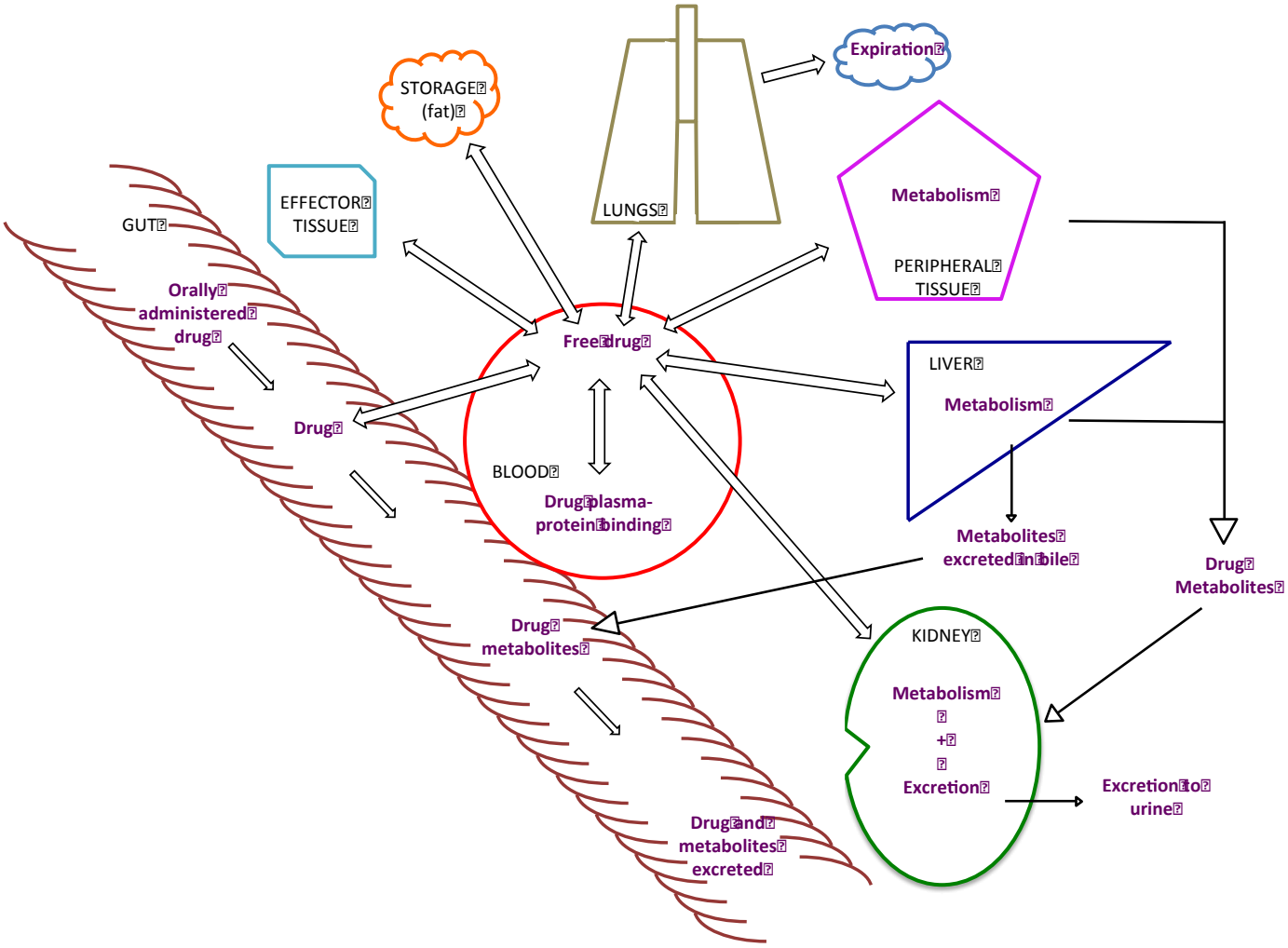

Figure 1.1 Mechanisms that may influence PK parameters of some clinically administered drugs (adapted from Lentz *et al.*, 2013, Part I). Multiple mechanisms may apply for an individual drug but not all mechanisms are relevant for all drugs.

The impact of the body and its processes on PK is complex and dynamic. Thus, analysis requires models to simplify the complexity into specific sections/compartments to describe the fate of a drug.

The one-compartment model assumes all compartments are in equilibrium with the central blood compartment and the drug (D) is instantly distributed throughout the body (K_a), with the rate of excretion equal in all tissues (k_{el}) (16) (Figure 1.2).

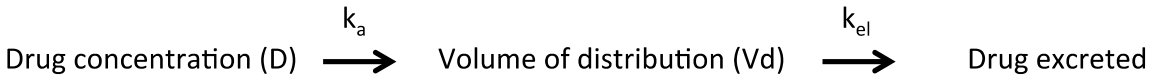

Figure 1.2 One-compartment model (adapted from Dhillon *et al.*, 2006)

Therefore, drug concentration (D) can be calculated if the volume of distribution (Vd) (17) in the compartment (whole body) is known as the drug enters the systemic circulation (time zero; T_0).

$$\frac{D}{Vd} = T_0$$

Equation 1.3 Drug concentration calculated from one compartment model

Consequently, the clearance of the drug from the compartment can be determined by the elimination rate constant (k_{el}), which is normally directly proportional to the concentration of the drug. Hence, the time taken for the drug to halve in concentration ($t_{1/2}$) is always the same. Primary factors that are directly influenced by physiology can be calculated using a first order, one compartment model:

$$\frac{\delta D}{\delta T} = -k_{el} \cdot T_0$$

Equation 1.4 Elimination rate constant at time zero

Taking into consideration the simplicity of the one compartment model, the results generated for Vd, K_{el} and $t_{1/2}$ provide a relatively useful insight into the movement, duration and intensity of drug action (18, 19).

The two compartment model adds one more layer of complexity to generate a hypothesis. Whilst the one compartment model assumes elimination is equal for each tissue, the two compartment model encompasses a central (highly perfused organs e.g. heart, liver, etc.) and peripheral compartment (less well perfused tissues e.g. fat) and estimates the elimination of a drug from each compartment (18) (Figure 1.3).

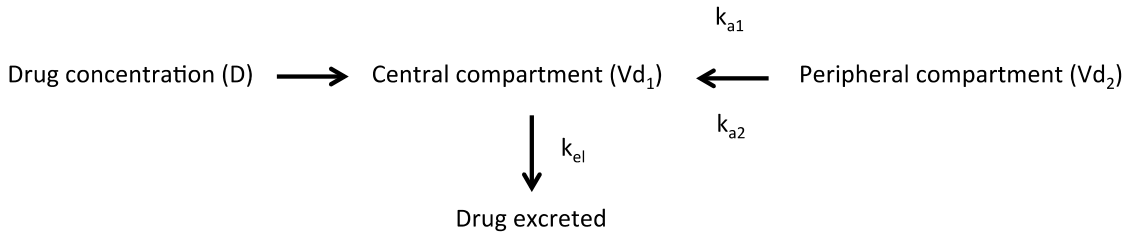

Ka_1 = rate constant from central to peripheral compartment

Ka_2 = rate constant from peripheral to central compartment

Figure 1.3 Two compartment model (adapted from Dhillon *et al.,* 2006)

Although the compartments are a poor representation of the human anatomy they are kinetically distinct. It is assumed the central compartment represents organs that are highly perfused, such as, the lungs, heart, kidneys, liver and brain, whilst the peripheral accounts for tissues that are less well perfused (and frequently cannot directly eliminate drugs), such as, muscle, skin and fat. Thus, analysis must consider the distribution of the drug from the central to the peripheral compartment, drug concentration throughout and elimination of the drug (20). In contrast to the one compartment model, this model does not assume instant equilibrium of the drug between both compartments and clearance (CL) is dependent on the rate constant for each compartment (21).

The two-compartment model can be applied to generate the Vd, K_{el} and $t_{1/2}$. However, since the model is more complex it is used to determine the total amount of drug in the body over time (area under the concentration-time curve; AUC). This measurement can predict the fraction of the dose reaching the systemic circulation (bioavailability; F) (22), assuming CL remains constant. Representative equations of the two-compartment model include:

A

$$\frac{D}{CL} = AUC$$

B

$$\frac{k_{el}}{Vd_{1}} = CL$$

Equation 1.5 Two compartment model use to determine the total amount of dug in the body over time (A) and clearance of the drug (B)

1.2 Drug absorption, distribution, and elimination

1.2.1 Biopharmaceutics drug disposition classification system

The biopharmaceutics classification system (BCS) (Figure 1.4a) is a guidance for the classification of drug compounds based upon their solubility and intestinal permeability at which point the rate limiting step can be defined (e.g. gastric clearance or permeability) and drugs that may be eligible for a waiver in *in vivo* bioequivalence studies can be identified (23). Following dissolution of the drug product, the BCS can be used to predict the rate and extent of drug absorption and elimination from the solid dose form (23). The BCS classifies drug substances based on solubility and permeability. A compound is considered highly soluble if the highest therapeutic concentration is dissolvable in ≤250 ml of aqueous media from pH 1-7.5 and highly permeable if ≥90% of the administered dose is absorbed (17).

The FDA approved application of the BCS with set boundaries to waiver *in vivo* bioequivalence assays for immediate release drugs in 2000 (24). Much controversy exists regarding the policy with some authorities suggesting the biowaiver should be extended whilst others argue it should be stopped. In 2010, the European Medicines Agency (EMA) extended the waiver to include class 3 compounds provided they dissolved very rapidly (25). Whilst the World Health Organisation (WHO) embraces the FDA and EMA concepts, it has further extended the waiver to include weakly acidic, highly permeable and highly soluble compounds at pH 6.8 (e.g. class 2) (26, 27).

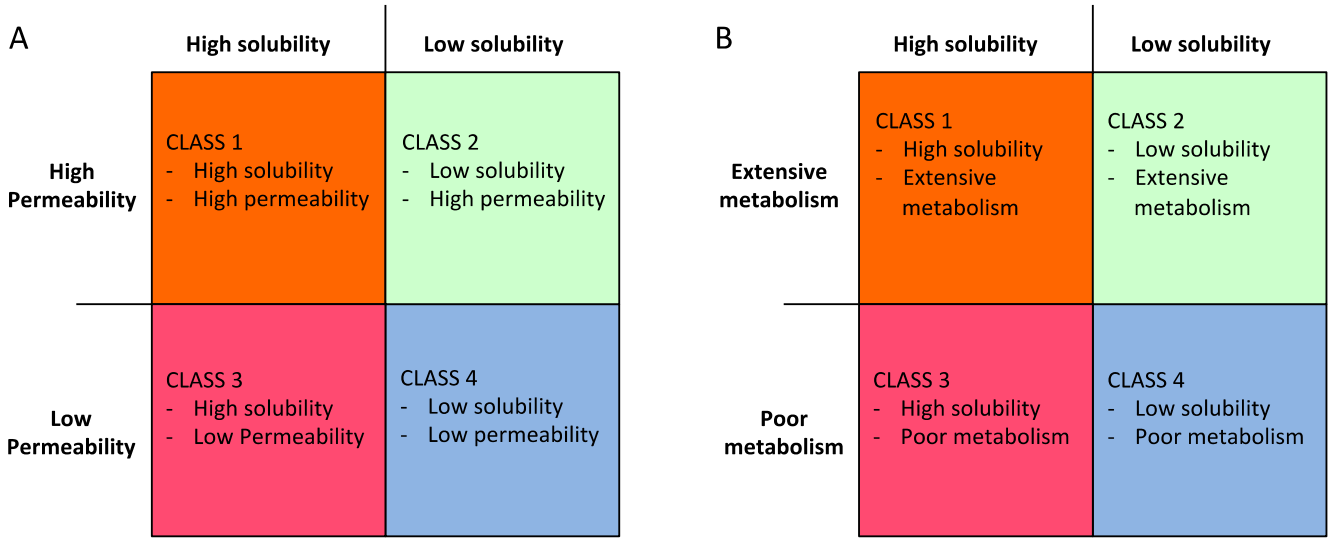

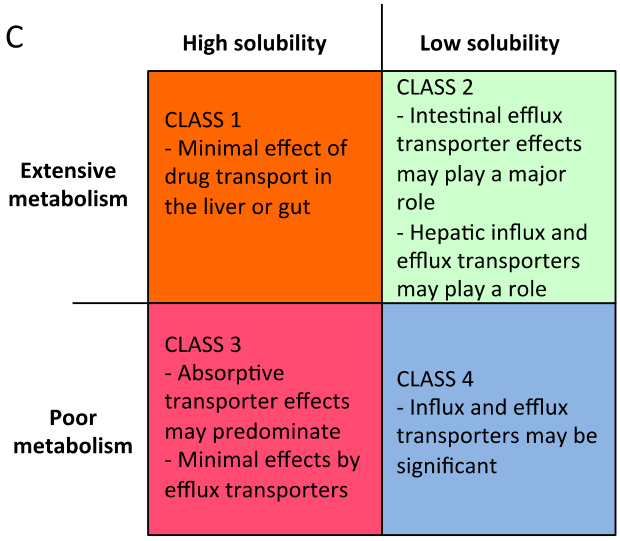

Figure 1.4 Diagram of; Biopharmaceutics Classification System (adapted from Amidon *et al.,* 1995) (A), Biopharmaceutics Drug Disposition Classification System (adapted from Benet *et al.,* 2005) (B) and manipulation of the Biopharmaceutics Drug Disposition Classification System to ascertain the effects of drug transporters for each class (C)

In contrast, the biopharmaceutics drug disposition classification system (BDDCS) (Figure 1.4b) developed by Wu and Benet (17) is used to classify compounds into four groups according to characteristics that affect drug disposition and potential DDIs, such as the route of elimination and solubility. In contrast to the BCS (28), phase I and II metabolism are regarded as appropriate markers of drug permeability (29).

Drugs metabolised ≥ 90% are characterised as class 1 or 2 depending on their solubility according to the BDDCS. Ambiguity arises when comparing compounds classified under the BCS or BDDCS (30). Tallinolol for example, is highly absorbed by the body and is categorised as a class 2 compound according to the BCS (31). However, it is poorly metabolised, thus when applying the BDDCS the drug is a class 4 compound and transport across the membrane is fundamental (31). By applying either method, drug absorption can be predicted. Nonetheless, the FDA (32, 33) requires absorption to be estimated as a product of metabolism and not permeability. Hence, the BDDCS must be applied. The BDDCS predicts the extent of metabolism but does not give an insight into the magnitude of absorption or elimination; instead it implies drug transporters are key factors. The effects of drug transporters can be predicted following oral administration (Figure 1.4c) (34).

Although the classification may not be suitable for every drug, the majority can be fitted to the BDDCS (17). According to Figure 1.4b and 1.4c, a drug that is extensively metabolised, membrane permeable and has high solubility, crosses the gut relatively independently, therefore effects of drug transporters will be minimal (class 1). Class 2 compounds are extensively metabolised, membrane permeable but have low solubility suggesting influx transporter effects are minimal in comparison to efflux transporters that may play a significant role. However, Fagerholm *et al.*, 2008, describes how varying intensities of 'high' permeability may determine whether a drug is a transporter substrate even though it is extensively metabolised (35). Class 3 and 4 compounds are poorly metabolised and have varying levels of solubility, suggesting both influx and efflux transporters play a major role in the absorption distribution, and elimination of the drug (28).

Whilst the BCS is part of the legal framework in waiving bioequivalence studies, there is no consensus with the BDDCS. However, they are regarded as complimentary classification systems that aid in improving drug disposition and DDI predictions to simplify and speed up the drug development process.

1.2.2 Transport

The route of administration, dose, physiochemical properties (lipophilicity, size, pH) and formulation of a drug all influence its absorption and subsequent distribution and elimination (22). A drug (unless administered intravenously) must cross numerous cell membranes by passive or facilitated diffusion, active transport or pinocytosis (36) before it reaches the systemic circulation.

The majority of drugs are weak organic acids or bases but lipophilicity varies depending on their charge. Lipophilic compounds flow across the cell membrane with ease down a concentration gradient in contrast to hydrophilic compounds that do not penetrate the lipid bilayer with ease (37). However, glucose does not demonstrate the same difficulties (38). Although glucose has poor lipid solubility it rapidly passes the cell membrane and facilitated diffusion is thought to be the mechanism responsible. Facilitated passive diffusion involves a chaperone that binds to a compound to aid the movement through the cell membrane after which the chaperone dissociates to carry the next molecule (37). The process does not require energy expenditure but the number of carriers and compound structure limits the process. Pinocytosis is dependent on energy and plays a minor role in the transport of non-protein compounds (39, 40). The lipid bilayer creates a crevasse, traps molecules and re-fuses to form interior vesicles that are released allowing the molecule to penetrate the cell. Lastly, active transport involves the energy dependent movement of endogenous molecules such as, vitamins, minerals, amino acids, drugs and xenobiotics against a concentration gradient (37).

1.2.3 Role of drug transporters

For a drug to reach the systemic circulation it must pass liver and intestinal transporters, which dictate drug concentrations that undergo, first pass metabolism (30, 41). By controlling bioavailability and absorption of drugs, uptake and efflux transporters regulate the disposition and efficacy profiles of orally administered drugs (42). The characterisation of the efflux transporter, ATP-binding cassette sub-family B member 1 (ABCB1; p-glycoprotein) in 1976 (43), highlighted the need for an improved understanding of transporters in influencing PK (30).

To date, over 400 membrane bound transport proteins have been identified in the human genome (42). In particular, the two transporter groups outlined below have been found to be influential in the safety, efficacy and disposition of many drugs (predominantly, but not exclusively, in the liver and intestine) (44, 45). As described later in chapter 4, to further understand the effects these proteins have on PK, some transporters have been cloned, transfected or knocked-down to characterise them in different models. Clinical DDI studies have suggested the PK of a drug is linked to the cross-talk between drug transporters and metabolism enzymes, rather than the proteins exerting their effects independently (46).

The solute carrier superfamilies, SLC and SLCO have been identified as the main uptake transporters involved in hepatic and intestinal drug transport of type I organic ions, zwitterions and cations, and type II organic anions, respectively (47). Transporter activity is not energy dependent, rather ion movement over the membrane creates a chemiosmotic gradient, which the proteins utilise to transport xenobiotics or endobiotics (4, 41, 48). The SLC superfamily comprises numerous proteins including, the organic anion transporters (OAT1; SLC22A6), organic cation transporters (OCT1; SLC22A1), the electroneutral cation transporters (OCTN1; SLC22A4), the equilibrative nucleoside transporters (ENT; SLC29) and the apical sodium dependent bile salt transporter (ABST; SLC10A1) (47). In contrast, the SLCO superfamily includes the organic anion transporting polypeptides (OATP) such as the main drug transporters, SLCO1B1 (OATP1B1) and SLCO1B3 (OATP1B3) (13). These sinusoidal membrane bound proteins transport many substrates including the angiotensin receptor antagonists, the HMG-CoA reductase inhibitors and protease inhibitors (49, 50).

The ATP-dependent binding cassette superfamily (ABC) constitutes a major group of hepatic and intestinal transporters involved in drug efflux (51). The superfamily comprises 49 large membrane bound proteins split into 7 main groups with all ATP-binding cassette members (ABC), including ABCB1 (p-glycoprotein), ABCCs (multidrug resistance proteins; MRPs) and ABCG2 (breast cancer resistance protein; BCRP) (51). The utilisation of ATP equips the transporters with a key energy source for the movement of compounds against a concentration gradient (52). Figure 1.7a and b illustrates selected drug transporters present in the liver and intestine, respectively.

Factors affecting the expression and activity of drug transporters such as, single nucleotide polymorphisms (SNPs), inhibitors, inducers and protein regulatory elements are crucial factors influencing drug absorption and distribution and will be discussed in more detail later (section 1.5).

A

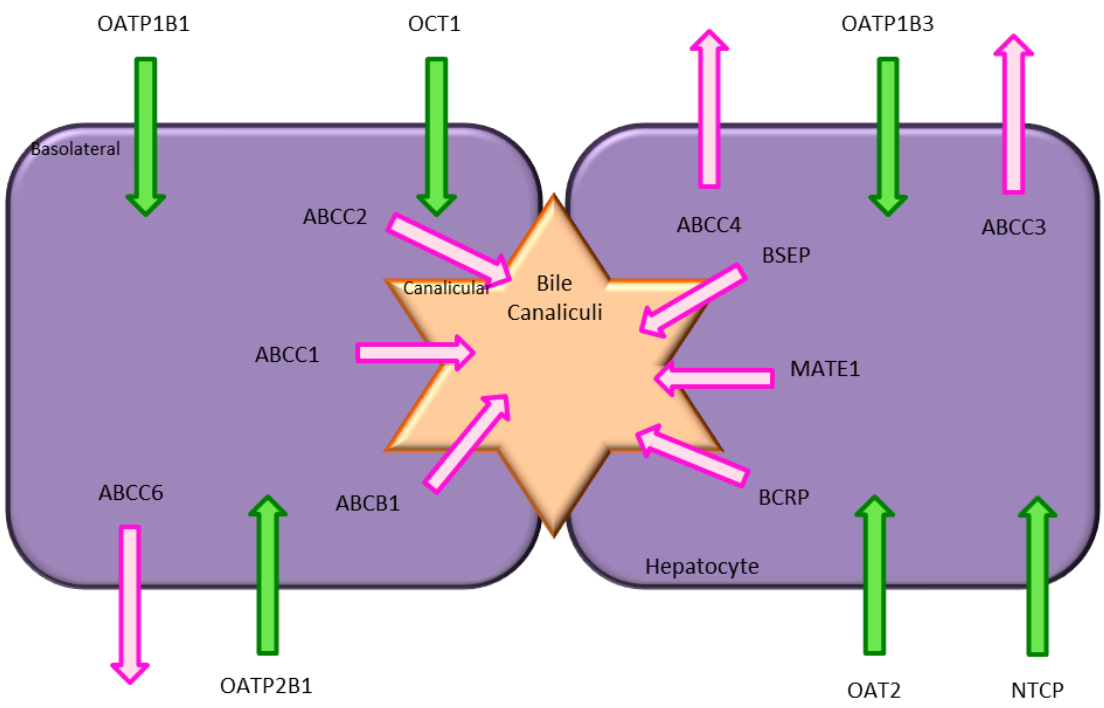

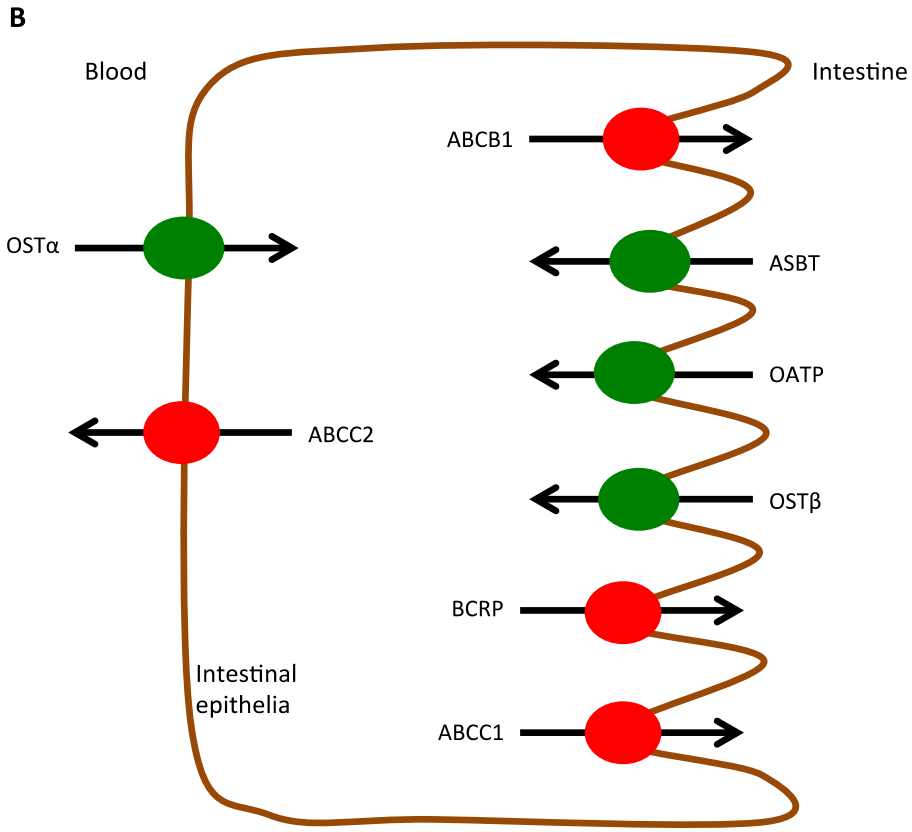

Figure 1.7 Selected transporters expressed on the membranes of human hepatocytes (A) and enterocytes (B). ABC, ATP-binding cassette protein; ASBT, apical sodium dependent bile acid transporter; BCRP, breast cancer resistance protein; BSEP, bile salt export port; MATE, multidrug and toxin extrusion protein; NTCP, sodium/taurocholate co-transporting polypeptide; OAT, organic anion transporter; OATP, organic anion transporting polypeptide; OCT, organic cation transporter; OST, organic solute transporter.

1.2.4 DDIs and drug transporters

Transporters can be major determinants of PK, efficacy and safety of compounds and can play an important role in DDIs (53). In the context of this chapter, Table 1.1 includes drug transporters with clinical influence and practical considerations required in drug development.

Selected Drug Transporter Inhibitors						
OATP1B1	**OATP1B3**	**OAT1**	**MATE1**	**ABCB1**	**ABCC2**	**ABCG2**
Atorvastatin	Rifampicin	Probenecid	Quinidine	Cyclosporine A	Cyclosporine	Estrone
Saquinavir	Cyclosporine A	Novobiocin	Cimetidine	Quinidine	Delaviridine	17β-Oestradiol
Ritonavir	Ritonavir		Procainamide	Tariquidor	Efavirenz	Fomitremorgin C
Lopinavir	Lopinavir			Verapamil	Emtricitabine	
Rifampicin						
Selected Drug Transporter Substrates						
OATP1B1	**OATP1B3**	**OAT1**	**MATE1**	**ABCB1**	**ABCC2**	**ABCG2**
Estrone-3-sulfate	Cholecystokinin 8	Adefovir	Metformin	Digoxin	Glutathione conjugates	Mitoxantrone
Olmesartan	Fexofenadine	Zidovudine	Tetraethylammonium	Loperimide	Methotrexate	Topotecan
Valsartan	Telmisartan	Methotrexate	N-methylpyridinium	Irinotecan	Etoposide	Methotrexate
Pitavastatin	Valsartan	Ciprofloxacin		Vinblastine	Valsartan	Irinotecan
Bromosulphophthalein	Digoxin			Paclitaxel	Olmesartan	
				Fexofenadine		

Table 1.1. Examples of human drug transporters with associated substrates and inhibitors involved in DDIs (data obtained from the literature, see references (4, 41, 54-63)).

Although less well recognised in comparison to CYPs, due to extent of transporter based DDIs, the FDA now requires investigation of drugs *in vitro* to determine their potential as substrates for the transporters outlined in Table 1.1 (64). In 2012, the International Transporter Consortium (ITC) gathered to collate their opinions on which transporters should be studied *in vitro*, *in vivo* and in clinical studies based on their clinical significance in determining drug absorption and distribution (ITC White Paper) (33, 64). The FDA updated their requirements in February 2012, stating 7 key transporters should be analysed. Further to the White Paper published in 2012, the ITC recommendations have now been updated. The ITC suggest 11 drug transporters should be considered for all NCEs (42). The emphasis of drug transporter analysis is the significance of their role on PKs. For example, inhibition of OATP1B1 by cyclosporine increases the AUC of pravastatin, pitavastatin and rosuvastatin, 10-fold, 5-fold and 7-fold, respectively (4). Inhibition of ABCB1 by quinidine results in 50%

less clearance of digoxin and an 86% increase in AUC of ritonavir (59). Similar to CYPs, drug transporter expression can be induced mediating effects on many victim drugs. For example, efavirenz and oltipraz upregulate the expression of ABCB1, ABCC2 and ABCG2 (63, 65). Drug transporters and DDIs are discussed further in Chapter 4 and 5.

1.3 Metabolism

1.3.1 Cytochrome P450 enzymes

In 1947, Williams *et al.*, identified detoxification mechanisms of the human body upon xenobiotic insult (66). Metabolism was categorised into 2 distinct phases: phase I including oxidation, reduction and hydrolysis and phase II: conjugation reactions (66). Williams *et al.*, 1947, proposed the liver was the main organ responsible for first past metabolism and posed as a major obstacle when regulating therapeutic drug concentrations. The human genome codes for a superfamily of over 50 membrane-bound, haem-containing cytochrome P450 genes (CYP) that are responsible for xenobiotic and endogenous compound metabolism (67). The superfamily is classified according to structure (>40% identical) (CYP1, CYP2, CYP3, etc.) and sub-classified with group members >55% identical (CYP2B, CYP2D etc.). Finally, an Arabic numeral is used to identify each individual enzyme (CYP1A2, CYP2D6, CYP2B2, etc.). Key members of this specialised xenobiotic metabolism group include CYP2C9, CYP2C19, CYP1A2, CYP2B6, CYP2D6, CYP3A5 and CYP3A4 (68) (Table 1.2). Although CYPs are located in the majority of organs their primary locations are the liver and intestine (69).

Enzyme	Abundance of CYP enzyme in the liver (% of total CYP genes)	Contribution to the metabolism of therapeutic drugs (%)
CYP1A2	12–13	4–6
CYP2A6	1–10	-
CYP2B6	3–5	25
CYP2C8	7	-
CYP2C9	12–17	10–11
CYP2C19	0.2–3	4
CYP2D6	4	25
CYP2E1	7–15	21–52
CYP3A4	30	>50
CYP3A5	29	-

Table 1.2. Relative liver content of selected cytochrome P450 enzymes and their quantitative role in drug metabolism (data obtained from the literature, see references (70-79)).

As Williams *et al.,* 1947 described, metabolism can occur via a number of processes; oxidation, reduction, hydroxylation and dealkylation. Generally, in order for drug oxidation to be achieved, the CYPs utilise the mono-oxygenase redox system (NADPH-P450 reductase) (80). The mechanism by which the NADPH-P450 reductase provides electrons for drug oxidation and how the redox cycle is maintained is highly complex (81). However, drug oxidation can be achieved efficiently by the transfer of one molecular oxygen atom to the drug, creating a more polar hydroxyl containing metabolite, with the other oxygen atom forming a water molecule (81).

1.3.2 CYP induction and inhibition

Over 80% of clinically administered drugs are metabolised by CYPs, therefore their involvement in DDIs are common (69). Induction or inhibition of CYP expression and activity (CYP1A1, CYP1A2, CYP2B6, CYP2C8, CYP3A4) can alter an

individual's PK by as much as 5-200 fold (76). Induction is usually a result of NR-mediated transcriptional activation where mRNA and protein expression are increased leading to the production of new CYP protein, which may take several days (2). Induction can significantly reduce the efficacy of the mediating drug (perpetrator) through autoinduction or of a coadministered drug (victim) by increasing their metabolism, resulting in decreased absorption, increased clearance and treatment failure (2). In contrast to induction, CYP inhibition is immediate and drug plasma concentrations may be increased by competitive inhibition (e.g. ketoconazole is a CYP3A4 substrate also) or by non-competitive inhibition (e.g. quinidine is a CYP2D6 inhibitor but not a substrate) (82). Inhibition of CYPs generally results in supra-therapeutic concentrations of a victim drug by a perpetrator drug, which can result in a higher incidence of concentration-dependent toxicities. However, most inhibition-mediated DDIs are rapidly reversible.

Levels of CYP expression and activity can also be modified by SNPs (see section 1.5 below) and functional variants have been noted for CYP1A2, CYP2C9, CYP2D6, CYP2B6 and CYP3A4 (75, 83). Inhibition, induction and SNPs result in large inter-individual variability in PK and drug response. Table 1.3 includes examples of the main human CYP substrates, inhibitors and inducers.

Selected CYP Inducers						
1A2	**2B6**	**2C8**	**2C9**	**2D6**	**2E1**	**3A4/5**
Omeprazole	Rifampicin	Rifampicin	Rifampicin	Rifampicin	Ethanol	Rifampicin
Tobacco	Phenobarbitol	Verapimil	Secobarbital	Dexamethasone	Isoniazid	Carbamazepine
Insulin	Carbamazepine	Rosiglitazone	Dehydroepiandrosteron	Glutethimide	Tabacco	Efavirenz
Broccoli	Phenytoin	Paclitaxel	Dexamethasone			Phenobarbitol
Bok Choy						Phenytoin
Cabbage						Nevirapine
						Glucocorticoids
						St Johns Wort
						Bile acids
						Vitamin D
Selected CYP Inhibitors						
1A2	**2B6**	**2C8**	**2C9**	**2D6**	**2E1**	**3A4/5**
Ciprofloxacin	Orphenadrine	Deferasirox	Valproic acid	Ritonavir	Disulfiram	Ritonavir
Verapamil	Curcumin	Gemfibrozil	Amiodarone	Cimetidine	Diethyldithiocarbamate	Clarithromycin
Cannabis	Ticlopidine	Lapatinib	Fluconazole	Haloperidol		Nefazodone
Peppermint tea	ThioTEPA	Trimethoprim	Sulfaphenazole	Quinidine		Ketoconazole
Fluvoxamine		Montelukast	Cyclizine	Bupropion		Erythromycin
Cimetidine		Quercetin	Quercetin	Histamine H1		Saquinavir
Grapefruit			Lovastatin	Doxorubicin		Indinavir
Cumin			St Johns Wort	Fluoxetine		Nelfinavir
				Celecoxib		Fluconazole
						Cimetidine
Selected CYP Substrates						
1A2	**2B6**	**2C8**	**2C9**	**2D6**	**2E1**	**3A4/5**
Haloperidol	Bupropion	Amiodarone	Celecoxib	Codeine	Benzene	Cyclosporine
Amitriptyline	Efavirenz	Carbamazepine	Tolbutamide	Metoprolol	Theophylline	Paclitaxel
Caffeine	Tamoxifen	Chloroquine	Losartan	Chlorpromazine	Ethanol	Ketoconazole
Tamoxifen	Valproic acid	Diclofenac	S-warfarin	Fluoxetine	Paracetamol	Dapsone
Erlotinib	Nevirapine	Ibuprofen	Phenytoin	Imipramine	Halothane	Amitriptyline
Naproxen	Methadone	Paclitaxel	Rosiglitazone	Amitriptyline	Sevoflurane	Citalopram
Estradiol	Cyclophosphamide	Torsemide	Ketamine	Encainide	Chlorzoxazone	Haloperidol
Phenacetin	Propofol	Cerivastatin	Suprofen	Phenacetin		Codeine
Warfarin		Rosiglitazone				Atorvastatin
						Ritonavir

Table 1.3. Examples of the main human CYPs with associated substrates, inhibitors and inducers involved in drug metabolism (data obtained from the literature, see references (2, 46, 55, 68, 70, 73, 74, 78, 81, 82, 84-109)).

1.4 Regulation of transporter and CYP expression

1.4.1 Nuclear receptors

Xenobiotic insult can have a profound effect on human health. Metabolism and transport mechanisms are regulated through the nuclear receptor (NR) superfamily of transcription factors (110). The superfamily recognises toxic byproducts acting as

xenosensors to modulate gene transcription through a variety of processes, depending on their classification (111). Although derived from one common ancestor (112), NRs are grouped into 6 categories according to their mechanism of action and distribution within a cell (Table 1.4).

Class Number	Nuclear receptors
1	Thyroid hormone receptors (TRs) Retinoic acid receptors (RARs) Vitamin D receptors (VDRs) Peroxisome proliferator-activated receptor (PPARs) Numerous orphan receptors - (Pregnane X receptor (PXR), constitutive androstane receptor (CAR))
2	Retinoid X receptor (RXR) Hepatocyte nuclear factor 4 (HNF4) Testicular receptor (TLX)
3	Steroid receptors (progestins, glucocorticoids (GR), mineralcorticoids (MR)) Oestrogen receptor (ER) and homologs (oestrogen related receptor (ERR))
4	Nerve growth factor 1B-like (NGF1B) Nuclear receptor related 1 (NURR1)
5	Steroidogenic factor like-1 (SF1)
6	Germ cell nuclear factor (GCNF)

Table 1.4 Classification of nuclear receptors

The general mechanism of NR activation is illustrated in Figure 1.8. NR substrates (endogenous or exogenous) cross the cell membrane and bind to the receptor. Two main ligand binding processes proceed: 1) the NR, (for example CAR) may be bound to chaperones and co-chaperones, such as, heat shock proteins (Hsp) in the cytoplasm. Upon ligand binding, the chaperone/co-chaperone complex dissociates allowing the receptor to translocate to the nucleus, forming a homo- or hetero-dimer and binding at upstream regulatory sites of target genes. NR co-activators, such as, the p160 family, are then recruited and transcriptional activation occurs (Figure 1.8a). However, if NR co-repressors such as, NR co-repressor 1 (NCOR1) are recruited, DNA binding and subsequent DNA transcription can be repressed. For some NRs an alternative pathway occurs (Figure 1.8b). Specifically, some NRs (PXR, TR, VDR) may already be located in the nucleus of the cell bound to their response elements as a homo- or hetero-dimer in the presence or absence of a substrate. The dimeric complex does not require chaperones or co-chaperones to translocate, rather co-repressors such as, NCOR1 suppress transcription. Upon ligand binding, the co-repressor dissociates and co-activator proteins are recruited, initiating gene transcription. The roles of NR co-regulators are discussed in more detail in section 1.4.7.

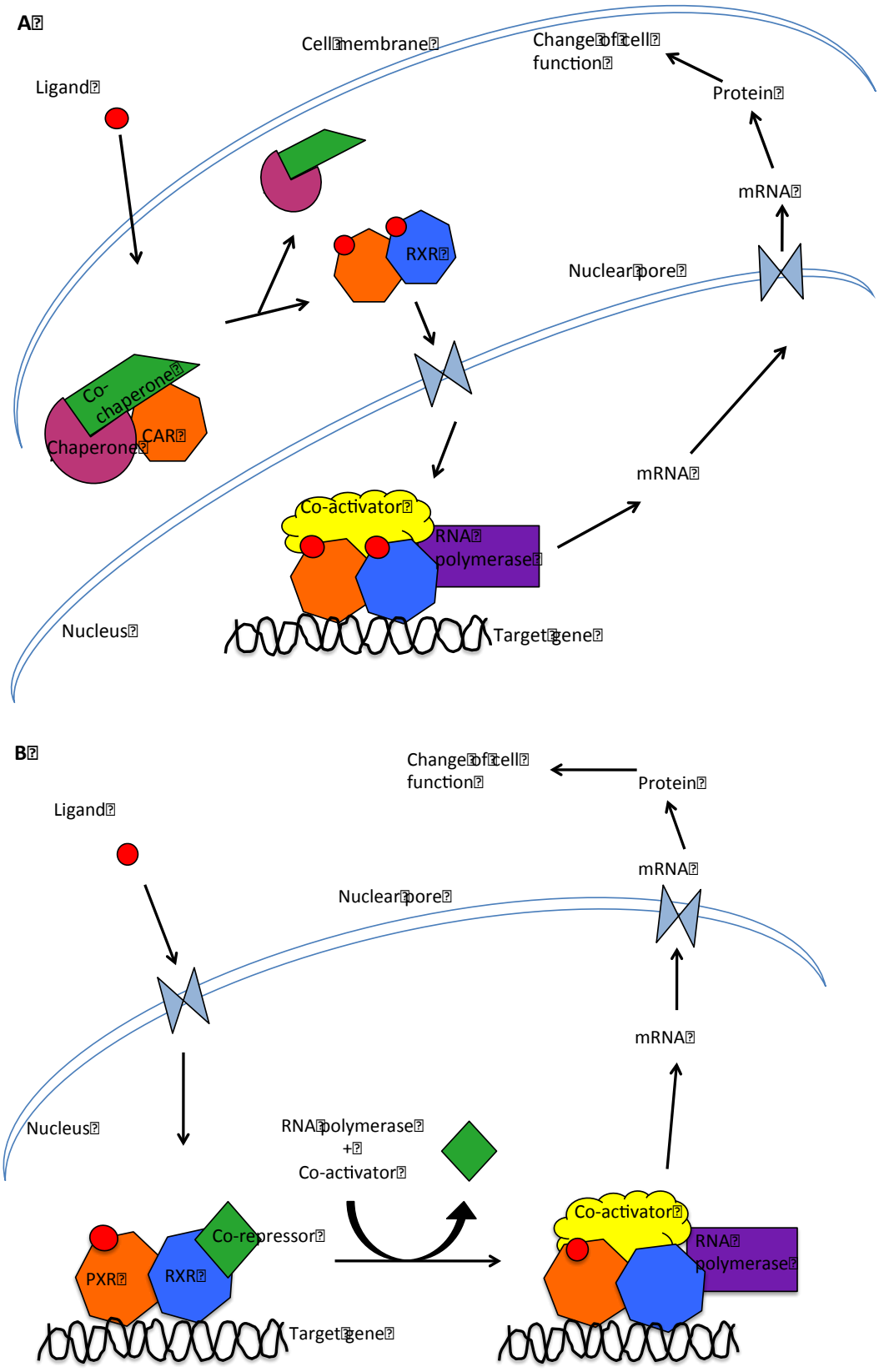

Figure 1.8 Activation of NR upon ligand binding via dissociation of chaperone/co-chaperone complex (A) or co-repressor dissociation (B)

1.4.2 Structure of nuclear receptors

NRs are composed of 5 distinct regions (Figure 1.9), originally defined by Krust *et al.*, 1986 (113):

1. The A/B region (N-terminal domain), contains transcriptional activation function (AF-1) primarily responsible for activation. A range of signaling cascades mediate the post translational phosphorylation of the region, resulting in variable activity (114). The A/B region varies considerably in length between NRs; for example, VDR has 23 amino acids compared to GR that has 550 amino acids. The NH_2 group also differs between NRs and the region is highly susceptible to SNPs, thus structure definition is yet to be complete (111). However, the region demonstrates cell and promoter selectivity, specific to cell action and AF-1 activity (115).

2. The DNA binding domain (DBD) contains the peptide sequence that specifically recognises and binds to the response elements in the target genes of the NR. It is a highly conserved domain comprising 2 zinc finger motifs, a C-terminal motif and an N-terminal motif; each motif contains 2 cysteine residues that chelate 1 zinc ion. The C-terminal sequence elements (P, D, T, A boxes) are key for identifying specific response elements contributing to DNA backbone binding and acting as an interface for dimerisation in the DBD (116). The major groove of DNA is bound to an α helix located in the core of the DBD (recognition helix) to ensure specific base binding. In addition, a second α helix of the DBD core intertwines the carboxyl group of the zinc finger forming a right angle with the recognition helix (117).

3. The hinge region allows rotation of the NR between the DBD and the LBD. Without causing any steric hindrance, the hinge allows surrounding domains to alter their conformational structure. The region is not well conserved between NRs, although most contain nuclear localisation signals (NLS) or elements that contribute to NR localisation from cytoplasm to nucleus (118). Polymorphisms are also common, many of which contribute to structure alterations and may modulate co-repressor interactions (119).

4. The ligand binding domain (LBD) is formed of 12 highly conserved α helices (H1-H12) split into 2 regions; a COOH-terminal comprising an activation function motif (AF-2) that acts as an interface for ligand-dependent transcription and a signature motif (120). The LBD is immensely flexible in shape and size allowing the binding of a range of diverse chemical structures. It is responsible for Hsp interaction, NR dimerisation and ligand dependent transcription and upon ligand binding a conformational change is evident (121).

5. The F region (C-terminal) is not present in all NRs and poorly conserved. The function of the C-terminal is not fully understood but it is thought to be responsible for co-activator recruitment to the LBD and 'fine tunes' NR activation (122).

Figure 1.9 Schematic representation of a typical nuclear receptor sequence

1.4.2.1 NR hormone response elements

Hormone response elements (HREs) are specific DNA sequences in target genes that NRs bind to mediate transcription (123). They are commonly found in regulatory sequences in the 5'-flanking region of the target gene, close to the promoter core but can also be found several kilobases (kb) upstream of the transcription activation site in the enhancer region (124). Copious analysis of endogenous and synthetic HREs, have determined that the core recognition motif is comprised of 6 base pairs (bp) (125). Further investigation has identified 2 consensus motifs: 1) a palindromic sequence of AGAACA that is separated by 3 nucleotides and preferentially recognised by class 3 NRs and 2) the remaining NRs recognise the direct repeat consensus motif AGG/TTCA (126). Although the consensus motifs represent ideal sequences, naturally occurring HREs show variation to those detailed above. Whilst most receptors bind as homo- or heterodimers to HREs composed of 2 core hexameric motifs, monomeric NRs are able to bind to a single hexameric motif. The half sites for dimeric HREs can be arranged as direct repeats (DR), inverted palindromes (IP) or palindromes (Pal) (127). A Pal is a nucleotide sequence with one strand that reads in the reverse order to the complimentary strand (the sequence is same whether it is read 5'-3' or 3'-5'). An IP is a nucleotide sequence that is the reversed compliment to another further downstream. A DR is a similar nucleotide sequence that is repeated in the same orientation within one strand (123).

1.4.2.2 NR binding – monomers, homodimers, heterodimers

Monomeric binding of orphan NRs to DNA can be achieved with high affinity. The monomeric NRs recognise the sequence by utilising the C-terminal extension (CTE) of the LBD, whilst recognition of specific amino acids is ensured by the DBD A box.

Extensive DNA receptor contacts, ensure affinity and specificity are achieved when the CTE binds the minor groove of DNA, extending the DBD connection further than the recognition sequence consensus half site.

Whilst the majority of non-steroidal NRs bind as heterodimers, some can bind to DNA as homodimers. Thyroid hormone receptor (TR), vitamin D receptor (VDR) and retinoic acid receptor (RAR) can bind as homodimers but DNA binding and transcriptional efficacy are significantly improved following heterodimerisation with RXR (a promiscuous partner) (128). In addition, monomeric and homodimeric receptors such as NGF1B and RAR, can form heterodimers with RXR. NGF1B/RXR heterodimers recognise the DRs rather than monomeric sequences whilst RAR/RXR heterodimers bind to Pal or IP.

DRs are asymmetric, hence heterodimers bind with 2 definitive polarities. RXR occupies the upstream half site on the DR3, 4 and 5 and the heterodimeric partner (e.g. TR, VDR, RAR) is present on the downstream half site (129).

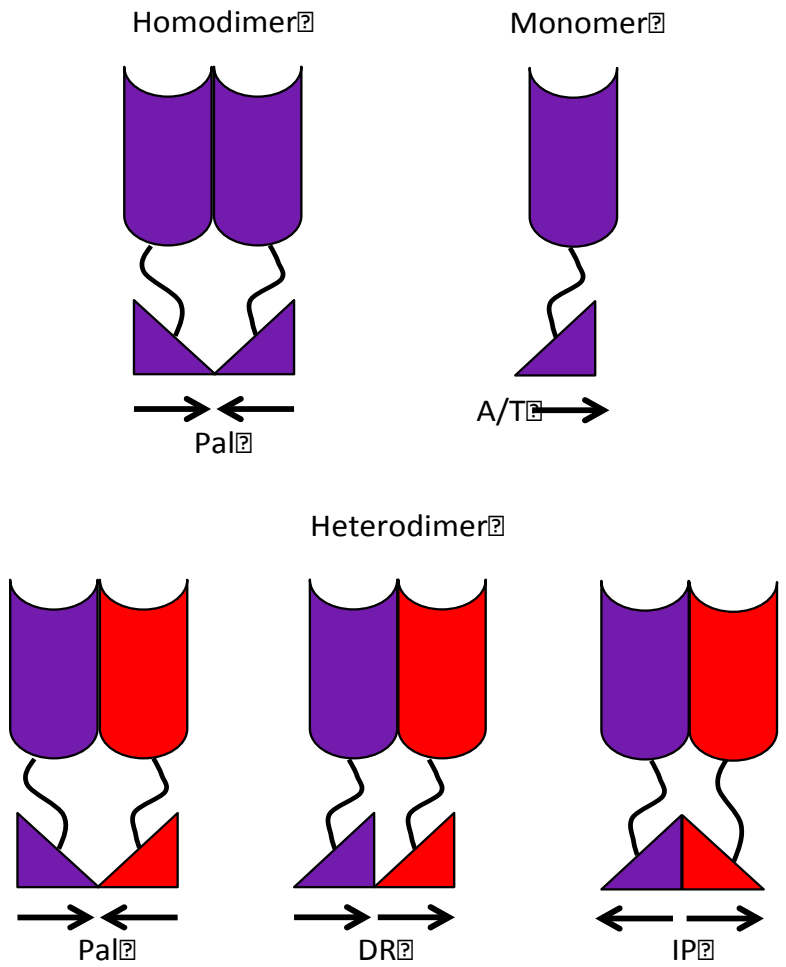

Figure 1.10 Examples of NR binding to their hormone response elements (Adapted from Aranda *et al.*, 2001)

Post-translational modifications (PTM) including methylation, phosphorylation, acetylation, ubiquitination and sumoylation regulate the functions of NRs (130). Furthermore, these PTMs can be subdivided into 2 groups: 1) alterations through the addition of other proteins (e.g. sumoylation, ubiquitination); or 2) the reversible addition or removal of functional groups on specific target proteins (e.g. phosphorylation). PTMs subtly alter NR functions, modulating the activity (positively or negatively) through steric hindrance, reducing the stability of the protein as well as manipulating the localisation of the intracellular proteins (131). Recently, it has been

found PTMs of NRs are fundamental in the pathophysiological formation of numerous diseases including diabetes, cancer and obesity (130).

1.4.3 Key NRs; PXR and CAR

The most widely studied NRs in terms of drug disposition are PXR and CAR. Both of these NRs exhibit promiscuous xenobiotic sensitivity although PXR appears to be more promiscuous than CAR. Mechanistically, these 2 fundamental NRs regulate the transcription of a broad range of drug metabolising enzymes and transporters often in a concerted manner (132, 133).

1.4.3.1 PXR

The 'adopted' orphan NR, PXR (NR1I2), is highly expressed in the liver and intestine, was initially named steroid X receptor (SXR) or pregnane-activated receptor (PAR) as a reflection of its versatility in substrate recognition (134). The 434 amino acid, 50 kDa protein located on chromosome 3, locus 3q12-q13.3 was isolated and cloned in 1998 (135). The promiscuity of PXR is deemed to be as a result of a large and flexible LBD that is able to accommodate a wide range of structures in contrast to other NRs (136). Human PXR (hPXR) and mouse PXR (mPXR) share approximately 90% structure similarity but the LBDs share less sequence homology. In addition, although they are activated by numerous ligands including, glucocorticoids, antifungals, macrolide antibiotics, pregnane derivatives and herbal remedies, they display different profiles (137). For example, species-specific differences are observed with rifampicin (RIF) and pregnenolone-16α-carbonitrile (PCN) (138). Whilst RIF is a potent inducer of hPXR, only a weak effect is prevalent for mPXR with the converse true for PCN, which is a weak activator of hPXR and a potent

activator of mPXR (138). The difference in species specificity poses a challenge when extrapolating pre-clinical models to analyse human drugs (139). Investigations into the binding characteristics and structure of PXR have been extensive (140). Identified upon RIF and hyperforin binding, in contrast to other NRs, the LBD of PXR can change shape and structure as well as vary significantly in its volume capacity (141).

1.4.3.2 Regulation of drug metabolism and transport by PXR

Upon ligand binding, PXR binds as a heterodimer with RXR to direct or everted repeats ((A/G)G(G/T)TCA) separated by 3 (DR3) or 6 (ER6) base pairs present on the enhancer region or proximal promoter region of CYP3A4, respectively (142). In addition to CYP3A4 induction, it has been demonstrated the basal expression of the enzyme is highly dependent on PXR (108). Indeed, a correlation between PXR and CYP3A4 expression has been reported in many tissues in the absence of enzyme inducers (61, 111, 143, 144). The most common DDI occurrence is observed in patients with complex drug regimens including, tuberculosis, human immunodeficiency virus, cancer or cardiovascular diseases. In particular, the macrolide antibiotic, rifampicin (RIF), a PXR substrate used in tuberculosis treatment, is associated with over 100 CYP3A4 substrate DDIs (137). Mechanistically, RIF binds 18 amino acid side residues of the PXR LBD, inducing CYP3A4 and resulting in decreased plasma drug concentrations due to an upregulation of clearance (145).

Another widely reported PXR agonist is the herbal medicine, St John's Wort. The herb contains many PXR ligands including hyperforin (146). Hyperforin does not bind directly to the α helix in the LBD, instead it induces a unique conformational change in 2 loops opposite the LBD to activate gene transcription (147). In addition to

CYP3A4, other CYPs and drug transporters activated by PXR include, CYP2B6, CYP2C8, CYP2C9, CYP2C19, ABCB1, OATP1B1, OATP1B3 and ABCC2 (132). Recent studies have shown PXR activation of genes is not dependent on the location of the attachment. CYP4F12, responsible for metabolising arachidonic acid, contains PXR binding sites located on the intron rather than the upstream promoter region (148). Paclitaxel, a mitotic inhibitor used in the treatment of ovarian or breast cancer is metabolised by CYP3A4 and CYP2C8, and removed from the hepatic cell by ABCB1 (149). Importantly, paclitaxel activates PXR, inducing gene transcription of CYP3A4, CYP2C8 and ABCB1; thus, efficacy is reduced with an increased incidence of development of drug resistance.

Over the last decade it has become more apparent PXR is responsible for coordinating the efflux, and, influx of compounds rather than just metabolic processes (38). The main transporters responsible for preventing therapeutic concentration are the efflux transporters hence they are more commonly studied. The PXR ligand, RIF, induces NR binding to the distal DR4 HRE 8kb upstream of the ABCB1 initiation site (150, 151). As described earlier, PXR CYP binding also occurs at the distal region, indicating the maximum induction of target genes is achieved through the distal enhancer regions (133). The use of PXR knock-out mice has demonstrated ABCC2 is regulated by PXR upon PCN or dexamethasone (DEX) exposure (152). In contrast to the CYPs, ABCB1 and ABCC2 bind to PXR/RXR and CAR/RXR heterodimers at the ER8 HRE on the upstream proximal promoter region. Pharmacokinetics is additionally influenced by influx transporters OATP1B1, OATP1B3 and NTCP all of which are also regulated by PXR (144, 150). Other regulatory targets of PXR include,

sulfotransferases (153), carboxylesterases (154), aldo-keto reductases (155) and uridine-5'-diphosphate glucuronosyl transferases (UGTs) (156).

1.4.3.3 CAR

Similar to PXR, CAR (NR1I3) is highly expressed in the liver and intestine. The 8.5kb NR located on chromosome 1, locus 1q23 was first identified in 1994 following cDNA screening of the conserved NR DBD using degenerate oligonucleotides (157). In the absence of a ligand, the NR can be constitutively active, bound as a heterodimer to RXR at DR5 HREs, as well as RARs and CYP2B, although it is largely sequestered inactive in the cytoplasm (158). Forman *et al.*, 1998, identified the first CAR ligands, androstenol and androstanol but rather than activating the NR, the compounds suppress the basal activity of CAR *in vitro*. However, the androstane metabolite binding still results in the dissociation of co-activators therefore, they are classed as inverse agonists rather than antagonists (159).

Activation of CAR was fully characterised using knock-out mice (107). CAR binding motifs within the proximal HRE consists of 2 DR hexamers separated by 4 amino acids (DR4), with complimentary DR4 binding motifs able to bind CAR (160). Phenobarbital (PB) was shown to reverse the suppression of the androstane metabolites on the proximal promoter region of CYP2B6 (161). Recently, activation of CAR by PB has been studied in greater detail. Shizu *et al.,* 2012, found PB mediates the down regulation of micro-RNA-122 (miR-122) (an intergenic miRNA, regulated through its own promoter) early in the activation-signaling cascade of CAR. The reduction in miR-122 results in 5'-adenosine monophosphate-activated protein kinase (AMPK) dependent activation of CAR, suggesting miRNA changes may be

connected to DDIs but further work is required to understand the relationship between miR-122 and AMPK (162).

X-ray crystallography shows CAR has a smaller ligand binding pocket compared to PXR, as well as a unique structural conformation change upon ligand binding (163). Ligand activation of CAR is also species specific; 1,4-bis[2-(3,5-dichloropyridyloxy)]benzene (TCPOBOP) is highly inducible of mouse CAR (mCAR) but not human CAR (hCAR), whilst 6-(4-chlorophenyl)imidazole[2,1-b]thiazole-5-carbaldehyde-O-(3,4-dichlorobenzyl)oxime (CITCO) is a potent agonist of hCAR but not mCAR (164). Despite possessing a relatively small ligand binding pocket, CAR mediates the transcription of a broad array of xenobiotic metabolism and transporter genes (133), sharing many target genes with PXR. Cross-talk of overlapping HRE binding suggests CAR and PXR coordinately regulate gene expression. Nonetheless, the NRs are activated by ligands in 2 distinct ways. PXR is exclusively dependent on ligand binding whereas CAR can be activated indirectly or by direct ligand binding (133). CAR is sequestered in the cytoplasm *in vivo* prior to ligand activation and subsequent translocation to the nucleus. However, in immortalised cell lines, CAR spontaneously accumulates in the nucleus (165). Ligand independent activation of CAR poses as a major obstacle for investigating drug activation *in vitro* but distinguishes it from other NRs.

1.4.3.4 Regulation of drug metabolism and transport by CAR

Transfection of CAR into HepG2 cells results in an increase of CYP3A4 mRNA implying crosstalk between CAR and PXR is a key factor to be considered (132). Phenobarbital (PB) is highly documented as an inducer of the CYP2B family but until

recently the mechanism of action was subject to debate. Of particular prominence is CYP2B6 as it metabolises approximately 25% of drugs (Figure 1.7). With the aid of CAR knock-out mice, induction of Cyp2b10 was absent when treated with PB (107). More so, it has been found that CAR HREs are present on the promoter region of CYP2B6 similar to mouse Cyp2b10 (107). During *in vitro* screening of CYP2B6 and CAR mRNA expression in 12 hepatocyte donors, Chang *et al* found a 278 fold and 240 fold increase in CYP2B6 and CAR mRNA expression, respectively, when treated with PB (166). In addition to CYP2B genes, aryl hydrocarbon (AhR) knockout mice have been used to dissect the activation mechanisms of CYP1A1 and CYP1A2. Located on the cis-ER8 element of both enzymes, this HRE is a CAR binding site, indicating their expression is regulated through this NR (167).

The CYP3A4 and CYP2B6 substrates carbamazepine and phenytoin (antiepileptics), are also CAR ligands (99). Activation of CAR by 100 μM phenytoin has been shown to increase CYP3A4 mRNA levels in human hepatocyte donors by 707%, as well as significant upregulation of CYP2C9, drastically reducing its efficacy through autoinduction. In addition, the systemic concentration of carbamazepine is significantly reduced due to an increase in the metabolism of the drug by CYP3A4 and CYP2C9, which are regulated through CAR (168).

In addition to CYPs, drug transporters have been identified as targets for CAR, although most are shared with PXR including, ABCB1, ABCC2, OATP1B1 and OATP1B3 (62, 169, 170). In contrast to PXR, contradictory data is reported for transcriptional regulation of drug transporters by CAR. Some groups report ABCC3 as a target for CAR (171) whereas others found no mRNA correlation (172).

Accordingly, it is crucial that data attained from target gene identification assays are accurately interpreted, given over 50% of genes induced by PB are not regulated through CAR (173). Other regulatory targets of CAR include, sulfotransferases (174), UGTs (175) and glutathione-s-transferases (176). Recent studies suggest although CAR plays a key role in induction, it is capable of repressing activation or suppressing transcriptional induction (111).

1.4.4 Indirect DDIs mediated through generation of toxic metabolites

In addition to DDIs affecting plasma exposure of the victim drug, PXR and CAR activation can result in an increase in drug metabolism leading to toxicity through overproduction of toxic metabolites. Paracetamol, an analgesic, is primarily metabolised in the liver into metabolically inactive sulfate and glucuronide metabolites (145). However, paracetamol is also metabolised by CYP2E1 into N-acetyl-p-benzo-quinone imine (NAPQI), a toxic metabolite. Induction of CYP2E1, CYP3A11 or CYP1A2 increases the production of NAPQI, resulting in an increased incidence of hepatotoxicity. Androstanol administration following paracetamol has been shown to inhibit CAR activity and reduce paracetamol hepatotoxicity in mice (177). It is conceivable that research and development into PXR and CAR antagonists may provide useful mechanisms to prevent DDIs (178). Studies have shown antagonists target their binding to the AF-2 domain of the C-terminal, altering the NR tertiary structure, hindering the binding/release of co-activators/co-repressors (136). Known PXR and CAR antagonists include ketoconazole (46), coumestrol (179), androstanol (180) and androstanol (178).

1.4.5 Cross-talk of HNF4α with *PXR and CAR in regulation of metabolism and transport*

Recently, HNF4α has been identified as a key determinant in CAR and PXR mediated expression of CYP3A4 (69). In the absence of HNF4α, induction of CYP3A4 is absent or significantly repressed, which is correlated to the lack of HNF4α binding on the CAR and PXR upstream HREs in the CYP3A4 enhancer region, indicating it is a fundamental mediator of CAR and PXR action (132). It has also been reported HNF4α null mice express significantly less mRNA of OATP1B1, OATP2B1 and ABCC2. However, PXR is positively upregulated in the null mice, demonstrating adaptive activation through NR cross-talk (181).

1.4.6 NR co-regulators

As described earlier, NRs are crucial for gene regulation but they lack the properties required for chromatin re-structuring or direct interaction with the polymerase. Transcriptional modulation involves a complex process of ligand binding, binding of the NR to target HREs, co-regulator recruitment, binding of the RNA polymerase II holocomplex (Pol II), chromatin condensation and activation of gene transcription (182). To directly mediate induction, NR co-regulators are recruited upon ligand binding (183) and a substantial number of co-regulator complexes are required for gene transcription. Functioning as mediators these complexes are capable of interpreting xenobiotic activation. Central to the discussion here, co-regulators are classified as, chaperones, co-chaperones, co-activators and co-repressors (184). Expression of proteins is dependent upon the interaction of Pol II (a constitutive group of 30 general transcription factors) with human DNA (185), in addition to non-constitutive co-regulator complexes that interact directly with the NRs (182). Further

to solely ‘bridging’ complexes, co-regulators possess many functions and contribute to transcriptional elongation, mRNA trafficking and RNA splicing (186). Currently, over 300 co-regulators have been reported, the majority of which are not restricted in their selectivity between NRs. Table 1.4 includes a literature based search of PXR and CAR co-regulators that have been shown to contribute to drug disposition and NR interactions.

1.4.6.1 NR chaperones and co-chaperones

Chaperones and their associated co-chaperones are proteins that assist in the non-covalent folding and assembly of nuclear receptor complexes in the cytosol. The general mechanism is initiated through the exposure of NR hydrophobic residues, which heat shock protein 70 (Hsp70) binds to. As the NR begins to fold, heat shock protein 90 (Hsp90) binds allowing completion of the folding and priming the LBD in a hormone binding state (187). The LBD is unstable in the absence of a ligand thus it cycles through an ATP-dependent chaperone complex reaction preparing the LBD for activation. Co-chaperones such as, stress induced phosphoprotein 1 (STIP1) and cytoplasmic CAR retention protein (CCRP) are involved in this ATP-dependent reaction by controlling the ATPase activity of chaperones, or by contributing directly to the NR folding. CCRP is over expressed in HepG2 cells stabilising CAR in the cytosol thus, upon TCPOBOP treatment, nuclear translocation is significantly enhanced (188). Ligand binding and NR heterodimerisation requires translocation to the nucleus which is aided by this chaperone/co-chaperone complex.

1.4.6.2 NR co-activators and co-repressors

Co-activators are described as proteins that are recruited through direct signals from NRs (sometimes when bound or unbound to ligands) to activate/enhance gene transcription (189). Although all co-activators contribute to gene expression, they can be split into 2 groups: primary co-activators interact directly with NRs whereas secondary co-activators do not bind to the receptor, rather they are members of a subunit complex (182). Some co-activators possess intrinsic histone acetylase (HAT) and methyltransferase activity, or, alternatively act as docking sites for such enzymes implicating them in chromatin relaxation (61). They are capable of modifying histone tails, protein kinases, SUMO ligases, ubiquitin and protein phosphatases (190).

Co-repressors bind to NRs that are inactive either through the absence of a ligand (e.g. nuclear receptor co-repressor 1; NCOR1) or in the presence of an antagonist or inverse agonist (e.g. ligand dependent co-repressor 1; LCOR, nuclear receptor interacting protein 1; RIP140) (184). In contrast to co-activators, co-repressors can recruit histone deacetylase enzymes (HDACs) to condense chromatin and repress gene expression. Co-activators and co-repressors play an integral role in the gene transcription pathway (191).

1.4.6.3 Activation mechanisms involving co-regulator proteins

Co-regulators are involved in coordinating the regulation of xenobiotic metabolism and transport, cell growth, differentiation and metabolic processes (186). Intensity of activation is influenced by PTMs including methylation, phosphorylation or acetylation (192). One important co-regulator is the nuclear receptor co-activator 1 (NCOA1). NCOA1 is a member of the p160 superfamily of co-activators that bind to

NR leucine repeats in the AF-2 region co-activator binding cleft that is produced upon ligand binding (192). CAR and PXR recruit other members of the p160 family including nuclear receptor co-activator 2 (NCOA2) and nuclear receptor co-activator 3 (NCOA3) (193). Binding of these co-activators recruits HAT and 3'-5'-cyclic adenosine monophosphate (cAMP) to enhance gene transcription (194). In the liver NCOA1 is phosphorylated at serine/threonine residues by kinases, the potency of this phosphorylation then regulates NR activation (17).

Co-repressors are also regulated by phosphorylation, which determines their localisation within the cell. Stimulation of phosphorylation reactions, initiates the transfer of co-repressors such as NCOR1 and nuclear receptor co-repressor 2 (NCOR2) to the cytoplasm, inhibiting their ability to repress mRNA transcription (195). Hence, kinase signaling cascades, co-regulators and NRs work in concert to regulate gene transcription.

In humans, the majority of co-regulators are constitutively expressed and their basal mRNA expression is subject to dynamic stimuli (except peroxisome proliferator-activated receptor gamma co-activator 1 alpha (PGC1α)). However, this is not always true in transformed cell lines (90). Co-regulators add another layer of complexity to NR activation and can sometimes contribute to human disease. For example, co-activator-associated arginine methyltransferase 1 (CARM1) over expression inhibits tumour suppressor protein 53 (p53) and induces antiapoptotic genes resulting in uncontrolled cell proliferation and prostate cancer (196). A lack of PGC1α expression contributes to reduced mitochondrial function, and may result in diabetes, Huntington's disease or cholesterol cholelithiasis (197-199). Similarly, upregulation

of NCOR1 is associated with embryonic mortality, CNS development defects and erythrocyte defects (200). Heat shock protein 90kDa (Hsp90) is correlated to expression levels of oncogenic proteins (201) and growth arrest DNA damage inducible 45 beta (Gadd45β) is linked with Alzheimer's disease and hepatic hypertrophy (202-204).

Gene	Description	Alias	Chromosomal location	Reference sequence	Regulatory activity/function	Gene ID
HSPA4	Heat shock 70kDa protein 4	Hsp70	5q31.1	NM_002154.3	Chaperone	3312
HSP90AA1	Heat shock protein 90α, cytosolic, class A, member 1	Hsp90	14q32.33	NM_005348.3	Chaperone	3320
PIH1D1	PIH1 domain containing 1	NOP17	19q13.33	NM_017916.2	Chaperone	55011
HSPA8	Heat shock 70kDa protein 8	HSC70, LAP1	11q24.1	NM_006597.4	Chaperone	3312
DNAJB1	DnaJ (Hsp40) homolog, subfamily B, member 1	Hsp40, HSPF1	19p13.2	NM_006145.1	Co-chaperone	3337
PTGES3	Prostaglandin E synthase 3 (cytosolic)	p23/TEBP	12q13.13	NM_006601.5	Co-chaperone	10728
REG3A	Regenerating islet-derived 3 alpha	Hip, PAP	2p12	NM_002580 .2	Co-chaperone	5068
DNAJC4	DnaJ (Hsp40) homolog, subfamily C, member 4	Hsp40	11q13	NM_005528.3	Co-chaperone	3338
VCP	Valosin-containing protein	p97	9p13.3	NM_007126.3	Co-chaperone	7415
CDC37	Cell division cycle 37	P50, CDC37	19p13.2	NM_007065.3	Co-chaperone	11140

Gene	Description	Alias	Chromosomal location	Reference sequence	Regulatory activity/function	Gene ID
PPID	Peptidylprolyl isomerase D	CYP-40	4q31.3	NM_005038.2	Co-chaperone	5481
STIP1	Stress-induced-phosphoprotein 1	HOP, P60	11q13	NM_006819.2	Co-chaperone	10963
PPP5C	Protein phosphatase 5, catalytic subunit	PP5	19q13.3	NM_006247.3	Co-chaperone	5536
DNAJA1	DnaJ (Hsp40) homolog, subfamily A, member 1	HSDJ, DJ-2	9p13.3	NM_001539.2	Co-chaperone	3301
DNAJC7	DnaJ (Hsp40) homolog, subfamily C, member 7	TPR2, DJC7	17q11.2	NM_003315.3	Co-chaperone	7266
FKBP4	FK506 binding protein 4, 59kDa	FKBP52, Hsp56	12q13.33	NM_002014.3	Co-chaperone	2288
FKBP5	FK506 binding protein 5	FKBP51, P54	6p21.31	NM_004117.3	Co-chaperone	2289
STUB1	STIP1 homology and U-box containing protein 1	CHIP, UBOX1	16p13.3	NM_005861.2	Co-chaperone	10273
NCOR1	Nuclear receptor co-repressor 1	N-CoR, TRAC1	17p11.2	NM_006311.3	Co-repressor	9611
Sin3A	SIN3 transcriptional regulator homolog A	SIN3 homolog A	15q24.2	NM_015477.2	Co-repressor	25942

Gene	Description	Alias	Chromosomal location	Reference sequence	Regulatory activity/function	Gene ID
NRIP1	Nuclear receptor interacting protein 1	RIP140	21q11.2	NM_003489.3	Co-repressor	8204
HDAC1	Histone deacteylase 1	HD1, RPD3	1p34	NM_004964.2	Co-repressor	3065
HDAC2	Histone deacteylase 2	HD2, YAF1	6q21	NM_001527.3	Co-repressor	3066
NR0B2	Nuclear receptor subfamily 0, group B, member 2	SHP, SHP1, DAX1	1p36.1	NM_021969.2	Co-repressor	8431
SREBF1	Sterol regulatory element binding transcription factor 1	SREBP1	17p11.2	NM_004176.4	Co-repressor	6720
NCOR2	Nuclear receptor co-repressor 2	SMRT, N-CoR2	12q24	NM_006312.5	Co-repressor	9612
LCOR	Ligand dependent nuclear receptor corepressor	MLR2	10q24	NM_032440.3	Co-repressor	84458
CARD16	Caspase recruitment domain family, member 16	COP, COP1	11q23	NM_052889.2	Co-repressor	114769
TMTC3	Transmembrane and tetratricopeptide repeat containing 3	SMILE	12q21.32	NM_181783.3	Co-repressor	160418
NRBF2	Nuclear receptor binding factor 2	COPR1	10q22.1	NM_030759.3	Co-activator	29982

Gene	Description	Alias	Chromosomal location	Reference sequence	Regulatory activity/function	Gene ID
MED1	Mediator complex subunit 1	TRAP220, TRIP2	17q12	NM_004774.3	Co-activator	5469
PSMC5	Proteasome (prosome, macropain) 26S subunit, ATPase, 5	SUG1, p45	17q23.3	NM_002805.5	Co-activator	5705
CARM-1	Coactivator-associated arginine methyltransferase 1	PRMT4	19p13.2	NM_199141.1	Co-activator	10498
Gadd45β	Growth arrest and DNA-damage-inducible, beta	GADD45BETA	19p13.3	NM_015675.3	Co-activator	4616
SMC1A	Structural maintenance of chromosomes 1A	CDLS2, SMC1	Xp11.22-p11.21	NM_006306.2	Co-activator	8243
CITED1	Cbp/p300-interacting transactivator, with Glu/Asp-rich carboxy-terminal domain, 1	MSG1	Xq13.1	NM_004143.3	Co-activator	12705
NCOA3	Nuclear receptor coactivator 3	AIB1, ACTR	20q12	NM_006534.3	Co-activator	8202
KAT2B	K(lysine) acetyltransferase 2B	CAF, P/CAF	3p24	NM_003884.4	Co-activator	8850
NCOA6	Nuclear receptor coactivator 6	ASC2, PRIP	20q11	NM_014071.3	Co-activator	23054
NCOA1	Nuclear receptor coactivator 1	RIP160, SRC1	2p23	NM_147223.2	Co-activator	8648

Gene	Description	Alias	Chromosomal location	Reference sequence	Regulatory activity/function	Gene ID
NCOA2	Nuclear receptor coactivator 2	GRIP1, SRC2	8q13.3	NM_006540.2	Co-activator	10499
PGC1α	Peroxisome proliferator-activated receptor gamma co-activator 1	PGC1, PPARGC1	4p15.1	NM_013261.3	Co-activator	10891
CREBBP	CREB binding protein	CBP/KAT3A	16p13.3	NM_004380.2	Co-activator	1387

Table 1.5 Selected co-regulators associated with PXR and CAR function

1.4.6.4 NR co-regulators and CYP regulation

Although many interactions can occur with the co-regulators included in Table 1.5, the following section details examples of their interactions with PXR and CAR in the regulation of CYP3A4. Key chaperones Hsp90 and co-chaperones cytoplasmic CAR retention protein (CCRP), FK506 binding protein 4 (FKBP4) and 5 (FKBP5) expression levels are linked to CAR and PXR activation (205).

Studies have shown that induction of CYP3A4 by RIF requires the binding of PXR, PGC1α and NCOA1 following the dissociation of NCOR1 (206). Transfection of PGC1α and to a lesser extent NCOA1 is correlated to dose-dependent increases in CYP2C9, CYP1A1, CYP3A4, CYP3A5 and ABCB1 of which all are PXR and CAR target genes. Whilst the effect is increased upon RIF binding, these data also demonstrate that PGC1α and NCOA1 are required for CYP3A4 basal expression (207).

Sterol regulatory element binding protein (SREBP1) is a NR co-repressor of the basic helix-loop-helix family (208). The co-repressor is membrane bound to the endoplasmic reticulum with its amino acid carboxy-terminals protruding into the cytoplasm. SREBP1 binds to the promoter regions of lipogenic genes inducing fatty acid and triglyceride production (208). A decrease in lipid metabolism in the liver is correlated to a decrease in drug metabolism through SREBP1 binding to PXR and CAR, inhibiting co-activator recruitment and preventing CYP3A4 production (209). Although the majority of CAR is sequestered in the cytoplasm, it is also found in the nucleus where it interacts with members of the p160 co-activator family (137). Small heterodimer partner (SHP) and the nuclear receptor protein, dosage-sensitive sex

reversal adrenal hypoplasia congenital critical region on X chromosome, gene 1 (NR0B1) binds to CAR inhibiting transactivation through preventing binding of the p160 family (210). In addition, complete repression of the NR is achieved due to the presence of an intrinsic repression domain on the C terminal of SHP. The co-repressor recruits additional proteins to a complex achieving this effect (211). Small heterodimer partner interacting protein leucine zipper protein (SMILE) is a novel co-repressor of CAR (212). SMILE recruits HDACs, binds to the AF-2 domain and hinders the interaction of the NR with co-activators thus repressing transcription and decreasing drug clearance (212).

1.4.7 NRs, co-regulators and drug discovery

In depth analysis of NRs is now applied during the drug discovery and development process, which has aided understanding of the mechanisms that underpin DDIs. As described earlier, PXR is thought to be involved in over 60% of unwanted DDIs (132). The promiscuity and uniqueness of CAR and PXR have lead pharmaceutical companies to conduct NR induction assays before advancing into clinical trials. This increased interest has intensified the requirement for accurate *in vitro* and *in vivo* models to predict NR activation (111). Cell based reporter gene assays are ordinarily used *in vitro* to determine NR activation whereas expression of drug disposition genes is routinely analysed in primary human hepatocytes (99, 213).

Co-regulators are emerging as critical factors for NR function and have therefore attracted interest as targets for modifying drug response and disease. Current targets include Hsp90, the chaperones inhibitor geldanamycin effectively prevents hormone dimerisation and enhances protein degradation making it a potentially useful

compound to treat breast cancer (205). Additionally, inhibitors for co-activators such as NCOA1 are being investigated as treatment strategies in breast cancer (214) and microRNAs of the co-repressor SMRT allow modulation of the transcription factor nuclear factor-kappaB (NF-κB) and interleukin 8 during the inflammatory response against microbial infection of innate immune cells (215). Species specific gene activation of NRs prevents accurate induction analysis in rodents but humanised rodent models exhibit responses closer to that of a human and are an invaluable tool in NR induction interactions (61).

1.5 Pharmacogenetics in drug response

Pharmacogenetics is the study of how genetic variants may result in altered responses to xenobiotics (216). With the application of genomic technology and analysis, pharmacogenetics can also be applied during drug discovery to analyse the complete target genome (111). Of particular clinical interest are single nucleotide polymorphisms (SNPs) in drug disposition genes.

The interindividual variability observed in xenobiotic PK is in part a result of genetic polymorphisms in ADME genes (217). Drug plasma concentrations are a consequence of numerous processes regulated by several proteins rather than the direct and sole influence of SNPs. Subsequently, polymorphisms in multiple genes may contribute to variable PK and their consideration during drug discovery and development may be warranted. SNPs with particular relevance to this thesis are discussed below.

CYP3A4 polymorphisms have been identified and related to drug concentrations of immunosuppressants and alpha-blockers. Two haplotypes resulting from *CYP3A4* SNPs are *CYP3A4**1B, rs52740574 and *CYP3A4**22, rs35599367. *CYP3A4**1B is a relatively newly identified haplotype associated with an increase in enzyme mRNA expression which is correlated to a decrease in the C_{max} of silodosin (218), although conflicting data exist for this SNP (219, 220). In contrast, *CYP3A4**22 is a SNP on intron 6 and is associated with an increase in tacrolimus exposure regulated through the presence of the C allele resulting in a defective enzyme (221, 222).

Numerous sequence alterations and SNPs have been documented for the influx transporter *SLCO1B1*, many of which vary between populations (223). Two distinct SNPs in particular have been associated with the differences in xenobiotic pharmacokinetics. The 521T>C, rs4149056 and 388A>G, rs2306283 collectively define 4 haplotypes: *SLCO1B1**1A, *SLCO1B1**1B, *SLCO1B1**5 and *SLCO1B1**15. *SLCO1B1**5 and *SLCO1B1**15 contain the 521C allele and this SNP has a dominant effect, which is associated with a decreased activity (224). This decrease in transporter activity is correlated to a 144%, 221% and 110% increase in AUC of atorvastatin, simvastatin and pravastatin, respectively (225). Additionally, the C_{trough} of the CCR5 antagonist, maraviroc is reduced by 53% (226) and the C_{max} of the protease inhibitor, lopinavir is significantly increased (49).

Efflux transporters are also subject to SNPs that can alter their activity and/or expression. The most commonly studied SNP in *ABCB1* is 3435C>T, rs1045642 which is associated with transporter expression and increased concentrations of sirolimus (227); however, data for this SNP is not very reproducible (104, 228).

Homozygous individuals with the C allele express 2-fold more ABCB1 than individuals homozygous for the T allele (heterozygotes have intermediate expression levels). The SNP is a synonymous silent mutation in the gene sequence therefore the mechanism governing expression is unknown (104, 229, 230).

SNPs in the promoter, DBD and LBD have significant functional consequences for *PXR* (231, 232). Polymorphisms associated with a decrease in PXR gene expression resulting in a decrease of CYP3A4 activity are 698789A>G (G allele), rs763645 and 44477T>C (T allele), rs1523130 (233). In contrast, an increase in PXR expression is associated with the T allele of the SNP 63396C>T, rs2472677 which significantly reduces the C_{max} of CYP3A4 substrates (234).

Similar to *PXR*, nonsynonymous SNPs in *CAR* are rare but those localised to the LBD have been shown to alter ligand binding as well as dimerisation with RXR, co-activator binding and nuclear localisation of the receptor (233). A significant decrease in basal and induced CYP3A4 and CYP2B6 activation is associated with the *CAR* SNP located on exon 5, 246A>G (allele), rs2307424 (60, 109). The 246A>G SNP is associated with early discontinuation of efavirenz containing regimens due to toxicity (109). It has been reported this SNP influences the PK significantly of efavirenz in Chilean patients (235). In contrast, a polymorphism located on exon 7, 380T>C, rs437470 is associated with reduced constitutive CAR activity but response to CITCO is not affected (60, 232).

1.6 Organotypic liver models

Regulatory and safety pressures to understand and accurately predict human response upon compound exposure are becoming increasingly more evident. As described in more detail below and in Chapter 2, *in vitro* strategies are currently applied to predict PK parameters, dose and DDIs. However, it is clear there is an urgency to improve current model systems.

Although the majority of drugs are biotransformed and eliminated by the liver (236), the organ contains numerous cells that work in concert to perform a range of tasks, for example, protein and fat metabolism, secretion of bile products and localised immune responses (236). Table 1.6 details representative cell types of the liver, their overlapping roles and the effect they have on CYP gene expression.

Cell	Type	Form	Function	Gene Expression
Hepatocyte	Paraenchymal	Highly differentiated epithelial cells, Comprise cell plates of the liver lobule	Xenobiotic biotransformation (Phase I and II enzymes) and elimination, Fat, steroid and protein metabolism, Sugar and vitamin storage, Size and polyploid number increases from zone 1 to zone 3, Efficient influx or efflux transport	Dependent upon growth factors, hormones and extracellular matrix
Liver sinusoidal endothelial cell	Non-parenchymal	Elongated cell possessing high number of pinocytotic vesicles	Maintain hepatic homeostasis, Function as antigen presenting cells, Improve passive diffusion contribute to hepatocyte exposure of soluble components, Xenobiotic biotransformation (Phase I and II enzymes) and elimination	Dependent upon growth factors, hormones and extracellular matrix
Hepatic stellate cell	Non-parenchymal	Reside in the space of Disse, Extensive dendrite-like extensions that wrap around the sinusoids	Involved in regulating liver injury, Store vitamin A, Produce a network of fibrillar collagens, elastin and heparan sulfate proteoglycans, Produce cytokines and growth factors for intracellular communications	Influence their own gene expression through production of growth factors and cytokines

Cell	Type	Form	Function	Gene Expression
Kupffer cell	Non-parenchymal	Mesenchymal origins, Localised within the sinusoidal on the luminal side of endothelial cells, Long cytoplamsic extensions	Resident macrophages in the liver, endocytic/phagocytic ability, Induced in liver injury, In constant contact with gut-derived material that are eliminated from the blood, Modulate the turn-over and metabolic ability of hepatocytes, Large and more active in zone 1, Zone 3 are more active in cytokine production	Influence gene expression of Phase I and II enzymes and transporters in hepatocytes through production of growth factors and cytokines
Cholangiocyte	Non-parenchymal	Form the cuboidal epithelium in the small interlobular bile ducts	Regulated localised hepatic immune response through secretion of cytokines, Interact directly with immune cells through adhesion molecules, Involved in absorption of organic anions/cations, lipids and in the regulation of bile secretion, Regulation of GSH	Influence gene expression of Phase I and II enzymes and transporters in hepatocytes through production of growth factors and cytokines
Hepatic progenitor cell	Non-parenchymal	Reside in the compartment within the canals of Hering, Bi-potential stem cells	Activated upon hepatic epithelial cell damage (>50%), Migrate from zone 1 to zone 3 to form mature hepatocytes of cholangiocytes, Support stem cell populations of all liver cells, Represent a target for drug induced toxicty that controls liver regeneration	Form new, mature hepatocytes that posses Phase I and phase II enzymes and transporters

Table 1.6. Representative cell types of the liver, their role and effect of gene expression (Adapted from LeCluyse *et al.*, *(237)*)

1.6.1 Current model systems

Although *in vitro* analysis cannot replicate the complexity of a human, the simplicity of using isolated hepatocytes allows analysis of specific components. Nevertheless, the accuracy of this model varies considerably depending on the isolation and culture conditions used (238, 239). A physiologically-relevant phenotype including cell differentiation, metabolism and transporter protein expression and tight regulation of cellular processes can be partially maintained in isolated human hepatocytes, if the environment closely resembles that of the liver (239). However, the artificial environment results in the formation of significantly different phenotypes. Groups standardising their culture preparations and medium observe variability in drug metabolism, suggesting the inconsistency *in vitro* is a reflection of the donor phenotype (56), which may complicate extrapolation but may provide an early evaluation of inter-individual variability.

1.6.1.1 Primary hepatocytes

Efficient secretion of key liver proteins (collagen, fibrinogen, laminin) can be achieved in mono-cell cultures of hepatocytes in suspension. Hepatocytes form spheroids that utilise the secreted proteins to encapsulate themselves. Cell viability is improved and *in vivo* cell-cell connections are established (240). The main disadvantage of this model is sub-optimal oxygen levels due to the uncontrollable size of the spheroid aggregates that are produced. Hence, current research is focusing on the generation of scaffolds that restrict spheroid aggregate size but maintain liver specific protein secretion (241).

Factors affecting the profile of 2-dimensional mono-cultured hepatocytes include:

- The quantity of fetal bovine serum (FBS) supplement (blood fraction containing low antibody content but high levels of growth factors). The serum is associated with an increase in hepatocyte surface attachment (242, 243) but a decrease in the formation of bile canaliculi (244).

- Increased hepatocyte plating density (~100%) maintains hepatic morphology and phenotype (increasing production of bile canaliculi) for ~1-2 days more, in contrast to cells plated at ~80% confluence (245).

- Specific individual donor genotypes can significantly alter the expression and/or activity of key drug disposition genes and hepatocyte architecture.

- Supplements including growth hormones and dexamethasone (DEX) maintain structure identity, integrity and gene expression of the hepatocyte. However, over use results in significant fibroblast growth and abnormal gene expression profiles (244).

- Whilst a matrigel/collagen matrix overlay increases the time in culture, hepatocytes take longer to produce a polygonal morphology and form cell-cell contacts (238). However, if a ‘sticky’ biomatrix is used, the hepatocyte spread across the culture plate is reduced and the cells are subject to extensive stress (238).

- The use of plastic culture dishes can result in a rapid reduction depletion of hepatocyte cell membrane polarity as well as variable cell attachments (237).

- A lack of relevant liver cell types in a mono-primary hepatocyte culture does not allow analysis of the concerted response upon xenobiotic exposure or accurate mechanisms to remove waste products making them more susceptible to toxicity (239).

- Culturing cells with a constant perfusion flow replicates the blood flow and oxygen levels in the liver (237).

1.6.1.2 Co-cultures

As described earlier, co-cultures enhance cell-cell communications through organised production of inter-cellular junctions (246, 247). Co-culture of hepatocytes with kupffer cells has been pivotal in understanding the *in vivo* effects of IL-2 on CYP3A4 metabolism (248). In addition, hepatocytes cultured with rat liver endothelial cells have allowed production of a robust assay to analyse the inflammatory cytokine production upon xenobiotic exposure (249). Nonetheless, co-cultures are still hindered by the lack of CYP expression, which is thought to be due to the absence of a hemodynamic environment (249).

1.6.1.3 HepaRG cells

Similar to HepG2 and Huh7 cells (described in more detail throughout Chapter 2), HepaRG cells are derived from hepatocellular carcinoma (249). In comparison to routinely used HepG2 and Huh7 cell lines, HepaRG cells are superior due to their ability to differentiate into hepatocyte-like cells. Grown to confluence, the mono-culture produces two equally representative cell types; a flat cholangiocyte cell and a rounded hepatocyte-like cell. However, to achieve the required morphology, phenotype and gene expression profile, HepaRG cells must be treated with 1% DMSO (249). Functional phase I and II metabolism enzyme activity is restored along with NR pathways that regulate xenobiotic biotransformation (e.g. PXR, CAR, AhR) (250, 251). To date, HepaRG cells are the most representative cell line of the human liver. However, their main limitation for toxicity and xenobiotic analysis is the high concentration of DMSO required in culture. Whilst gene expression profiles are restored, the level of expression is significantly greater than those observed *in vivo*, hence response to prototypical inducers such as RIF is misrepresented (237).

1.6.1.4 Stem cells

Numerous cell types, cell-cell communications, gene expression profiles and a constant hemodynamic environment are all examples of significant obstacles when producing a characteristic organotypic liver model. Despite ethical concerns, stem cells represent a promising alternative as a renewable cell source. For the purpose of the work herein, stem cells are discussed in two classes; adult stem cells and pluripotent stem cells. Pluripotent stem cells are capable of constant replication and differentiation to form all three layers of the liver (ectoderm, mesoderm, endoderm). To date, there are many established methods for the controlled differentiation of pluripotent stem cells into hepatocytes (115, 252, 253) but gene expression profiles closely relate those of fetal levels rather than adults. Similarly, adult stem cells self-renew and are capable of differentiating into all liver cell types (described in Table 1.6). Specific to the liver, hepatic progenitor cells (resident liver stem cells) are crucial in liver re-generation, which is initiated upon exposure to specific growth factors (254). Importantly, the main advantages of adult stem cells are availability and potential to generate donor panels for analysis of inter-individual variability and polymorphisms (237).

1.6.2 Advanced technologies

In addition to the models described above, throughout the last decade technological advances have enabled more complex liver models to be engineered, although the majority remain in optimisation. Examples of manufactured novel devices include:

- Microfluidic perfusion array; the 96-well automated format system has a continuous perfusion across the plates that replicates liver blood flow. The hepatocytes are maintained in 3-dimensional (3-D) aggregates optimizing gas and nutrient transport

across the porous barrier. With the co-culture of numerous cell types, cell-cell contacts are maintained, replicating gene expression and liver protein profiles, induction/inhibition responses and cell viability for 3-4weeks (255).

- Bioengineered micropatterned liver platform; hepatocytes are co-cultured with stromal cells to support the formation of hepatocyte colonies within a miniaturised multiwell system. Cells remain viable in culture for up to six weeks with accurate *in vivo* morphologies, functional bile canaliculi, phase I and II metabolism enzymes and transport functions (256).

- Biochip dynamic flow system; living cells are inserted into microfluidic compartments that are connected by a circulating blood partition to simulate the effect *in vivo*. Co-culture of hepatocytes with non-parenchymal cells correlates significantly with the responses observed *in vivo* (257).

- 3-D liver tissue culture scaffold; this multi-well plated model accommodates mono or co-cultures in addition to static or flow conditions. The cells remain differentiation for numerous weeks allowing the model to be characterised for use in induction assays and inflammatory responses (258).

- 3-D scaffolds with dynamic flow; Silicon pores are utilised as scaffolds for 3-D co-culture aggregates to form and ensure oxygen flow. Thus, histotypic morphology and cell organisation are optimised. The platform of the model is scalable to *in vivo* and replicates the different zones within the liver. Living cells used in the model retain gene expression profiles of transcription factors, CYPs, transporters and NRs for several weeks (259).

Immortalised hepatic cells are discussed further in Chapter 2 but an advantage of hepatoma cells is their suitability as an alternative cell source during optimisation of

dynamic flow organotypic mechanical devices due to their low cost and availability (236).

1.7 Thesis aims

The primary aim of this thesis was to investigate and understand the differences and similarities in the expression profiles of drug disposition genes, between transformed hepatic cell lines and primary human hepatocytes. Primary human hepatocytes were also analysed to determine uptake contribution, induction and genotype of key drug disposition-relevant genes. This was achieved as follows:

1. Comparison of the gene expression profiles of key drug transporters and metabolising enzymes between hepatoma cell lines and primary human hepatocytes. PXR and CAR co-regulators were identified and gene expression compared between the two cell types. Selected co-regulators were then chosen to determine any correlation with CYP3A4 expression and activity.

2. Upon identification of Gadd45β and PGC1α correlation with CYP3A4, genetic manipulation was applied to determine if a more physiologically relevant phenotype could be achieved. The two co-activators were transiently transfected into HepG2 cells using Lipofectamine2000. Western blotting, HPLC and Taqman analyses were completed to determine protein expression, CYP3A4 activity and mRNA expression, respectively. Off-target effects were determined by microfluidic analysis.

3. Optimisation and application of a robust *in vitro* assay using AtuFect01 and specific oligomers to selectively inhibit OATP1B1 in primary human hepatocytes was developed to determine the role of OATP1B1 in the hepatic uptake of xenobiotics. OATP1B1 inhibition was analysed at the mRNA and activity level using Taqman expression assays and [^{3}H] estrone 3 sulfate uptake, respectively. Atorvastatin was used to selectively inhibit the drug transporter and off-target effects were determined using microfluidic analysis.

4. The impact of the prototypical inducer rifampicin, as well as, rifabutin and rifapentine on the mRNA expression of CYP3A4, ABCB1, ABCC1, ABCC2, OATP1B1 and OATP1B3 mRNA was determined. Primary human hepatocyte donors (6) were treated with 0, 0.5, 5 and 10 μM of drug for 24 hours and gene expression analysis used to analyse the effects on the drug disposition genes.

5. The effect of VDR gene expression and *VDR* SNPs were analysed to determine if the NR contributed to differences in PXR, CYP3A4, ABCB1 or OATP1B1 mRNA expression in D2 intestinal biopsies. Gene expression and genotype analysis (of 5 *VDR* SNPs) were completed on 84 human intestinal samples and linear regression used to determine any correlations.

CHAPTER 2

A comparison of key drug disposition gene expression including NRs and their co-regulators in primary human hepatocytes and hepatoma cell lines

2.1 Introduction

Initial predictions of drug response and drug-drug interactions are made following high-throughput *in vitro* screening. Such assays are indispensible in the pharmaceutical industry to determine the mechanism and safety of new chemical entities (NCEs). However, they often fail when extrapolated to predict *in vivo* response due to unsuitable pharmacokinetic or poor pharmacodynamic prediction (260).

As described in Chapter 1 (Section 1.2 and 1.3) cytochrome P450 3A4 (CYP3A4), ATP binding cassette transporters (ABC), organic anion transporting polypeptides (OATP) and nuclear receptors (NR) contribute to the detoxification of xenobiotics and endogenous compounds (53, 102, 261). The transcription of CYPs and transporters is regulated through PXR, CAR and their co-regulators (111). Previous reports have shown extensive correlations between NR expression and CYP activity (67, 111, 123, 137, 139, 261) but to date there is no comprehensive and simultaneous analysis on the expression of NR co-regulators and CYP3A4 in multiple hepatic models.

Variable drug response between individuals is common (due to genotype, drug-drug interactions (DDIs), etc.), but advances in the laboratory investigating the complete metabolic profile and transport of a compound have improved *in vitro* predictions (244). Hence, *in vitro* analysis is vital, but limitations arise when predicting an *in vivo* response. In many cases, the models used are not representative of primary cells in intact organ systems and relying on over-expression systems does not completely avoid the problem. The majority of transfected systems do not generate

physiologically relevant expression levels of the protein of interest.

To date, the main *in vitro* approaches used to investigate drug metabolism are liver microsomes or whole cell systems. Liver microsomes (subcellular fractions) efficiently retain their CYP function years after extraction from liver tissue. However, they only possess the uridine-5'-disphosphate glucuronosyltransferases (UGTs) from the phase II class of metabolism enzymes (67). Drug incubations with microsomes are limited to 2 hours and involve the assessment of metabolism in the absence of intact cells, significantly restricting their use.

Metabolically active cell systems (primary human hepatocytes/transformed immortalised hepatic cell lines) are used as an alternative tool. Primary human hepatocytes are regarded as the 'gold standard' model of hepatic function and are therefore used widely to simulate drug metabolism, toxicity and transport *in vitro* to quantitatively predict the effect *in vivo* (13, 53, 244, 262). For example, hepatocyte studies of aceclofenac, an anti-inflammatory, directly match the metabolic profile observed *in vivo* (86, 244). In addition, current regulatory guidelines require all NCEs to be analysed in at least three human hepatocyte donors (46).

Hepatoma cell lines, including Huh7 and HepG2 have the advantage of low cost, commercial availability and extensive use in *in vitro* investigations of hepatotoxicity (263), gene regulation in disease and drug response (264) and mechanisms of infection of certain pathogens (265). HepG2 and Huh7 cells were derived from hepatocellular carcinomas that were extracted from a 15-year old and 57-year old male, respectively. Studies have outlined fundamental differences in the gene

expression profile of hepatoma cell lines, compared to primary human hepatocytes. When grown to confluence, CYP3A4 activity is induced in Huh7 cells (105) but the same effect has not been observed for HepG2 cells. Olvasky *et al.*, 2010, found Huh7 and HepG2 cells were unable to express specific liver function genes to mimic the biological response of the cell upon xenobiotic treatment (266). In addition, it has been well documented that hepatoma cell lines are unable to exhibit CYP3A4 expression and activity that resemble primary human hepatocytes (101, 239, 267, 268). Consequently, recent studies have focussed on characterising the gene expression profiles of key drug transporters (261), NRs (105) and CYPs (105, 148, 269) between different cell lines. Previous investigations have shown there is a significantly lower basal expression of CAR, PXR and their co-activators (SRC-1, TIF-2, GRIP) in contrast to an increase in basal levels of co-repressors (NCOR1, SMRT) when compared to primary human hepatocytes (270). Another factor for consideration when extrapolating from hepatoma cells is fluctuations in gene expression across passage number and culture conditions (271).

The aim of this study was to understand the disparities in the gene expression profile of key drug disposition genes including CYP3A4, CYP2B6, ABCB1, ABCC1, ABCC2, SLCO1B1, SLCO1B3, SLCO1A2, SLCO3A1, NRs CAR and PXR and their co-regulators in hepatoma cells (HepG2 and Huh7 cells) versus primary human hepatocytes. From initial studies, two co-activators were selected using strict criteria to determine if their expression varied over passage number and was subsequently correlated to CYP3A4 activity in the HepG2 cell, to ultimately define the mechanisms in transcriptional regulation that underpin the levels of CYP3A4 activity.

2.2 Methods and Materials

2.2.1 Materials.

Vivid® CYP screening kit assays, primary human hepatocytes, Williams E media, optiMEM media, cryopreserved hepatocyte recovery medium (CHRM®), CHRM® supplements, Hanks balanced salt solution (HBSS) and Dulbecco's modified eagle medium (DMEM) were purchased from LifeTechnologies, Ltd (Paisley, Scotland). Fetal bovine serum (FBS) was purchased from BioSera Co, Ltd (East Sussex, UK). Taqman reagents and assays, reverse transcription products and real time-qPCR master mix were obtained from Applied Biosystems (Warrington, UK). HepG2 cells were purchased from American Tissue Culture Collection (ATCC, Ltd). Huh-7 cells were purchased from European Collection of Cell Cultures (ECCAC, HPA). 96-well plates pre-coated with collagen IV were purchased from BD Biosciences (Oxford, UK). All other reagents were of analytical grade and purchased from Sigma-Aldrich (Poole, UK).

2.2.2 Cell Line Maintenance

DMEM with the addition of 10% FBS (v/v) was used to maintain Huh7 and HepG2 cells. Cells were seeded in T175 flasks and placed in a humidified incubator (37 ^{o}C, 5% CO_2). Cells were sub-cultured when approximately 75-85% confluent (~3 days) using the standard trypsin and centrifugation method. Previous investigations have shown optimum gene expression occurs at passage (p) 10 (271). Hence as a control, cells were passaged until p10, used for analysis and then removed to waste. For comparative passage analysis, cells were passaged 21 times and analysis completed at passage 5, 10, 15 and 20.

2.2.3 Primary Hepatocytes

Cryopreserved human hepatocytes from 3 donors (Table 2.1) were thawed in a 37 ^{o}C water bath for approximately 2 min. Once thawed, 50 ml of pre-warmed CHRM® was added to the hepatocytes, centrifuged for 10 min at 100 x g and the supernatant fraction discarded. The hepatocytes were re-suspended in plating media prepared as Williams E media with phenol red (500 ml) supplemented with 1 µM dexamethasone, a 1% solution of penicillin-streptomycin, 4 µg/ml insulin, 5% FBS, 2 mM GlutaMAX™ and 15 mM HEPES (CHRM® supplement A).

Donor	Viability	Gender	Donor Demographics	
			Age/Race	Characteristics
Hu8089	91 %	Male	36year old, Caucasian	Alcohol abuse, smoking
Hu8085	97 %	Female	1 year old, Caucasian	No alcohol abuse, no smoking
Hu4244	89 %	Male	3 year old, Caucasian	No alcohol abuse, no smoking

Table 2.1 Human donor demographics of the cryopreserved hepatocytes used in the study

2.2.4 Cell viability

Cell viability and density of primary human hepatocytes were calculated using trypan blue exclusion. A 0.4% solution of trypan blue was prepared in buffered isotonic salt solution to pH 7.2. 100 µl of cell solution was added to 100 µl of trypan blue stock, loaded onto a haemocytometer and counted under a light microscope. A cell viability of > 80% was required for all experiments.

$$\text{Cell viability (\%)} = \frac{\text{Number of dead cells (blue)}}{\text{Number of total cells}} \times 100$$

Cell viability of Huh7 and HepG2 cells was calculated using a Countess™ automated cell counter (LifeTechnologies, UK). 10 µl of cell suspension was added to 10 µl of trypan blue and placed on a Countess™ slide. Using specific algorithms the Countess™ measured the approximate size, concentration and viability of the cells.

2.2.5 Plating and maintaining primary human hepatocytes

Cells were seeded in 96-well plates pre-coated with collagen at a density of 4.5 x 10^4 cells/well and incubated for 24 h at 37 ºC with 5% CO_2 and 95% humidity. Plating media was replaced with 100 µl William's E media supplemented with optiMEM media and a maintenance cocktail of 0.1 µM dexamethasone, a 0.5% solution of penicillin-streptomycin, 2 mM GlutaMAX™, 15 mM HEPES, 6.25 µg/ml human recombinant insulin, 6 µg/ml human transferrin, 6 µg/ml selenous acid, 1.25 µg/ml bovine serum albumin and 5.35 µg/ml linoleic acid (CHRM® supplement B) (LifeTechnologies, Ltd), 24 h prior to mRNA extraction (to allow formation of cell-cell contacts and bile canaliculi).

2.2.6 Extraction and Quantification of mRNA

Trizol reagent (1 ml) was added to 2-5 x 10^6 cells for lysis. The resulting sample was incubated for 5 min at 37 ^oC followed by centrifugation (12000 x g for 2 min at 2-8^oC). The supernatant fraction was then removed to a fresh eppendorf. Chloroform (200 µl/1ml Tri) was added and the eppendorf shaken vigorously. Incubation at 37 ^oC for 3 min followed. Samples were centrifuged at 12000 x g for 15 min at 2-8 ^oC. The upper aqueous phase was transferred to a fresh eppendorf, isopropanol was added (500 µl/1ml Tri) and the solution incubated at 37 ^oC for 10 min. Centrifugation at 12000 x g for 10 min at 2-8 ^oC followed and the supernatant was discarded. Ethanol (75%;

1ml/1ml Tri) was added to the pellet, the solution was vortexed and centrifuged at 7500 x g for 5 min at 2-8 ^{o}C. The supernatant fraction was removed and the pellet air-dried for 5-10 min. RNase free water (20 µl/1ml Tri) was used to re-dissolve the pellet, which was then incubated for 10 min at 58 ^{o}C. Samples were stored at -80^{o}C. Quantification of mRNA was achieved by spectrophotometry using a Nanodrop1000. The absorbance of UV light at 260 nm determined the concentration (ng/µl) and the 260:280 nm ratio was used to assess protein contamination (ratio >1.90 was required for all experiments).

2.2.7 Synthesis of cDNA from mRNA

Reverse transcription of mRNA to cDNA was completed using a Taqman® reverse transcription (RT) assay. RT mixtures were made to 50 µl volume with RNase free water. RT mixtures included; 10X Taqman® RT buffer (5 µl), $MgCl_2$ (5.49 mM), reverse transcriptase (1.75 µl), RNA (2 µg), dNTP (50 µM), random hexamers (2.5 µM) and RNase inhibitor (1 µM). A GeneAmp PCR 9700 (Applied Biosystems, UK) was used to run a thermal cycle of: 10 min at 25 ^{o}C, 30 min at 48 ^{o}C, 5 min at 95 ^{o}C and a hold phase at 4 ^{o}C. Concentrated cDNA was diluted with sigma water to produce a working stock of 20ng/µl.

2.2.8 Quantitative real time-PCR

A Chromo4™ real-time PCR (LifeTechnologies, UK) was used to determine the gene expression of selected genes. All samples were completed in triplicate for primary human hepatocytes, Huh7 and HepG2 cells. Real time-PCR solutions were prepared for each well as follows; 12.5 µl of 2X Taqman® Master Mix, 1.25 µl of 20X

Taqman® custom assay, 9.25µl sigma water and 2 µl of 20ng/µl of cDNA. Table 2.2 details the assays (Applied Biosystems) used for each gene with its ID.

PCR conditions were 15 min at 95 ^{o}C (to activate polymerase, denature cDNA and initiate PCR) followed by 50 cycles of 15 sec at 94 ^{o}C (denaturation) and 60 seconds at 60 ^{o}C (annealing/extension of the product). Fluorescence was collected at the end of each cycle.

No template controls and *no reverse transcriptase* controls were completed in duplicate to ensure no contamination, specific amplification and maximum amplification, respectively. For the custom array 4 housekeeping genes were analysed to determine the most constant expression throughout all samples (18s, GUSB, HPRT1, GAPDH). In all other experiments, GAPDH was used as a housekeeping gene (C(t) values were consistent in every sample). A geometric mean was calculated for the 4 housekeeping genes and the value used to normalise the expression data. For all other experiments, data were compared to GAPDH and normalised to the primary hepatocyte (or control) sample using the comparative threshold cycle (C(t)) method ($Ct=2^{\wedge-\Delta\Delta C(t)}$). To ensure only gene amplification was measured the C(t) was set to ignore any aberrant fluorescence such as that from primer-dimer formation.

Gene	Description	Alias	Chromosomal location	Reference sequence	Assay ID	Gene ID
CYP3A4	Cytochrome P450, family 3, subfamily A, polypeptide 4	CP33, CYP3A	7q21.1	NM_017460.5	Hs00604506_m1	1576
CYP2B6	Cytochrome P450, family 2, subfamily B, polypeptide 6	CPB6, CYP2B	19q13.2	NM_000767.4	Hs04183483_g1	1555
ABCB1	ATP-binding cassette, subfamily B (MDR/TAP), member 1	ABC20, P-GP	7q21.12	NM_000927.4	Hs00184500_m1	5243
ABCC1	ATP-binding cassette, subfamily C (CFTR/MRP), member 1	MRP, ABCC	16p13.1	NM_004996.3	Hs01561502_m1	4363
ABCC2	ATP-binding cassette, subfamily C (CFTR/MRP), member 2	ABC30, MRP2	10q24	NM_000392.3	Hs00166123_m1	1244
SLCO1A2	Solute carrier organic anion transporter family, member 1A2	OATP1A2, OATP-A	12p12	NM_134431.3	Hs00203184_m1	6579
SLCO1B1	Solute carrier organic anion transporter family, member 1B1	OATP1B1, OATP2	12p	NM_006446.4	Hs00272374_m1	10599
SLCO1B3	Solute carrier organic anion transporter family, member 1B3	OATP1B3, OATP8	12p12	NM_019844.3	Hs00251986_m1	28234
SLCO3A1	Solute carrier organic anion transporter family, member 3A1	OAPT3A1, OATPD	15q26	NM_013272.3	Hs00203184_m1	28232
HSPA4	Heat shock 70kDa protein 4	Hsp70	5q31.1	NM_002154.3	Hs00382884_m1	3312

Gene	Description	Alias	Chromosomal location	Reference sequence	Assay ID	Gene ID
HSP90AA1	Heat shock protein 90α, cytosolic, class A, member 1	Hsp90	14q32.33	NM_005348.3	Hs00743767_sH	3320
PIH1D1	PIH1 domain containing 1	NOP17	19q13.33	NM_017916.2	Hs00215579_m1	55011
DNAJB1	DnaJ (Hsp40) homolog, subfamily B, member 1	Hsp40, HSPF1	19p13.2	NM_006145.1	Hs00428680_m1	3337
HSPA8	Heat shock 70kDa protein 8	HSC70, LAP1	11q24.1	NM_006597.4	Hs00941880_m1	3312
PTGES3	Prostaglandin E synthase 3 (cytosolic)	p23/TEBP	12q13.13	NM_006601.5	Hs00832847_gH	10728
DNAJC4	DnaJ (Hsp40) homolog, subfamily C, member 4	Hsp40	11q13	NM_005528.3	Hs00268602_m1	3338
VCP	Valosin-containing protein	p97	9p13.3	NM_007126.3	Hs00997642_m1	7415
CDC37	Cell division cycle 37	P50, CDC37	19p13.2	NM_007065.3	Hs00606477_m1	11140
PPID	Peptidylprolyl isomerase D	CYP-40	4q31.3	NM_005038.2	Hs00234593_m1	5481
STIP1	Stress-induced-phosphoprotein 1	HOP, P60	11q13	NM_006819.2	Hs00428979_m1	10963

Gene	Description	Alias	Chromosomal location	Reference sequence	Assay ID	Gene ID
PPP5C	Protein phosphatase 5, catalytic subunit	PP5	19q13.3	NM_006247.3	Hs00196577_m1	5536
DNAJA1	DnaJ (Hsp40) homolog, subfamily A, member 1	HSDJ, DJ-2	9p13.3	NM_001539.2	Hs00266011_m1	3301
DNAJC7	DnaJ (Hsp40) homolog, subfamily C, member 7	TPR2, DJC7	17q11.2	NM_003315.3	Hs00268602_m1	7266
FKBP4	FK506 binding protein 4, 59kDa	FKBP52, Hsp56	12q13.33	NM_002014.3	Hs00427038_g1	2288
FKBP5	FK506 binding protein 5	FKBP51, P54	6p21.31	NM_004117.3	Hs01561006_m1	2289
STUB1	STIP1 homology and U-box containing protein 1	CHIP, UBOX1	16p13.3	NM_005861.2	Hs00195300_m1	10273
NCOR1	Nuclear receptor co-repressor 1	N-CoR, TRAC1	17p11.2	NM_006311.3	Hs01094540_m1	9611
Sin3A	SIN3 transcriptional regulator homolog A	SIN3 homolog A	15q24.2	NM_015477.2	Hs00292479_m1	25942
NRIP1	Nuclear receptor interacting protein 1	RIP140	21q11.2	NM_003489.3	Hs00942766_s1	8204
HDAC1	Histone deacteylase 1	HD1, RPD3	1p34	NM_004964.2	Hs00606262_g1	3065

Gene	Description	Alias	Chromosomal location	Reference sequence	Assay ID	Gene ID
HDAC2	Histone deacteylase 2	HD2, YAF1	6q21	NM_001527.3	Hs00231032_m1	3066
NR0B2	Nuclear receptor subfamily 0, group B, member 2	SHP, SHP1, DAX1	1p36.1	NM_021969.2	Hs00222677_m1	8431
SREBF1	Sterol regulatory element binding transcription factor 1	SREBP1	17p11.2	NM_004176.4	Hs00231674_m1	6720
NCOR2	Nuclear receptor co-repressor 2	SMRT, N-CoR2	12q24	NM_006312.5	Hs00196955_m1	9612
LCOR	Ligand dependent nuclear receptor corepressor	MLR2	10q24	NM_032440.3	Hs00287120_m1	84458
CARD16	Caspase recruitment domain family, member 16	COP, COP1	11q23	NM_052889.2	Hs00430993_m1	114769
TMTC3	Transmembrane and tetratricopeptide repeat containing 3	SMILE	12q21.32	NM_181783.3	Hs00699202_m1	160418
NRBF2	Nuclear receptor binding factor 2	COPR1	10q22.1	NM_030759.3	Hs00852466_g1	29982
MED1	Mediator complex subunit 1	TRAP220, TRIP2	17q12	NM_004774.3	Hs00191130_m1	5469
PSMC5	Proteasome (prosome, macropain) 26S subunit, ATPase, 5	SUG1, p45	17q23.3	NM_002805.5	Hs00267687_m1	5705

Gene	Description	Alias	Chromosomal location	Reference sequence	Assay ID	Gene ID
CARM-1	Coactivator-associated arginine methyltransferase 1	PRMT4	19p13.2	NM_199141.1	Hs00406354_m1	10498
Gadd45β	Growth arrest and DNA-damage-inducible, beta	GADD45BETA	19p13.3	NM_015675.3	Hs00169587_m1	4616
SMC1A	Structural maintenance of chromosomes 1A	CDLS2, SMC1	Xp11.22-p11.21	NM_006306.2	Hs00196849_m1	8243
CITED1	Cbp/p300-interacting transactivator, with Glu/Asp-rich carboxy-terminal domain, 1	MSG1	Xq13.1	NM_004143.3	Hs00366310_m1	12705
NCOA3	Nuclear receptor coactivator 3	AIB1, ACTR	20q12	NM_006534.3	Hs01105251_m1	8202
NCOA5	Nuclear receptor coactivator 3	CIA	20q12-q13.12	NM_020967.2	Hs00253115_m1	57727
NCOA6	Nuclear receptor coactivator 6	ASC2, PRIP	20q11	NM_014071.3	Hs00204160_m1	23054
NCOA1	Nuclear receptor coactivator 1	RIP160, SRC1	2p23	NM_147223.2	Hs00186661_m1	8648
NCOA2	Nuclear receptor coactivator 2	GRIP1, SRC2	8q13.3	NM_006540.2	Hs00197990_m1	10499
PGC1α	Peroxisome proliferator-activated receptor gamma co-activator 1	PGC1, PPARGC1	4p15.1	NM_013261.3	Hs01016724_m1	10891

Gene	Description	Alias	Chromosomal location	Reference sequence	Assay ID	Gene ID
CREBBP	CREB binding protein	CBP/KAT3A	16p13.3	NM_004380.2	Hs00231733_m1	1387
NR1I1	Nuclear receptor subfamily 1, group 1, member 1	VDR	12q13.11	NM_000376.2	Hs00172113_m1	7421
NR1I2	Nuclear receptor subfamily 1, group 1, member 2	PXR	3q12	NM_003889.3	Hs01114267_m1	8856
NR1I3	Nuclear receptor subfamily 1, group 1, member 3	CAR	1q23.3	NM_005122.4	Hs00901571	9970

Table 2.2 List of genes analysed using real-time PCR. Assay ID is the Applied Biosystems reference number and gene ID is the NCBI reference number. Dye - FAM: 6-carboxyfluorescein

2.2.9 Measurement of CYP3A4 enzyme activity

Cells (4.5 x 10^4/well) were seeded in a black 96-well plate and CYP3A4 activity assessed using a Vivid® CYP450 screening assay. The Vivid® substrate is metabolised specifically by the CYP3A4 enzyme into highly fluorescent products in aqueous solution. CYP450 baculosomes plus reagent (positive control), Vivid® regeneration system, Vivid® substrate and Vivid® NADP+ were placed at room temperature for 10 min until just thawed, mixed by inversion and then stored on ice until ready to use. Vivid® substrate was reconstituted in acetonitrile (2 mM stock solution, assay final concentration 3 μM). 2X Vivid® CYP450 reaction buffer was diluted in nanopure water (final concentration 100 mM). 40 μl of the 1X Vivid® CYP450 reaction buffer was dispensed into the selected wells in triplicate. A master pre-mix was prepared for the control wells by combining 1X Vivid® CYP450 reaction buffer (50.52 μl/well), Vivid® regeneration system (1.04 μl/well) and CYP450 baculosomes plus reagent (0.52 μl/well). Final P450 concentration was 5 nM. Two negative controls were included: one excluding the Vivid® regeneration system and one excluding the CYP450 baculosomes plus reagent (1X Vivid® CYP450 reaction buffer was used to ensure all volumes were equal). A master pre-mix was prepared for the test wells by combining 1X Vivid® CYP450 reaction buffer (51.04 μl/well) and Vivid® regeneration system (1.04 μl/well). 50 μl of master pre-mix was added to the selected wells and the plate incubated at 37 ^oC for 20 min. During this incubation a 10X Vivid® mix was prepared by combining 1X Vivid® CYP450 reaction buffer (9.22 μl/well), Vivid® substrate (0.16 μl/well) and Vivid® NADP+ (1.04μl/well). The reaction was initiated by adding 10 μl of the 10X Vivid® mix to the wells.

Fluorescent measurements were recorded every minute for 20 min at ambient temperature using a Tecan Magellan plate reader at 530 nm excitation, 605 nm emission and analysed using XFluor software.

Activity endpoint assay calculation:

CYP3A4 Activity (%) =

$$1 - \left(\frac{\text{Relative fluorescence of hepatic cell line}}{\text{Relative fluorescence of primary human hepatocytes}} \right) \times 100$$

2.2.10 Data Analysis.

All data presented for the Huh7 and HepG2 cells is the mean of three independent isolations completed in triplicate. The primary hepatocyte data for the CYP3A4 activity analysis and mRNA expression was mean of three donors completed in duplicate. Normality of all data was assessed using a Shapiro-Wilk test and for gene expression data statistical analysis conducted using paired t-test or Wilcoxon signed-rank test for normally or non-normally distributed data, respectively. For comparison of CYP3A4 activity and co-activator expression, statistical analysis was conducted using Spearman's or Pearson test for normally or non-normally distributed data, respectively. Statistical analyses were conducted using Stats Direct (Version 2.4.6 Stats Direct Ltd). Results were considered significant if; *, $p < 0.05$; **, $p < 0.01$; ***, $p < 0.001$.

2.3 Results

2.3.1 Relative gene expression of key drug transporters and metabolism enzymes

Previous work has shown differences in the expression of key drug transporters and metabolism enzymes between hepatic cells but significance varies between studies (261). Hence, initial work focused on assessing the gene expression of ABCC1, ABCC2, ABCB1, CYP3A4, CYP2B6, OATP1A2, OATP1B1, OATP1B3 and OATP3A1 in hepatoma cell lines (HepG2 and Huh7) compared to primary human hepatocytes. Figure 2.1, shows all of the genes analysed had a lower expression in hepatoma cells compared to primary human hepatocytes. In addition, excluding ABCB1 and CYP3A4, gene expression varied between HepG2 and Huh7 cells. As a whole, Figure 2.1 shows Huh7 cells express approximately 25% more of these genes than HepG2 cells and the majority of genes expressed in HepG2 cells were significantly less than the primary human hepatocytes. In agreement with the literature (105, 236, 270) CYP3A4 was expressed ~50% less in hepatoma cells compared to primary human hepatocytes ($p=0.02$). Expression of CYP2B6 was near absent in HepG2 cells compared to a 30% expression in Huh7 cells when compared to primary human hepatocytes.

The efflux transporters ABCC1 and ABCC2 were expressed significantly less (~65%) in HepG2 cells compared to primary human hepatocytes and ~40% and 10% less in Huh7 cells. In contrast, both cell lines expressed significantly less ABCB1 (80%, $p=0.005$) compared to primary human hepatocytes. The expression of OATP influx transporters varied considerably between cell types. In comparison to OATP1A2 and OATP1B1, OATP1B3 and OATP3A1 had greater expression in HepG2 cells although

this was also significantly lower than that observed in the primary human hepatocytes (42% (p=0.001) and 92%, respectively).

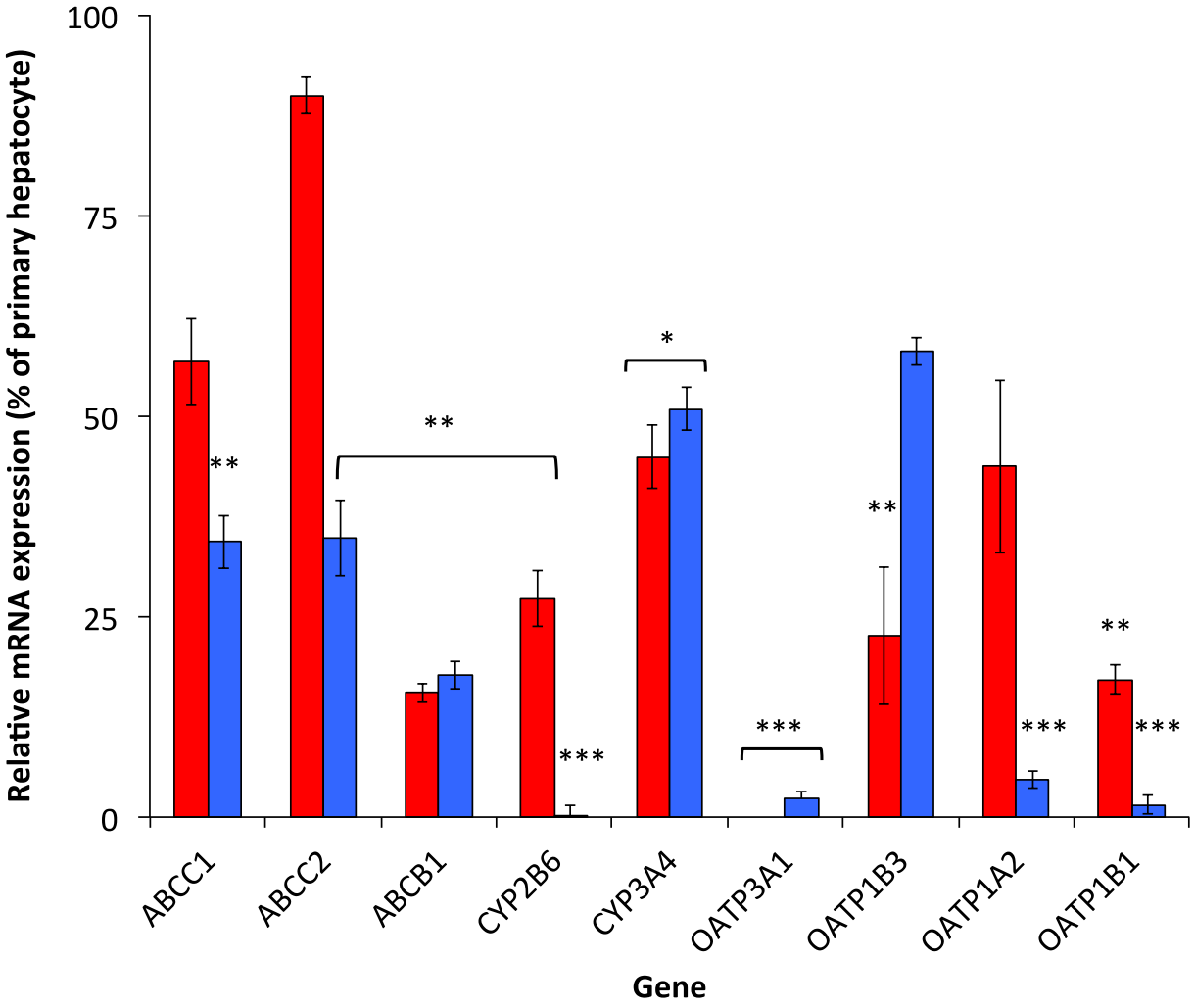

Figure 2.1 Relative gene expression of efflux / influx drug transporters and CYPs in Huh7 (♦) and HepG2 (♦) cells compared to primary human hepatocytes. Data are normalised to GAPDH house keeping gene and to a pool of 3 primary human hepatocyte donors using the comparative C(t) method ($C(t)=2^{\wedge -ddC(t)}$). Data are expressed as the mean of 3 independent isolations completed in duplicate ± standard deviation. $p<0.05$ *, $p<0.01$ **, $p<0.0001$ ***

2.3.2 PXR and CAR gene expression

The expression of the key drug disposition genes analysed in Figure 2.1 are tightly regulated by xenobiotic sensors PXR and CAR (133). The expression of PXR and CAR was analysed in HepG2 and Huh7 cells at passage 10 (Figure 2.2). CAR expression was undetectable in Huh7 cells ($p>0.0001$) whereas HepG2 cells expressed 20% of CAR ($p=0.004$) in comparison to primary human hepatocytes. The expression of PXR was consistent in both cell lines, but expression was ~80% less when compared to primary human hepatocytes ($p=0.007$ and $p=0.008$ for Huh7 and HepG2 cells, respectively).

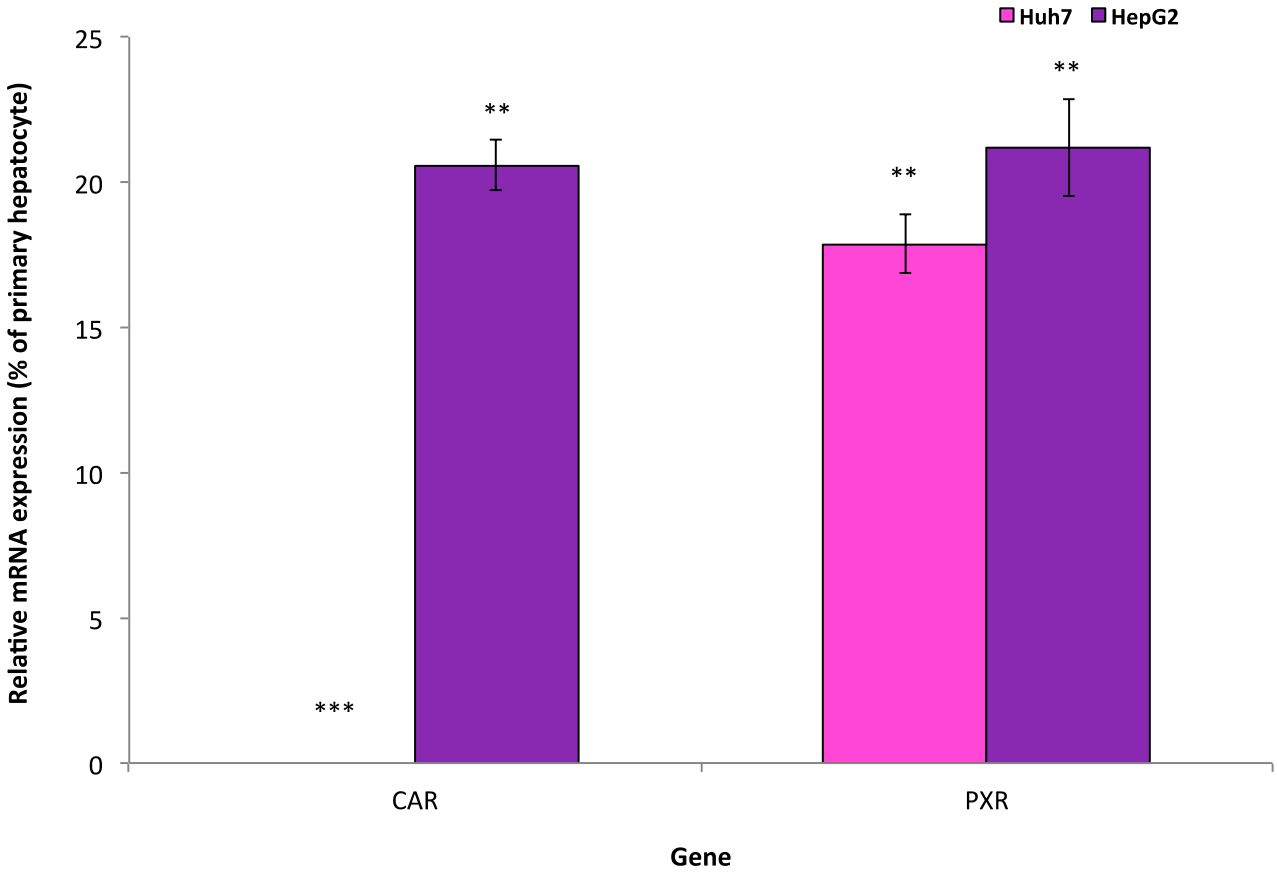

Figure 2.2 Relative gene expression of NRs CAR and PXR in Huh7 and HepG2 cells compared to primary human hepatocytes. Data were normalised to GAPDH house keeping gene and to a pool of 3 primary human hepatocyte donors using the comparative C(t) method ($C(t)=2^{\wedge -ddC(t)}$). Data are expressed as the mean of 3

independent isolations completed in duplicate ± standard deviation. $p<0.05$ *, $p<0.01$ **, $p<0.0001$ ***

2.3.3 CYP3A4 activity versus cell passage number

As shown in Figure 2.1, CYP3A4 gene expression was expressed ~50% less in HepG2 and Huh7 cells compared to primary human hepatocytes. The next step was to determine if the same effect was observed at the activity level and whether the activity of CYP3A4 varied as cell line passage number increased, comparing all data to primary human hepatocytes. A CYP3A4 Vivid® fluorescent assay was used to kinetically measure the activity of CYP3A4 in HepG2 cells (Figure 2.3). At passage 5, CYP3A4 activity was 78% of the primary human hepatocyte but as passage number increased, CYP3A4 activity decreased. At passage 10, CYP3A4 activity was 49% (Figure 2.3), paralleled to 53% mRNA expression (Figure 2.1) both compared to primary human hepatocytes. At passage 20, CYP3A4 activity was reduced to 26% ($p=0.0082$). Furthermore, at passage 25 activity decreased to 17% ($p=0.006$) of the primary human hepatocyte activity.

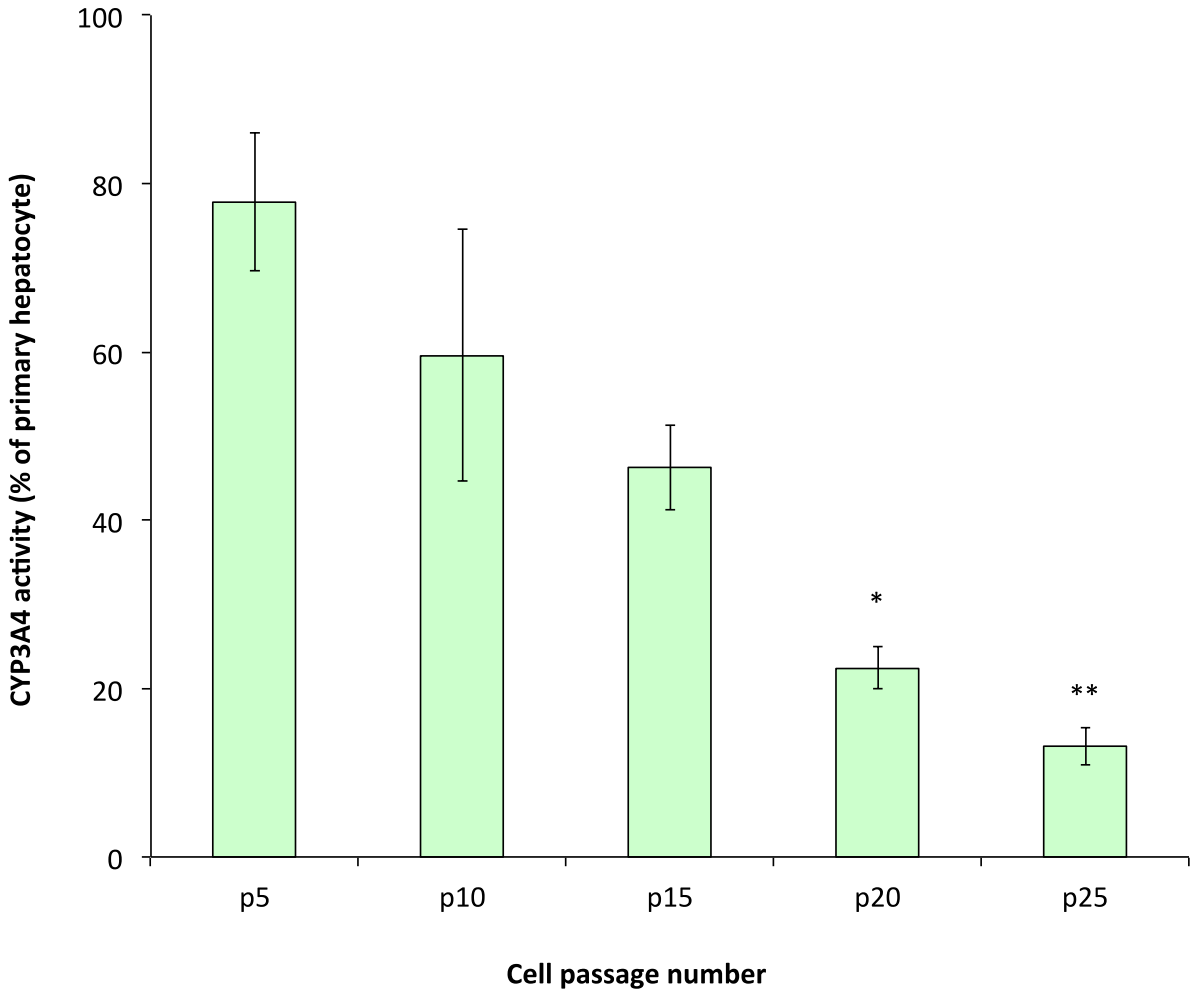

Figure 2.3 Relative activity of CYP3A4 in HepG2 cells compared to primary human hepatocytes. Data are compared to 3 primary human hepatocyte donors and expressed as the mean of 3 independent isolations completed in duplicate ± standard deviation. $p<0.05$ *, $p<0.01$ **, $p<0.0001$ ***.

2.3.4 PXR and CAR co-regulator gene expression array

Chaperones retain NRs in complexes within the cytoplasm preventing/hindering their transcriptional activation. Along with a reduced expression of CAR and PXR, all chaperones were under-expressed in the cell lines compared to primary human hepatocytes (Figure 2.4a). Whilst there was a difference in expression of NR chaperones between Huh7 and HepG2 cells, the expression of all 4 chaperones was

consistent in each cell type. HSPA8, HSPA4 and HSP90AA1 were expressed 50% less compared to primary human hepatocytes in HepG2 cells in contrast to 10% in Huh7 cells (p=0.009, p=0.002, p=0.002 for HSPA4, HSP90AA1 and HSPA8, respectively). PIH1D1 basal expression was maintained in HepG2 cells when compared to primary human hepatocytes but 95% less in Huh7 cells (p=0.02).

Co-chaperones are components of the binding complex retaining NRs in the cytoplasm. Similar basal levels of DNAJB1 was observed in HepG2 and Huh7 cells compared to primary human hepatocytes (Figure 2.4b) as well as PPP5C, STUB1, FKBP4 and DNAJC4 in HepG2 cells. Whilst FKBP5 and PTGE3S were found to be expressed ~80% less (p=0.004, p=0.003 for PTGE3S and p=0.002, p=0.002 for FKBP4 in Huh7 and HepG2 cells, respectively) compared to primary human hepatocytes, basal expression was comparable between cell lines. In contrast, VCP (p=0.04), STIP1 (p=0.05) and PPP5C (p=0.004) were significantly over-expressed in Huh7 cells and PPID (p=0.002), CDC37 (p=0.009), DNAJA1 (p=0.004), VCP (p=0.002) and DNAJC7 (p=0.002) were significantly under-expressed in HepG2 cells compared to primary human hepatocytes.

Co-repressors involved in preventing gene transcription are shown in Figure 2.4c. The cell lines displayed very different gene expression profiles. All co-repressors were significantly under-expressed in Huh7 cells, excluding HDAC2 and HDAC1 when compared to primary human hepatocytes. In comparison, TMTC3 was expressed 350% (p=0.007) more in Huh7 cells when compared to primary human hepatocytes and 429% more compared to HepG2 cells. In HepG2 cells, Sin3A, SREBF1, NCOR1

and NRIP1 presented similar basal expression levels to the primary human hepatocytes.

A similar trend was observed for co-activator expression (Figure 2.4d). Variable results were presented for each gene between cell types. However, HepG2 cells displayed basal levels comparable to primary human hepatocytes for NRBF2, CARM1, NCOA1, PSMC5, NCOA6 and SMC1A. Gadd45β and PGC1α exhibited similar expression in Huh7 and HepG2 cells when compared to primary human hepatocytes. Expression of PGC1α and Gadd45β in Huh7 cells was 8% ($p=0.002$) and 2% ($p=0.003$), respectively and expression in HepG2 cells was 11% ($p=0.0004$) and 8% ($p=0.004$), respectively.

Throughout the NR co-regulator analysis, HepG2 cells were found to present gene expression closer to primary human hepatocytes when compared with Huh7 cells. Hence, further analysis was completed with HepG2 cells.

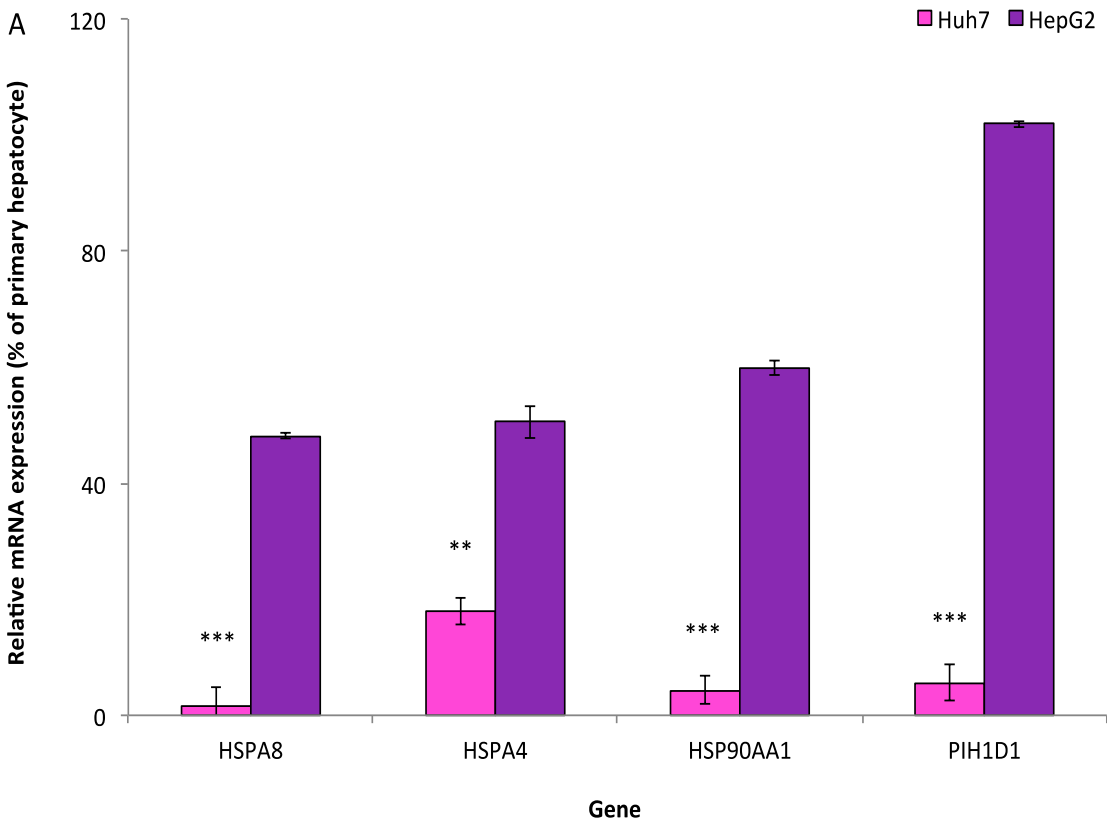
A
Huh7
HepG2
Relative mRNA expression (% of primary hepatocyte)
120
80
40
0
***
**
***
***
HSPA8
HSPA4
HSP90AA1
PIH1D1
Gene

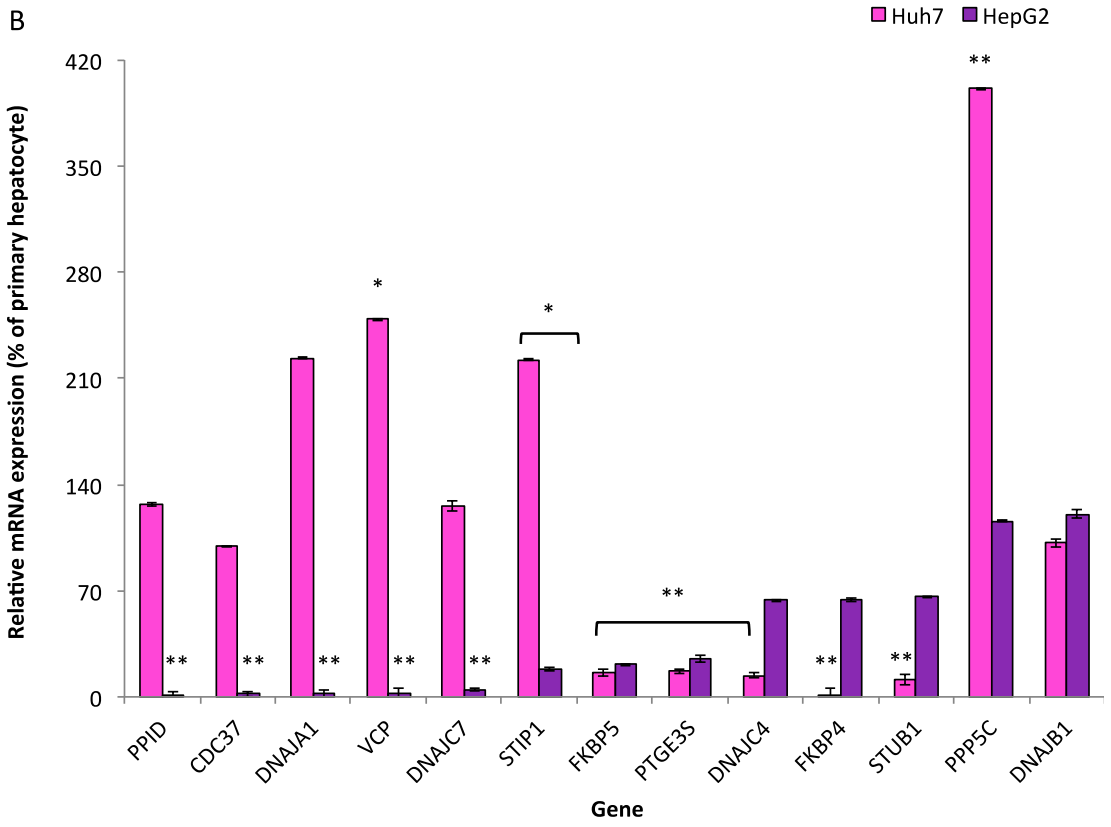
B
Huh7
HepG2
Relative mRNA expression (% of primary hepatocyte)
420
350
280
210
140
70
0
**
**
**
*
**
*
**
**
**
**
**
PPID
CDC37
DNAJA1
VCP
DNAJC7
STIP1
FKBP5
PTGE3S
DNAJC4
FKBP4
STUB1
PPP5C
DNAJB1
Gene

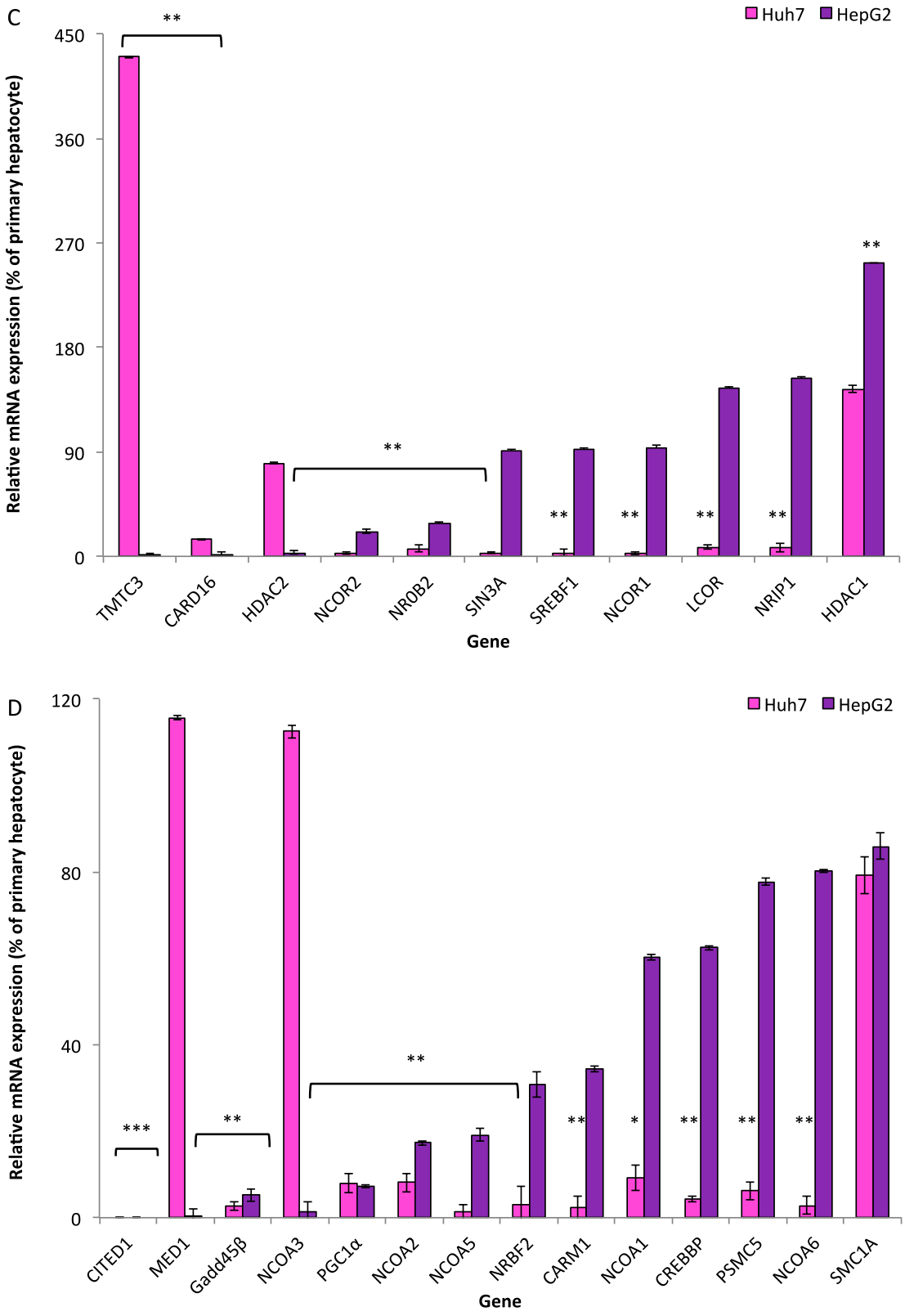

Figure 2.4 Relative gene expression of NR chaperones (A), NR co-chaperones (B), NR co-repressors (C) and NR co-activators (D) in Huh7 and HepG2 cells, compared to primary human hepatocytes. Data are normalised to a geometric mean of

4 house keeping genes and to a pool of 3 primary human hepatocyte donors using the comparative C(t) method ($C(t)=2^{\wedge -ddC(t)}$). Data are expressed as the mean of 3 independent isolations completed in duplicate ± standard deviation. $p<0.05$ *, $p<0.01$ **, $p<0.001$ ***

2.3.5 Selection of Gadd45β and PGC1α

To determine whether the decrease in CYP3A4 activity and mRNA expression in hepatoma cell lines was a result of altered NR co-regulator expression, a strict criterion was applied. The selection criteria included:

- mRNA expression in the co-regulator assay (Figure 2.4) was <20% for both cell lines compared to primary human hepatocytes
- there was evidence in the literature of CYP interactions
- the co-regulators modulate the expression/activity of CAR and PXR
- there was evidence in the literature of cell maintenance/growth regulation by the co-regulator

Based on these selection criteria, Gadd45β and PGC1α were progressed for further analysis.

2.3.6 Gadd45β and PGC1α gene expression versus HepG2 cell passage number

The expression of Gadd45β and PGC1α was determined over 25 passages with results recorded every 5 passages (Figure 2.5). In agreement with Figure 2.4d, Gadd45β and PGC1α expression at passage 10 was found to be 14% ($p=0.007$) and 8% ($p=0.004$)

when compared with primary human hepatocytes. As cell passage increased the expression of both co-activators decreased, at passage 25 Gadd45β and PGC1α expression was 0.68% (p=0.001) and 1.69% (p=0.001) compared to primary human hepatocytes, respectively.

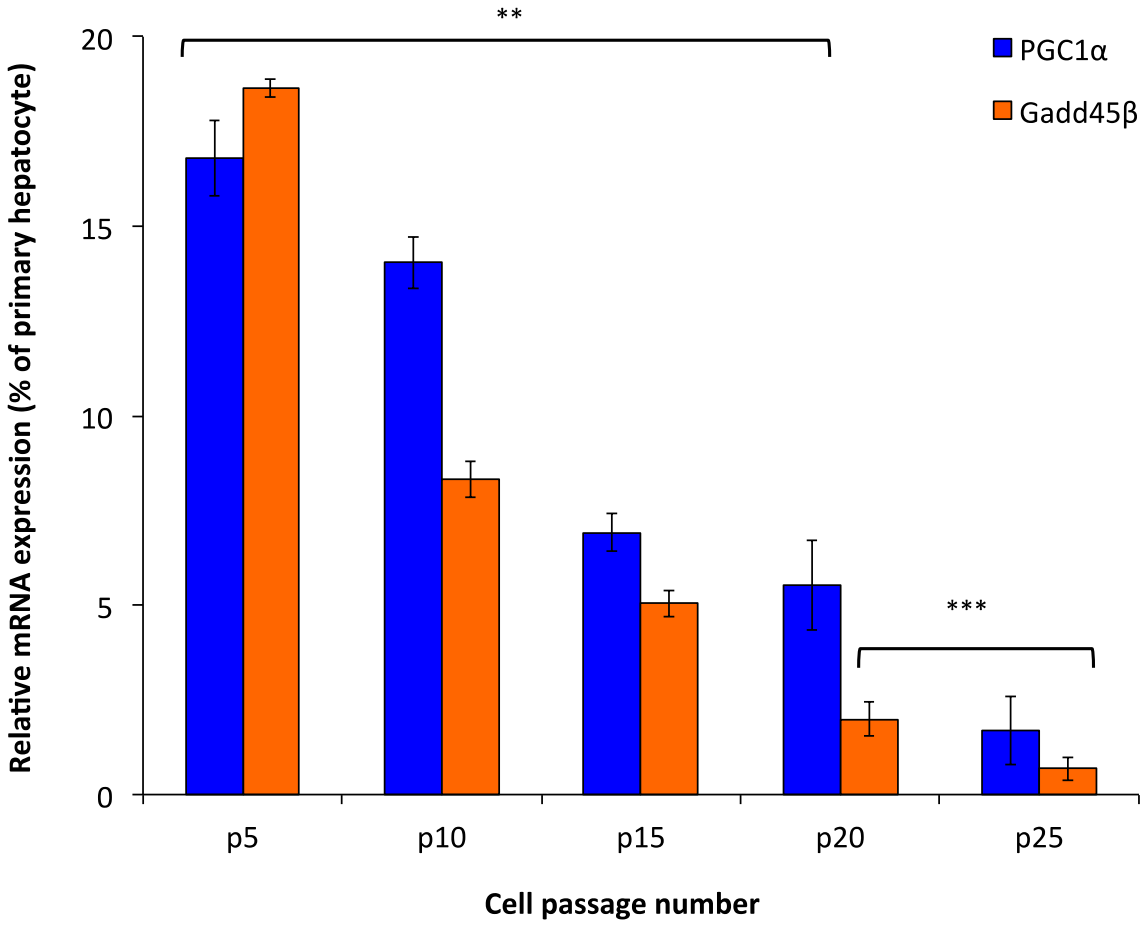

Figure 2.5. Relative gene expression of Gadd45β and PGC1α in HepG2 cells over 25 passages, compared to primary human hepatocytes. Data are normalised to GAPDH house-keeping gene and to a pool of 3 primary human hepatocyte donors using the comparative C(t) method ($C(t)=2^{\wedge -ddC(t)}$). Data are expressed as the mean of 3 independent isolations completed in duplicate ± standard deviation. $p<0.05$ *, $p<0.01$ **, $p<0.0001$ ***

2.3.7 Correlation of CYP3A4 activity with cell passage and Gadd45β/PGC1α gene expression

As shown in Figure 2.5 and 2.3, expression of Gadd45β and PGC1α and activity of CYP3A4 decreased significantly over cell passage, respectively. Linear regression analysis was used to determine the relationship between Gadd45β/PGC1α mRNA expression in HepG2 cells (compared to primary human hepatocytes) and the activity of CYP3A4 in primary human hepatocytes. A significant linear relationship was observed for Gadd45β and CYP3A4 activity (r^2=0.88) (Figure 2.6a) as well as PGC1α gene expression and CYP3A4 activity (r^2=0.93) (Figure 2.6b).

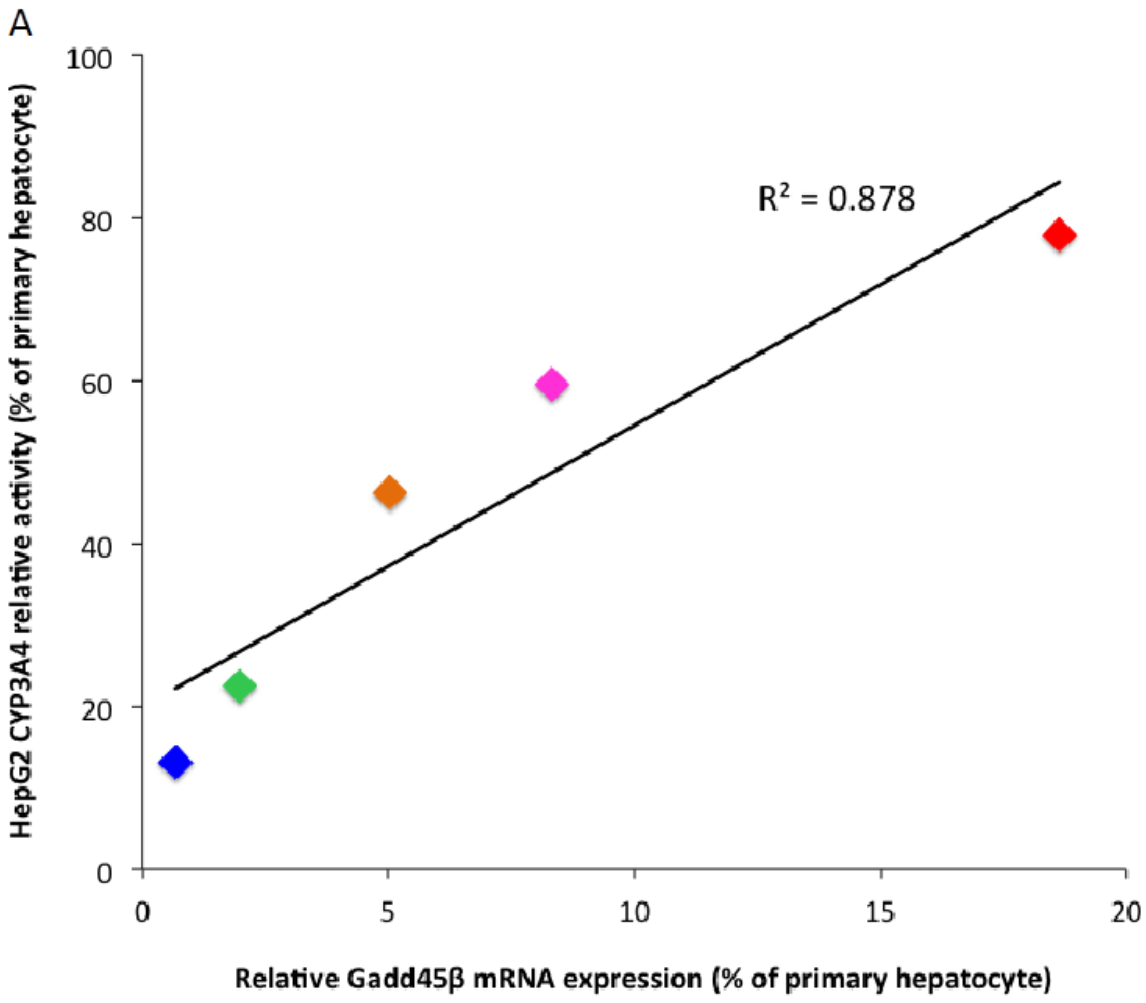

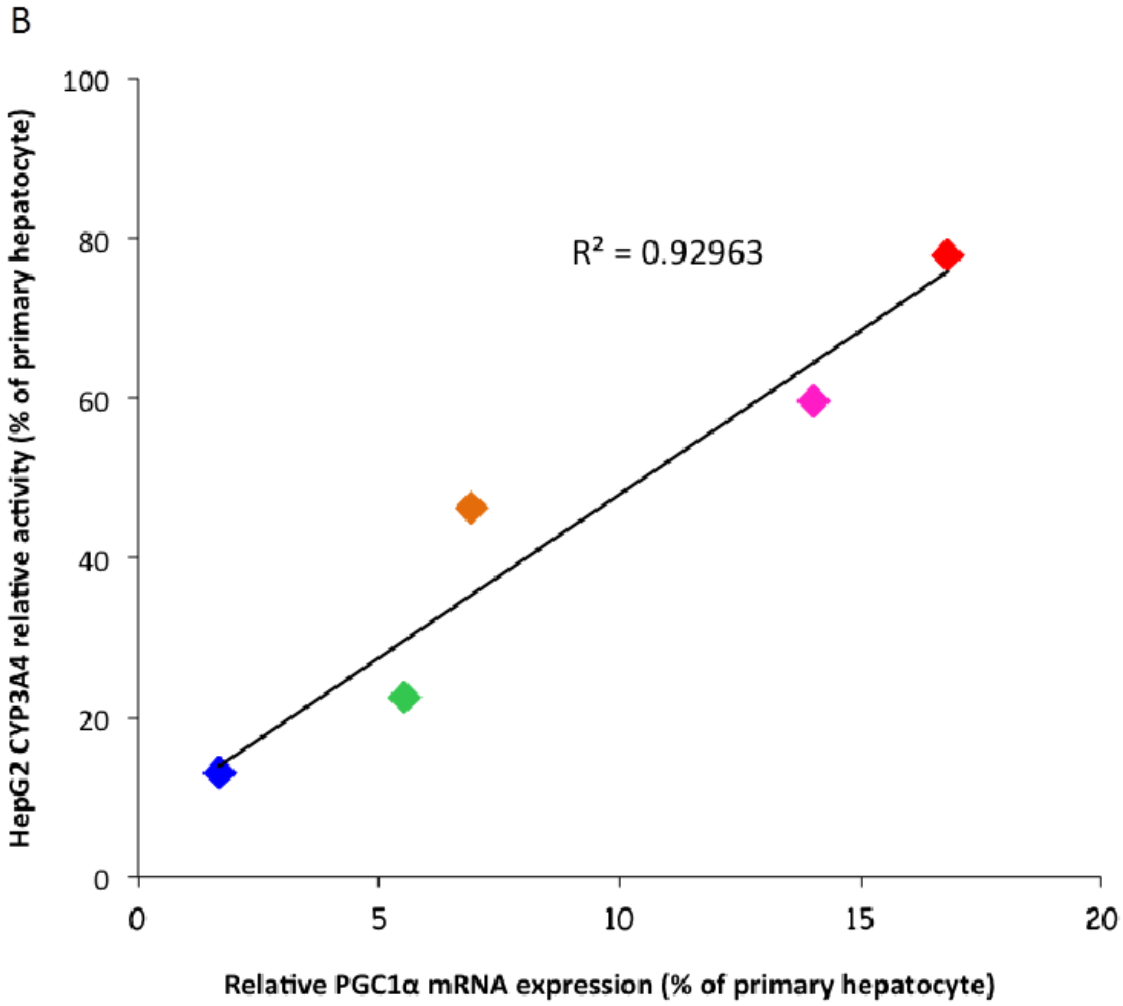

Figure 2.6. Relative gene expression of Gadd45β (A) and PGC1α (B) with CYP3A4 activity in HepG2 cells across 20 passages (p5 (◆), p10 (◆), p15 (◆), p20 (◆), p25 (◆). Expression data are normalised to GAPDH house keeping gene and to a pool of 3 primary human hepatocyte donors using the comparative C(t) method ($C(t)=2^{\wedge -ddC(t)}$). Activity data was calculated as relative fluorescent units/min as a percent of 3 primary human hepatocyte donors. Data are expressed as the mean of 3 independent isolations completed in duplicate.

2.4 Discussion

The bioavailability and disposition of a drug is largely governed by biotransformation mechanisms and transport. These mechanisms occur in the intestine but the liver is clearly a major organ for metabolic clearance. Traditional analyses are completed using established *in vitro* models but many more are in development and validation stages. Although hepatic cell lines are widely used as they retain many hepatic functions, they have limitations with numerous reports recording lower levels of drug transporters and CYPs (84, 105, 261, 272) than primary hepatic cells, which have very similar gene expression profiles to liver tissue (268, 273). Some studies have reported extremely low levels of CYP3A4 mRNA and protein in HepG2 cells that are not induced upon rifampicin (RIF) treatment (274). Nonetheless, cell lines have been pivotal in defining mechanisms for transcriptional regulation including, constitutive activation of CYP2B6 and CYP3A4 by CAR through its accumulation in the nucleus due to a lack of cytoplasmic CAR retention protein (CCRP, designated DNAJC7 in the NCBI database) (164, 165). Therefore, they provide tools for drug metabolism, toxicity and absorption studies.

Primary human hepatocytes display common hepatic functions, similar levels of gene expression and metabolism observed *in vitro* and *in vivo* (271). Analysis can be completed on suspension hepatocytes that retain hepatic function for 4-6 hours (275) or on cultured hepatocytes that display hepatic capabilities for ~24 hours post plating (244), meaning both methods can be utilised in drug metabolism or toxicity studies. Interestingly, cryopreservation of primary human hepatocytes is linked with a selective decrease in gene expression, drug metabolism (275) and a loss of specific sub-types including diploid and tetraploid cells accompanied with decreased cell

viability (271). Although inter-individual variation between human hepatocyte donors is high, the greatest asset of using isolated hepatocytes is the ability to assess active drug transport, metabolism and response to metabolite formation.

This chapter focussed on characterising the gene expression profiles of HepG2 and Huh7 cell lines in comparison with primary human hepatocytes to consequently determine any relationships between NR co-regulators and CYP3A4. It should be noted that the results and conclusions are based on mRNA expression data, which may not always correlate to protein expression or activity. However, strong correlations for efflux transporters and CYPs are well documented in the literature (261, 276). Protein expression analysis of all genes would be required to completely correlate data, but due to challenges in proteomic assessment of nuclear and membrane bound proteins (277) and the number of candidates selected, mRNA analysis was deemed to be the most appropriate alternative.

Although clear similarities were found for some genes, variability was observed between cell lines and primary human hepatocytes. Initially, work focussed on assessing the quantitative differences of key drug transporter and metabolism enzyme gene expression (Figure 2.1). Of the 3 efflux transporters investigated (ABCB1, ABCC1, ABCC2), ABCC2 expression was found to be similar to primary human hepatocytes. The most abundantly expressed efflux transporter in the human liver is ABCC2 (261) suggesting analysis of this transporter may be completed with more confidence in Huh7 cell lines. However, the most abundantly expressed influx transporter of the liver, OATP1B1 was found to have significantly lower levels of expression in the cell lines (~1-20%). Synergistic transport by OATP1B1 and ABCC2

has been identified as a crucial mechanism of both proteins involved in the transport of substrates including, HMG-CoA reductase inhibitors (e.g. simvastatin, rosuvastatin, pravastatin) hence, biliary secretion should be analysed with caution in the two hepatic cell lines investigated. OATP1B1 is an important mediator of CYP3A4 metabolism due to the large overlap in substrate affinity as well as governing access of substrates to the enzyme (30, 278). Hence, it may be a contributing mechanism for the low CYP3A4 metabolic activity reported in these cells.

ABCB1 has a low expression in the human liver but is significantly induced during regeneration and cholestasis (279). ABCB1 and CYP3A4 were significantly under expressed in both hepatic cell lines compared to primary human hepatocytes. In contrast, an up-regulation of CYP3A4 expression has been observed in confluent Huh7 cells but the mechanism by which this occurs is yet to be determined (105). CYP3A4 mRNA expression and activity in HepG2 cells were found to be a poor representation of primary human hepatocytes (Figure 2.1 and 2.3, respectively). Additionally, the passaging process correlated to a decrease in CYP3A4 activity (Figure 2.3), as previously observed (84, 280). CYP3A4 activity was comparable to values noted by others (101). The major drug disposition genes analysed in Figure 2.1 are targets of the NRs CAR and PXR, which regulate their transcription thus it was also important to consider NR expression.

NRs CAR and PXR are strict regulators of drug metabolism, cell growth, differentiation, apoptosis and cell migration. One would therefore predict variable NR expression in immortalised cells, as demonstrated in Figure 2.2. In agreement with

previous studies (111), relative to primary human hepatocytes, HepG2 and Huh7 cells expressed diminished levels of CAR and PXR. CAR and PXR control the expression of the genes analysed in Figure 2.1, hence their reduced expression in hepatoma cell lines (compared to primary human hepatocytes) is a likely consequence of significantly low levels of the NRs (94). Albeit minimal, detection of CYP3A4 and NR mRNA in HepG2 and Huh7 hepatoma cells implies gene expression is not fully eradicated by known molecular mechanisms such as methylation alterations and/or chromatin condensation. CAR and PXR are also regulated by a number of transcriptional modifiers (Table 1.4). Comparative analysis of these transcription factors between HepG2 and Huh7 hepatic cell lines and primary human hepatocytes showed significant disparities in gene expression profiles (Figure 2.4).

The cellular chaperones are essential in coordinating the translocation of proteins. The major chaperone Hsp90 is responsible for not only positively folding DNA but supports and contributes to protein degradation (281), chromatin remodelling (282) and cytoskeleton movement (283). The mechanisms by which Hsp90 orchestrates these functions are currently under investigation. However, due to its diverse abilities and correlation with oncogenic proteins Hsp90 has the potential to be targeted for cancer and immunological dysfunction treatments (282, 284). The chaperones investigated herein (HSPA4, HSPA8, HSP90AA1, PHI1D1, Figure 2.4a) were under expressed in HepG2 cells and significantly under expressed in Huh7 cells when compared to primary human hepatocytes. Within the liver and primary human hepatocytes nuclear translocation of CAR predominantly occurs via activation cascades. However, it has been noted within transformed hepatic cell lines that CAR spontaneously accumulates in the nucleus (285). Hence, the low expression of

chaperones in hepatoma cell lines here may be a result of this spontaneous mechanism.

In contrast to the chaperones, the majority of co-chaperones expressed in Huh7 cells were over-expressed when compared to primary human hepatocytes, whilst the majority were under expressed in HepG2 cells (Figure 2.4b). Co-chaperones serve to stabilise the chaperone conformation and extend the binding region to the NR (205). Inhibition of these co-chaperones (VCP, CDC37) has been shown to result in lethal perinatal outcomes in knockout mice (286). The dissociation of the chaperone/co-chaperone complex from NRs *in vivo* is highly dependent upon hydrolysis of ATP. *In vitro* co-chaperones have been found to dynamically exchange on chaperones leading to many behavioural displays by the NR (205). Co-chaperones (FKBP4, FKBP5, PPP5C) primarily attenuate or potentiate receptor activity and binding of hormones involved in cell growth and survival. Therefore, the over-expression of these genes in immortalised cells is not surprising. In addition, the lack of chaperone expression may also contribute to the low expression observed in the HepG2 cells. In contrast to work herein, DNAJC7 has been reported to be significantly over-expressed in HepG2 cells compared to Huh7 cells or primary human hepatocytes and is associated with higher levels of CAR in the cytoplasm (188). Possible reasons for the discrepancy in co-chaperone expression may be due to the maintenance buffer used, media supplements, cell passage number or if the cells have diverged.

Co-repressors bind to unliganded, antagonist or inverse agonist bound NRs to prevent the interactions and actions of co-activators (184). Similar to all the co-regulators analysed, Huh7 cells poorly expressed co-repressors in comparison to HepG2 cells

(Figure 2.4c). However, TMTC3 strongly competes with the co-activators NCOA2 and PGC1α (212) and therefore, the significant over expression of TMTC3 in Huh7 cells may contribute to the significantly reduced expression of the co-activators (Figure 2.4c and 2.4d). TMTC3 recruits HDAC1 and HDAC2, thus the expression of the co-repressors may be a consequence of this signalling cascade. The same trend was not observed for HepG2 cells. Expression of SREBF1 is associated with decreased xenobiotic clearance and regulation of cholesterol and triglyceride synthesis (208). Expression of this co-repressor was significantly lower in Huh7 cells but HepG2 cells expressed similar levels of the gene to primary human hepatocytes. Regulation of this gene is crucial to ensure optimum lipid metabolism suggesting HepG2 cells may be more reliable in this context.

The NCOA family of co-activators function as intermediate signalling genes to enhance transcription and it has also been demonstrated they play a key part in general metabolism (287). Conflicting data exist for NR co-activator expression in hepatoma cell lines (192, 207). We found NCOA1, NCOA2, NCOA3, NCOA5 and NCOA6 were under expressed in both cell lines compared to primary human hepatocytes suggesting the transformed cell lines may utilise alternative pathways. To restore CYP3A4 activity and inducibility, studies have also found transfection of NCOA1 and PGC1α genes increases PXR, hepatocyte nuclear factor 4 α (HNF4α) and CYP3A4 gene expression in HepG2 cells. However, CYP3A4 activity and induction was not restored (96, 288). Gadd45β is known to mediate numerous cellular functions including: apoptosis, cell growth and DNA repair by interacting with cyclin and cyclin-dependent kinases (203). Hence, one may predict increased expression of the co-activator in immortalised cells but this was not apparent (Figure 2.4d).

Activation of PXR by Gadd45β has no effect on cell growth *in vitro*, rather HepG2 cells have been found to differentiate into epithelial-mesenchyma (202). In addition, an over expression of CAR is correlated to an upregulation of Gadd45β (203); the converse may also be expected which is demonstrated herein (Figure 2.1 and 2.4d). PGC1α regulates adaptive thermogenesis, gluconeogenesis, mitochondrial activity and oxidative metabolism, making it a crucial hepatospecific transcription factor. In comparison to primary human hepatocytes, PGC1α was significantly under-expressed in Huh7 and HepG2 cell lines, as observed previously (207, 288).

In comparison to the environment *in vivo*, cultured hepatoma cell lines experience different stimuli in terms of cell stress, growth factors, tissue specific functions and xenobiotic exposure which may contribute to the significantly altered phenotype observed here. It is feasible to hypothesise that the hepatoma cell may adapt to its artificial environment with its primary aim to preserve life in the most efficient way possible rather than preservation of hepatic functions, since selective pressures will be different. The analysis completed clearly outlines the extent of gene expression disparities between hepatoma cells and primary human hepatocytes and the caution that should be applied when utilising the cells for drug metabolism and transport studies.

Cell passage can alter the phenotype and morphology of cell lines, which are particularly apparent at high passage number (67, 289). CYP3A4 activity (Figure 2.3) and NR co-activator Gadd45β and PGC1α expression were significantly reduced as HepG2 cell passage number increased (Figure 2.5). Linear correlations between Gadd45β/PGC1α expression and CYP3A4 activity in HepG2 cells were observed

(Figure 2.6). Whilst the correlation for Gadd45β and CYP3A4 is novel, the association of PGC1α and CYP3A4 is consistent with previous work (288).

In summary, we have determined the extent of the disparities between hepatic cell lines (HepG2 and Huh7) and primary human hepatocytes by comprehensively analysing the expression of key drug disposition genes, PXR, CAR and their co-regulators, which has not previously been assessed. Potential reasons for altered gene profiles in HepG2 and Huh7 cells were elucidated and Gadd45β and PGC1α were identified as potential mediators for the lack of CYP3A4 activity and expression in HepG2 cells and were therefore selected for work aimed at restoration of metabolic function in Chapter 3.

CHAPTER 3

Determinants of transcriptional regulation of CYP3A4 activity in hepatoma cell lines

3.1 Introduction

Primary human hepatocytes are extensively used in *in vitro* drug metabolism and toxicity screening (262). However, despite them being the current 'gold standard' (244), limitations are evident (246, 249) (see Chapter 2, Section 2.3 for more detail).

Accuracy of predictions from early stage *in vitro* assays in drug discovery are often hindered by the use of cell lines due to their altered metabolic processes and lack of hepatospecific functions (105). Comparisons between cell lines and primary human hepatocytes are discussed in more detail in Chapter 2 but the mechanism of sustaining CYP levels by both cell types is achieved through the concerted role of tissue specific and ubiquitously expressed transcription factors (96). For example, the expression of CYP3A4 is directed by co-regulators, with co-activators representing the primary target of physiological signals (95, 96, 193). Furthermore, based on the significance between PGC1α, Gadd45β and CYP3A4 found in Chapter 2, it was deemed appropriate and beneficial to determine the impact on CYP3A4 upon upregulation of the 2 co-activators.

NR co-activator, peroxisome proliferator-activated receptor-gamma co-activator 1-alpha (PGC1α), is a member of the PGC1 family expressed in the cell nucleus on chromosome 4 (290). It is involved in mitochondrial biogenesis, drug metabolism (although levels are relatively low in the liver in comparison to the heart where mitochondria are abundant (291)), adaptive thermogenesis and gluconeogenesis (290). PGC1α binds the N-terminal regions of histone acetylase proteins (HAT) (e.g. p300, CBP, SRC-1) or forms a complex at its C-terminal region with protein mediator complex (TRAP/DRIP) (292, 293). This binding displaces any present co-repressor

proteins, allowing access of DNA to the transcriptional complex, subsequently initiating gene transcription (294). In contrast to other co-activators, PGC1α has a distinctive architecture, comprising a RNA recognition motif (RRM) at the C-terminal and a rich serine/arginine (RS) domain (252).

The main mechanism of PGC1α binding is dependent upon cell type and nutritional status but primarily it forms a complex to 3'-5'-cyclic adenosine monophosphate (cAMP) at its proximal promoter region, inducing the cAMP signaling pathway (291). Previous studies have demonstrated PGC1α is key in the regulation of NRs including hepatocyte nuclear factor 4α (HNF4α) (295), constitutive androstane receptor (CAR) (252) and pregnane x receptor (PXR) (137), all of which are responsible for influencing the expression of cytochrome P450 enzymes (CYPs) and transporters (137). Martinez-Jimenez *et al.,* 2006a, showed co-transfection of PGC1α and HNF4α increased the expression of CYP1A1, CYP1A2 and CYP2C9, but the same effect was not observed when the genes were transfected alone (207). In contrast, when PGC1α was transfected alone, Martinez-Jimenez *et al.,* 2006b achieved a significant increase in CYP1A1, CYP1A2 and CYP2C9 as well as a moderate increase in CYP2D6, CYP3A4 and CYP3A5 (96). However, Novotna *et al.,* 2012, succeeded in increasing HNF4α, PXR, aryl hydrocarbon receptor (AhR) and fibrinogen protein but did not observe any increase in CYP enzyme expression (288).

Growth arrest and DNA damage inducible 45 beta (Gadd45β) is a NR co-activator that responds immediately to external stress including, inflammation (cytokines) and oxidative stress (296). Similar to PGC1α, Gadd45β modulates numerous processes that are cell specific. It is involved in DNA repair, apoptosis and cell cycle regulation

(297, 298). The main mechanism of Gadd45β is activation of the p38 mitogen-activated protein kinase (MAPK) pathway (297), where MTK1/MEKK4 form a complex directly with Gadd45β, repressing apoptosis and enhancing cell proliferation (299, 300). One would therefore speculate that Gadd45β expression may be greater in hepatoma cells in comparison to primary human hepatocytes. However, unregulated growth observed in hepatoma cells has been shown to be associated with a negative correlation of Gadd45β expression (301). Qiu *et al.,* (2007) and results from Chapter 2 have demonstrated Gadd45β expression is significantly reduced in HepG2 and Huh7 cells compared to primary human hepatocytes. Upon activation of PXR and CAR, the DR4 promoter region of Gadd45β binds directly to the NRs, activating the p38 MAPK pathway altering cell morphology but not cell growth (203). Although current literature details no specific link between Gadd45β and CYP3A4, the activation pathway detailed above allows speculation that Gadd45β may contribute to xenobiotic activation of NRs (203).

Having identified a positive correlation between the mRNA expression of Gadd45β or PGC1α and CYP3A4 activity in Chapter 2, the aim of this chapter was to determine whether manipulation of Gadd45β and PGC1α expression in hepatoma cells, can produce a more physiologically relevant phenotype.

3.2 Methods and Materials

3.2.1 Materials.

Primary human hepatocytes, Vivid® CYP screening kit, Lipofectamine2000, Williams E media, optiMEM media, CHRM®, Hanks balanced salt solution (HBSS) and Dulbecco's modified eagle medium (DMEM), OptiMEM media and western blotting reagents were purchased from LifeTechnologies, Ltd (Paisley, Scotland). β-Actin (Ab6276), PGC1α (Ab54481), Gadd45β (Ab105468) primary antibodies and secondary antibodies (Ab97240 and Ab6721) were sourced from AbCam (Cambridge, UK). Fetal bovine serum (FBS) was purchased from BioSera Co, Ltd (East Sussex, UK). Taqman reagents and assays, reverse transcription products and real-time qPCR master mix were obtained from Applied Biosystems (Warrington, UK). HepG2 cells were purchased from American Tissue Culture Collection (ATCC, USA). Purified plasmids were purchased from GeneCopoeia (MD, USA). Chemically competent 5α E.coli and BsaAI restriction digest enzyme were purchased from New England BioLabs (Herts, UK). HPLC grade acetonitrile (ACN), methanol (MeOH) and diethyl ether were purchased from Fisher Scientific (Loughborough, UK). A 3 µm C18, 100 x 4.6 mm Fortis® column was obtained from Fortis® Technologies Ltd (Neston, UK). Plasmid midi-prep kits, CelLytic™ M, midazolam hydrochloride (MDZ), 1'-hydrozymidazolam and all other products were of analytical grade and purchased from Sigma-Aldrich (Poole, UK).

3.2.2 Cell Line Maintenance.

HepG2 cells were passage and maintained as described in section 2.2.2. HepG2 cells were passaged until p10, used for analysis and then removed to waste.

3.2.3 Thawing and plating of cryopreserved primary human hepatocytes.

Cryopreserved human hepatocytes were thawed as previously described in section 2.2.3. Donor demographics are detailed in Table 2.1.

3.2.4 Cell viability

Cell viability and density of primary human hepatocytes were calculated using trypan blue exclusion as described in section 2.2.4.

3.2.5 Plating and maintaining primary human hepatocytes

24 h prior to midazolam (MDZ) treatment cells were seeded in 96-well plates pre-coated with collagen at a density of 4.5 x 10^4 cells/well and incubated for 24 h at 37 ºC with 5% CO_2 and 95% humidity as described in section 2.2.5. Plating media was replaced with 100 µl William's E media supplemented with optiMEM media and CHRM® supplement B (LifeTechnologies, Ltd).

3.2.6 Cell treatment

24 hours post plating, plating media was replaced with maintenance media (as described in section 2.2.5) for primary human hepatocytes or replaced with fresh DMEM/10% FBS for HepG2 cells containing rifampicin (RIF) at concentrations spanning the therapeutic range (0.5, 5 and 10 µM) for 24 hours. Following 24 h incubation with RIF, cells were washed twice in HBSS and incubated for 60 min with 3.37 µM MDZ.

3.2.7 Transformation of chemically competent 5-α E. coli

Purified pEZ-M02 vectors containing Gadd45β and PGC1α (Figure 3.1 and 3.2) were transformed separately into *E. coli*. Agar plates were produced containing 100 μg/ml ampicillin to select for positive colonies. One vial of DH 5-α chemically competent *E. coli* was defrosted per transformation. Plasmid DNA (10 pg) was added to a vial of *E. coli* and incubated on ice for 30 min, cells were heat shocked at 42 ^{o}C for exactly 30 sec and then placed back on ice. Warmed SOC medium (950 μl, 37 ^{o}C) was added to the vial and the solution placed in an incubator at 37 ^{o}C and shaken at 250 rpm for 1 hour. A range of culture dilutions (1:1, 1:10, 1:100) were streaked onto warmed agar plates whilst ensuring enough space was allowed for growth and separation and incubated at 37 ^{o}C overnight. Following incubation, single colonies were removed from the agar plate and added to Luria Bertani (LB) broth (4 ml) and incubated overnight at 37 ^{o}C and 250 rpm. 100 μl of the overnight incubation was added to 25 ml of LB broth containing 100 μg/ml ampicillin to select for positive colonies and incubated at 37 ^{o}C overnight at 350 rpm.

A

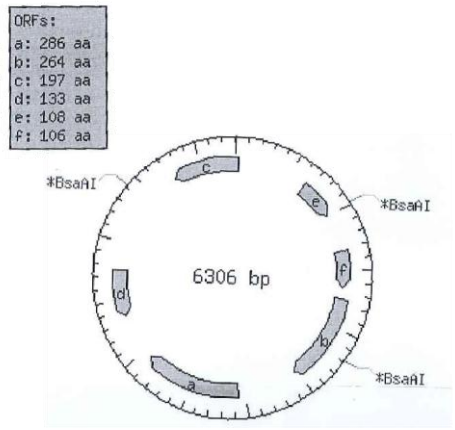

B

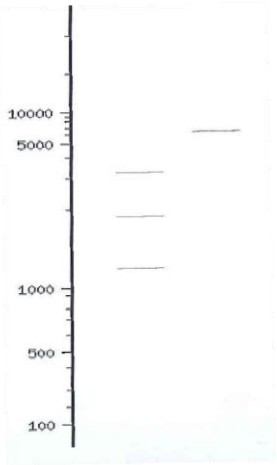

C

	Ends	Coordinates	Length (bp)
1	BsaAI-BsaAI	2177-5421	3245
2	BsaAI-BsaAI	5422-992	1877
3	BsaAI-BsaAI	993-2176	1184

Figure 3.1. Details, restriction sites within the pEZ-M02 plasmid containing Gadd45β (A) plasmid virtual digest results and (B) and the size of the digest products (C).

A

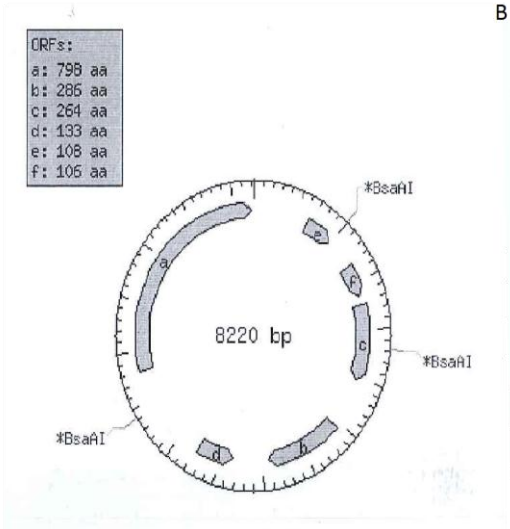

B

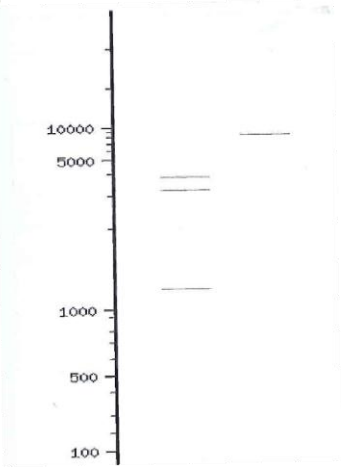

C

	Ends	Coordinates	Length (bp)
1	BsaAI-BsaAI	5422-992	3791
2	BsaAI-BsaAI	2177-5421	3245
3	BsaAI-BsaAI	993-2176	1184

Figure 3.2. Details, restriction sites within the pEZ-M02 plasmid containing PGC1α (A) plasmid virtual digest results and (B) the size of the digest products (C).

3.2.8 Restriction endonuclease analysis of DNA samples

To ensure the gDNA of *E. coli* contained PGC1α and Gadd45β, restriction enzyme digest was completed. Using the vector information sheet and the NEB cutter software, BsaAI was shown to produce 3 distinct bands when the vector was cut to determine the correct insertion via virtual digest (see vector maps, Figure 3.1 and 3.2). The dsDNA was extracted using a Sigma Midiprep kit; overnight positive cultures (25 ml) were centrifuged at 5000 x g for 10 min. Resuspension/RNase A solution (2 ml) was used to resuspend the pellet and lysis buffer (2 ml) added to lyse the cells. To neutralise the cell solution, neutralisation solution (2 ml) was added. To neutralise the lysate, 1.5 ml of binding solution was added to the solution and the cell lysate left to settle for 5 min. The cleared lysate was transferred to a column and centrifuged at 3000 x g for 2min. The column was washed twice with wash solution 1 and 2, spinning the column at 3000 x g for 2 min after each wash. Finally, 0.5 ml of elution solution was added to the column, centrifuged at 3000 x g for 5 min and the dsDNA collected in a clean tube. Quality/quantity of the plasmid determined using a Nanodrop1000 spectrophotometer. Plasmid DNA (500 ng) was added to BsaAI for 1 hour at 37 ^{o}C and resulting digest products pictured on an ethidium bromide 0.8% agarose gel. Following confirmation of the correct digest products, transformed *E. coli* were grown and extracted using the Midiprep kit as previously described. Quantification of the plasmid was again analysed using spectrophotometry and working aliquots (10 μg) frozen at -80 ^{o}C.

3.2.9 Transient transfection of PGC1α and Gadd45β into HepG2 cells using nucleofection

Initially transfection was completed using nucleofection. To obtain maximum transfection efficiency 5 μg of purified plasmid DNA was combined to appropriate solutions as described by Amaxa. The cells were passaged 4 days before nucleofection in 10% FBS/DMEM culture medium to achieve a confluence of 80%. HepG2 cells (1 x 10^6). Nucleofector V supplement (0.5 ml) and 2.25 ml of Nucleofector solution were combined with 1 x 10^6 cells in a nucleofector cuvette. The cuvette was loaded into the Nucleofector and the program for high transfection efficiency selected (T28). Following nucleofection, the cuvette was rinsed with pre-warmed culture medium (500 μl) and transferred to a 6 well plate containing culture medium (1.5 ml). The plates were then incubated (37 ^oC, 5% CO_2) ready for analysis. However, due to significant cell death (>95%), nucleofection was deemed to be an inappropriate method in transfecting HepG2 cells.

3.2.10 Transient transfection of PGC1α and Gadd45β into HepG2 cells using calcium chloride

Due to significant cell death using the nucleofector, calcium chloride was subsequently used as a delivery method of the plasmid DNA. HepG2 cells were seeded in 24 well plates in 10% FBS/DMEM culture medium at a density of 4.5 x 10^5, 24 hours prior to transfection. On the day of transfection the culture medium was replaced. 20 μg of plasmid DNA was placed in a polypropylene tube, made to 450 μl with 0.1X TE buffer and 50 μl of 2.5 M $CaCl_2$ added, vortexed and incubated at room temperature for 5 min. 500 μl of 2X HEBs buffer (280 mM NaCl, 50 mM Hepes, 1.5 mM Na_2HPO_4, 10 mM KCl, 12 mM dextrose) was prepared and the DNA/$CaCl_2$

solution added drop by drop whilst vortexing the HEBs buffer. The solution was left to equilibrate at room temperature for 30 min then added dropwise to the cells and placed back in the incubator for 4 hours. The media was aspirated off the cells and washed in 500 µl of fresh media, which was also removed. Cells were then glycerol shocked by adding 500 µl of HEBs/glycerol (25 ml 2X HEBs, 7.5 ml glycerol, 17.5 ml distilled water) and left to incubate at room temperature for 3min. The solution was aspirated off the cells and again washed in fresh media. 500 µl of fresh media was added to each well and the cells incubated at 37 ^{o}C, 5% CO_2 for 24, 48 and 72 hours, ready for mRNA, activity, toxicity and protein analysis. The calcium chloride method was successful in achieving significant upregulation of Gadd45β and PGC1α but efficiency was not very high so other methods were investigated.

3.2.11 Transient transfection of PGC1α and Gadd45β into HepG2 cells using Lipofectamine2000

A third attempt of transfecting HepG2 cells was completed using Lipofectamine2000. A range of Lipofectamine2000 volumes were analysed (0.4-1.1 µl) whilst maintaining plasmid DNA concentration at 0.2 µg. Additionally, a range of plasmid DNA concentrations (0.02 - 0.64 µg) were analysed whilst maintaining Lipofectamine2000 volume at 0.8 µl. Optimum transfection conditions were deemed to be 0.6 µl Lipofectamine 2000 and 0.16 µg plasmid DNA incubated for 24 hours. Transfections were performed according to the manufacturer's instructions. In brief, 24 hours prior to transfection 5 x10^4 HepG2cells (~80% confluent, recommended by Invitrogen) were plated in 96-well plates in culture medium (10% FBS/DMEM, 100 µl) so that on the day of transfection they were ~95% confluent. Media was replaced in each well (50 µl) and incubated for 30 min. Plasmid DNA was then diluted in optiMEM media

(25 µl) and incubated at room temperature for 10 min whilst Lipofectamine2000 was diluted with optiMEM media (25 µl), vortexed and incubated for 5 min. Following incubation, the DNA and Lipofectamine2000 solutions were combined (50 µl) and incubated at room temperature for a further 20min. Transfection complexes were added directly to the media of appropriate wells and mixed gently by 'criss-crossing' the plate. Plates were then incubated (37 ^{o}C, 5% CO_2) until ready for analysis.

3.2.12 Assessment of cell viability

Primary hepatocytes were seeded in a 96-well plate and cell viability was measured using a fluorometric assay. Mitochondrial activity was assessed by the cleavage of the tetrazolinium salt, 4-[3-(-4-Iodophenyl)-2-(4-nitrophenyl-2H-5-tetrazolio]-1,3-benzene disulphonate (WST-1) by dehydrogenase (according to the manufacturer's protocol). Maintenance media was aspirated to waste and cells were incubated with 100 µl of WST-1 (1 mL WST-1 reagent/10 mL maintenance media) at 37 ºC, 5% CO_2, 95% humidity, for 1 h. Each plate contained samples, blanks and controls with three replicates each and absorbance was measured at 450 nm using a SPECTRAmax v2.1.28 absorbance reader. Cells were assessed for toxicity using WST-1 reagent at all time points.

3.2.13 mRNA and cDNA Quantification

mRNA was extracted using Trizol reagent and reverse transcribed using standard methodology as described in section 2.2.6 and 2.2.7.

3.2.14 Quantitative real time-PCR

Real time-PCR (Chromo4™) was used to determine the gene expression of two NR co-regulators (PGC1α and Gadd45β). All samples were completed in triplicate. Real time-PCR solutions and PCR conditions were as described in section 2.2.8. Table 3.1 details the assay sequence (Applied Biosystems) of each gene with its ID.

Gene	Assay ID	Assay Sequence (FAM)
PGC1α	Hs01016719_m1	AAGGCAATTGAAGAGCGCCGTGTGA
Gadd45β	Hs00199608_m1	AGTTGATGAATGTGGACCCAGACAG

Table 3.1. Applied Biosystems Assay ID and the gene sequence that was amplified by real-time PCR. Dye - FAM: 6-carboxyfluorescein

No template controls and *no reverse transcriptase controls* were also completed in duplicate to ensure no contamination, specific amplification and maximum amplification, respectively. 2 house-keeping genes were analysed to determine the most constant expression throughout all samples (18s, GAPDH). All data were compared to the housekeeping gene GAPDH and normalised to the primary hepatocyte sample using the comparative threshold cycle (Ct) method ($Ct=2^{\wedge-\Delta\Delta C(t)}$). To ensure only gene amplification was measured the Ct was set to ignore any aberrant data such as primer degradation.

3.2.15 Protein Extraction

Cells were washed in hanks balanced salt solution (HBSS) and lysed in CelLytic™ M solution (125 µl/1 x 10^6 cells) containing 10 % protease inhibitor cocktail. The cell lysate solution was incubated at room temperature for 15 min on an orbital shaker

(125 rpm). The resulting solution was transferred to a clean eppendorf and centrifuged for 15 min at 13.9 x g to pellet the cell debris. The protein containing supernatant fraction was removed and concentration determined using a BCA assay.

3.2.16 Protein Concentration

The Bicinchoninic Acid (BCA) assay (Kader *et al.*, 1997) was used to determine whole cell protein concentration. Whilst protein samples were thawed on ice for 30 min, bovine serum albumin (BSA) standards were prepared in a flat-bottomed 96-well clear plate. BSA (50 mg) was dissolved in 1 mL of CelLytic™ M solution containing 10 % protease inhibitor cocktail. All standards and samples were completed in duplicate. 40 µl of standard/sample was added to each well and 1:2 dilutions completed across the plate to achieve a range of concentrations (1-2000 µg/ml). Reagent A and reagent B were prepared and combined in a 1:50 dilution respectively to produce the standard working stock of which 80 µl was dispensed across the wells. The plate was incubated for 30 min at 60 ^{o}C, cooled and absorbance measured on a Tecan Magellan plate reader at 562 nm and analysed using XFluor software.

Reagent A: 1 g sodium bicinchoniate, 2 g sodium carbonate, 0.16 g sodium tartrate, 0.4 g sodium hydroxide, 0.95 g sodium bicarbonate, made to 100 ml with deionized water and adjusted to pH 11.25 with 10 mM sodium hydroxide.

Reagent B: 0.4 g cupric sulphate (5X hydrated) made to 10 ml using deionized water.

3.2.17 Protein Quantification

50 µg of total cell protein was added to 10 µl of sample buffer, 1 µl of NuPage reducing agent and made to 21 µl using deionised water. Samples were heated to 70 ^{o}C for 10 min and centrifuged for 30 sec to gather any condensation. 20 µl of the

sample was loaded onto NuPage 4-12% bis-tris gels and electrophoresed for 1.5 hours at 180 V. The gel was released from the slide, placed onto iBlot gel stacks and transferred onto a nitrocellulose membrane using iBlot gel transfer programme for 6 min according to manufacturer's instructions.

For Gadd45β and PGC1α the membrane was blocked in 5% BSA/0.01% tween-tris buffered saline (T-TBS) for 2 hours at room temperature, washed in 0.01% T-TBS for 5 min (completed 3 times) followed by an overnight incubation at 4 ^{o}C and 150 rpm with the primary antibody (1/1000 in 3% non-fat dried milk (NFDM)/ 0.01% T-TBS). For the positive control β-actin, the membrane was blocked in 10% NFDM overnight at 4 ^{o}C and 150 rpm. The following day the membrane with Gadd45β and PGC1α was washed in 0.01% T-TBS for 5 min (completed 3 times) and incubated with the secondary antibody containing horseradish peroxidase (HRP) (1/3000 in 2% NFDM/ 0.01% T-TBS) for 2 hours at 4 ^{o}C and 150 rpm. For β-actin, the membrane was washed in 0.01% T-TBS for 5 min (completed 3 times) and incubated with the primary antibody (1/5000 in 2% NFDM/ 0.01% T-TBS) at 4 ^{o}C and 150 rpm. Following a 2 hour incubation with the β-actin primary antibody, the membrane was washed in 0.01% T-TBS for 5 min (completed 3 times) and incubated with the secondary antibody containing HRP (1/2000 in 2% NFDM/ 0.01% T-TBS) for 1 hour at 4 ^{o}C and 150 rpm. After incubation with the secondary antibodies all membranes were washed for 5 min in 0.01% T-TBS (completed 3 times) followed by two 20 min washes in 0.01% T-TBS.

Enhanced chemiluminescence (ECL) was used to visualise the bands produced on the membrane. Following the final wash, the nitrocellulose membrane was blotted dry and ECL solution added for approximately 30 seconds. The membrane was blotted dry and in the dark room, X-ray film placed on top of the blot and film exposed for 20

sec for β-actin and 20 min for Gadd45β and PGC1α. The X-ray film was placed in developing solution until the image was revealed (approximately 30 sec), it was then removed and placed in fixing solution for 1 min, and water for 1 min.

3.2.18 Densitometry

Western blot films were transferred onto the computer using a GS800 densitometer scanner and the Quantity One 4.6.1 (Basic) BioRad programme (BioRad, USA). Relative protein band density was determined using Total Lab Quant programme. Optical band density and relative protein quantification was determined by selecting each sample and normalising it against β-Actin (loading control). The background signal of the ECL treated nitrocellulose membrane was subtracted from the normalised protein band density measurement for each sample.

3.2.19 Measurement of CYP3A4 enzyme activity

CYP3A4 activity was determined as described in section 2.2.9.

Activity endpoint assay calculation:

CYP3A4 Activity (%) =

$$1 - \left(\frac{\text{Relative fluorescence of transfected cells}}{\text{Relative fluorescence of control cells}} \right) \text{ x } 100$$

3.2.20 HPLC analysis of midazolam and its 1'-hydroxy metabolite

MDZ, 1'-hydroxymidazolam, and RIF were made in a solution of HPLC grade methanol to obtain a final concentration of 1 mg/ml; all stock solutions were stored at -20 ˚C until use, within 1 month. Previous reports suggest MDZ (302, 303), 1'-

hydroxymidazolam (304, 305) and RIF (306) are stable in solution at -20^{o}C for at least 30 days. Following 60 min incubation with MDZ at 37 ^{o}C, MDZ and 1'-hydroxymidazolam were analysed in the media of: control HepG2 cells (non-transfected control-optiMEM media (NTCO)), Gadd45β, PGC1α and complex transfected HepG2 cells and 6 primary human hepatocyte donors. MDZ was chosen as a selective CYP3A4 substrate at a concentration of 3.37 μM as described previously (89, 236, 307, 308). Additional samples were also incubated with rifampicin (RIF) (0.5, 5, 10 μM) for 24 hours to determine the effect of the transfections on induction potential. Prior to separation, the compounds were extracted from the media to ensure a clean sample passed through the C18 column. Briefly, 100 μl of media was removed from the cells to an eppendorf following incubation with MDZ. Metabolism was stopped by the addition of 500 μl of diethyl ether. The eppendorf was placed on a turntable for 30 min at room temperature followed by 5 min centrifugation at 17,000 x g, 4 ^{o}C. To ensure only the supernatant fraction (containing the compound) was removed from the sample, the eppendorf was placed at -80 ^{o}C for 20 min to allow the aqueous media to freeze. The organic phase supernatant fraction was transferred to a glass tube and placed in a vacuum centrifuge for 20 min at 37 ^{o}C (to ensure stability of the compounds) and evaporated until dry. The resulting pellet was resuspended in 125 μl of solvent (25% ACN/ 75% H_2O). MDZ and 1'-hydroxymidazolam were chromatographically separated using a Thermo Finnigan HPLC (Thermo Scientific, Herts, UK) and a Fortis® column (3 μm, C18, 100 x 4.6 mm; Fortis® Technologies Ltd, Neston, UK).

Conditions were as follows:

Mobile phase A	5% ACN, 94.95% H_2O, 0.05% formic acid – pH 3.14
Mobile phase B	70% ACN, 25% MeOH, 4.95% H_2O, 0.05% formic acid – pH 4.45
Wash bottle	50% H_2O, 50% MeOH
Internal wash reservoir	100% H_2O
Flow rate	1 ml/min^{-1}
Injection volume	50 µl
Detector	PDA
Peak algorithm	ICIS
Plot type	Total scan

Gradient mobile phase run conditions:

Time (min)	Mobile Phase A (%)	Mobile Phase B (%)
0.0	90	10
0.5	90	10
0.6	70	30
4.0	40	60
4.1	0	100
6.0	0	100
6.1	90	10
8.0	90	10

After each sample, the needle was washed twice with 5 ml of wash bottle solution followed by 250 µl of the internal wash reservoir to ensure all solute was removed. Calibration curves were prepared using 8 calibration points, containing blank media and a range of concentrations for MDZ and 1'-hydroxymidazolam (0.138 - 13.81 µM). A linear through zero calibration curve was used. Absorbance was monitored using the PDA surveyor across a total scan. Peaks of interest; MDZ and 1'-hydroxymidazolam were quantified using XCalibur software and an ICIS peak algorithm to determine peak area. A baseline window of 40, area noise factor 5 and peak noise factor 10 was set as a standard for each sample.

Precision and accuracy were determined by analysing 3 sets of quality controls (QCs) (low, 0.5 μM; medium, 1.5 μM and high, 11.5 μM) in each run, on 3 consecutive days. Precision was determined by calculating the standard deviation at each QC concentration. Accuracy was defined as the percent deviation from the nominal concentration. Limit of detection (LOD) was expressed as the concentration that yielded a signal-to-noise ratio of 3:1 (MDZ, 54 nM and 1'-hydroxymidazolam, 97 nM). The limit of quantification (LOQ) for accuracy and precision was set to < 20%. LOQ analysis complied with the European guidelines (27). Average recovery of MDZ and 1'-hydroxymidazolam was determined by comparing the peak area of the drug extracted from the 3 QCs against direct injection samples (the same concentration of drug in reconstitution solution) (recovery was 93% for MDZ and 92% for 1'-hydroxymidazolam).

3.2.21 Microfluidic Assay

To ensure no off-target effects were apparent following transfection and induction with 0.5 and 10 μM of RIF after 24 h, key drug disposition genes (see Table 4.2 for details of genes analysed) were analysed in control and transfected HepG2 cells and 3 primary human hepatocyte donors (see Table 2.1 for donor details) using microfluidic analysis. mRNA (100 ng per reaction) was added to custom Taqman microfluidic cards and centrifuged at 1200 x g for 2 min. Quantification of genes (Table 4.2) was recorded in real time using an Applied Biosystems 7900HT PCR system. PCR conditions were 30 min at 50 ^{o}C (to reverse transcribe the mRNA, activate polymerase, denature cDNA and initiate PCR) followed by 40 cycles of 15 sec at 94.5 ^{o}C (denaturation), 30 seconds at 97 ^{o}C (annealing) and 60 seconds at 59.7 ^{o}C (extension of the product). Fluorescence was collected at the end of each cycle.

A geometric mean was calculated for 6 housekeeping genes (18s, UBC, ACTB, B2M, GAPDH, HPRT1) and the value used to normalise the expression data. Gene expression was then quantified against untreated cells using the comparative threshold cycle (C(t)) method ($Ct=2^{\wedge-\Delta\Delta C(t)}$). To ensure only gene amplification was measured the C(t) was set to ignore any aberrant fluorescence such as that from primer-dimer formation.

3.2.22 Data analysis

Each data point is the average of 3 independent samples completed in triplicate. 6 primary hepatocyte donors (see Table 5.1 for donor details) were analysed in duplicate to determine CYP3A4 activity and metabolism of MDZ on the HPLC. Normality was assessed using Shapiro Wilk and data were assessed using Mann Whitney for non-normal and unpaired t test for normally distributed data. Results were considered significant if; *, $p < 0.05$; **, $p < 0.01$; ***, $p < 0.001$. Statistics were calculated using Stats Direct (Version 2.4.6 Stats Direct Ltd).

3.3 Results

3.3.1 *BsaAI restriction enzyme digest to confirm the presence of Gadd45β and PGC1α*

pEZ-M02 vectors containing Gadd45β and PGC1α were grown in chemically competent 5-α *E.coli*. Following extraction of single colonies, BsaAI restriction enzyme was used to determine if the plasmid DNA was present and its correct orientation. Figure 3.1a and 3.2a show the restriction sites of pEZ-M02 containing Gadd45β and PGC1α, respectively and the BsaAI restriction sites with the vector. Figure 3.1b and 3.2b show a virtual digest of band orientation that is produced if the insert is present, in addition to this, Figure 3.1c and 3.2c detail the approximate size of the bands produced in each digest.

Figure 3.3 shows a representative agarose gel of positive colonies that were identified following the transformation of chemically competent 5α E.coli with the pEZ-M02 plasmids and confirmed the orientation and presence of Gadd45β and PGC1α in each. The band patterns for each colony selected matched the virtual digest for each plasmid as they contained the required DNA in the correct orientation.

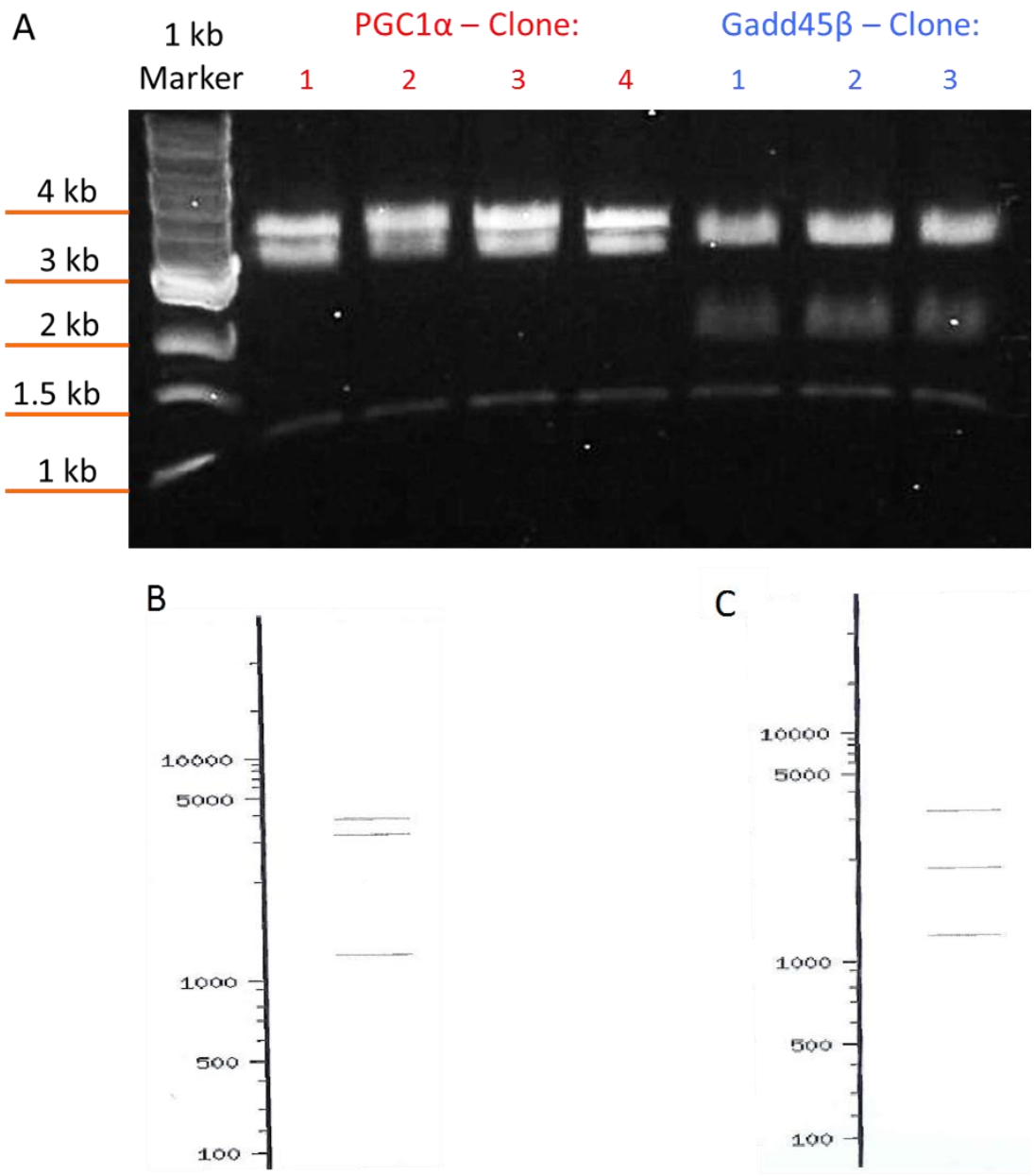

Figure 3.3. Representative agarose gel BsaAI restriction enzyme digest of pEZ-M02 plasmids containing PGC1α and pEZ-M02 plasmids containing Gadd45β (A), a virtual digest of PGC1α (B) and Gadd45β (C).

3.3.2 Optimisation of Gadd45β and PGC1α transfection via Lipofectamine2000

Following initial attempts to use nucleofection (resulted in >95% cell death) and calcium chloride (large amounts of DNA required/sample) as techniques of transfection it was decided the best method to use was Lipofectamine2000. To

determine the optimum plasmid DNA concentration, Lipofectamine2000 volume and incubation time, a range of preliminary experiments were conducted. According to manufacturer's instructions (LifeTechnologies Ltd, Paisley, UK) the optimum volume of Lipofectamine2000 ranges from 0.4-1.1 µl/96-well and plasmid DNA concentrations range from 0.02-1 µg. A matrix of Lipofectamine2000 volumes against a constant DNA concentration (0.2 µg/96-well) was set out as described in section 3.2.11. Figure 3.4a shows the effect of increasing volumes of Lipofectamine2000, using 0.2 µg plasmid DNA, on the mRNA expression of Gadd45β and PGC1α and Figure 3.4b shows the associated toxicity of increasing volumes of Lipofectamine2000.

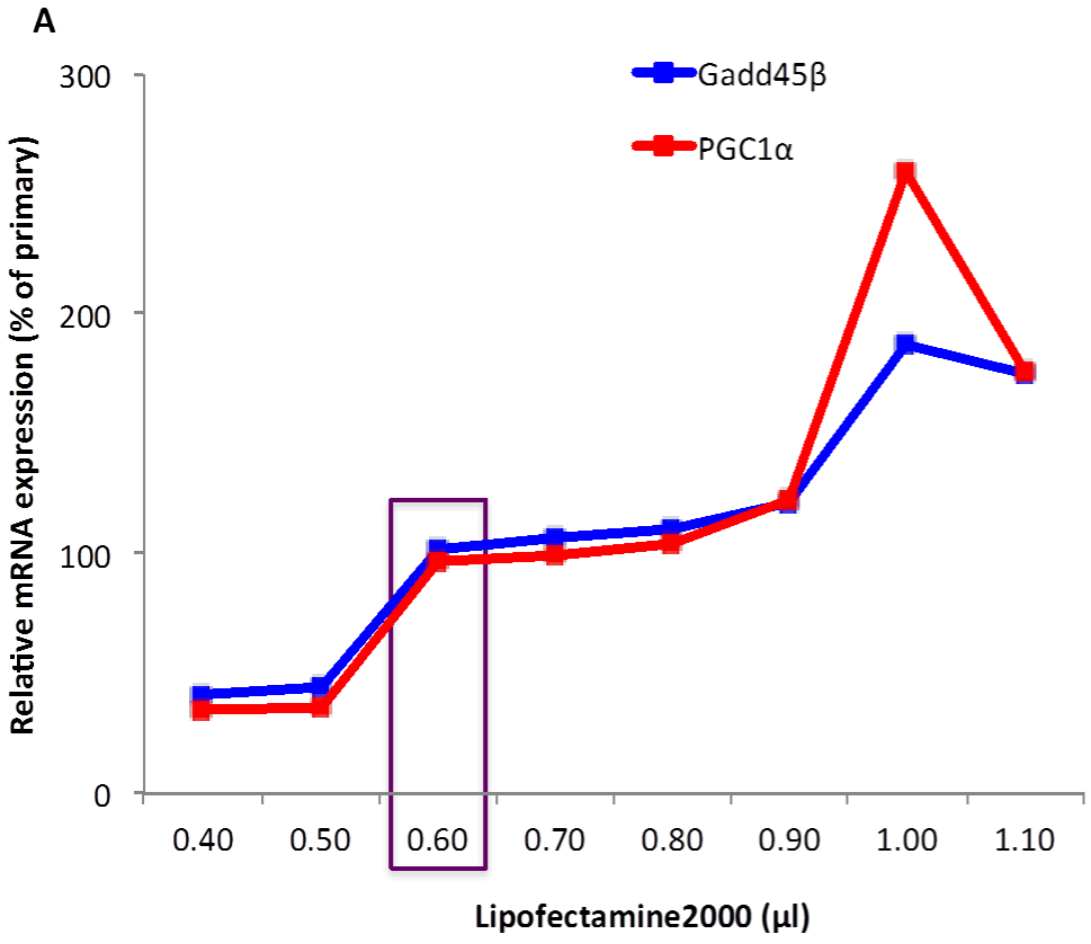

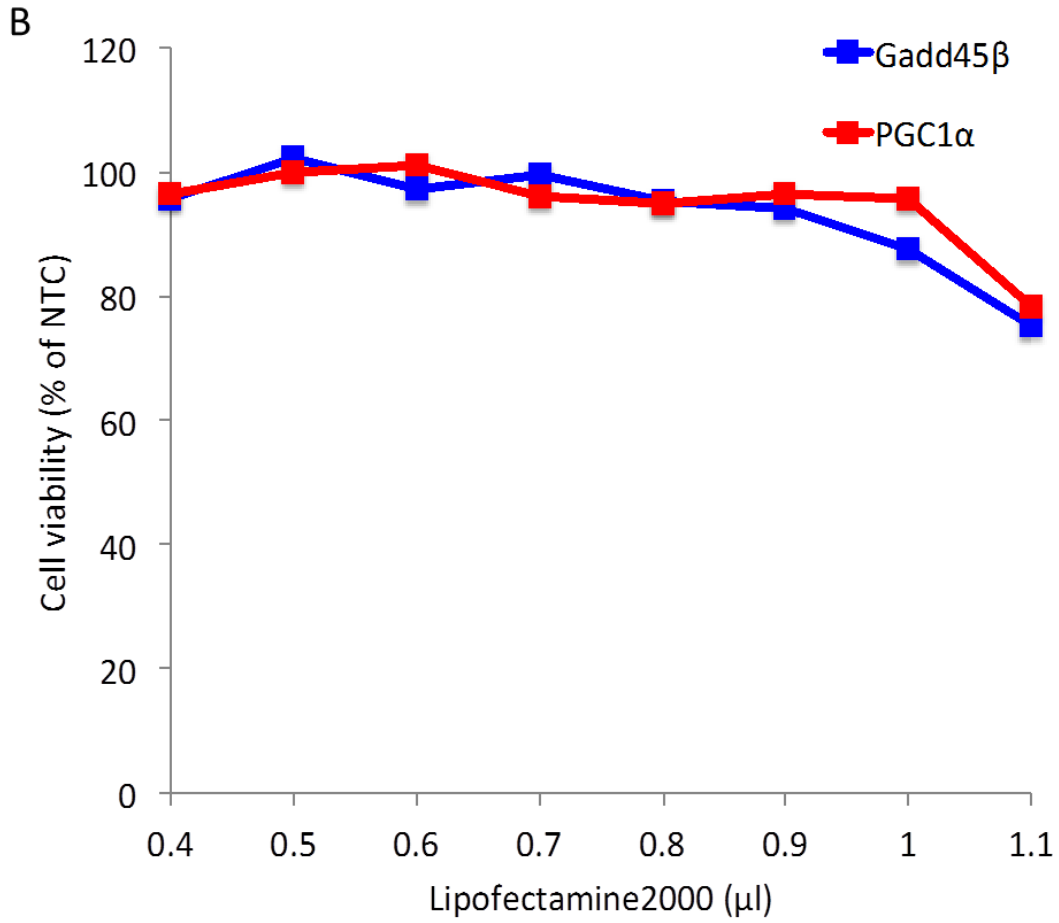

Figure 3.4. Relative mRNA expression of Gadd45β (-) and PGC1α (-) (A) and cell viability (B) following the transfection of plasmid DNA into HepG2 cells using 0.4-1.1 µl of Lipofectamine2000 and 0.2 µg DNA.

A sizeable increase in Gadd45β and PGC1α mRNA expression was achieved with larger volumes of Lipofectamine2000 (Figure 3.4a). A positive correlation in Lipofectamine2000 volume and cell viability was observed (Figure 3.4b). Using ≥1 µl of Lipofectamine2000/96-well resulted in ≥25% cell toxicity. Compared to primary human hepatocytes, 100% mRNA expression was achieved for both genes when using as little as 0.6 µl of Lipofectamine2000 with no associated cell toxicity.

In addition, a matrix of plasmid DNA concentrations against a constant Lipofectamine2000 volume (0.8 µl/96-well) was set out as described in section 3.2.11. Figure 3.5a shows the effect of increasing concentrations of plasmid DNA and holding Lipofectamine2000 volume at 0.8 µl, on the mRNA expression of Gadd45β and PGC1α and Figure 3.5b shows the associated toxicity with increasing concentrations of plasmid DNA.

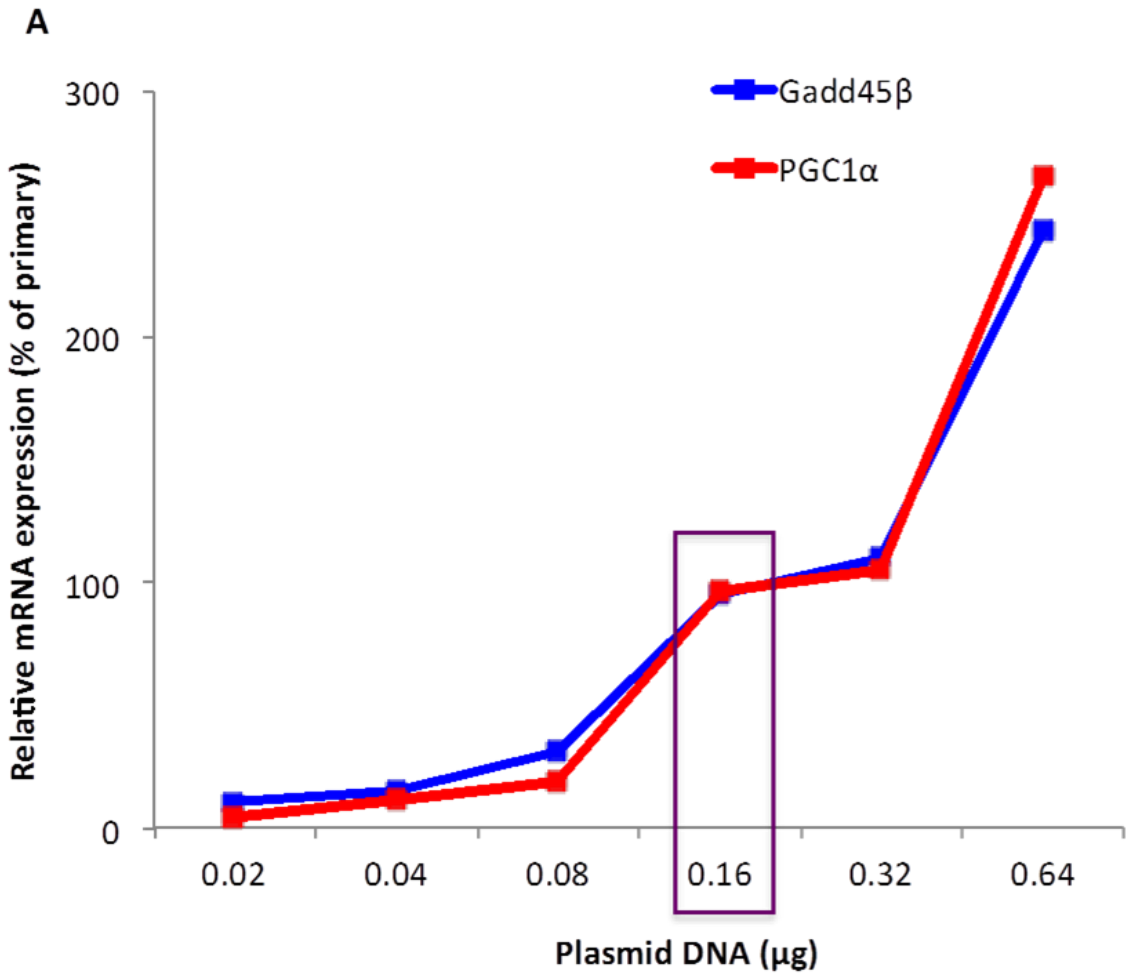

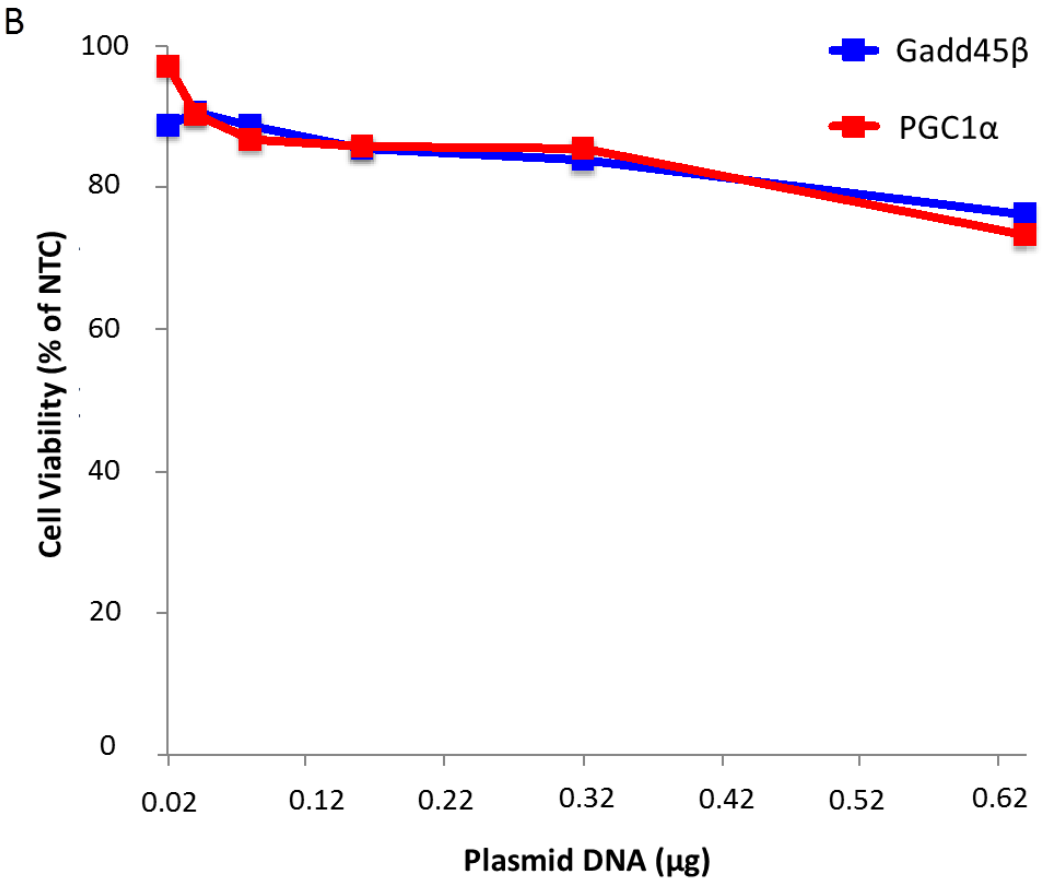

Figure 3.5. Relative mRNA expression of Gadd45β (-) and PGC1α (-) (A) and cell viability (B) following the transfection of plasmid DNA into HepG2 cells using 0.02-0.64 µg of plasmid DNA and 0.8 µl Lipofectamine2000.

An increase in Gadd45β and PGC1α mRNA expression was achieved when higher concentrations of plasmid DNA were transfected (Figure 3.5a). A correlation was observed between plasmid DNA concentrations and cell viability (Figure 3.5b). Using >0.32 µg of plasmid DNA/96-well resulted in ≥20% cell toxicity. Compared to primary human hepatocytes, 100% mRNA expression was achieved for both genes when using as little as 0.16 µg of plasmid DNA with no associated cell toxicity.

For subsequent experiments, 0.6 µl of Lipofectamine2000 and 0.16 µg of plasmid DNA were used for transient transfections.

To achieve mRNA expression similar to primary human hepatocytes it was key to determine if incubation time had an effect on the level of mRNA expression of Gadd45β and PGC1α and/or toxicity. Gadd45β and PGC1α mRNA expression decreased as incubation time increased (Figure 3.6). A 24 hour incubation achieved 115% Gadd45β mRNA expression and 119% PGC1α mRNA expression when compared to primary human hepatocytes.

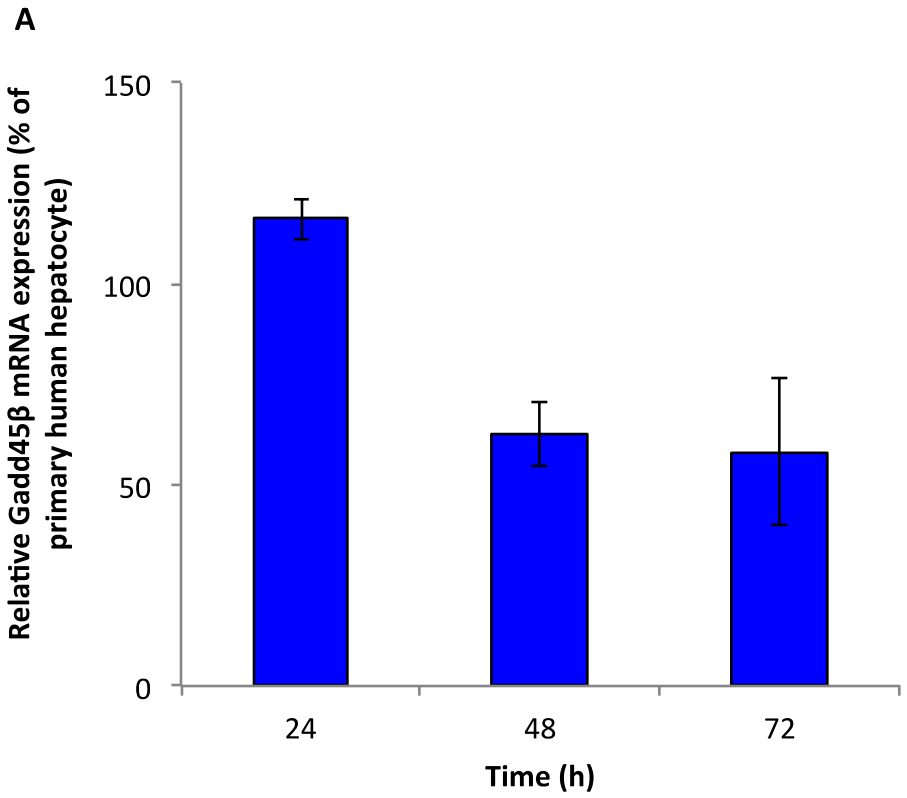

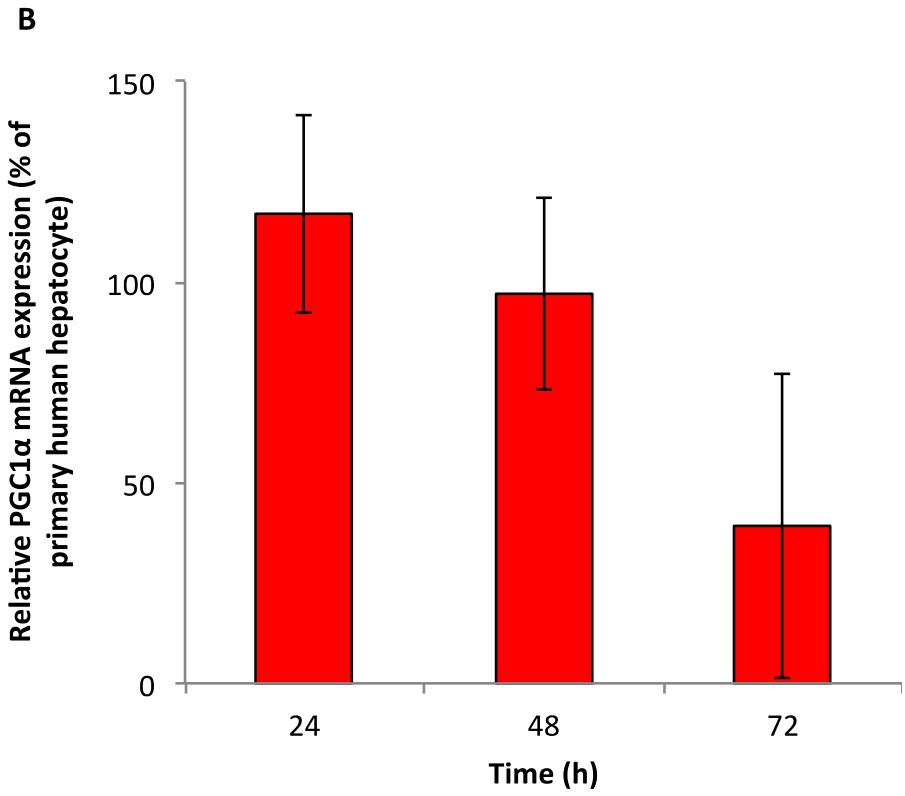

Figure 3.6. Relative mRNA expression of Gadd45β (A) and PGC1α (B) following the transfection of plasmid DNA into HepG2 cells using Lipofectamine2000 for 24, 48 and 72 hours.

In addition, it was favourable to determine if optimum mRNA expression could be achieved with the plasmid DNA transfected into HepG2 cells as a complex. Figure 3.7 shows mRNA expression of Gadd45β and PGC1α when transfected as a complex into HepG2 cells with varying concentrations of plasmid DNA. 24 hour incubations achieved the highest levels of mRNA expression, consistent with the data from single transfections. All plasmid DNA ratios were made to a final concentration of 0.16 µg/96-well, as determined in earlier optimisation assays, except for the complex (1:1) where the total plasmid DNA concentration was 0.32 µg. The complex (1:1) transfection achieved 105% and 109% mRNA expression of Gadd45β and PGC1α, respectively when compared to primary human hepatocytes.

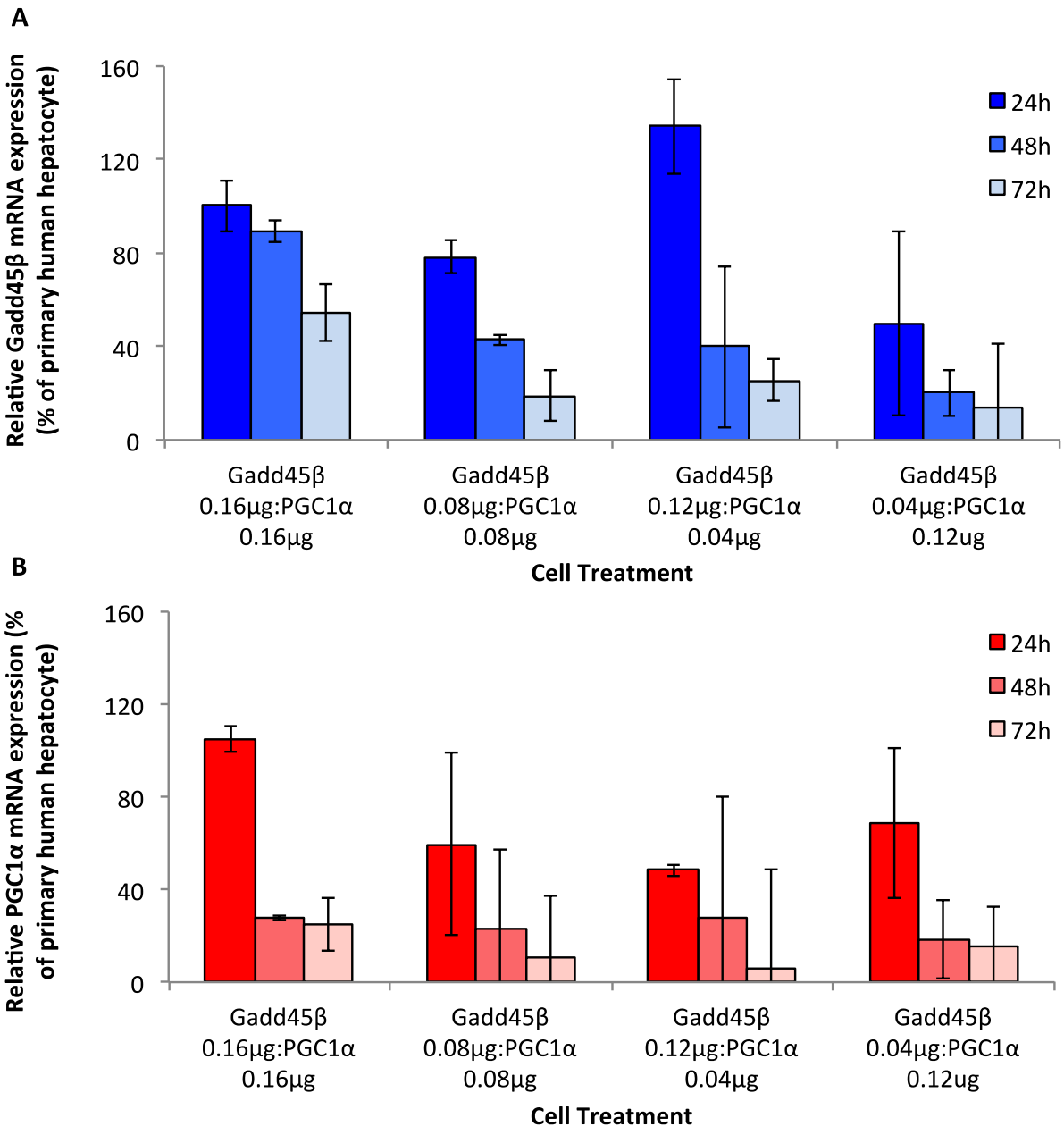

Figure 3.7. Relative mRNA expression of Gadd45β (A) and PGC1α (B) following the transfection of plasmid DNA into HepG2 cells using Lipofectamine2000 for 24, 48 and 72 hours.

It was crucial to determine the effect of incubation times and transfection complexes on cell viability. Figure 3.8 shows the cell viability of transfected HepG2 cells after 24, 48 and 72 hours with a range of plasmid DNA concentrations. All plasmid DNA

concentrations were made to a final quantity of 0.16 µg/96-well, as determined in earlier optimisation assays, except for the complex (1:1) transfection where the total plasmid DNA concentration was 0.32 µg. For all time points and plasmid DNA ratios no associated toxicity was observed (Figure 3.8).

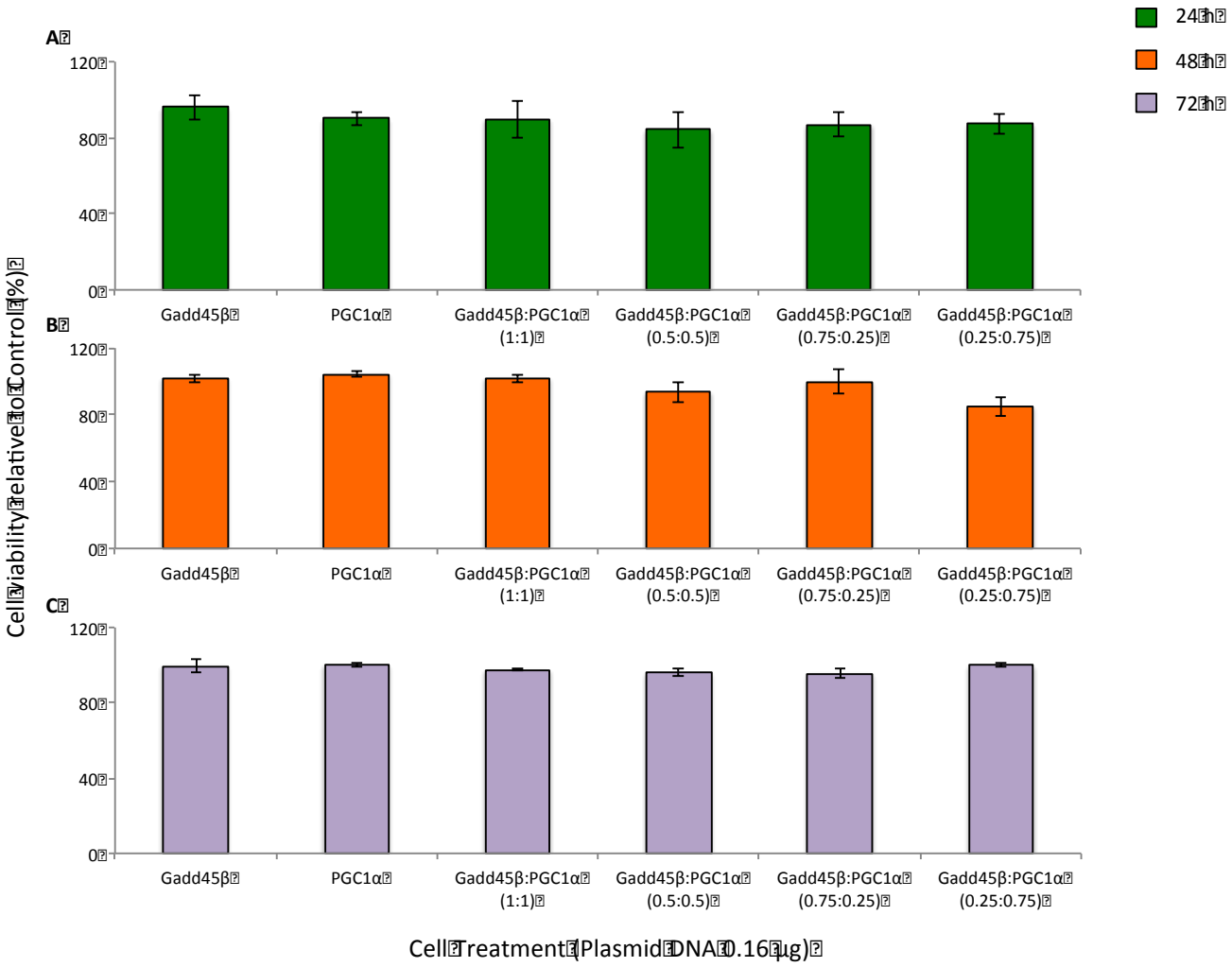

Figure 3.8. Cell viability of HepG2 cells following the transfection of plasmid DNA using Lipofectamine2000 for 24 (A), 48 (B) and 72 (C) hours.

Although the complex transfection used a double amount of plasmid DNA compared to single transfections, it was encouraging to find the complex did not interfere with gene expression or associate with any toxicity. Therefore, to assess whether the genes

had an additive effect on expression and activity of CYP3A4, subsequent experiments compared single transfections (0.6 µl of Lipofectamine2000 and 0.16 µg of single plasmid DNA) to complex transfections (0.6 µl of Lipofectamine2000 and 0.16 µg of each plasmid DNA).

3.3.3 Determination of Gadd45β and PGC1α protein expression using Western blot analysis

HepG2 cells were transfected with plasmid DNA containing Gadd45β, PGC1α and a complex of Gadd45β and PGC1α under optimal conditions as described in section 3.3.2. As shown in Figure 3.6 and 3.7, transfection of Gadd45β and PGC1α increased the mRNA expression similar to that of primary human hepatocytes. However, to determine if protein expression was also increased to levels observed in the primary human hepatocyte a western blot analysis was set up as described in section 3.2.13.

To ensure equal transfer of protein, ponceau red was used to stain the nitrocellulose membrane. In addition, β-actin was used as a loading control. As shown in Figure 3.9, β-actin levels were consistent across all samples.

From the results shown in Figure 3.9, Gadd45β and PGC1α protein was present at much lower levels in the control HepG2 cells (NTCO) compared to primary human hepatocytes (10 - 35%) (Figure 3.9, Table 3.2). Transfection of Gadd45β and PGC1α into HepG2 cells resulted in higher levels of protein compared to NTCO. In agreement with mRNA results, the highest levels of protein were achieved following 24 h incubations, with very little protein present for 48 or 72 h incubations. Single transfection of Gadd45β and PGC1α positively increased the respective protein levels

after 24 hours. An increase in Gadd45β protein was observed in HepG2 cells transfected with PGC1α, with the same effect observed for PGC1α protein levels in HepG2 cells transfected with Gadd45β (this effect was not observed at the mRNA level). However, only a slight additive effect was observed following the complex (1:1) transfection (Figure 3.9, Table 3.2). Levels of protein were consistent across all 24 h incubations. 24 hours was confirmed as the optimum incubation time for single and complex transfections (Figure 3.9).

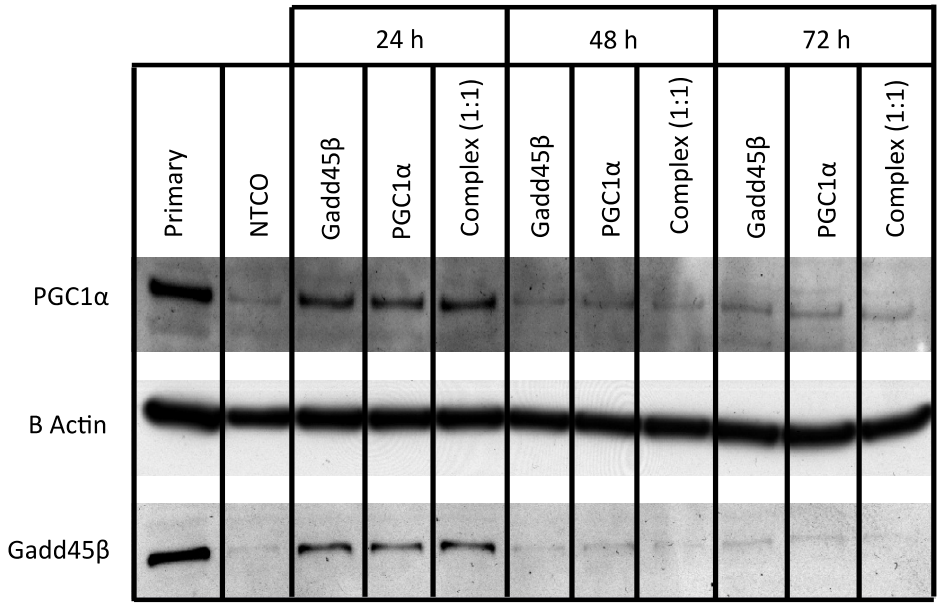

Figure 3.9. Representative immunoblot following the transfection of HepG2 cells with Gadd45β and PGC1α for 24, 48 and 72 hours.

		% of Primary human hepatocyte		
Incubation Time (h)	Plasmid DNA (0.16 μg)	n1	n2	n3
24	Gadd45β	90	69	91
	PGC1α	98	77	86
	Gadd45β:PGC1α (1:1)	92:98	89:85	89:95
48	Gadd45β	89	20	85
	PGC1α	41	15	60
	Gadd45β:PGC1α (1:1)	82:45	27:20	89:52
72	Gadd45β	106	26	95
	PGC1α	54	23	46
	Gadd45β:PGC1α (1:1)	86:57	22:25	49:30
NTCO	Gadd45β	32	15	35
	PGC1α	28	10	13

Table 3.2. Relative protein expression of transfected HepG2 cells with Gadd45β and PGC1α as a percent of primary human hepatocyte protein levels

3.3.4 Fluorescent analysis of CYP3A4 rate of activity

Following the confirmation of successful transient transfection, a preliminary analysis of CYP3A4 activity rate was determined in complex (1:1) transfected HepG2 cells, primary human hepatocytes and control HepG2 cells (NTCO) using a Vivid® fluorescent assay (Figure 3.10).

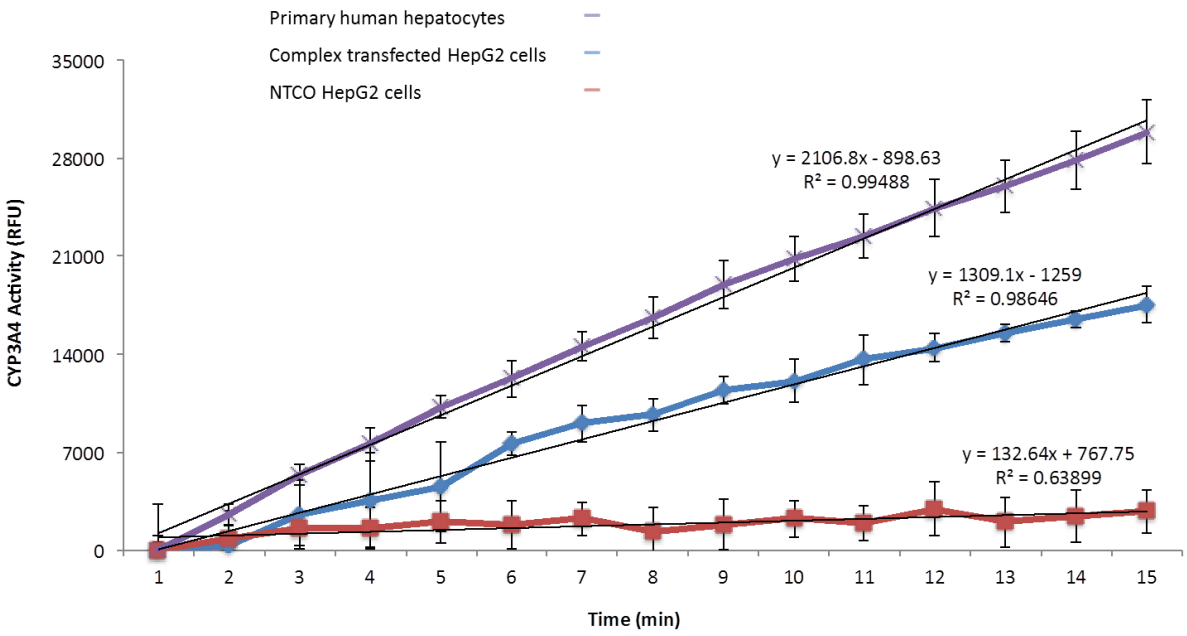

Figure 3.10. Effect of HepG2 cell complex transfection on the activity of CYP3A4 after 24 h incubation. Values are expressed as the mean relative fluorescent unit ± S.D of 3 independent experiments completed in triplicate. Primary human hepatocyte data are the mean relative fluorescent unit of 3 donors completed in duplicate

The rate of CYP3A4 activity was greatest in primary human hepatocytes (2106 RFU/min) compared to complex transfected (1309 RFU/min) and control cells (132 RFU/min) (Figure 3.10). Complex transfected HepG2 cells enhanced the activity of CYP3A4 by 54% compared to control cells (Table 3.3).

	Rate of CYP3A4 Activity (RFU/min)	% of Primary human hepatocyte	±S.D.
Primary human Hepatocyte	2106	100	9
Complex transfected HepG2	1309	62	18
NTCO HepG2 cells	132	6	34

Table 3.3. CYP3A4 activity rate

3.3.5 Validation of HPLC-PDA method for quantification of MDZ and 1'-hydroxymidazolam in mammalian cell medium

To confirm the activity of CYP3A4 in the transfected HepG2 cells and their inducibility upon RIF treatment, MDZ was used as a probe substrate and the formation of its main metabolite (1'-hydroxymidazolam) was quantified using high performance liquid chromatography (HPLC).

The retention time was 4.38 ± 0.1 min for MDZ and 4.79 ± 0.1 min for 1'-hydroxymidazolam. The retention time for RIF was 5.69 ± 0.1 min, therefore it did not interfere with either peak of interest. A chromatogram representing the top standard concentration (13.81 μM) and the maximum concentration of RIF used (10 μM) is shown in Figure 3.11.

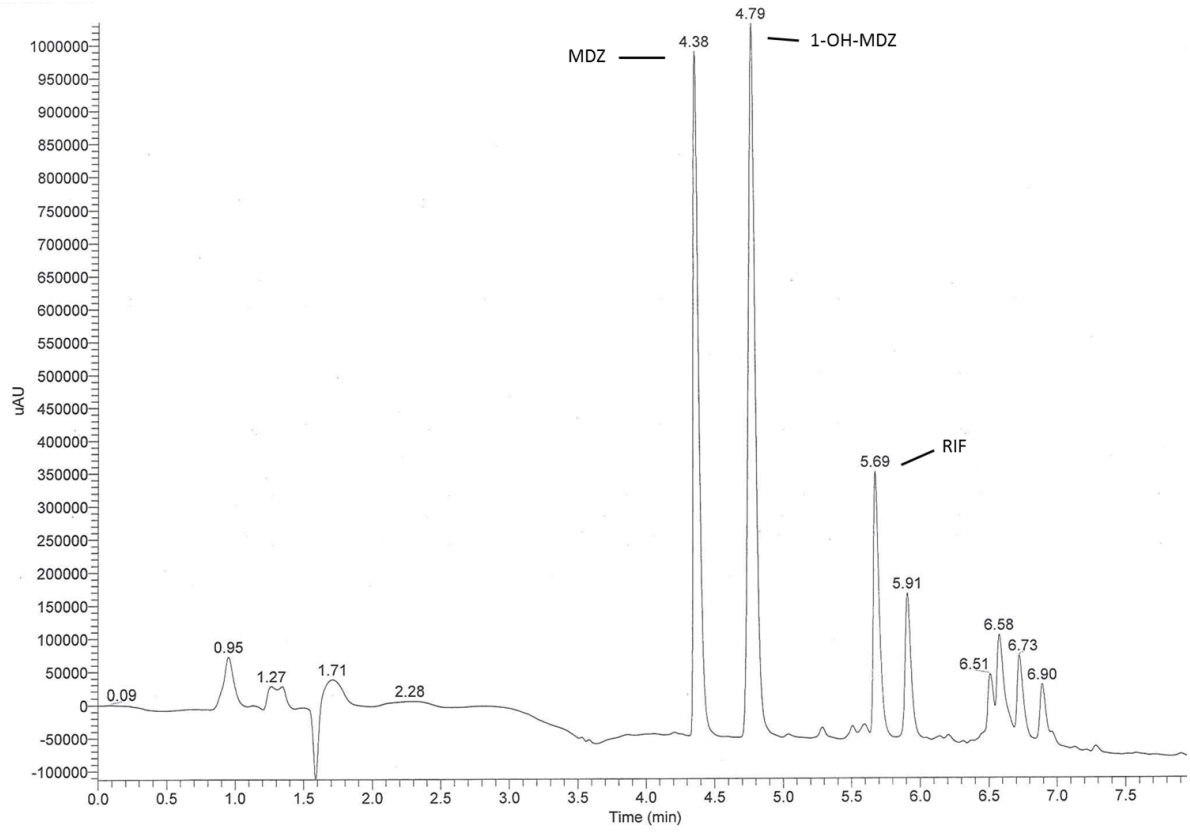

Figure 3.11. Representative chromatogram of 4X the top standard concentration (50 μM) of MDZ and 1'-hydroxymidazolam and the maximum concentration of RIF (10 μM). Y axis is absorbance and X axis is time.

The regression coefficient (r^2) of all calibration curves was ≥0.994. A linear through zero regression was selected as MDZ and 1'-hydroxymidazolam showed an excellent linear response up to 13.81 μM (Figure 3.12). All data, including precision and accuracy varied <15%, in accordance with European guidelines (27).

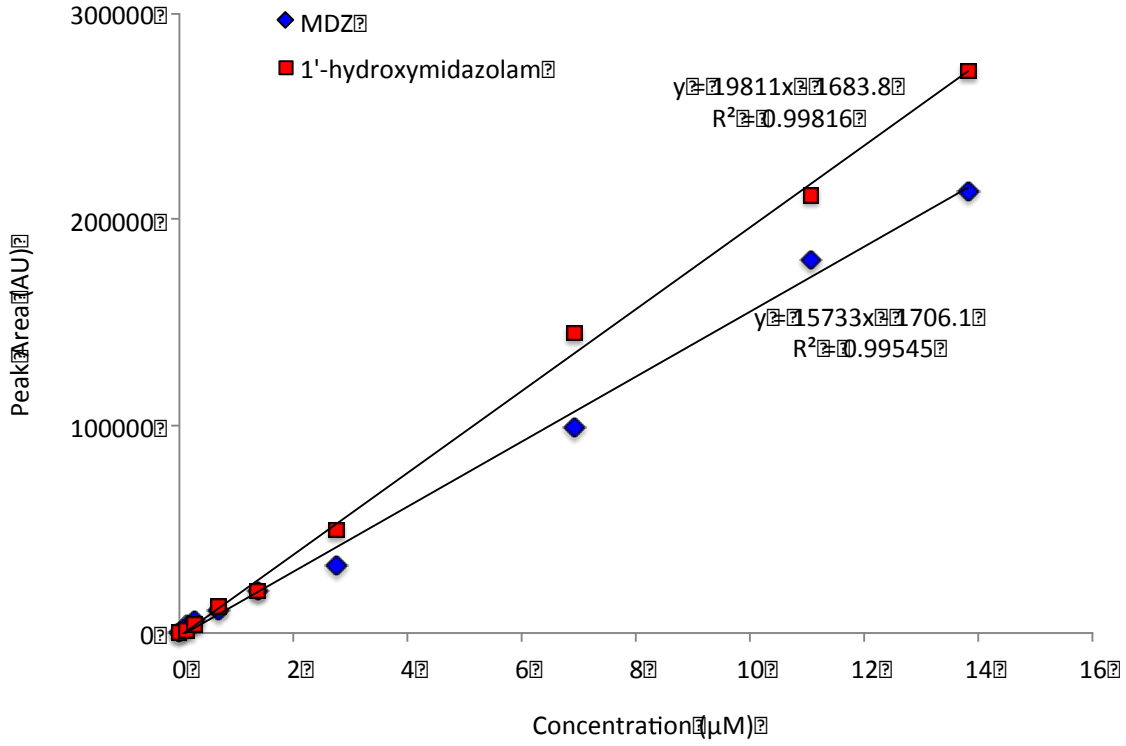

Figure 3.12. Representative calibration curve of MDZ and 1'-hydroxymidazolam peak area

3.3.6 Quantification of MDZ and 1'-hydroxymidazolam in mammalian cell medium

Basal activity of CYP3A4 was greatest in primary human hepatocytes with 1.38 µM of 1'-hydroxymidazolam produced (Figure 3.13). Compared to primary human hepatocytes, basal activity of CYP3A4 was 23% in control cells (in comparison to 6% observed in the fluorescent analysis (Figure 3.10)). However, similar to the fluorescent assay, basal activity of CYP3A4 in complex transfected HepG2 cells was 65% compared to primary human hepatocytes (Figure 3.13). Single transfection of HepG2 cells with Gadd45β or PGC1α produced 1.11 and 1.35 µM of 1'-hydroxymidazolam, respectively.

To determine inducibility, cells were treated with 0.5, 5 and 10 µM of RIF (Figure 3.13). Primary human hepatocytes produced significantly more 1'-hydroxymidazolam

when treated with 5 and 10 µM of RIF compared to control cells. Significant induction was observed when cells were treated with >0.5 µM RIF in NTCO and complex transfected HepG2 cells. Complex transfected cells produced 2 µM of 1'-hydroxymidazolam ($p<0.0001$) when treated with 10 µM RIF compared to 1.71 µM ($p<0.0001$) by primary human hepatocytes. HepG2 cells transfected with PGC1α DNA required at least 5 µM of RIF for statistically significant production of 1'-hydroxymidazolam whilst Gadd45β transfected HepG2 cells required 10 µM of RIF for statistically significant production (Figure 3.13).

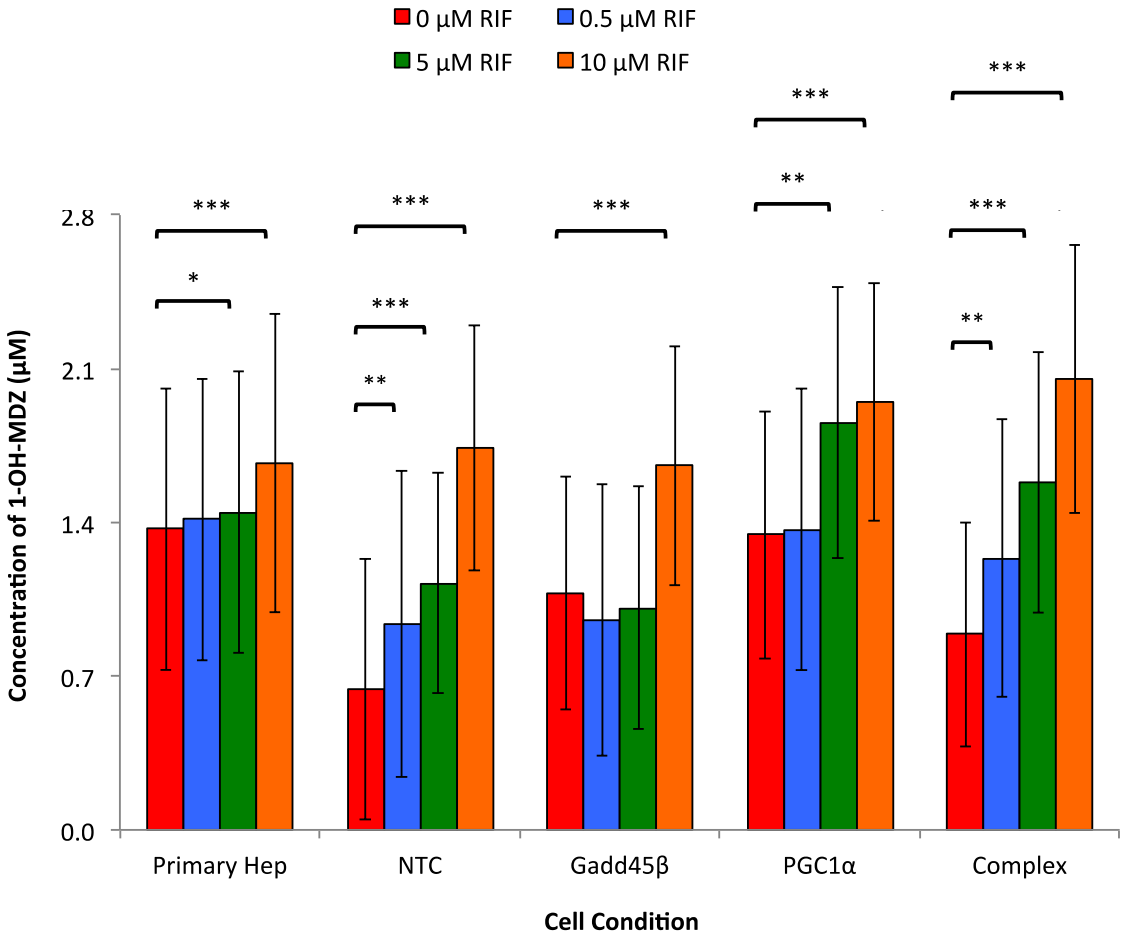

Figure 3.13. Conversion of MDZ to 1'-hydroxymidazolam in primary human hepatocytes, transfected HepG2 cells and induced cells with 0.5, 5 and 10 µM of RIF. Data are expressed as the mean of 3 independent experiments completed in triplicate

± S.D. for HepG2 cells and the mean of 6 donors completed in triplicate ± S.D. for the primary human hepatocytes.

3.3.7 Assessment of potential off-target effects following transfection

To determine if transfection of HepG2 cells using Lipofectamine2000 and plasmid DNA (Gadd45β and PGC1α) had any off-target effects in control or RIF induced cells, the mRNA expression of 40 genes involved in the regulation, metabolism and disposition of drugs was investigated (see Table 4.2). 10 of the 40 genes were not detected in the analysis (CAR, CYP1A2, CYP2C19, UGT1A4, OATP1B1, OATP1B3, OATP2B1, OATP10A1, ABCB11 and HDAC2). The lack of gene detection was in agreement with previous analysis (89, 261, 273, 309, 310). Figure 3.14 shows that treatment with Lipofecatmine2000/plasmid DNA for 24 h altered the expression of 6 genes analysed (PXR, HNF4α, CYP3A4, HDAC1, Gadd45β and PGC1α).

No notable changes in the mRNA expression of either UDP-glucuronosyltransferases (Figure 3.14e and 3.14f) or transporters (Figure 3.14g and 3.14h) were observed.

Compared to NTCO a small increase in VDR mRNA expression was observed in complex transfected HepG2 cells (Figure 3.14a). However, this effect was not observed when expression was compared to primary human hepatocytes (Figure 3.14b). No notable changes were apparent in FXR mRNA expression (Figure 3.14a and 3.14b). PXR and HNF4α mRNA expression were increased in all transfected cell types when compared to NTCO and primary human hepatocytes (Figure 3.14a and 3.14b).

Of the 4 cytochrome P450 enzymes detected in the assay, the greatest effect was observed in CYP3A4 mRNA expression. Compared to control cells, CYP3A4 expression was increased by ~150% in all transfected cell types (Figure 3.14c). In comparison to primary human hepatocytes, CYP3A4 mRNA expression was increased to similar levels in all transfected cell types (Figure 3.14d).

In agreement with single gene analysis (Figure 3.6), an increase in Gadd45β and PGC1α mRNA expression was observed in single Gadd45β and PGC1α transfected cells, repsectively, with both genes increased in complex transfected HepG2 cells (Figure 3.14i and 3.14j). In contrast, HDAC1 mRNA expression was decreased in all transfected cell types when compared to NTCO (Figure 3.14i) or primary human hepatocytes (Figure 3.14j). No notable changes in any other co-regulator were observed.

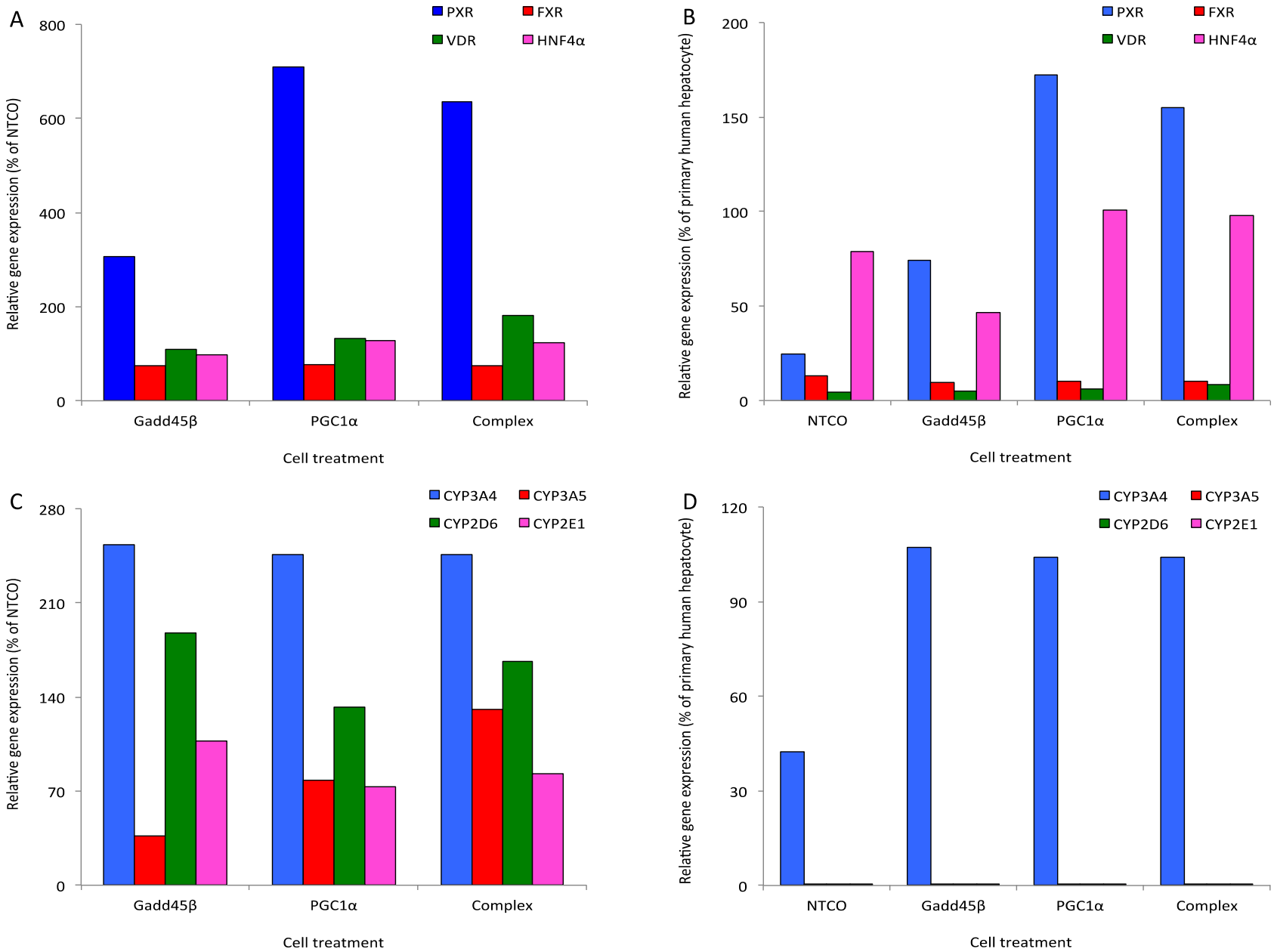
A
PXR
FXR
VDR
HNF4α
Relative gene expression (% of NTCO)
800
600
400
200
0
Gadd45β
PGC1α
Complex
Cell treatment
B
PXR
FXR
VDR
HNF4α
Relative gene expression (% of primary human hepatocyte)
200
150
100
50
0
NTCO
Gadd45β
PGC1α
Complex
Cell treatment
C
CYP3A4
CYP3A5
CYP2D6
CYP2E1
Relative gene expression (% of NTCO)
280
210
140
70
0
Gadd45β
PGC1α
Complex
Cell treatment
D
CYP3A4
CYP3A5
CYP2D6
CYP2E1
Relative gene expression (% of primary human hepatocyte)
120
90
60
30
0
NTCO
Gadd45β
PGC1α
Complex
Cell treatment

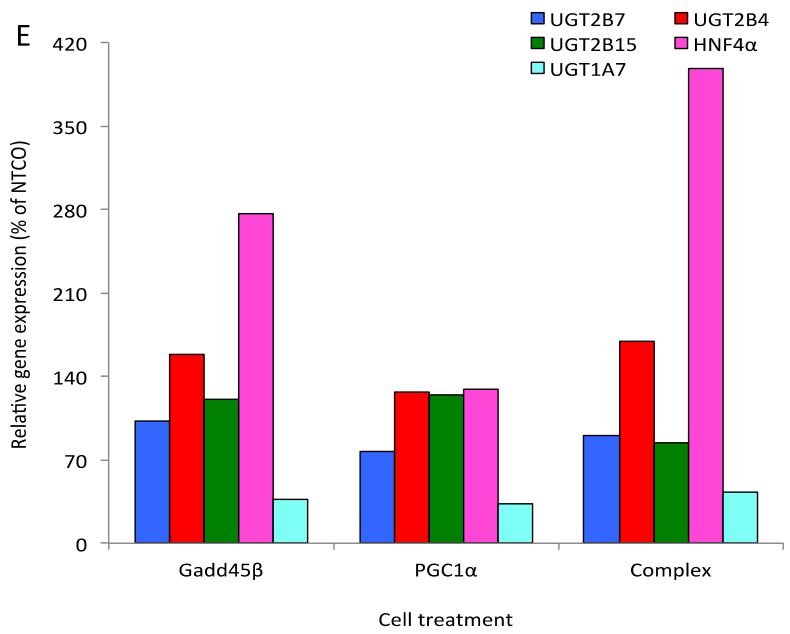
E
UGT2B7
UGT2B4
UGT2B15
HNF4α
UGT1A7
Relative gene expression (% of NTCO)
420
350
280
210
140
70
0
Gadd45β
PGC1α
Complex
Cell treatment

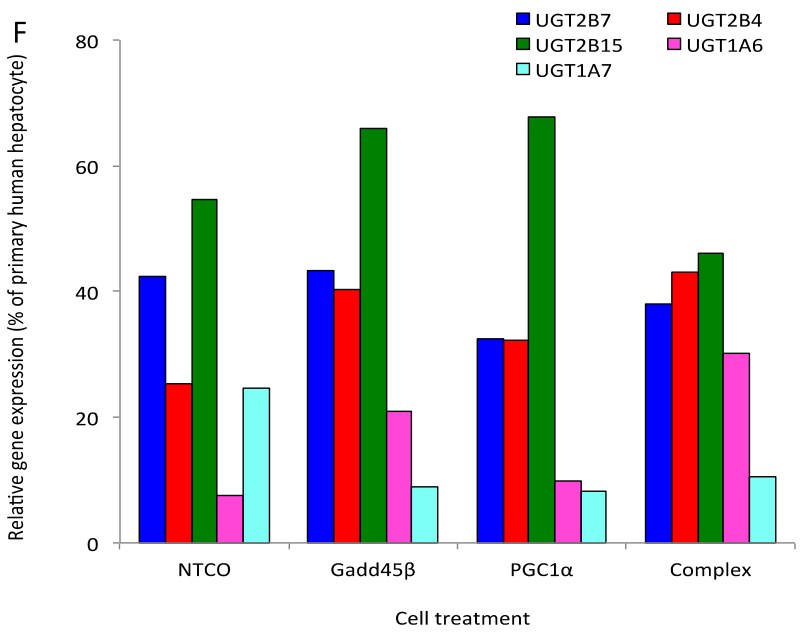
F
UGT2B7
UGT2B4
UGT2B15
UGT1A6
UGT1A7
Relative gene expression (% of primary human hepatocyte)
80
60
40
20
0
NTCO
Gadd45β
PGC1α
Complex
Cell treatment

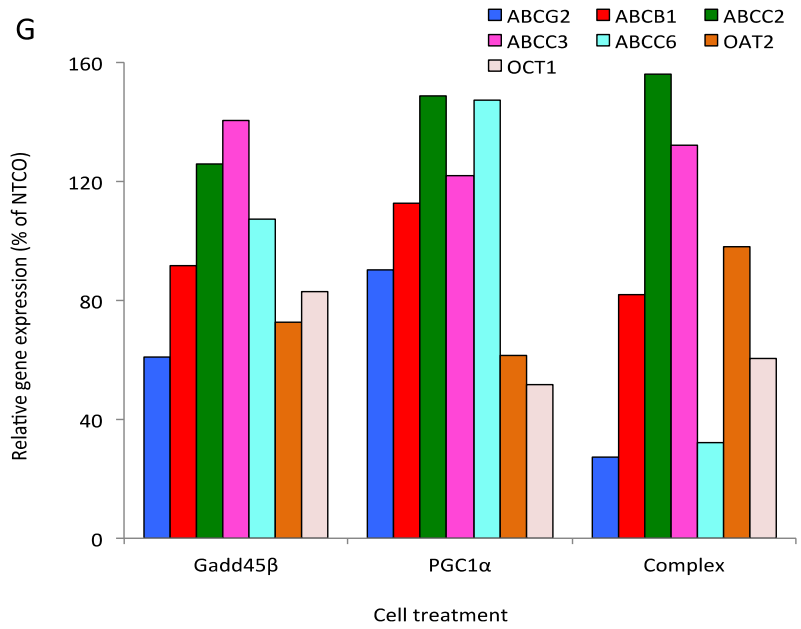
G
ABCG2
ABCB1
ABCC2
ABCC3
ABCC6
OAT2
OCT1
Relative gene expression (% of NTCO)
160
120
80
40
0
Gadd45β
PGC1α
Complex
Cell treatment

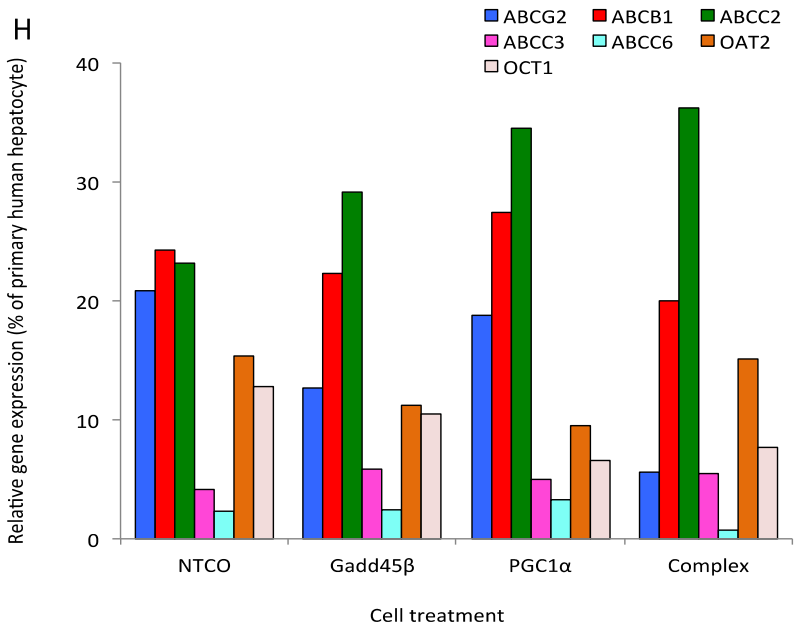
H
ABCG2
ABCB1
ABCC2
ABCC3
ABCC6
OAT2
OCT1
Relative gene expression (% of primary human hepatocyte)
40
30
20
10
0
NTCO
Gadd45β
PGC1α
Complex
Cell treatment

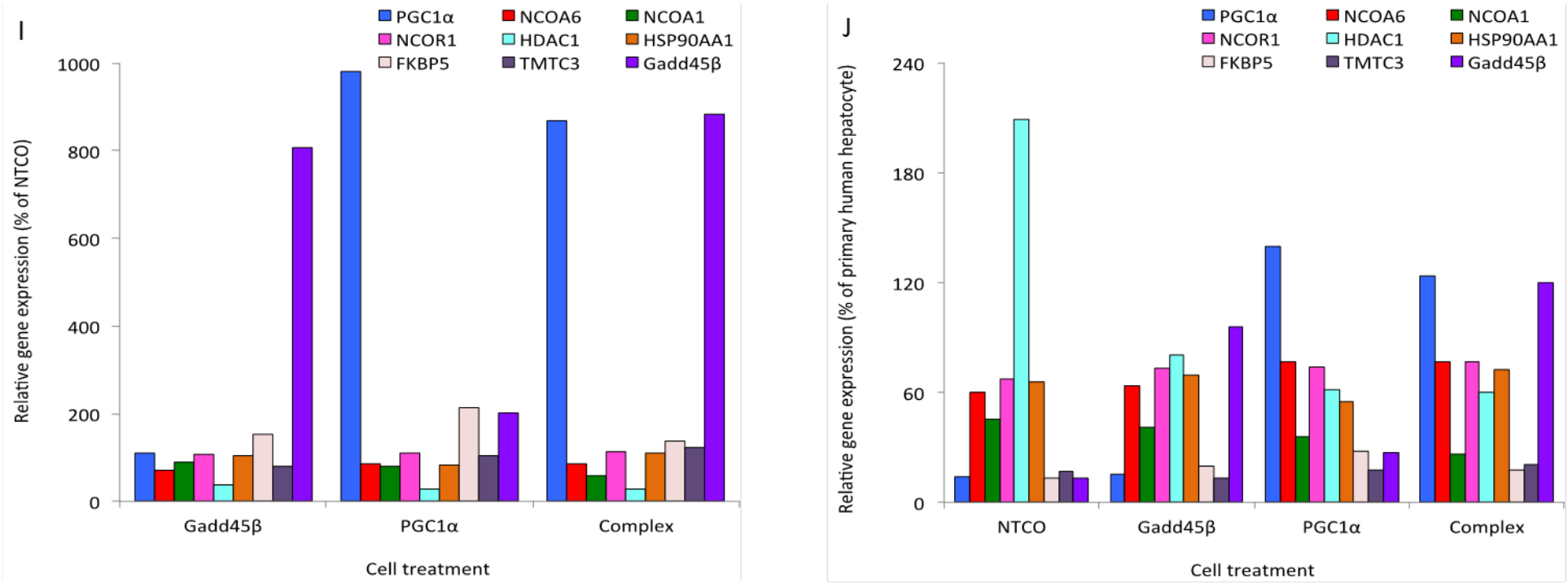

Figure 3.14. The effect of Gadd45β, PGC1α and complex transfected HepG2 cells on the mRNA expression of common nuclear hormone receptors (A,B), cytochrome P450's (C,D), uridine diphospho glucuronosyltransferases (E,F), transporters (G,H) and nuclear receptor co-regulators (I,J) following 24 h incubation. Each bar shows the mean of 2 independent experiments completed in duplicate as a percent of 3 human hepatocyte donors.

A concentration dependent increase in PXR (Figure 3.15a), HNF4α (Figure 3.15b), CYP3A4 (Figure 3.15c) and HDAC1 (Figure 3.15d) mRNA expression was observed in transfected cells treated with 0, 0.5 and 10 μM of RIF. HNF4α, HDAC1 and PGC1α mRNA expression was not altered in control cells (NTCO) treated with increasing concentrations of RIF. No notable changes in Gadd45β mRNA expression were observed in any cell type (Figure 3.15e). An increase in PGC1α mRNA expression was observed following treatment with 10 μM of RIF (Figure 3.15f).

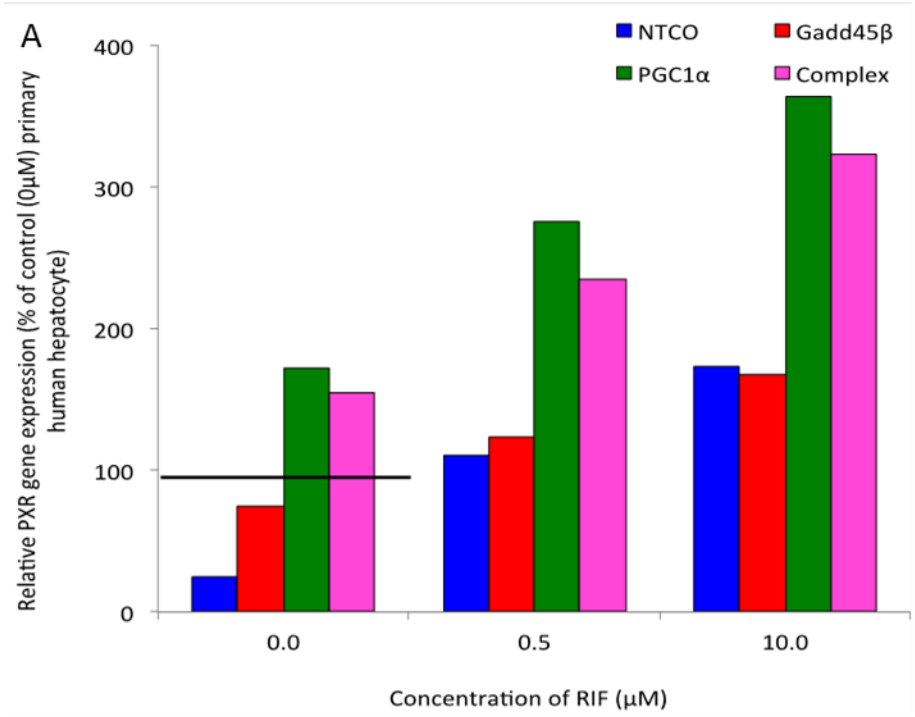
A
NTCO
Gadd45β
PGC1α
Complex
Relative PXR gene expression (% of control (0μM) primary human hepatocyte)
400
300
200
100
0
0.0
0.5
10.0
Concentration of RIF (μM)

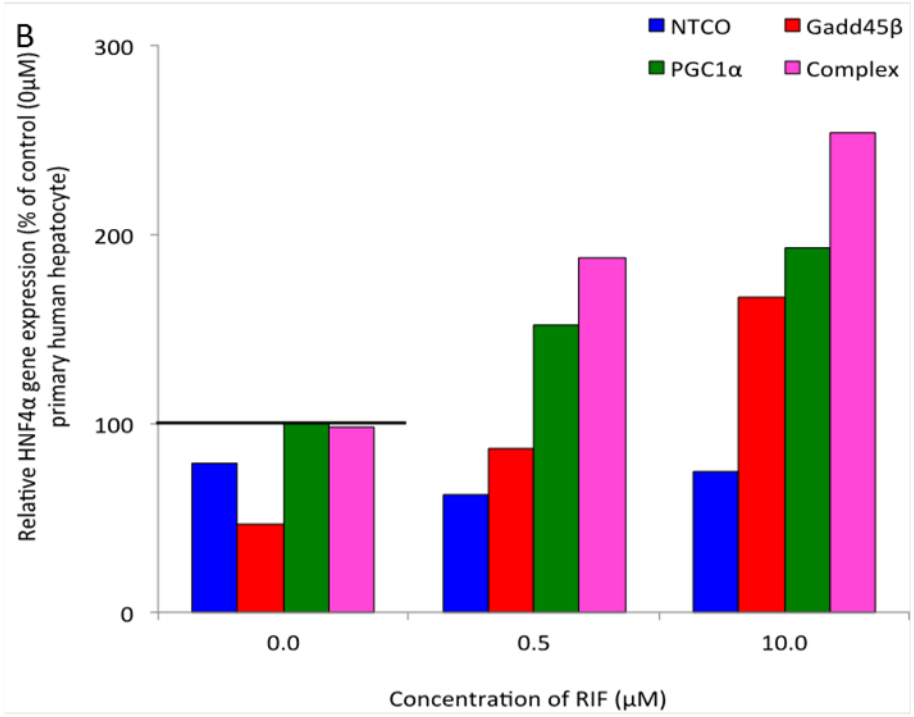
B
NTCO
Gadd45β
PGC1α
Complex
Relative HNF4α gene expression (% of control (0μM) primary human hepatocyte)
300
200
100
0
0.0
0.5
10.0
Concentration of RIF (μM)

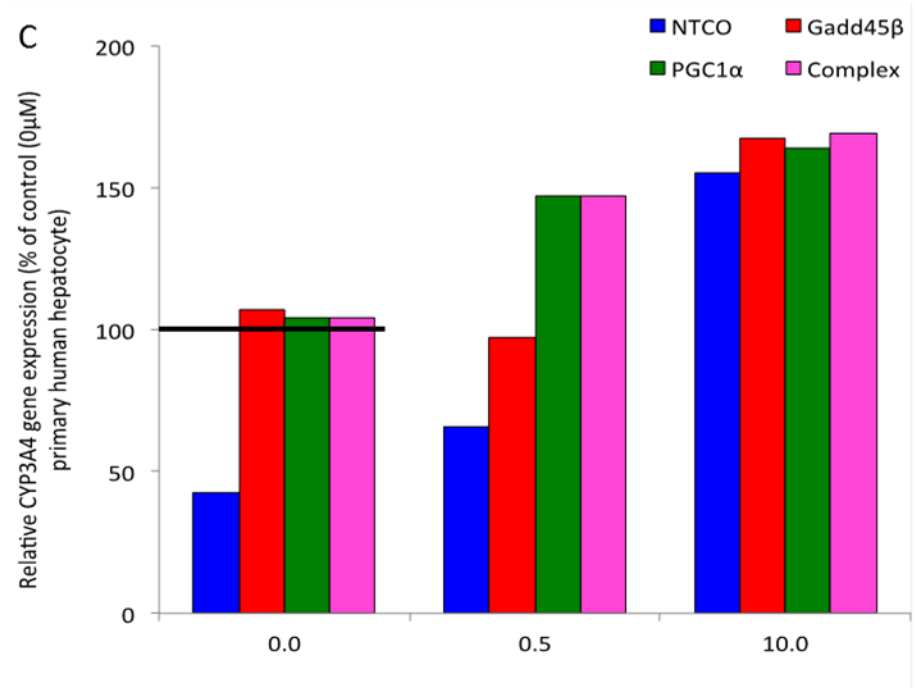
C
NTCO
Gadd45β
PGC1α
Complex
Relative CYP3A4 gene expression (% of control (0μM) primary human hepatocyte)
200
150
100
50
0
0.0
0.5
10.0

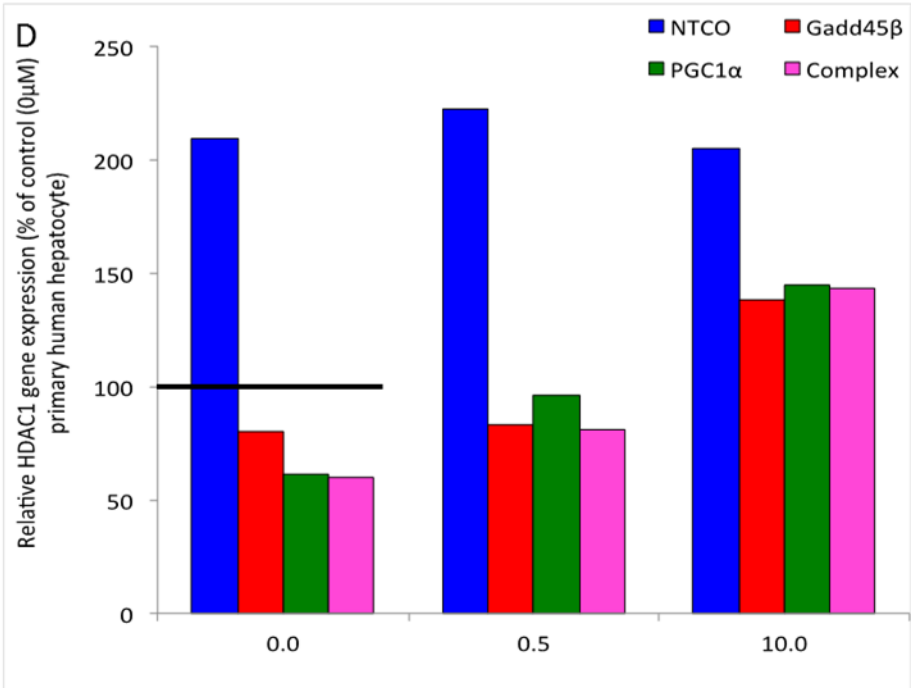
D
NTCO
Gadd45β
PGC1α
Complex
Relative HDAC1 gene expression (% of control (0μM) primary human hepatocyte)
250
200
150
100
50
0
0.0
0.5
10.0

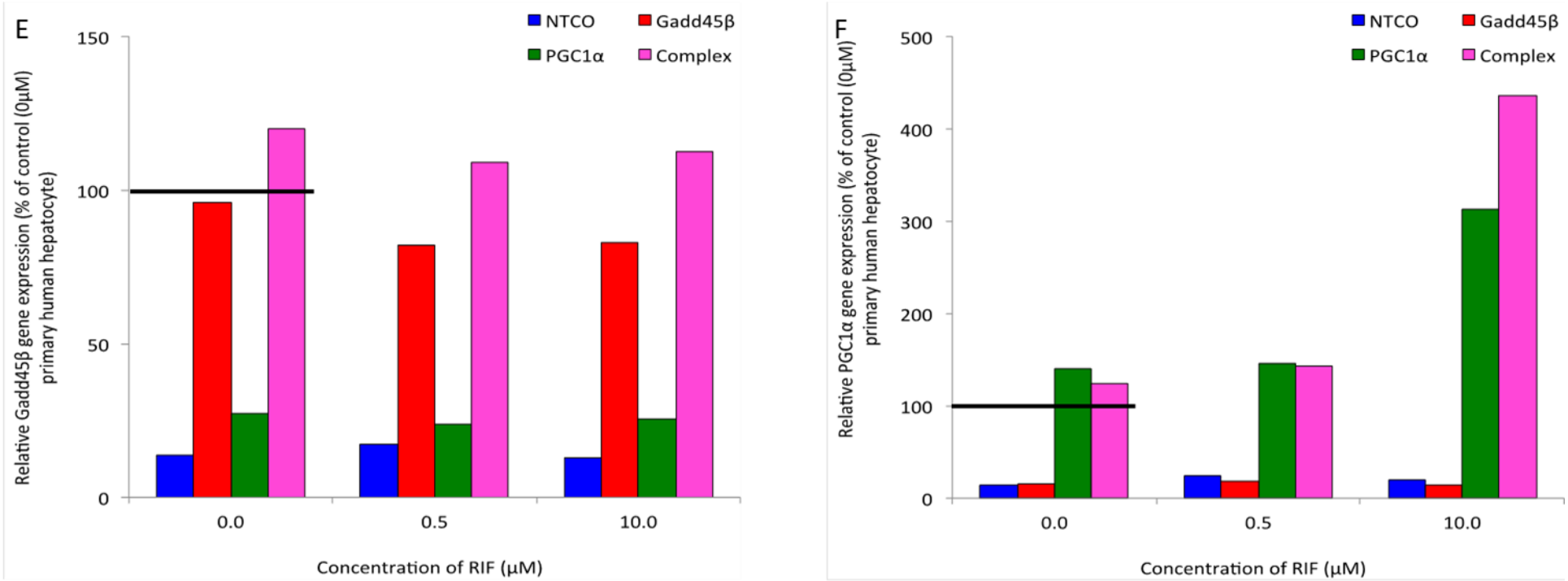

Figure 3.15. The effect of Gadd45β, PGC1α and complex transfected HepG2 cells on the mRNA expression of PXR (A), HNF4α (B), CYP3A4 (C), HDAC1 (D) Gadd45β (E) and PGC1α (F) following 24 h treatment with 0.5 and 10 μM of RIF. Each bar shows the mean of 2 independent experiments completed in duplicate as a percent of 3 human hepatocyte donors.

3.4 Discussion

As described in Chapter 2, the loss of hepatic phenotype in HepG2 and Huh7 cells is partly due to the altered expression of transcriptional regulators including; chaperones, co-chaperones, co-activators and co-repressors. Importantly, the down regulation of one co-activator can alter the activity of numerous transcription factors, resulting in distinct biological events (311). Indeed, we have shown lower levels of the *Gadd45β* and *PGC1α* genes in HepG2 cells correspond to a deficient expression and activity of CYP3A4, with the levels reducing further as cell passage increases, in comparison to primary human hepatocytes. However, restoration of the regulatory proteins may not be sufficient to restore CYP expression to primary human hepatocyte levels.

Whilst previous studies have demonstrated the role of PGC1α alone or in combination with other NR co-activators for CYP expression (95, 207, 288), this work defines a novel role of the co-activators Gadd45β and PGC1α in the constitutive expression and activity of CYP3A4. The prominent effect of PGC1α on CYP3A4 is further demonstrated here. Although expression in the liver is relatively low, PGC1α stimulates genes that regulate adaptive thermogenesis in the liver as well as activating mitochondrial processes and Phase I metabolism (312, 313). Temperature, physical exercise, food and insulin alter PGC1α levels (312). Whilst fasting induces PGC1α and CYPs (314), insulin suppresses basal PGC1α and CYP expression (96, 315). Previous studies have reported PGC1α activates CYP genes via interaction with NRs, PXR and HNF4α and the co-activator nuclear receptor co-activator 1 (NCOA1) (92, 95). Our results have demonstrated PGC1α transfection and complex (Gadd45β and PGC1α) transfection increases PXR mRNA expression (Figure 3.14). However, upon

induction with rifampicin (RIF), HNF4α mRNA expression was induced in both transfections compared to control cells (Figure 3.15). Further investigation is warranted to determine if media supplements could be utilised to further enhance CYP3A4 activity and expression by PGC1α.

Gadd45β positively regulates apoptosis, preventing the proliferation of damaged cells following exposure to xenobiotics (316). Ligands of the NRs, CAR and PXR, directly induce Gadd45β independent of two alternative pathways: transforming growth factor beta (TGF-β) activation initiated by Smad3 and Smad4 (317) or nuclear factor kappa-light-chain-enhancer of activated B cells (NF-κB) activation via upstream regulatory regions (12). Previous reports have found Gadd45β-/- mice compensate for the lack of co-activator by over expressing other co-activators, for example, NCOA1 and mediator complex subunit 1 (Med1) (202). However, this mechanism was not observed here or in Chapter 2. Transfection of Gadd45β in HepG2 cells positively upregulated the mRNA expression of PXR and CYP3A4 but no effect was observed for CAR, suggesting the primary target of Gadd45β is PXR. Gadd45β transfected cells displayed a similar induction profile upon RIF treatment for PXR and HNF4, whereas Gadd45β mRNA expression was not affected (Figure 3.15).

Two critical objectives required for successful transfection of Gadd45β and PGC1α in HepG2 cells were to increase Gadd45β and PGC1α mRNA and protein expression significantly, and to ensure specificity to Gadd45β and PGC1α to ultimately produce a cell line with a CYP3A4 phenotype similar to primary human hepatocytes. Figure 3.6 shows Gadd45β and PGC1α mRNA were increased to ~110% of the primary human hepatocytes following treatment with individual plasmid DNA for 24 h. When

transfected as a complex for 24 h, mRNA expression was ~100% of the primary human hepatocytes (Figure 3.7). In the current study, Gadd45β, PGC1α and complex transfections were screened against 40 genes to determine off-target effects (Figure 3.14). Similar to previous work, 10 genes were not detected in the analysis (89, 261, 273, 309, 310) and no major differences in mRNA were observed for genes that were not directly linked (according to the literature) to Gadd45β and PGC1α. The transfections were selective to CYP3A4 in comparison to previous studies that upregulated numerous isoforms (95, 96, 288, 309). In accordance with the findings of other groups (96, 288, 318), PXR, HNF4α, Gadd45β, PGC1α and CYP3A4 mRNA expression was, as expected, greatly increased in transfected HepG2 cells. In contrast, the co-repressor HDAC1 was reduced to mRNA levels similar to primary human hepatocytes, suggesting a negative feedback loop was in effect. In contrast to prior studies, similar to the primary human hepatocytes, all 6 genes listed above, were induced following treatment with the potent CYP3A4 inducer RIF (Figure 3.15) (288). These data demonstrate clearly that the current complex and single transfections can specifically increase Gadd45β and PGC1α mRNA, and protein with no overt off-target effects. Therefore, the transfections used in this study appear to be more specific than those previously applied.

Expression of hepatocyte nuclear factor 1 (HNF1) is regulated by HNF4α (319). HNF1 mediates the expression of hepatospecific features such as fibrinogen and albumin (320, 321). Thus, to determine the restoration extent of hepatospecific function and phenotype, future work should analyse the secretion of these proteins in the transfected cells.

Figure 3.9 and Table 3.2 show Gadd45β and PGC1α protein was increased to ~89% of the primary human hepatocytes following treatment with plasmid DNA for 24 h. Specific to protein expression, transfection of HepG2 cells with Gadd45β resulted in an increase of PGC1α protein, and *vice versa*. However, when transfected as a complex, an additive effect was observed. The exact mechanism of this process requires further investigation, but post-translational effects may play a role that result in stabilisation of the protein with no change in mRNA.

Preliminary investigation of CYP3A4 activity was assessed using a CYP3A4 Vivid probe assay (Figure 3.10). In comparison to control HepG2 cells (NTCO), CYP3A4 activity was increased by 54% in complex transfected HepG2 cells but 38% less activity compared to primary human hepatocytes (Table 3.3). In contrast, Novotna *et al.,* (271) and Martinez-Jimenez *et al.,* (96) could not increase CYP3A4 activity or mRNA expression in their stably transfected HepG2 cells with PGC1α. Whilst both groups achieved restoration of PGC1α mRNA expression it should be noted the transfections optimised were for the generation of a stable cell line, in contrast to transient transfections herein. Furthermore, the aim of this work was to achieve mRNA expression similar to the primary human hepatocytes rather than over-expressing the gene (in contrast to Martinez-Jimenez *et al*., (96)). It should also be noted the data generated by Novotna *et al*., (271) compared transfections to control HepG2 cells rather than primary human hepatocytes. Further work utilised the specific CYP3A4 substrate, MDZ to determine CYP3A4 activity by the production of 1-hydroxymidazolam in single and complex transfected cells (Figure 3.12). CYP3A4 responded significantly to Gadd45β and PGC1α transfections with production of 1-hydroxymidazolam similar to the levels observed by primary human hepatocytes.

Comparable to the mRNA expression but in contrast to the protein expression, complex transfected cells displayed no additive effect. However, the complex cells responded significantly to the CYP3A4 inducer, RIF, with a dose dependent response. The single transfections did not portray the same pattern with induction observed at 10 μM for Gadd45β and 5 μM for PGC1α. It is interesting to note that although the single transfections resulted in higher mRNA expression and activity, the complex transfection maintained and enhanced the cell induction potential similar to the primary human hepatocytes.

The lack of exact correlations between Gadd45β and PGC1α mRNA levels and the target gene, CYP3A4, may be a consequence of: 1) the initially low expression of CYP3A4 in HepG2 cells that may not be restored sufficiently by over expressing just two co-activators; other key co-regulators may still be absent or over expressed; 2) the adenoviral vector expression of Gadd45β and PGC1α are different from the endogenously expressed mRNA. The distinct 3' and 5' untranslated regions (introns) that govern translation efficiency may differ, leading to discrepancies between the protein and mRNA levels in the transfected and control cells.

CYP3A4 is the main CYP isoform in the liver, responsible for metabolising over 50% of therapeutically administered drugs (41). Individual variability in the metabolism of CYP3A4 substrates can result in toxicity, therapeutic failure or tolerance and may be a consequence of single nucleotide polymorphisms (SNPs). Hence, SNPs altering the expression of co-activators Gadd45β and PGC1α could influence CYP3A4 expression and activity. Further analysis is warranted to identify any co-regulator SNPs that may

contribute significantly to CYP3A4 expression and this could be preliminarily investigated using the approach presented here.

In conclusion, this chapter highlights the importance of rigorous optimisation of assay conditions to utilise key technologies to their full potential. In this case, a transfection method was developed to specifically increase Gadd45β and PGC1α expression in HepG2 cells to produce a cell line with a CYP3A4 phenotype, similar to primary human hepatocytes without significant off-target effects. The significant roles of NR co-activators in sustaining NR and hence CYP3A4 expression, are reinforced herein along with the emphasis that NR co-regulators work in concert to regulate gene expression. The overall strategy can be employed for other proteins of interest such as ABCB1 or OATP1B1, which clearly utilise different mechanisms. It is particularly interesting for OATP1B1, which was undetectable here but is an essential pre-requisite for uptake and subsequent CYP3A metabolism. In addition, knock-out of NR co-repressors may be of benefit to further enhance CYP3A4 activity or induction response. Further work to produce a stable cell line expressing Gadd45β and PGC1α could allow future application of this strategy in determining CYP3A4 mediated DDIs in early drug discovery.

CHAPTER 4

The use of siRNA to dissect the relative contribution of OATP1B1 to the hepatic uptake of xenobiotics

4.1 Introduction

Perhaps the two most critical tasks for drug metabolism departments are to predict human pharmacokinetics and dose accurately (307) and to provide a realistic assessment of the potential for new chemical entities (NCE) to cause drug-drug interactions (DDIs)(322). Historically, many of these evaluations have focused on cytochrome P450's (CYPs) but it has become evident over the last decade that transporters can play a significant role in the disposition of many drugs (278).

The organic anion transporting polypeptides (OATPs) have received considerable attention since they have been shown to mediate the sodium-independent uptake of a broad array of organic amphiphilic compounds including bile acids, thyroid hormones, antibiotics and anti-hypertensives (41). In addition, the inhibition of OATPs has been implicated in a number of DDIs where drugs such as cyclosporine have been shown to significantly increase (up to 20-fold) the plasma exposure of a number of drugs including atorvastatin (323), lovastatin (324), pravastatin (325, 326), rosuvastatin (327) and pitavastatin (328). While CYP3A4 may contribute to the increase in plasma exposure observed for atorvastatin and lovastatin, the lack of involvement of this isoform in the metabolism of rosuvastatin, pitavastatin or pravastatin suggests that the inhibition of OATPs is a more likely cause for these DDIs (329).

Human embryonic kidney cell lines heterologously expressing relevant OATP isoforms have been commonly used to detect OATP inhibitors (13, 330, 331). However, a robust characterisation of the cell line and selection of an appropriate control substrate has been shown to be critical in obtaining clinically relevant data

(13, 332). Furthermore, several groups have now started to utilise the emerging OATP1B1 inhibition data available to create *in silico* models (13, 331).

In addition to their use in determining inhibitors of OATPs, recombinant cell lines expressing OATP1B1, OATP1B3 and OATP2B1 have been invaluable in elucidating the major role they play in the hepatic uptake of anionic drugs (333). Mutation studies have identified both the transmembrane domain (334) and even the key amino acid residues that confer OATP activity (335). However, the broad substrate overlap between OATP1B1 and OATP1B3 in particular has hampered the identification of specific substrates for individual isoforms (331).

Many groups have utilised hepatocytes to obtain an overall assessment of hepatic uptake (336). Soars *et al*., (262) developed a high-throughput "media loss" assay in suspended hepatocytes to predict the clearance of 36 drugs where hepatic uptake was suspected to be involved in drug disposition. Subsequent studies have used the more traditional "oil spin" technique to confirm the utility of this approach by expanding datasets (337, 338) and providing a more detailed analysis of the individual kinetic processes involved (339). Several groups have shown that uptake data can be used to predict the profile of drugs such as atorvastatin, (340) and valsartan (341) as well as clearance. Most recently, Jones *et al*., (2012) used sandwich-cultured hepatocytes in conjunction with physiologically based pharmacokinetic modelling to incorporate efflux processes into these predictions.

Attempts to attribute hepatic uptake to individual transporters have primarily focused on the relative activity factor (RAF) approach, which has been used successfully in

the CYP field (342). Hirano et al., (2004) used estrone-3-sulfate (E3S) and cholecystokinin 8 (CCK-8) as probes for OATP1B1 and OATP1B3, respectively. However, the data obtained using this technique has yet to be confirmed using an alternative methodology. In addition, the RAF approach requires a specific substrate to elucidate the role of a particular transporter, which is often not available. Therefore, an investigation into other potential tools such as siRNA may facilitate our understanding in this area.

The promise of siRNA as a gene knockdown technique was highlighted by the seminal study of Fire et al., (1998). In subsequent years, siRNA has been used as a powerful tool to confirm target validation and more recently in the explosion of RNA interference therapeutics, which are currently under development for respiratory, cardiovascular, and oncological diseases (343, 344). However, the use of this technique in the drug disposition area has primarily focused on the inhibition of key efflux transporters such as P-glycoprotein and breast cancer resistance protein expressed either in recombinant cell lines (345) or in sandwich cultured hepatocytes (346). To date, the number of studies investigating the use of siRNA to knockdown drug transporters in human hepatocytes has been limited and often the level of functional knockdown obtained in such studies has precluded their use in assigning the individual transporter responsible for hepatic uptake (347). Previous studies with AtuFect01-based siRNA lipoplexes have demonstrated effective and specific mRNA and protein knockdown (348-350). Of importance, the small quantities of AtuFect01 required to complex the siRNA are important since the three positive charges of siRNA are able to bind one molecule of AtuFect01 correlating to reduced toxicity (350).

The aims of this chapter were two-fold: to develop and characterise a robust *in vitro* assay to selectively inhibit OATP1B1 in human hepatocytes using a siRNA approach; and to determine the relative role of OATP1B1 in the hepatic uptake of a range of drugs.

4.2 Methods and Materials

4.2.1 Materials

All chemicals and reagents were of the highest available grade. Olmesartan, valsartan, rosuvastatin, atorvastatin and pitavastatin were sourced from Sequoia Research Products Ltd. (Oxford, UK). Lopinavir was supplied by Moravec Chemicals (Brea, CA). [^{3}H]-estrone-3-sulfate (specific activity 2120 GBq/mmol) was purchased from PerkinElmer Life Sciences (Boston, MA, USA). AtuFECT01 was kindly supplied by Silence Therapeutics (Berlin, Germany). Cryopreserved hepatocyte recovery medium (CHRM® media), Williams E Media, plating and supplement media, OATP siRNA duplex oligoribonucleotides, Quant-iT Ribogreen Assay kit, cryopreserved human hepatocytes (same donors used in chapter 2; Table 2.1), plating cocktail, maintenance cocktail, RNase free DNase kit, Vivid® CYP450 screening assay and 96-well collagen coated plates were purchased from Invitrogen Ltd (Paisley, Scotland, UK). WST-1 reagent was purchased from Roche Applied Science (Hertfordshire, UK). RNeasy 96 kit and QuantiTect Probe one step RT-PCR Master Mix Kit was obtained from Qiagen Ltd (Crawley, UK). 96-well plates pre-coated with collagen IV were purchased from BD Biosciences (Oxford, UK). All other chemicals were purchased from Sigma-Aldrich (Poole, Dorset, UK) unless otherwise indicated.

Donor	Viability	Gender	Donor Demographics	
			Age/Race	Characteristics
Hu8089	91 %	Male	36year old, Caucasian	Alcohol abuse, smoking
Hu8085	97 %	Female	1 year old, Caucasian	No alcohol abuse, no smoking
Hu4244	89 %	Male	3 year old, Caucasian	No alcohol abuse, no smoking

Table 4.1 Human donor demographics of the cryopreserved hepatocytes used in the study

4.2.2 Thawing and plating of cryopreserved primary human hepatocytes

Cryopreserved human hepatocytes were thawed as previously described in section 2.2.3. Donor demographics are detailed in Table 4.1.

4.2.3 Cell viability

Cell viability and density of primary human hepatocytes were calculated using trypan blue exclusion as described in section 2.2.4.

4.2.4 Plating and maintaining primary human hepatocytes

Cells were seeded in 96-well plates pre-coated with collagen at a density of 4.5 x 10^4 cells/well and incubated for 24 h at 37 ºC with 5% CO_2 and 95% humidity as described in section 2.2.5. Media was replaced with 100 µl William's E media supplemented with optiMEM media and a maintenance cocktail of 0.1 µM dexamethasone, a 0.5% solution of penicillin-streptomycin, 2 mM GlutaMAX™, 15 mM HEPES, 6.25 µg/ml human recombinant insulin, 6 µg/ml human transferrin, 6 µg/ml selenous acid, 1.25 µg/ml bovine serum albumin and 5.35 µg/ml linoleic acid (CHRM® supplement B) (Invitrogen), 1 h prior to siRNA treatment. The same volume of optiMEM media was added to the non-transfected control cells (NTCO).

4.2.5 Determining cell density

To ensure the cells were plated at an optimum density varying numbers of cells (15,000, 30,000, 45,000, 75,000 and 100,000) were plated in a 96-well collagen coated plate and incubated at 37 ^oC, 5% CO_2 humidified incubator for four hours. Density was assessed using a light microscope to determine confluence and comparison of [^{3}H] E3S uptake.

4.2.6 OATP1B1 siRNA in plated primary human hepatocytes

For siRNA treatment, AtuFect01 and OATP1B1 siRNA were vortexed for 1 min in a polystyrene bijou and incubated for 30 min at 37 ºC prior to addition to the cells (final concentration of AtuFect01 was 1 µg/ml and siRNA was 40 nM). The OATP1B1 siRNA oligomer was purchased as a kit from Sigma Aldrich. The kit contained 3 siRNA sequences for OATP1B1 and the first sequence quoted below achieved the greatest inhibition of OATP1B1.

OATP1B1 siRNA sequences:

A. 5'-
CACUAUCAGGAUAACUCCUACUGAUAUCAGUAGGAGUUAUCCUGAUAG
UG-3'

B. 5'-
CCUCACAUGUCAUGCUGAUUGUUAAUUAACAAUCAGCAUGACAUGUGAGG
-3'

C. 5'-
GGCAGAUAGUGAAACACAUUGUUAAUUAACAAUGUGUUUCACUAUCUGCC
-3'

Cells were incubated with AtuFect01:siRNA complex at 37 ºC with 5% CO_2 and 95% humidity from 4 to 192 h. For the 192 h timepoint, cells were treated with lipid/siRNA complex for 144 h and media was replaced with control media for the subsequent 48 h to ensure cell viability. All experiments were conducted in triplicate.

Four control conditions were also included: maintenance media (Non-transfected control (NTC)), optiMEM control (Non-transfected optiMEM control (NTCO)), phosphatase and tensin homolog (PTEN) (siRNA positive control) and luciferase (negative control). 25 µl of each condition was added to the maintenance media, which provided the required nutrients to maintain cell viability and incubated at 37 ^{o}C, 5% CO_2 humidified incubator for the required time.

Phosphatase and tensin homolog (PTEN) and luciferase (sequences below) were used as positive and negative controls, respectively, throughout the experiment.

PTEN sequence: 5' - AGUUGUUGGGUUACACCGUGAUA - 3'

Luciferase product number: AM4629 (LifeTechnologies/Ambion)

4.2.7 Assessment of cell viability

Primary hepatocytes were seeded in a 96-well plate and cell viability was measured using a fluorometric assay. Mitochondrial activity was assessed by the cleavage of the tetrazolinium salt, 4-[3-(-4-Iodophenyl)-2-(4-nitrophenyl0-2H-5-tetrazolio]-1,3-benzene disulphonate (WST-1) by dehydrogenase (according to the manufacturer's protocol). Maintenance media was aspirated to waste and cells were incubated with 100 µl of WST-1 (1 mL WST-1 reagent/10 mL maintenance media) at 37 ºC, 5% CO_2, 95% humidity, for 1 h. Each plate contained samples, blanks and controls with three replicates each and absorbance was measured at 450 nm using a SPECTRAmax v2.1.28 absorbance reader. Cells were assessed for toxicity using WST-1 reagent at all time points.

4.2.8 Isolation of mRNA

β-mercaptoethanol (100 µl) was added to the cells following the removal of the WST-1 reagent. A further 100 µl of RNase free 70% ethanol was added to each well, mixed using a pipette and transferred to a 96-well RNeasy plate. The plate was centrifuged at 5600 x g for 4 min at room temperature and the subsequent flow-through was discarded. The DNase I pellet was dissolved in 550 µl of RNase free water, inverted to allow mixing and 3850 µl of RDD buffer was added. DNase I enzyme (80 µl) was pipetted into each well and left to incubate at room temperature for 15 min. RW1 buffer (800 µl) was then added to each well, the plate was again incubated at room temperature for 5 min and centrifuged at 5600 x g for 4 min. The flow-through was discarded, 800 µl of RPE buffer/80% ethanol was added to each well, centrifuged at 5600 x g at room temperature for 5 min. This step was completed twice with a centrifugation of 10 min on the second wash. The RNA was then eluted into an elution microtube rack. RNase free water (50 µl) was added to the membrane of each well, incubated at room temperature for one minute and centrifuged at 5600 x g at room temperature for 4 min. This step was completed twice. The flow-through was labeled and stored at -80^{o}C for future use.

4.2.9 RNA Quantification

Total RNA was quantified fluorometrically using a Quant-iT Ribogreen RNA assay kit. The 20X TE buffer (10 mM Tris-HCl, 1mM EDTA, pH 7.5) was diluted with RNase free H_20 and 95 µl added to a ribogreen assay plate. The mRNA was aliquot to each well (5 µl). The provided standard solution (20 µl) was added to wells for a standard curve of which sample mRNA was serial diluted and aliquot (5 µl). A 1 in 150 dilution of the ribogreen dye was completed with diluted TE buffer. The

ribogreen dye (100 µl) was added to each well, the plate was wrapped in foil away from light and incubated at room temperature for 5 min. The Soft Max Pro Plate Reader was used to read the fluorescence produced with excitation at 485nm and emission at 530nm.

4.2.10 Quantitative real-time polymerase chain reaction analysis

Purified mRNA samples (2 µl) were analysed by one-step quantitative real time RT-PCR performed on an Mx3005P real-time thermo cycler with MxPro software (Stratagene, La Jolla, CA). The mRNA samples were thawed on ice and 2 µl added to a 96-well Abgene semi-skirted PCR plate. Qiagen's One Step Quantitect Probe RT-PCR kit was used to reverse transcribe the mRNA to cDNA and amplify the gene. qPCR solutions were prepared for each well as follows; 10 µM probe, 10 µM forward and reverse primer (purchased from Eurogentec, sequences below), 12.5 µl 2X master mix, 10.075 µl RNase free H_20 and 0.25 µl reverse transcriptase to make a final volume of 23 µl. Primers and probe sequences were as follows:

OATP1B1 primer and probe sequences:

Forward primer - 5'-CTGGGTTTCCACTCAATGGT–3'

Reverse primer - 5'-TCAATCAGAGCCCCAAAATA–3'

Probe (FAM) - 5'-CGAGCACTAGGAGGAATTCTAGCTCCAA–3'

No template controls, *no reverse transcriptase controls* and a standard curve were generated in duplicate to ensure no contamination, specific amplification and maximum amplification, respectively. Quantification was recorded in real time using a Stratgene MXP3005P Real Time Thermocycler. PCR conditions were 15 min at 95

^{o}C (to activate polymerase, denature cDNA and initiate PCR) followed by 50 cycles of 15 sec at 94 ^{o}C (denaturation) and 60 seconds at 60 ^{o}C (annealing/extension of the product). Fluorescence was collected at the end of each cycle. Relative quantification of gene expression was determined by comparing cycle threshold values to that obtained from a standard curve prepared from untreated controls. Data were normalised to total RNA determined by Ribogreen assay.

4.2.11 Microfluidic Assay

mRNA (100 ng per reaction) was added to custom Taqman microfluidic plates and gene expression normalised and quantified as described in section 3.2.21.

Table 4.2

Gene	Description	Alias	Chromosomal location	Reference sequence	Regulatory function	Reference
NR1I2	Nuclear receptor subfamily 1, group I, member 2	PXR	3q12-q13.3	NM_033013.2	Nuclear receptor	Meyer zu Schwabedissen *et al.,* 2009
NR1H4	Nuclear receptor subfamily 1, group H, member 4	RIP14	12q23.1	NM_005123.3	Nuclear receptor	Meyer zu Schwabedissen et al., 2010
NR1I3	Nuclear receptor subfamily 1, group I, member 3	CAR	1q23.3	NM_005122.4	Nuclear receptor	Meyer zu Schwabedissen et al., 2009
NR1I1	Nuclear receptor subfamily 1, group I, member 1	VDR	12q13.11	NM_000376.2	Nuclear receptor	Lindh *et al.,* 2011
NR2A1	Nuclear receptor subfamily 2, group A, member 1	HNF4A	20q13.12	AY680696.1	Nuclear receptor	Kamiyama *et al.,* 2007
PPARGC1A	Peroxisome proliferator activated receptor gamma coactivator 1 alpha	PGC1α	4p15.1	NM_013261.3	Nuclear receptor co-regulator	Itoh *et al.*, 2006
NCoA1	Nuclear receptor coactivator 1	SRC1	2p23	NM_147233.2	Nuclear receptor co-regulator	Muangmoonchai *et al.,* 2001
NCoA2	Nuclear receptor coactivator 2	GRIP-1	8q13.3	NM_006540.2	Nuclear receptor co-regulator	di Masi *et al.,* 2009
NCoA6	Nuclear receptor coactivator 6	PRIP	20q11	NM_014071.3	Nuclear receptor co-regulator	Surapureddi *et al.,* 2008
NCOR1	Nuclear receptor co-repressor 1	TRAC1	17p11.2	NM_006311.3	Nuclear receptor co-regulator	Moore *et al.,* 2002
HDAC1	Histone deacetylase 1	HD1	1p34	NM_004964.2	Nuclear receptor co-regulator	Bae *et al.,* 2004
HDAC2	Histone deacetylase 2	RPD3	6q21	NM_001527.3	Nuclear receptor co-regulator	Ponugoti *et al.,* 2007
HSP90AA1	Heat shock protein 90kDa alpha (cytosolic), class A member 1	Hsp90	14q32.33	NM_005348.3	Nuclear receptor co-regulator	Squires *et al.,* 2004
TMTC3	Transmembrane and tetratricopeptide repeat containing 3	SMILE	12q21.33	NM_181783.3	Nuclear receptor co-regulator	Xie *et al.,* 2009
CYP3A4	Cytochrome P450, family 3, subfamily A, polypeptide 4	CYP3A3	7q21.1	NM_017460.5	Metabolism enzyme	Martinez-Jimenez *et al.,* 2007

Gene	Description	Alias	Chromosomal location	Reference sequence	Regulatory function	Reference
CYP3A5	Cytochrome P450, family 3, subfamily A, polypeptide 5	CP35	7q21.1	NM_000777.3	Metabolism enzyme	Niemi *et al.,* 2005]
CYP2B6	Cytochrome P450, family 2, subfamily B, polypeptide 6	CPB6	19q13.2	NM_000767.4	Metabolism enzyme	Wang *et al.,* 2003
CYP2D6	Cytochrome P450, family 2, subfamily D, polypeptide 6	CPD6	22q13.1	NM_001025161.1	Metabolism enzyme	Westerink *et al.,* 2007
CYP1A2	Cytochrome P450, family 1, subfamily A, polypeptide 2	CP12	15q24.1	NM_000761.3	Metabolism enzyme	Landi *et al.,* 1999
CYP2C9	Cytochrome P450, family 2, subfamily C, polypeptide 9	CYP2C10	10q24.1	NM_000771.3	Metabolism enzyme	Holstein *et al.,* 2012
CYP2C19	Cytochrome P450, family 2, subfamily C, polypeptide 19	CYP2C	10q24	NM_000769.1	Metabolism enzyme	Goldstein *et al.,* 1994
CYP2E1	Cytochrome P450, family 2, subfamily E, polypeptide 1	CYP2E	10q24.3	NM_000773.3	Metabolism enzyme	Nelson *et al.,* 2004
UGT2B4	UDP glucuronosyltransferase 2 family, polypeptide B4	UGT2B11	4q13	NM_021139.2	Metabolism enzyme	Congiu *et al.,* 2009
UGT2B7	UDP glucuronosyltransferase 2 family, polypeptide B7	UGT2B9	4q13	NM_001074.2	Metabolism enzyme	Ohtsuki *et al.,* 2012
UGT2B15	UDP glucuronosyltransferase 2 family, polypeptide B15	UGT2B8	4q13	NM_001076.3	Metabolism enzyme	Ohtsuki *et al.,* 2012
UGT1A1	UDP glucuronosyltransferase 1 family, polypeptide A1	UGT1A	2q37	NM_000463.2	Metabolism enzyme	Fisher *et al.,* 2001
UGT1A4	UDP glucuronosyltransferase 1 family, polypeptide A4	UGT1D	2q37	NM_007120.2	Metabolism enzyme	Ji *et al.,* 2012
UGT1A9	UDP glucuronosyltransferase 1 family, polypeptide A9	UGT1AI	2q37	NM_021027.2	Metabolism enzyme	Zhou *et al.,* 2013
SLCO1B1	Solute carrier organic anion transporter family, member 1B1	OATP1B1	12p	NM_006446.4	Influx transporter	Shitara *et al.,* 2011
SLCO1B3	Solute carrier organic anion transporter family, member 1B3	OATP1B3	12p12	NM_019844.3	Influx transporter	Shitara *et al.,* 2011
SLCO2B1	Solute carrier organic anion transporter family, member 2B1	OATP2B1	11q13	NM_007256.4	Influx transporter	Fahymayr *et al.,* 2010

Gene	Description	Alias	Chromosomal location	Reference sequence	Regulatory function	Reference
SLC10A1	Solute carrier family 10 (sodium/bile acid cotransporter family), member 1	NTCP	14q24.1	NM_003049.3	Influx transporter	Funk *et al.,* 2008
SLC22A7	Solute carrier family 22 (organic anion transporter), member 7	OAT2	6p21.1	NM_153320.2	Influx transporter	Funk *et al.,* 2008
SLC22A1	Solute carrier family 22 (organic cation transporter), member 1	OCT1	6q25.3	NM_153187.1	Influx transporter	Fahrmayr *et al.,* 2010
ABCG2	ATP-binding cassette, sub-family G (WHITE), member 2	BCRP	4q22	NM_004827.2	Efflux transporter	Muller *et al.,* 2011
ABCB11	ATP-binding cassette, sub-family B (MDR/TAP), member 11	BSEP	2q24	NM_003742.2	Efflux transporter	Stieger *et al.,* 2011
ABCB1	ATP-binding cassette, sub-family B (MDR/TAP), member 1	P-gp	7q21.12	NM-000927.4	Efflux transporter	Muller *et al.,* 2011
ABCC2	ATP-binding cassette, sub-family C (CFTR/MRP), member 2	MRP2	10q24	NM_000392.3	Efflux transporter	Ieri *et al.,* 2009
ABCC3	ATP-binding cassette, sub-family C (CFTR/MRP), member 3	MRP3	17q22	NM_003786.3	Efflux transporter	Le Vee *et al.,* 2009
ABCC6	ATP-binding cassette, sub-family C (CFTR/MRP), member 6	MRP6	16p13.1	NM_001171.5	Efflux transporter	Keppler 2011

Table 4.2 List of genes including description, function, chromosomal location and reference sequence analysed in the microfluidic assay

4.2.12 Uptake assays using primary human hepatocytes

Prior to the assay, cells were washed 3 times with hepatocyte buffer (Dulbecco's modified Eagle's medium; 1 litre powder supplemented with 2.34 g/l HEPES and 0.4 g/l D-fructose, pH 7.4) pre-warmed to 37ºC. After the third wash, cells were pre-incubated at 37ºC for 60 min in 200 µl of pre-warmed Krebs Henseleit solution; uptake assays were initiated with the addition of substrate prepared in hepatocyte buffer. [^{3}H]-E3S final substrate concentration was 5 nM and test substrates were made

to a final concentration of 1 µM. To estimate passive uptake atorvastatin (ATV) was added to the selected wells (at the same time as the probe and test substrates) varying in concentration (0.1-500 µM) to determine complete OATP1B1 inhibition (ATV IC_{50} in hepatocytes was 5.9 µM). In all cases the final concentration of dimethyl sulfoxide (DMSO) did not exceed 1% (v/v). Optimum substrate incubation time was also determined. Optimisation time-points were completed from 15–240 sec. Initial studies showed that the uptake of all substrates investigated was linear under the conditions used. Uptake assays containing [^{3}H]-E3S were terminated after 1 min (2 min for assays containing test substrates) via the addition of ice-cold hepatocyte buffer to ensure the reaction had terminated. Cells were washed a further two times with ice-cold hepatocyte buffer before all buffer was aspirated.

For uptake studies using [^{3}H]-E3S, cells were lysed by incubating with 500 µl of 0.1% (v/v) Triton X-100 for 30 min at room temperature. Following the addition of 5 mL scintillation cocktail, the amount of radioactivity in the cells was determined using a Packard 2200CA Tri-Carb liquid scintillation counter (Packard Instrument Co, Pangbourne, UK). For all other uptake studies cells were lysed by incubating with 500 µl of methanol:acetonitrile (50:50) for 1 min. The samples were placed at -20 ºC for 1 h and then centrifuged at 2000 g for 15 min. 100 µl of the supernatant fraction plus 100 µl of water were transferred to Agilent 96-well microtitre plates for LC-MS/MS analysis (see below).

To calculate the contribution by OATP1B1 the following equation was applied:

$$\text{OATP1B1 Inhibition (\%)} = 1 - \left(\frac{(\text{OATP1B1} - \text{ATV})}{(\text{NTCO} - \text{ATV})} \right) \times 100$$

4.2.13 LC-MS/MS analysis of hepatocyte uptake samples

Mass spectrometric analysis for rosuvastatin, pitavastatin, olmesartan, valsartan, and lopinavir was conducted on a ThermoScientific TSQ Quantum Ultra Mass spectrometer (ThermoScientific, Hemel, UK) using an Accela High pressure Quaternary Pump for separation. Analysis was by multiple reaction monitoring using a heated electrospray ionisation source, in either positive or negative ion mode. Tube lens and collision energy were optimised for each compound.

Assay optimisation and validation for all 5 compounds had already been conducted in house within AstraZeneca, Charnwood, UK. In these analyses, chromatographic separation was achieved using a Waters Acquity UPLC BEH C18 (2.1 x 100 mm, 1.7 μm) column. The mobile phase consisted of water with 0.1% (v/v) formic acid with the organic phase being methanol containing 0.1% (v/v) formic acid. All chromatography was performed using a generic gradient (t = 0 min 5% organic, t = 0.25 min 5% organic, t = 2 min 100% organic, t = 3 min 100% organic, t = 3.1 min 5% organic, t = 4 min 5% organic). The flow rate was set at 0.6 ml/min, with the column temperature set at 60 ºC.

4.2.14 Measurement of CYP3A4 enzyme activity

Primary hepatocytes (4.5 x 10^4/well) were seeded in a black 96-well plate and CYP3A4 activity assessed using a Vivid® CYP450 screening assay as described in Section 2.2.9.

Activity endpoint assay calculation:

CYP3A4 Activity (%)

$$= 1 - \left(\frac{\text{Relative fluorescence of OATP1B1 siRNA treated cells}}{\text{Relative fluorescence of control cells}} \right) \times 100$$

4.2.15 Data analysis

Within the study each assay was conducted in triplicate. To estimate passive transport into human hepatocytes, the OATP1B1 inhibitor atorvastatin was added to incubations at a final concentration of 500 µM. The following equation was used to estimate % inhibition of OATP1B1:

Where OATP1B1 siRNA was defined as uptake of the test compound conducted with cells treated with OATP1B1 siRNA for 144 h, ATV was uptake of test compound with the addition of 500 µM atorvastatin conducted with cells treated with OATP1B1 siRNA for 144 h and NTCO was uptake of test compound conducted with hepatocytes treated with control media.

All optimisation experiments were completed in triplicate using human hepatocyte donor Hu8089. Upon method application and off target assessment experiments were completed in triplicate for all 3 human hepatocyte donors (Table 2.1/4.1).

Normality was assessed using Shapiro Wilk and data were assessed using Mann Whitney for non-normal and unpaired t test for normally distributed data. Results were considered significant if; *, $p < 0.05$; **, $p < 0.01$; ***, $p < 0.001$. The IC_{50} of

atorvastatin was calculated using a non-compartmental model (WinNonLin, version 4.1).

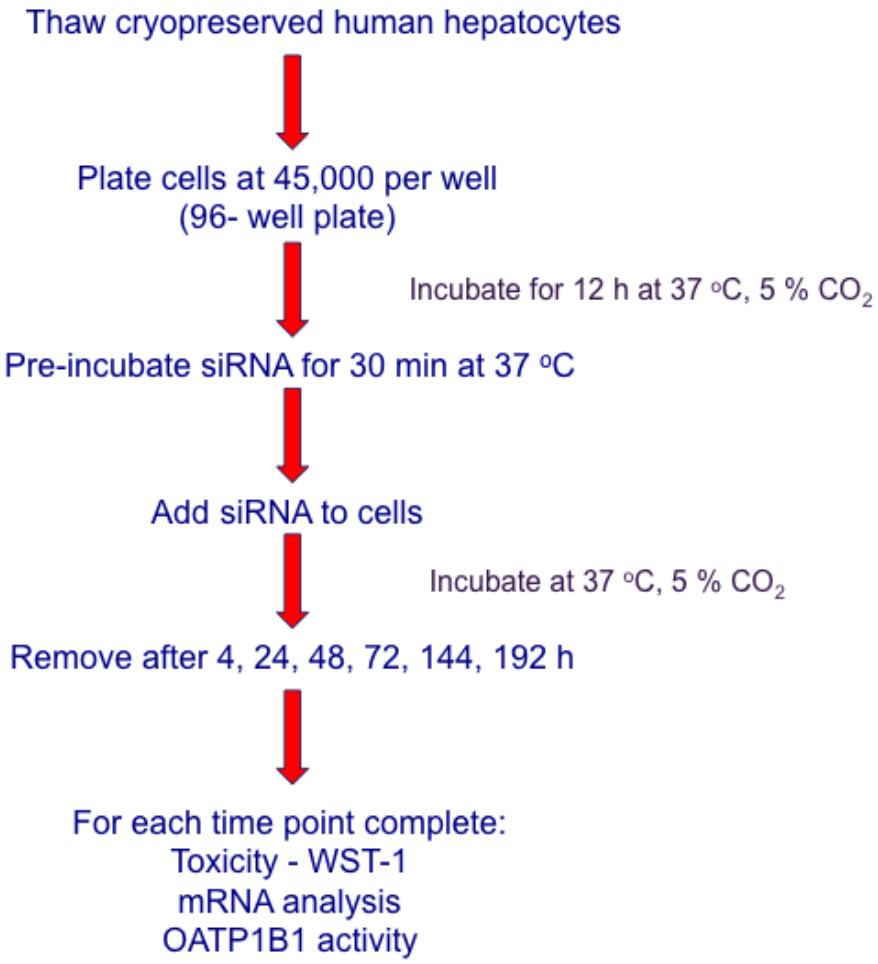

Figure 4.2 Schematic of the siRNA process

4.3 Results

4.3.1 Initial optimisation of siRNA delivery to human hepatocytes using AtuFect01

Initial work focused on assessing the utility of AtuFect01 to deliver siRNA specific to phosphatase and tensin homolog (PTEN) gene. Previous work in the laboratory showed this siRNA could knockdown PTEN in other cell types (data not shown). Therefore, this experiment aimed to validate AtuFect01 delivery of siRNA to primary human hepatocytes. Luciferase was used as a negative control to ensure specific inhibition. Figure 4.3A shows the effect of PTEN siRNA treatment on PTEN mRNA expression after human hepatocytes were exposed to the AtuFect01/siRNA complex for 4, 24, 48 and 72 hours. PTEN mRNA expression decreased with exposure time to the AtuFect01/siRNA complex resulting in a 98% reduction by 72 h, compared to cells which had been incubated with control optimum media (NTCO). Figure 4.3B shows that the decrease in PTEN mRNA over time was not associated with cytotoxicity as assessed by mitochondrial dehydrogenase activity. In subsequent experiments, PTEN was included as a positive control for AtuFect01 and luciferase was used as a negative control.

4.3A

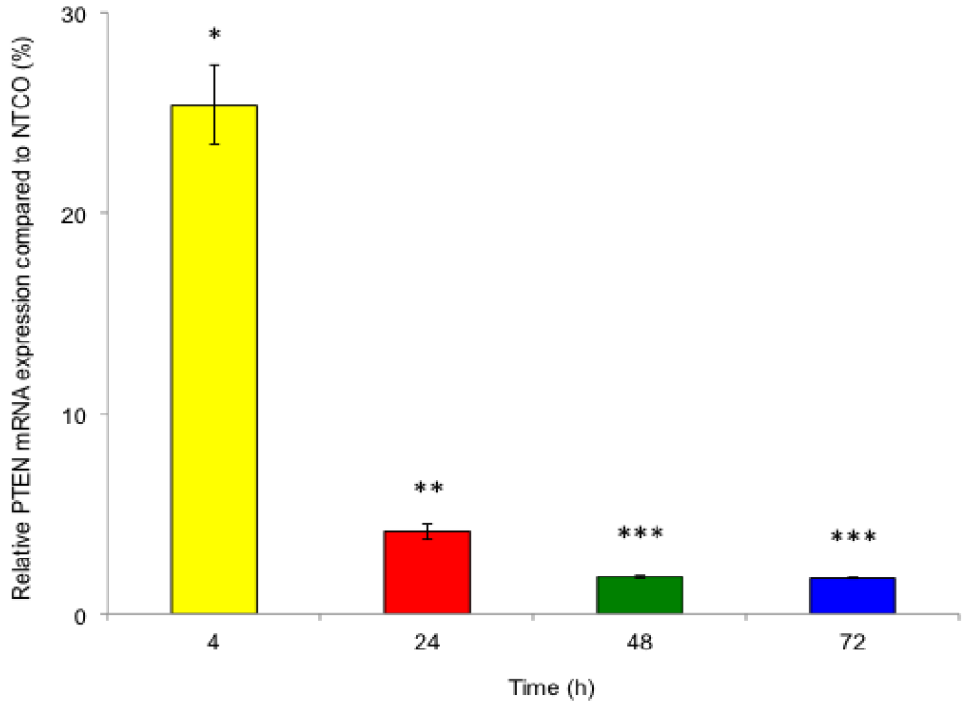

4.3B

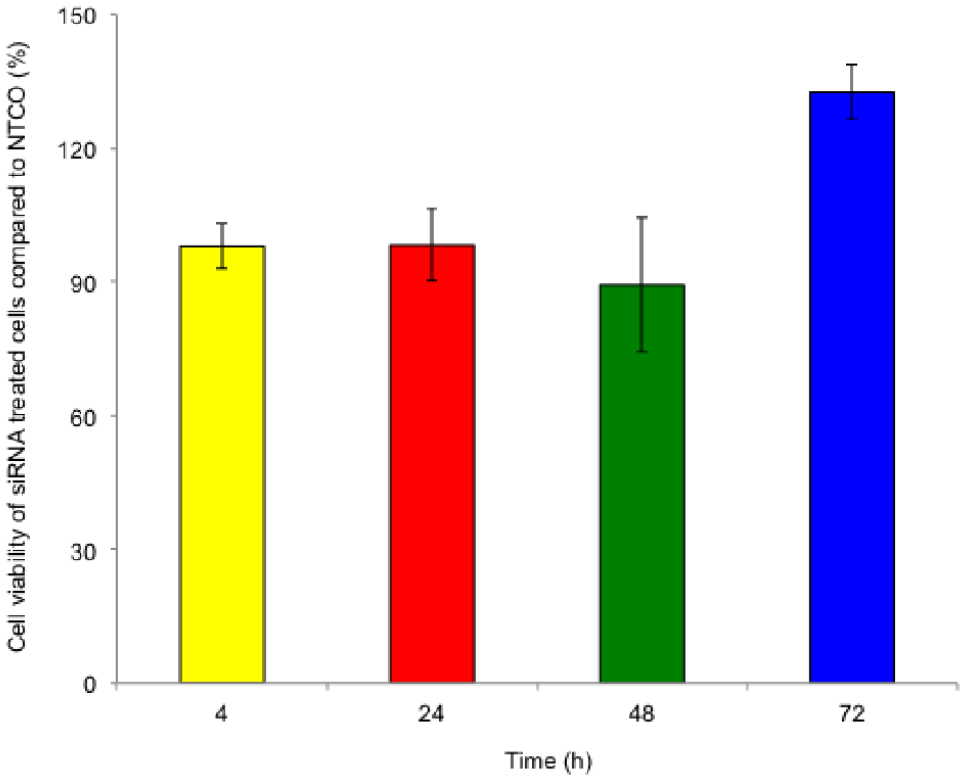

Figure 4.3 The effect of PTEN siRNA treatment on PTEN mRNA (A) and cell viability (B) after treatment for 4, 24, 48 and 72 h relative to non-transfected control-

optiMEM (NTCO). Each bar shows the mean ± S.D. of 3 wells. The conditions were statistically compared using an unpaired T test or Mann Whitney; * = $p < 0.05$, ** = $p < 0.01$,*** = $p < 0.001$.

4.3.2 Initial optimisation of estrone 3 sulfate uptake into human hepatocytes

The significant overlap in substrate selectivity for individual OATP isoforms has hampered the selection of specific OATP1B1 substrates (331, 351). However, it has been suggested that the uptake of E3S at low substrate concentrations may be selective for OATP1B1 (352, 353). Therefore, the uptake of E3S at a final substrate concentration of 5 nM was selected as a probe of OATP1B1 activity. Initial studies investigated the linearity of E3S uptake into hepatocytes with respect to both time and cell density. Uptake was linear over 3 min (Figure 4.4B) and also across the cell densities investigated (15,000 to 45,000 cells per well) (Figure 4.4A). An incubation time of 1 min and a cell density of 45,000 cells/well were chosen for siRNA studies due to a 75% increase in E3S uptake compared to 30,000 cells/well and well confluence was 95% (Figure 4.4).

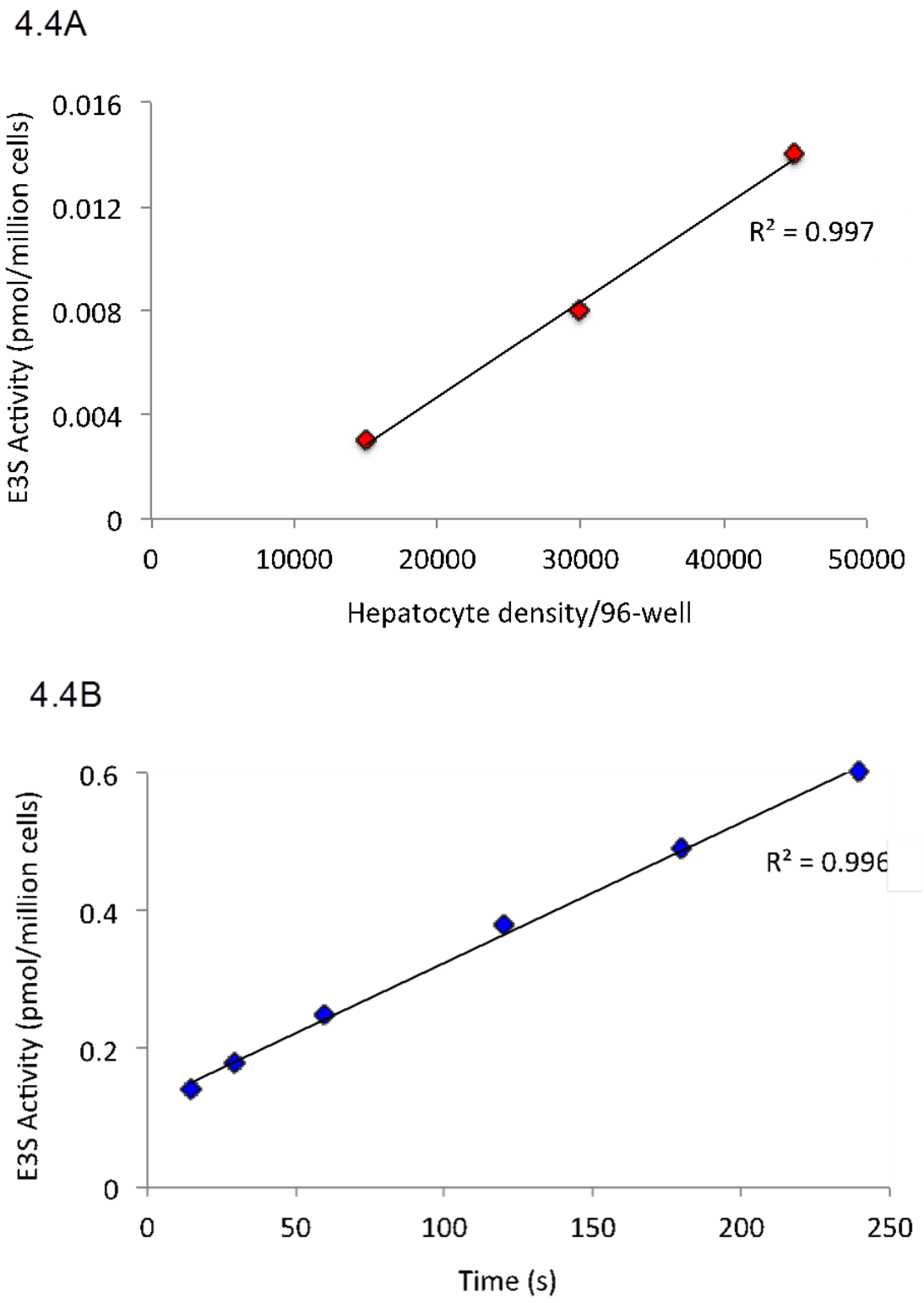

Figure 4.4 Effect of hepatocyte cell and number (A) and incubation time (B) on E3S uptake

Since E3S uptake into human hepatocytes has active and passive components and

siRNA will only knockdown active transport, it was crucial to obtain an estimate of passive uptake. Historically, uptake studies conducted at 4 ^{o}C have been used to give an estimation of passive uptake but recent data have shown this to be inaccurate since membrane permeability varies with temperature (354). Therefore, the use of ATV as a competative OATP1B1 inhibitor to estimate passive permeability was investigated. Initial studies with a range of ATV concentrations (0.1–500 µM) showed that ATV inhibited uptake of E3S into human hepatocytes with an IC_{50} of 5.9 µM (Figure 4.5). The addition of 500 µM ATV in uptake studies completely inhibited the active component of estrone-3-sulfate uptake and these assay conditions were used to estimate the passive permeability component.

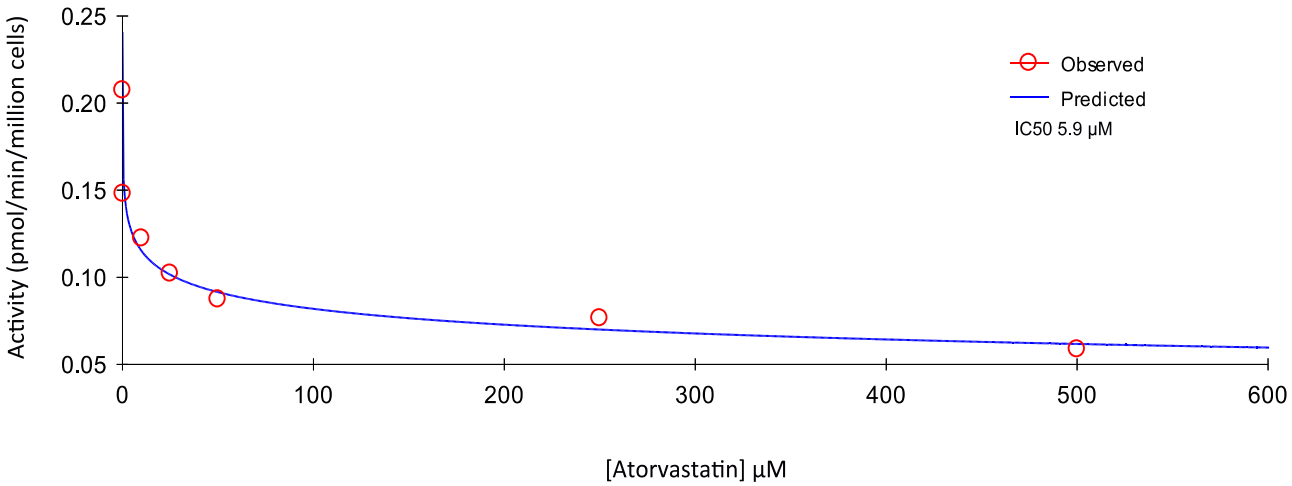

Figure 4.5 Inhibition of E3S uptake in human hepatocytes

4.3.3 Delivery of OATP1B1 siRNA to human hepatocytes

The effect of the lipid/OATP1B1 siRNA complex on human hepatocyte cytotoxicity (Figure 4.6A), OATP1B1 mRNA expression (Figure 4.6B) and uptake of E3S (Figure 4.6C) was assessed over 192 h. Figure 4.6A shows that although cell viability decreased over the time course investigated, even after 192 h, cell viability was

deemed to be within acceptable limits (>80% of controls). OATP1B1 mRNA decreased between 24 and 144 h of exposure to lipid/siRNA complex with a maximal knockdown of 98% observed compared to controls after 144 h (see Figure 4.6B). The uptake of E3S also decreased over 144 h with a 93% decrease in uptake observed at 144 h (see Figure 4.6C). It should be noted that the uptake of E3S into human hepatocytes treated with control media did not decrease over the time course investigated (24-192 h, Figure 4.7C) which agrees with previous studies that showed OATP activity was retained in long-term cultures of human hepatocytes (355).

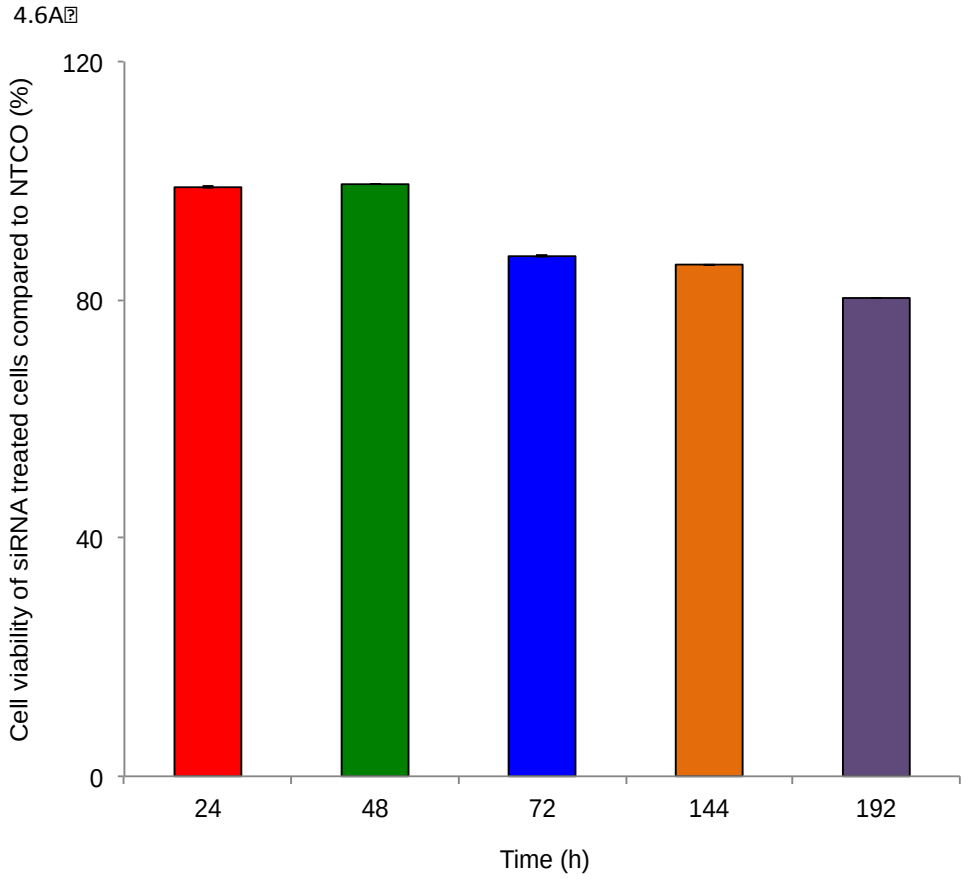

4.6B

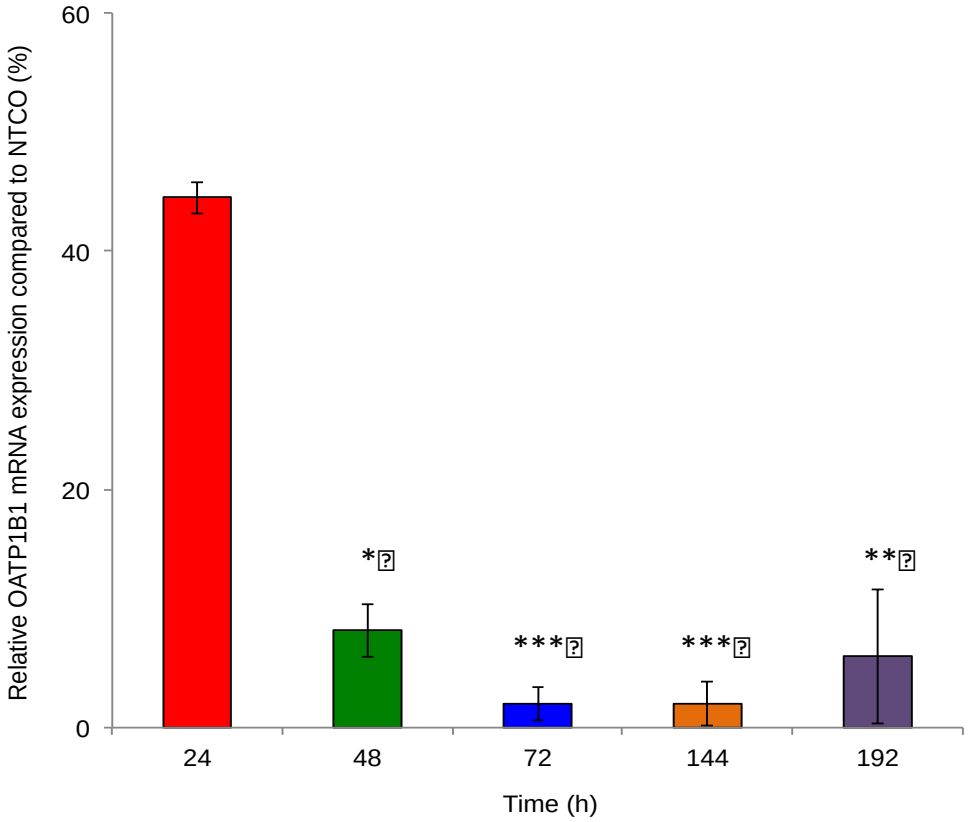
60
40
20
0
Relative OATP1B1 mRNA expression compared to NTCO (%)
*
***
***
**
24
48
72
144
192
Time (h)

4.6C

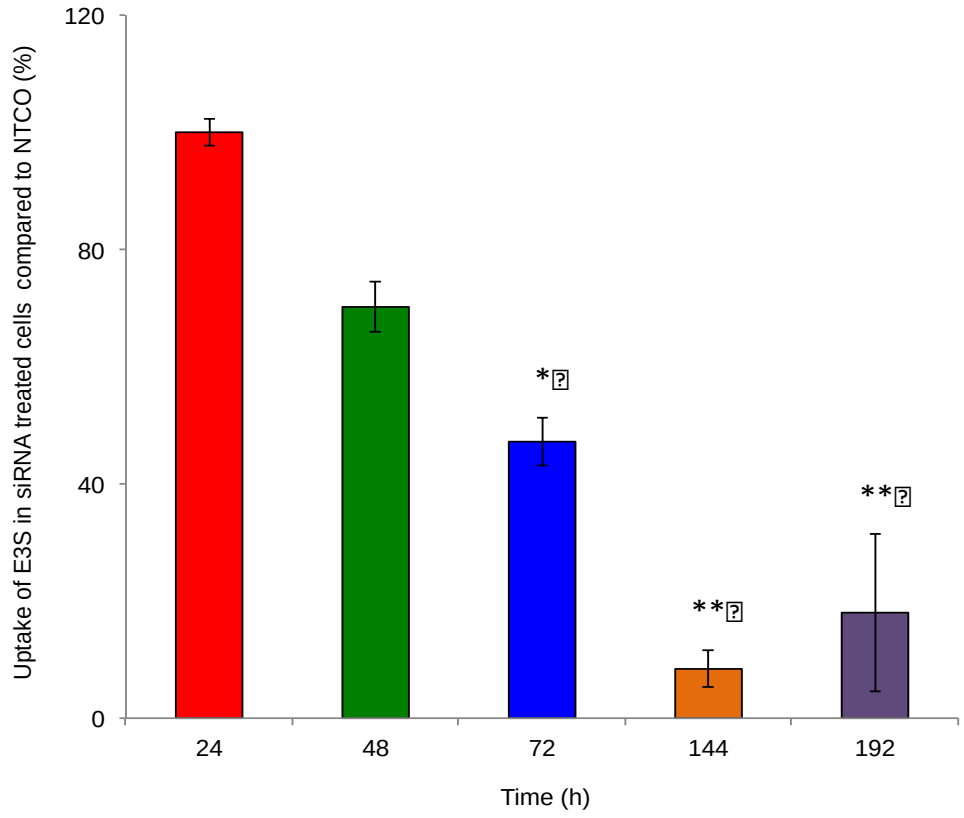
120
80
40
0
Uptake of E3S in siRNA treated cells compared to NTCO (%)
*
**
**
24
48
72
144
192
Time (h)

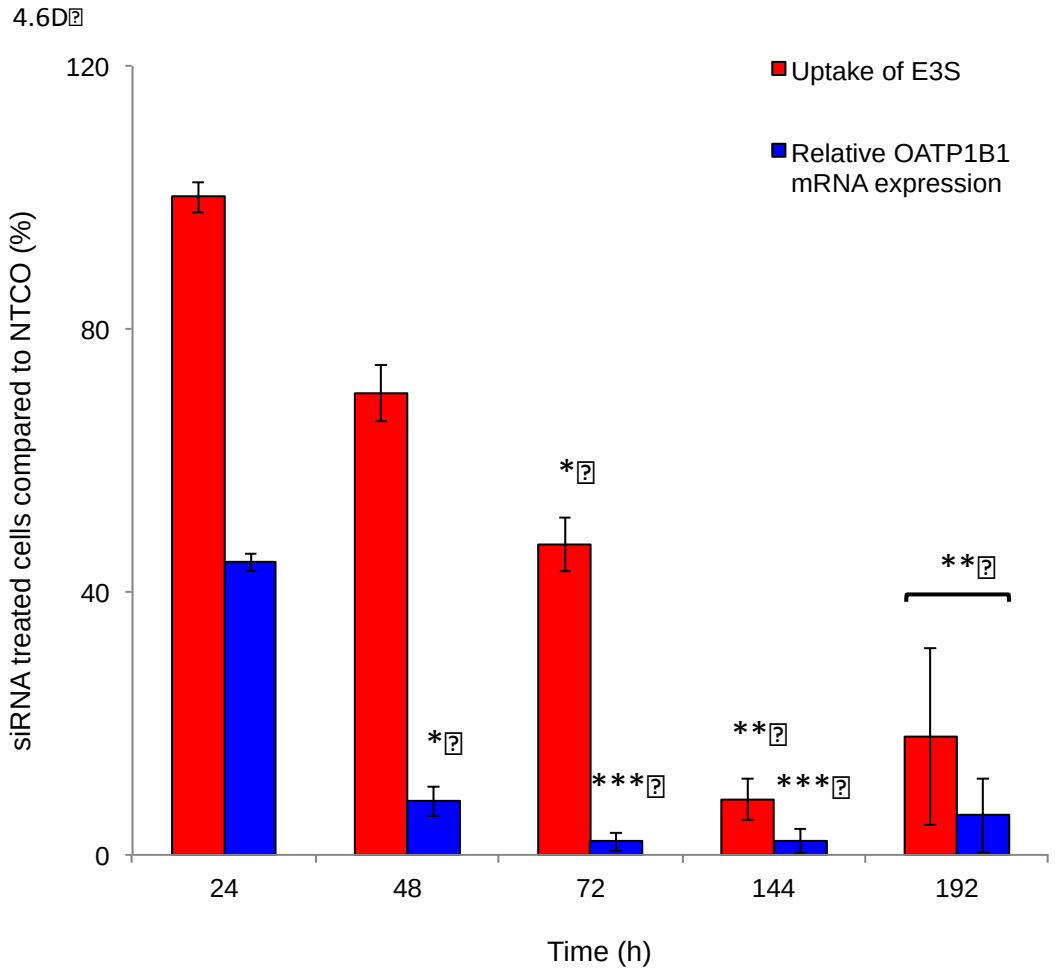

Figure 4.6 The effect of OATP1B1 siRNA on cell viability (A), OATP1B1 mRNA (B), E3S uptake (C) and OATP1B1 mRNA and E3S combined (D) after treatment with siRNA for 24, 48, 72, 144 and 192 h. Each bar shows the mean ± S.D. of 3 wells. The conditions were statistically compared using a Shapiro Wilks and Unpaired T test; * = $p < 0.05$, ** = $p < 0.01$,*** = $p < 0.001$.

144 h was selected as the optimum time for siRNA treatment; achieving the greatest inhibition of OATP1B1 mRNA, E3S uptake without any associated toxicity.

To examine the inter-donor variability in knockdown of OATP1B1 mRNA and inhibition of E3S uptake, two further human hepatocyte donors were treated with lipid/siRNA complex for 144 h. Figure 4.7A shows that the knockdown in OATP1B1

mRNA in donors Hu4244 and Hu8085 was consistent with results observed for donor Hu8089 (94% decrease for both Hu4244 and Hu8085). In addition, the reduction in E3S activity was also consistent between donors (82, 90 and 93% for Hu4244, Hu8085 and Hu8089, respectively, see Figure 4.7B).

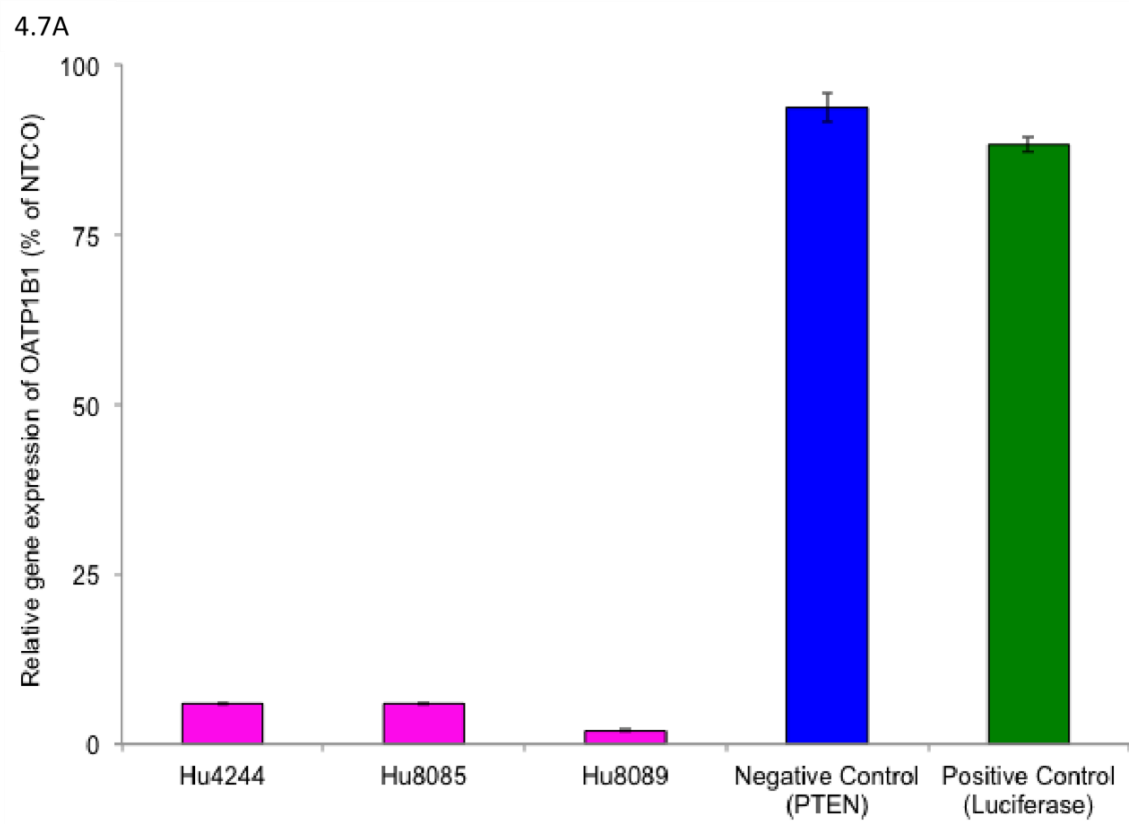

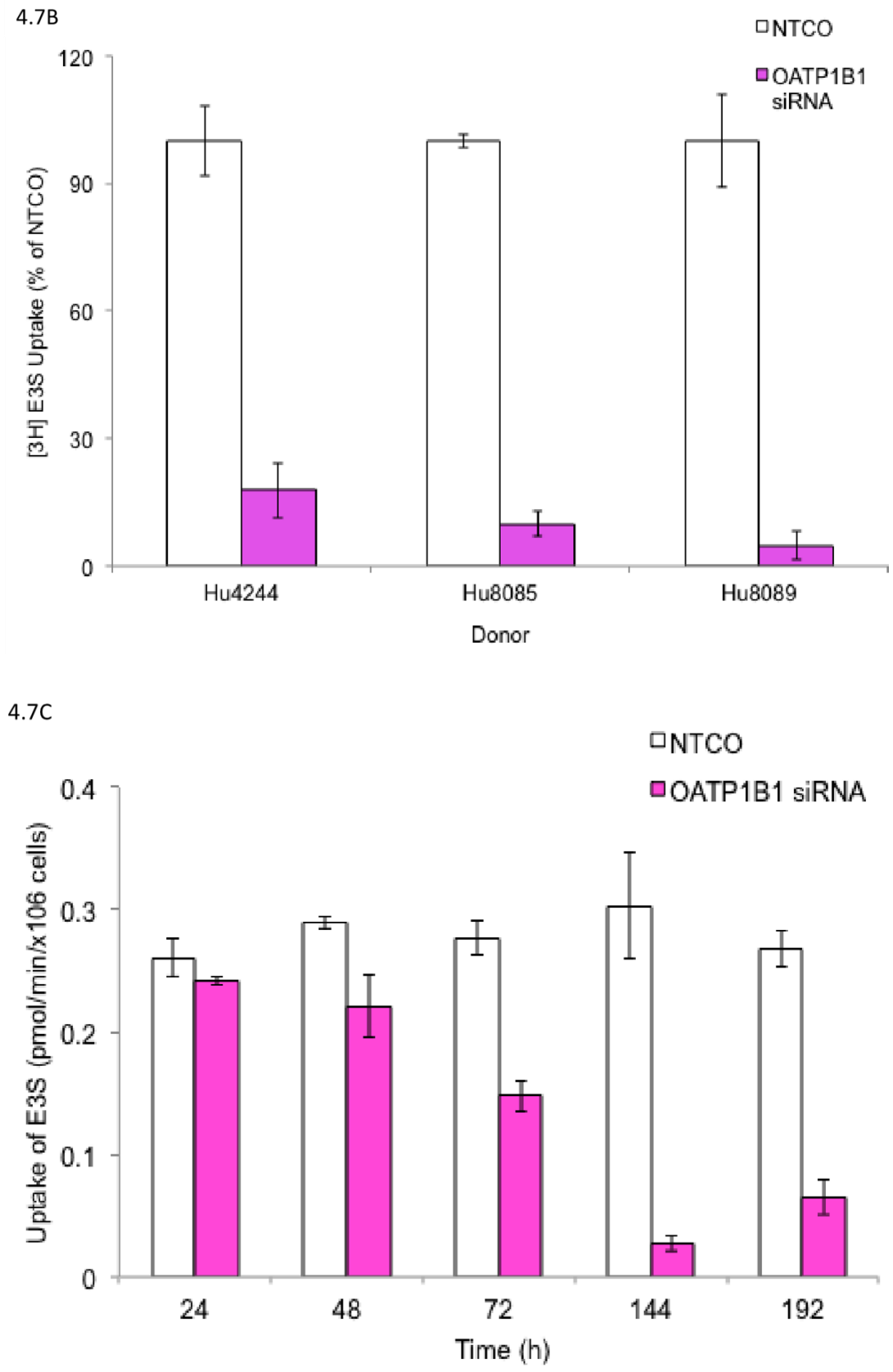

Figure 4.7 The effect of OATP1B1 siRNA on OATP1B1 mRNA (A) and E3S (B) in three different donor of human hepatocytes following treatment with siRNA for

144 h and the uptake of E3S over time in control and siRNA treated cells for one donor (C). Values are expressed as a percentage relative to NTCO. Each bar shows the mean±S.D. of 3 replicates. The results were statistically compared using an unpaired T test or Mann Whitney; ***, $p<0.001$.

4.3.4 Assessment of potential off-target effects using OATP1B1 siRNA delivery

To determine if OATP1B1 siRNA had any off-target effects, the mRNA expression of 40 genes involved in the regulation, metabolism and disposition of drugs was investigated (see Table 4.1 and Figure 4.8). Figure 4.8 shows that treatment with OATP1B1 siRNA for 144 h had no significant effect on the investigated nuclear receptors or nuclear receptor co-regulators.

No notable changes in the mRNA expression of either UDP-glucuronosyltransferases (see Figure 4.8D), influx transporters (Figure 4.8E) or efflux transporters (see Figure 4.8F) were observed. Overall, no significant (classified as either 50% increase or decrease in gene expression) off target effects were observed for the 40 genes investigated following treatment with OATP1B1 siRNA.

Figure 4.8C shows that of the 8 CYP genes investigated the greatest effect was a 27% decrease in CYP3A4 mRNA expression. While this decrease in expression was not considered significant, the high importance of CYP3A4 in drug metabolism prompted further studies. Therefore, CYP3A4 activity was assessed in human hepatocytes which had been treated with OATP1B1 siRNA for 144 h and compared with those incubated with control medium. For the three donors investigated CYP3A4 actvity only decreased 3% following OATP1B1 siRNA treatment (Figure 4.9).

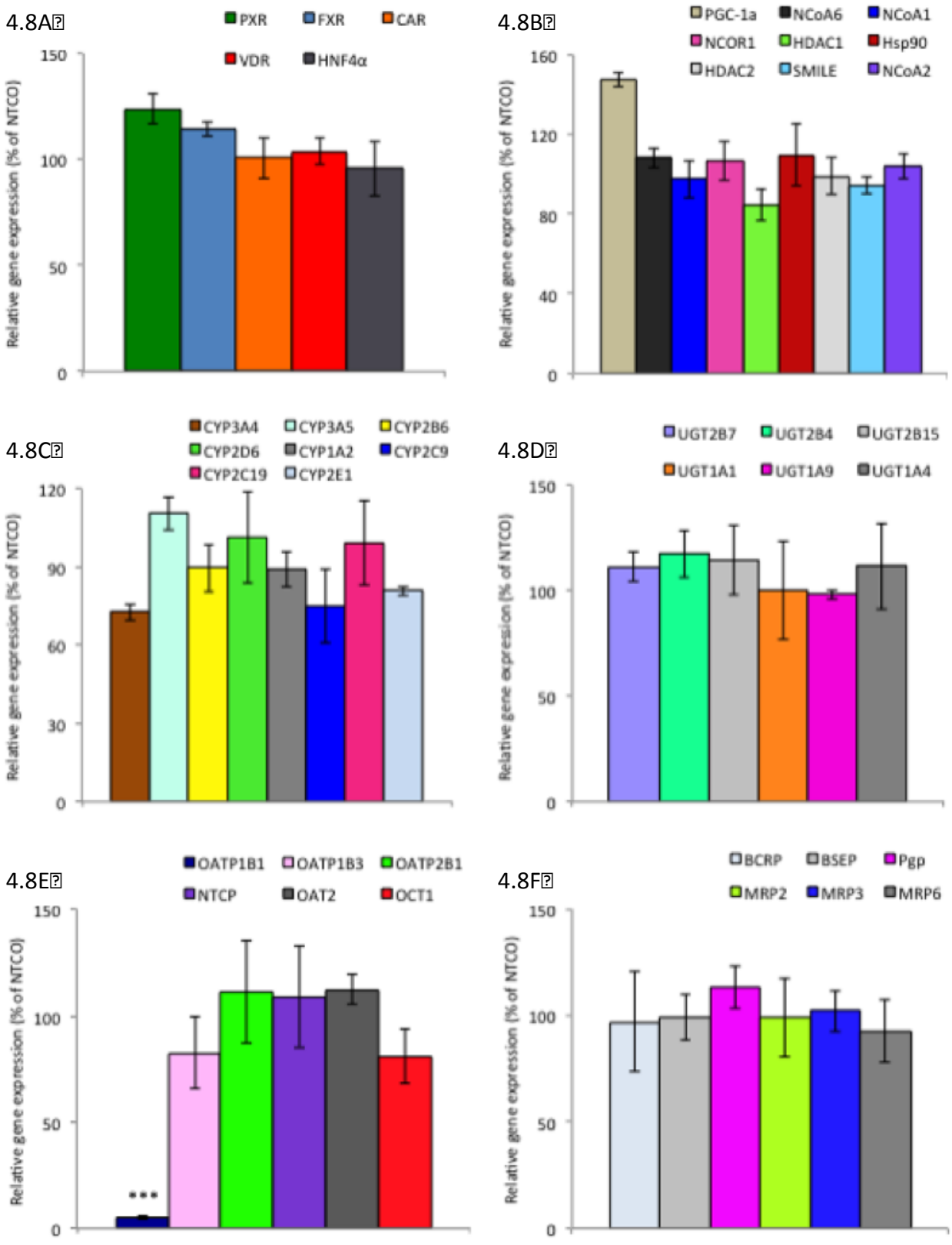

Figure 4.8 The effect of OATP1B1 siRNA on the hepatic mRNA expression of common nuclear hormone receptors (A), co regulators (B), cytochrome P450's (C), uridine diphospho glucuronosyltransferases (D), uptake transporters (E) and efflux

transporters (F) after 144 h of siRNA treatment. Each bar shows the mean ± S.D. of 3 donors completed in triplicate. The conditions were statistically compared using a Shapiro Wilks and Unpaired T test; ***, $p < 0.001$.

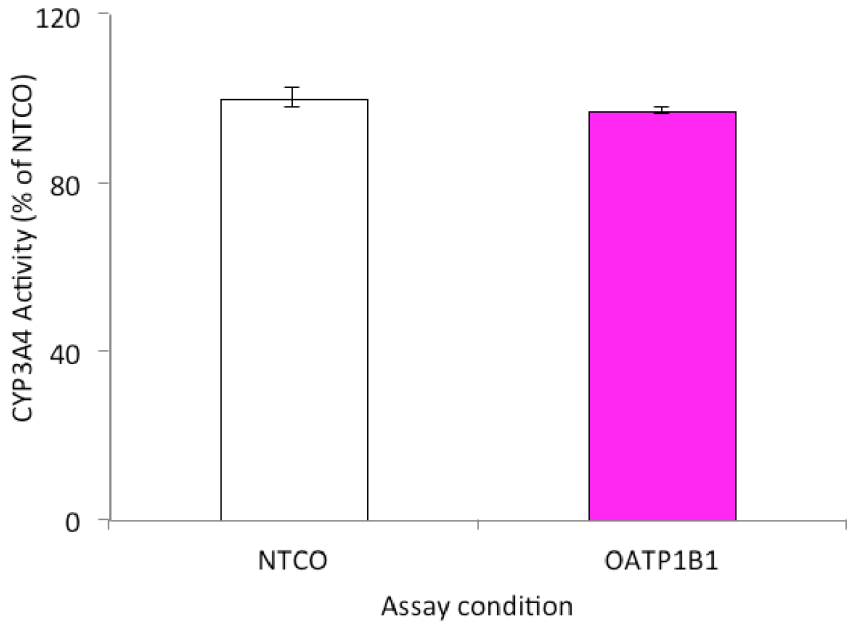

Figure 4.9 Effect of OATP1B1 siRNA oligo complex on the activity of CYP3A4 in plated human hepatocytes after 144 h. Values are expressed as the mean±S.D of 3 donors completed in triplicate. Calculated from the rate in relative fluorescent units (RFU) per minute in siRNA treated cells, expressed as a percent (%) of the rate in control cells (NTCO).

4.3.5 Determination of relative contribution of OATP1B1 to the hepatic uptake of five drugs

Initial work determined that the uptake of two angiotensin II inhibitors (valsartan and olmesartan), two HMG-co-enzyme A reductase inhibitors (rosuvastatin and pitavastatin) and a HIV protease inhibitor (lopinavir) into human hepatocytes was

linear with respect to time (up to 120 sec) (Figure 4.10). The uptake of each drug into hepatocytes with or without siRNA treatment was then assessed and the relative contribution of OATP1B1 was calculated accounting for passive uptake (see Methods section for details). A schematic of the siRNA process is shown in Figure 4.2. Table 4.2 shows that lopinavir, pitavastatin, olmesartan and rosuvastatin were predominantly taken up into human hepatocytes by OATP1B1 (64–89%, 84–98%, 42–62% and 64–72%, respectively). For these drugs, the percentage contribution of OATP1B1 was consistent across the three donors investigated (low inter-donor variability). By contrast, the inter-donor variability in OATP1B1 contribution for valsartan was much greater (28-71%), suggesting this may not be the main uptake transporter of the compound. Interestingly, the data obtained using this siRNA approach was in good agreement with that determined previously using the relative activity factor method (RAF) approach (Table 4.2).

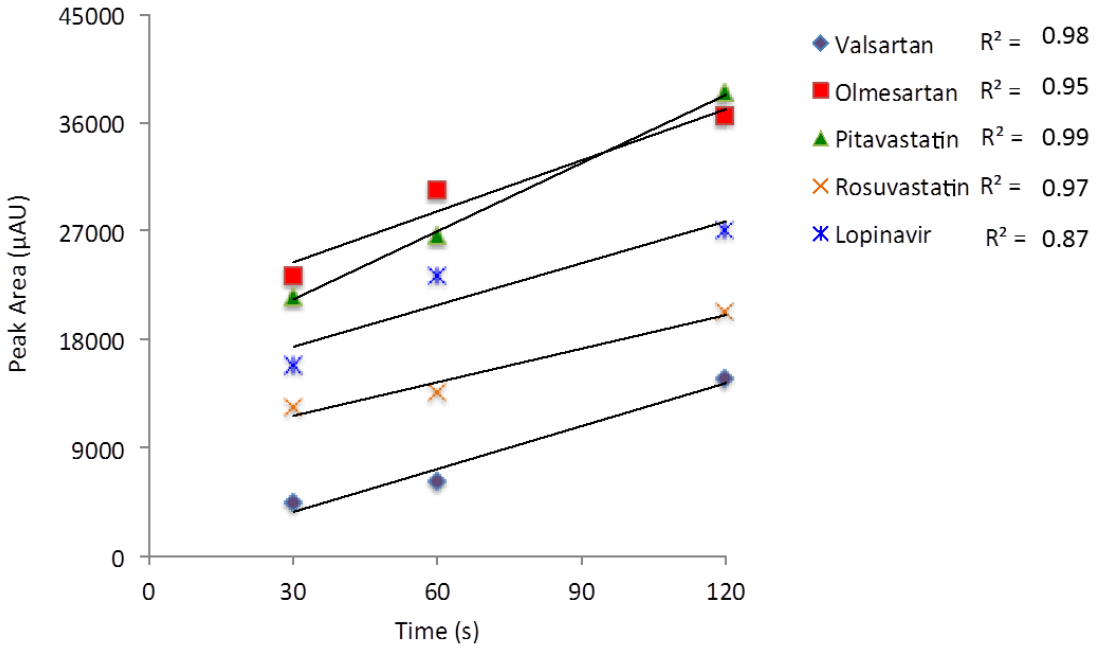

Figure 4.10 Effect of incubation time on the uptake of selected compounds in primary human hepatocytes

In contrast to the siRNA method, the RAF approach simultaneously defines the uptake of the influx transporters OATP1B1 and OATP1B3 hence it requires a selective substrate for both transporters and a HEK293 transfected cell for each gene. It uses E3S and cholecystokinin (CCK-8) as substrate probes for OATP1B1 and OATP1B3, respectively. It estimates the OATP1B1 and OATP1B3 mediated portion of uptake of selected compounds by:

$$R_{act,\ OATP1B1} = \frac{CL_{Hep,E3S}}{CL_{OATP1B1,E3S}} \qquad R_{act,OATP1B3} = \frac{CL_{Hep,CCK8}}{CL_{OATP1B3,CCK8}}$$

$$CL_{hep,test,OATP1B1} = CL_{OATP1B1,test} \cdot R_{actOATP1B1} \qquad CL_{hep,test,OATP1B3} = CL_{OATP1B3,test} \cdot R_{actOATP1B3}$$

$$CL_{hep,test} = CL_{hep,test,OATP1B1} + CL_{hep,test,OATP1B3} \qquad (356)$$

	OATP1B1 uptake contribution (%)				
Compound	**SiRNA**			**RAF**	**Reference**
	Hu4244	**Hu8085**	**Hu8089**		
Olmesartan	62	42	54	44-62	Yamada et al., 2007
Rosuvastatin	72	66	64	66-84	Kitamura et al., 2008
Pitavastatin	84	98	90	88-95	Hirano et al., 2004
Valsartan	43	28	81	22-71	Yamashiro et al., 2006
Lopinavir	64	69	89	Data not available	

Table 4.2 Percentage contribution by OATP1B1 for the hepatic uptake of selected compounds.

The passive component of uptake for the five drugs investigated ranged from 28-62% for low $logD_{7.4}$ drugs such as valsartan and olmesartan ($logD_{7.4}$ -1.1 and -1.6 respectively) to 37% for pitavastatin, which has a $logD_{7.4}$ of 1.2. These findings are consistent with those observed by Yabe *et al*., (2011) using rat hepatocytes.

4.4 Discussion

OATPs play a pivotal role in the disposition of anionic drugs across a number of therapeutic areas (333). However, the lack of selective substrates/inhibitors for the individual OATP isoforms has hampered progress in identifying the relative importance of OATP1B1, OATP1B3 and OATP2B1 to the hepatic uptake of drugs. Obtaining this added level of detail when characterising the disposition of drugs in development could be critical in determining the potential impact of known polymorphisms of OATP1B1 (357) or the fraction of drug transported by a particular isoform to produce more accurate DDI predictions. Indeed, this has been the case for CYPs when utilising fraction metabolised data (358). To address this issue, the current study has focused on the development of a method for determining the role of OATP1B1-mediated uptake of compounds into human hepatocytes using a siRNA approach. This method was then applied to quantify OATP1B1-mediated uptake for five commonly prescribed drugs (Table 4.2).

Two critical objectives required for successful utilisation of siRNA to knockdown of OATP1B1 in human hepatocytes were to inhibit OATP1B1 mRNA and activity significantly and to ensure specificity to OATP1B1. Figure 4.6B shows that OATP1B1 mRNA was reduced by 98% following treatment with siRNA for 144 h which is consistent with the results of Liao *et al*., (2010) who also observed a ~98% knockdown of OATP1B1 mRNA after 96 hours. However, minimal effects on OATP1B3 and OATP2B1 mRNA were observed in the current study (inhibition of 12% and increase of 10% respectively), while up to 50% inhibition of OATP1B3 and a 70% increase in OATP2B1 mRNA were observed in the previous study by Liao *et al*., (2010). In addition, Liao *et al*., (2010) screened a mixture of OATP1B1, 1B3 and

2B1 siRNA and showed a >50% change in mRNA for 5 non-target genes including CYP2B6 (70% increase). In the current study OATP1B1 siRNA was screened against 40 genes (Figure 4.8) and no significant differences in mRNA were observed (including CYP2B6 where only a 10% increase was observed). These data demonstrate clearly that the current siRNA/lipid complex can specifically inhibit OATP1B1 mRNA with no overt off target effects. Therefore, the siRNA oligos used in this study appears to be more specific to OATP1B1 than that used previously.

Although the transport of estrone-3-sulfate has been shown previously by some investigators to be mediated by OATP1B1, OATP1B3 and OATP2B1 (351), it has been reported to be selective for OATP1B1 at low substrate concentrations (352, 353). The active uptake of estrone-3-sulfate at a final substrate concentration of 5 nM was decreased by ~50% following treatment with siRNA for 72 h (Figure 4.6C) which was similar to the 65% knockdown of activity observed by Liao *et al*., (2010) after 96 h of OATP1B1 siRNA treatment. However, an 82-93% decrease in the active uptake of estrone-3-sulfate was observed in the three different human hepatocyte donors studied after 144 h of OATP1B1 siRNA treatment (Figure 4.6C). The high level of inhibition and the consistency of estrone-3-sulfate uptake across multiple hepatocyte donors suggest that these assay conditions are suitable to assess OATP1B1 mediated uptake in human hepatocytes. By contrast, Liao et al., (2010) required a mixture of OATP1B1, 1B3 and 2B1 siRNA to inhibit estrone-3-sulfate uptake by 70-80% suggesting that the method was not isoform-specific. It is interesting to note that maximal inhibition of estrone-3-sulfate uptake required 144 h of exposure to OATP1B1 siRNA (Figure 4.6C) whereas maximal inhibition of OATP1B1 mRNA was achieved after 72 h (Figure 4.6B). These differences provide information on

protein turnover for OATP1B1 in human hepatocytes and offer a guide to the timescales required to obtain meaningful knockdown of this transporter. A potential limitation of the current study is that OATP1B1 protein expression was not assessed. Commercial antibody's against OATP1B1 are currently available but suffer from a lack of specificity. Therefore, the high level of knockdown observed in the current study indicates that these data would be of limited value. Because of this and the availability of functional activity data, protein expression was not assessed.

The application of a siRNA approach to dissect the role of OATP1B1 in the hepatic uptake of 5 drugs is shown in Table 4.2. The remarkable similarity in the results obtained using either the siRNA or RAF approach agrees with the hypothesis that the uptake of estrone-3-sulfate (5nM) by OATP1B1 is concentration dependent. Therefore, these data provide additional evidence that the RAF approach proposed by Hirano *et al*., 2004, is a suitable method to determine the relative contribution of OATP1B1 to the hepatic uptake of drugs. However, the RAF method relies on prior availability of specific transporter substrates and although CCK-8 is specific for OATP1B3 the availability of specific substrates for other transporters (including those of determined and as yet undetermined importance), limits broad applicability of the RAF approach. Since the siRNA approach does not require selective substrates, the methodology has clear advantages in determining the relative contribution of other transporters to drug disposition. Along with ready to use reagents and easy transfection methods, the process can readily be applied for high throughput application with minimal off target effects. However, there are disadvantages of using siRNA including cost and specific knockdown times. The use of specific inhibitors to determine drug transport has been discussed previously (Soars et al., 2012). Key

disadvantages include the requirement of additional substrates and *in silico* modeling to generate robust data. Soars et al. (2012), in particular noted a 10-fold under prediction of inhibition when using various substrates.

Further evidence to support the role of OATP1B1 in the disposition of the 5 drugs investigated in Table 4.2 can be found in pharmacokinetic studies conducted with patients who have genetic polymorphisms in *SLCO1B1* (coding for OATP1B1). In particular, studies comparing the pharmacokinetics of substrates in patients with the common allele compared with those who have the *SLCO1B1*15* haplotype (associated with reduced function) have been informative (357). Ieiri *et al*., (2007) showed a 3.1-fold higher pitavastatin AUC in patients homozygous for *SLCO1B1*15*. This is consistent with findings of this study, which suggest that OATP1B1 has a major role in pitavastatin disposition (Table 4.2). A significantly higher exposure of both rosuvastatin (359) and lopinavir (49) have also been reported for *SLCO1B1*15*, although the magnitude of difference was less than that observed for pitavastatin. This indicates that the involvement of OATP1B1 in the disposition of these drugs is more moderate (Table 4.2), and that other uptake/clearance pathways also contribute. Olmesartan pharmacokinetics have also been investigated according to *SLCO1B1*15* haplotype but differences in AUC were not statistically significant (360). Finally, Maeda *et al*., (2006) saw no significant difference in valsartan AUC in *SLCO1B1*15* heterozygotes. This suggests that the role of OATP1B1 in hepatic uptake of valsartan might be at the lower range of the 28-81% contribution observed in this study and/or other mechanisms of clearance predominate for this drug.

In conclusion, this chapter highlights the importance of rigorous optimisation of assay conditions to utilise key technologies to their full potential. In this case a siRNA method was developed to specifically inhibit OATP1B1-mediated uptake into human hepatocytes without significant off-target effects. The application of this technique to elucidate the role of OATP1B1 in the hepatic uptake of 5 drugs was then demonstrated. Future application of this strategy is likely to have broad importance in determining relative contribution that individual transporters play in drug disposition.

CHAPTER 5

Induction of influx and efflux transporters and CYP3A4 in primary human hepatocytes by rifampicin, rifabutin and rifapentine

5.1 Introduction

To prevent accumulation and toxicity of xenobiotics, biotransformation and transport of foreign compounds occurs, whereby the lipophilic structures are converted into water soluble metabolites that are easily excreted. Whilst these mechanisms serve to protect the body, they reduce the bioavailability of orally administered compounds. Induction is the process in which a compound, such as, rifampicin (RIF), initiates/enhances the expression of a gene, for example cytochrome P450 3A4 (CYP3A4) or drug transporters, thereby altering the pharmacokinetics (PK) of the perpetrator (RIF) or victim drug (e.g. midazolam (MDZ)), contributing to numerous clinically significant drug-drug interactions (DDIs).

Tuberculosis (TB) is a major global health problem caused by the bacteria *mycobacterium tuberculosis* (361-364). In 2011 there were over 8.7 million new cases of TB and 1.4 million deaths (365). As a single infection it is the worlds second biggest killer worldwide (to human immunodeficiency virus (HIV)) with over 95% of the mortalities occurring in low- and middle-income countries. Although the prevalence of TB has dropped by 41% since 1990 it is responsible for over 25% of deaths in HIV infected patients (366). However, the efforts to achieve the Millennium Development Goal to suppress TB infection by 2015 is on target (367).

Current treatment is effective, with combined therapy of isoniazid, RIF, pyrazinamide and ethambutol (368). However, to avoid relapse and occurrence of multi-drug resistant TB, treatment is prescribed for 6 months (369). Rifamycins, bactericidal antibiotics, inhibit bacteria DNA-dependent RNA synthesis. The drug binds adjacent to the RNA polymerase active centre thereby blocking RNA synthesis through steric

occlusion, which prevents extension of RNA products beyond 2-3 nucleotides in length (370). Rifamycins represent a key drug class used in first line TB regimens (371). First identification of the compounds was in 1972 due to their treatment shortening potential (372). However, the optimal and maximum dose for RIF or RPT was never established in mouse models or in humans (373). The renewed interest in this class of drugs is driven by the potential of further treatment shortening times and related drug-drug interactions (DDIs). Drug resistance commonly occurs through mutations in the rpoB portion of the β subunit in RNA polymerase (374). Although the drugs are well tolerated, hepatotoxicity and flu-like syndrome are common.

RIF is a potent antibactericidal and inducer of cytochrome P450 (CYP) and phase 2 metabolising enzymes (89, 95, 375). Clinically significant DDIs are common due to induction of CYP3A4 and key drug transporters due to a lower maximum concentration (C_{max}) and area under the curve (AUC) of co-administered drugs (375) (examples and more detail are included in Chapter 1).

Rifabutin (RBT), a semi-synthetic derivative of rifamycin B is considered a less potent inducer and is often used in place of RIF for patients receiving antiretroviral drugs for HIV to reduce risk of drug interactions (85, 376, 377). Although bioavailability of RBT is 85% (compared to 95% for RIF) it has a much longer half-life ($t_{1/2}$) (28-62 h compared to 2.3-5.1 h for RIF) and is therefore effective in patients with a lower CD4+ T cell count as these individuals are more susceptible to developing drug resistance (85, 376, 378).

Rifapentine (RPT) a lipophilic, cyclopentyl RIF antibiotic derivative has a lower mean inhibitory concentration against *mycobacterium TB* in comparison to RIF and a longer half-life (~17 h), suggesting it is a possible alternative for the current RIF regimen (379). Substitution of RPT for RIF may reduce treatment duration required for cure, but its induction potential is comparatively understudied (375, 380). RPT sterilising activity is dose-dependent in an established mouse model of TB, with eradication possible in three months or less when high-dose RPT is substituted for RIF in a multidrug treatment regimen (375, 381). However, dose increases resulted in less than dose-proportional increases in RPT exposures in the clinic (368, 381, 382). In addition, the mean AUC of oral MDZ, a CYP3A4 probe, decreased by 75% when co-administered with RIF, compared to 92% when co-administered with RPT, each given at 10 mg/kg daily (383).

The aim of this chapter was to evaluate the impact of the prototypical inducer RIF as well as RBT and RPT *in vitro* on the mRNA expression of CYP3A4, ABCB1, ABCC1, ABCC2, OATP1B1 and OATP1B3 in six primary human hepatocyte donors.

5.2 Methods and Materials

5.2.1 Materials

Primary human hepatocytes, Williams E media, optiMEM media, cryopreserved hepatocyte recovery medium (CHRM®), CHRM® supplements and Hanks balanced salt solution were purchased from LifeTechnologies, Ltd (Paisley, Scotland). Taqman reagents and assays, reverse transcription products and real time-qPCR master mix were obtained from Applied Biosystems (Warrington, UK). 24-well plates pre-coated with collagen IV were purchased from BD Biosceinces (Oxford, UK). Rifampicin (R3501), rifabutin (R3530), rifapentine (R0533) and all products were of analytical grade and purchased from Sigma-Aldrich (Poole, UK).

5.2.2 Primary human hepatocytes

Cryopreserved human hepatocytes were thawed as previously described in section 2.2.3. Donor demographics are detailed in Table 5.1.

Donor	Viability	Gender	Age	Race
Hu1389	96 %	Female	36 year old	Caucasian
Hu1414	95 %	Male	68 year old	Caucasian
Hu4228	94 %	Female	47 year old	Indian
Hu4248	95 %	Female	12 year old	Caucasian
Hu1413	95 %	Female	72 year old	African American
Hu4197	91 %	Male	31 year old	Caucasian

Table 5.1 Human donor demographics of the cryopreserved hepatocytes used in the study

5.2.3 Cell viability

Cell viability and density of primary human hepatocytes were calculated using trypan blue exclusion as described in section 2.2.4.

5.2.4 Plating and maintaining primary human hepatocytes

Cells were seeded in 24-well plates pre-coated with collagen at a density of 2 x 10^5 cells/well and incubated for 24 h at 37 ºC with 5% CO_2 and 95% humidity as described in section 2.2.5.

5.2.5 Primary human hepatocyte treatment

24 hours post plating, plating media was replaced with maintenance media (as described in section 2.2.5) containing rifampicin (RIF), rifabutin (RBT) or rifapentine (RPT) at concentrations spanning the therapeutic range (0.5, 5 and 10 μM) for 24 hours.

5.2.6 mRNA and cDNA Quantification

mRNA was extracted using Trizol reagent and reverse transcribed using standard methodology as described in section 2.2.6 and 2.2.7.

5.2.7 Quantitative real time-PCR

A Chromo4™ real-time PCR (LifeTechnologies, UK) was used to determine the gene expression of selected genes (Table 5.2) as described in section 2.2.8.

Gene	Description	Alias	Chromosomal location	Reference sequence	Assay ID	Gene ID
CYP3A4	Cytochrome P450, family 3, subfamily A, polypeptide 4	CP33, CYP3A	7q21.1	NM_017460.5	Hs00604506_m1	1576
ABCB1	ATP-binding cassette, subfamily B (MDR/TAP), member 1	ABC20, P-GP	7q21.12	NM_000927.4	Hs00184500_m1	5243
ABCC1	ATP-binding cassette, subfamily C (CFTR/MRP), member 1	MRP, ABCC	16p13.1	NM_004996.3	Hs01561502_m1	4363
ABCC2	ATP-binding cassette, subfamily C (CFTR/MRP), member 2	ABC30, MRP2	10q24	NM_000392.3	Hs00166123_m1	1244
SLCO1B1	Solute carrier organic anion transporter family, member 1B1	OATP1B1, OATP2	12p	NM_006446.4	Hs00272374_m1	10599
SLCO1B3	Solute carrier organic anion transporter family, member 1B3	OATP1B3, OATP8	12p12	NM_019844.3	Hs00251986_m1	28234

Table 5.2. Information on genes analysed using real-time PCR. Assay ID is the Applied Biosystems reference number and gene ID is the NCBI reference number. Dye - FAM: 6-carboxyfluorescein

5.2.8 Data Analysis.

All primary human hepatocyte data herein was mean of six donors completed in triplicate. Normality of all data was assessed using a Shapiro-Wilk test and statistical analysis conducted using paired t-test or Wilcoxon signed-rank test for normally or non-normally distributed data, respectively. Statistics were calculated using Stats Direct (Version 2.4.6 Stats Direct Ltd). Results were considered significant if; *, $p < 0.05$; **, $p < 0.01$; ***, $p < 0.001$.

5.3 Results

5.3.1 OATP1B1 and OATP1B3 gene expression

RIF significantly upregulated the expression of OATP1B1, with maximal induction observed at 10 μM (2-fold increase, p=0.03) (Figure 5.1a). Treatment with RBT or RPT had no significant impact on the expression of OATP1B1.

No significant induction of OATP1B3 was observed upon treatment with RIF or RPT at any concentration (Figure 5.1b). However, the expression was significantly induced when incubated with 5 μM RBT (4-fold increase, p=0.04). Whilst the mean expression of OATP1B3 was greater with 10 μM RBT, the increase was not significant; large donor variability was observed at 10 μM RBT, with the top whisker regarded as an outlier (outlier = ≥1.5 times the interquartile range (IQR)). Interestingly, the data observed for OATP1B1 and OATP1B3 were much more variable between donors treated with RIF and RBT in comparison to RPT.

5.3.2 ABCC1 and ABCC2 gene expression

RIF, RBT and RPT had no significant impact at any concentration on the mRNA expression of ABCC1 (Figure 5.2a). A dose-dependent increase in expression was observed when cells were treated with RBT however, the same trend did not occur for RIF and RPT. Large variability in ABCC1 expression was observed for all drugs.

Expression of ABCC2 was consistent across all donors when treated with RIF, RBT or RPT (Figure 5.2b). Whilst a dose-dependent increase in ABCC2 expression was observed for all drugs, only RIF significantly upregulated ABCC2, with maximal induction at 10 μM (3-fold increase, p=0.03).

5.3.3 CYP3A4 and ABCB1 gene expression

A significant induction of CYP3A4 was observed at the lowest concentration of RIF (0.5 μM, 11-fold, p=0.04). A concentration-dependent profile was observed for CYP3A4 when treated with RIF with maximal induction observed at 10 μM (5 μM, 35-fold increase, p=0.03; 10 μM, 80-fold increase, p=0.02) (Figure 5.3a). RBT also significantly upregulated the expression of CYP3A4 at 5 μM (10-fold increase, p=0.05), with greatest induction observed at 10 μM (20-fold increase, p=0.05). Treatment with RPT displayed large donor variability and although a dose-dependent increase in CYP3A4 expression was observed, the difference when compared to the control was not significant. When analysed as an average of the 6 donors RPT did not significantly induce the expression of CYP3A4 but significant induction was observed in 3 of 6 donors when analysed individually.

In contrast to CYP3A4, when treated with the 3 rifamycins, the expression of ABCB1 was comparable between donors (Figure 5.3b). RIF elicited a significant upregulation of ABCB1 from 5 μM (5-fold increase, p=0.03). A concentration-dependent upregulation was observed with greatest induction observed at 10 μM (10-fold increase, p=0.03). Treatment with RBT had no significant impact on ABCB1 expression. However, ABCB1 was the only gene significantly induced by RPT (4-fold increase; p=0.04) at 10 μM.

In comparison to previous studies (4), the results herein suggest the rifamycins' potency as CYP3A4 inducers as rifampicin > rifabutin > rifapentine.

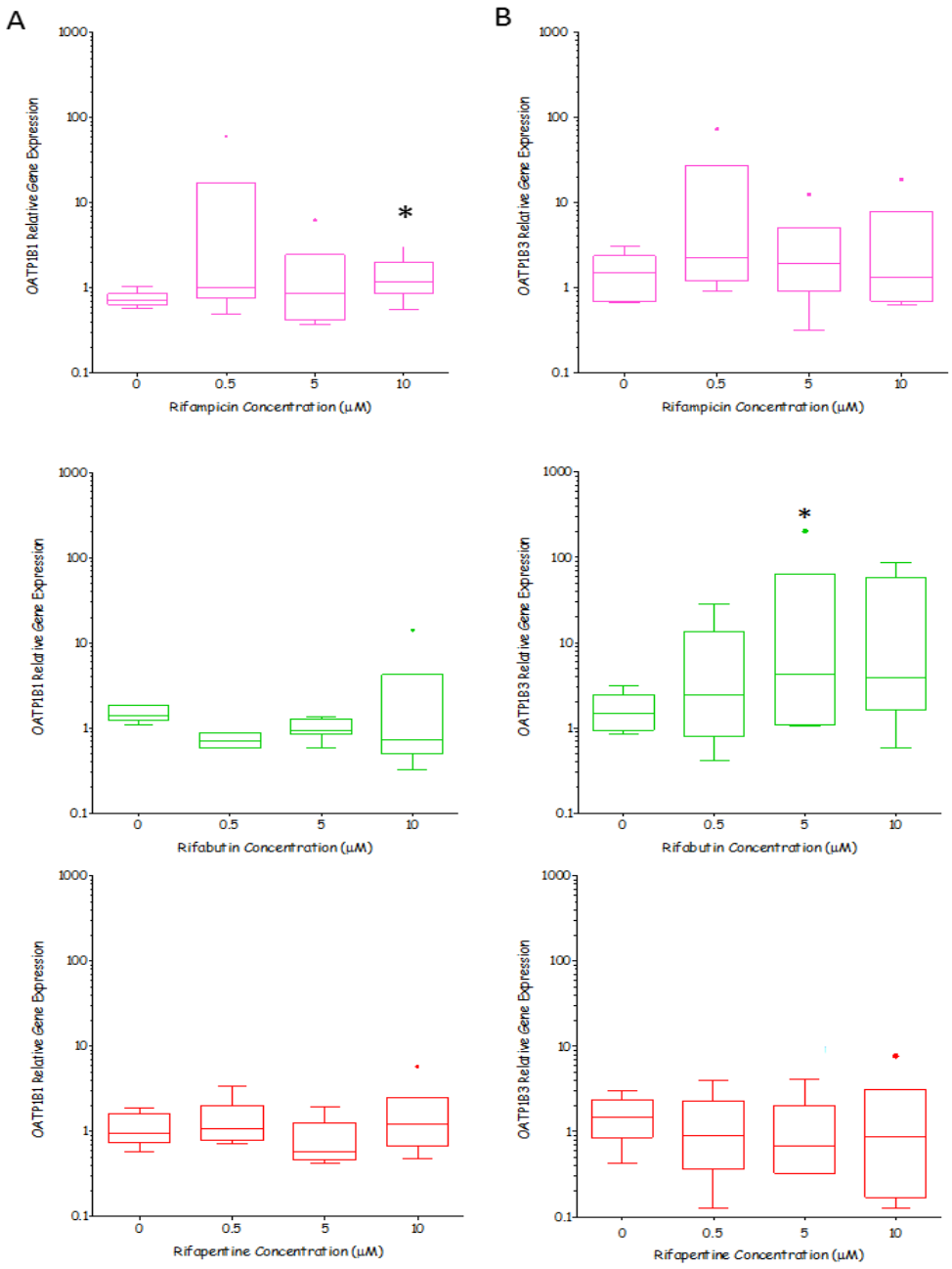

Figure 5.1. Relative gene expression of OATP1B1 (A) and OATP1B3 (B) in primary hepatocytes when incubated with RIF, RBT or RPT at 0, 0.5, 5 and 10 µM. Data was normalised to GAPDH housekeeping gene and to control primary hepatocytes (0 µM) using the comparative C(t) method ($C(t)=2^{\wedge -ddC(t)}$). Tukey box plot represents the mean of 6 donors completed in triplicate with box showing inter-quartile range (IQR) and whiskers representing <1.5 x IQR. Data outside 1.5 x IQR are labelled as outliers (•).

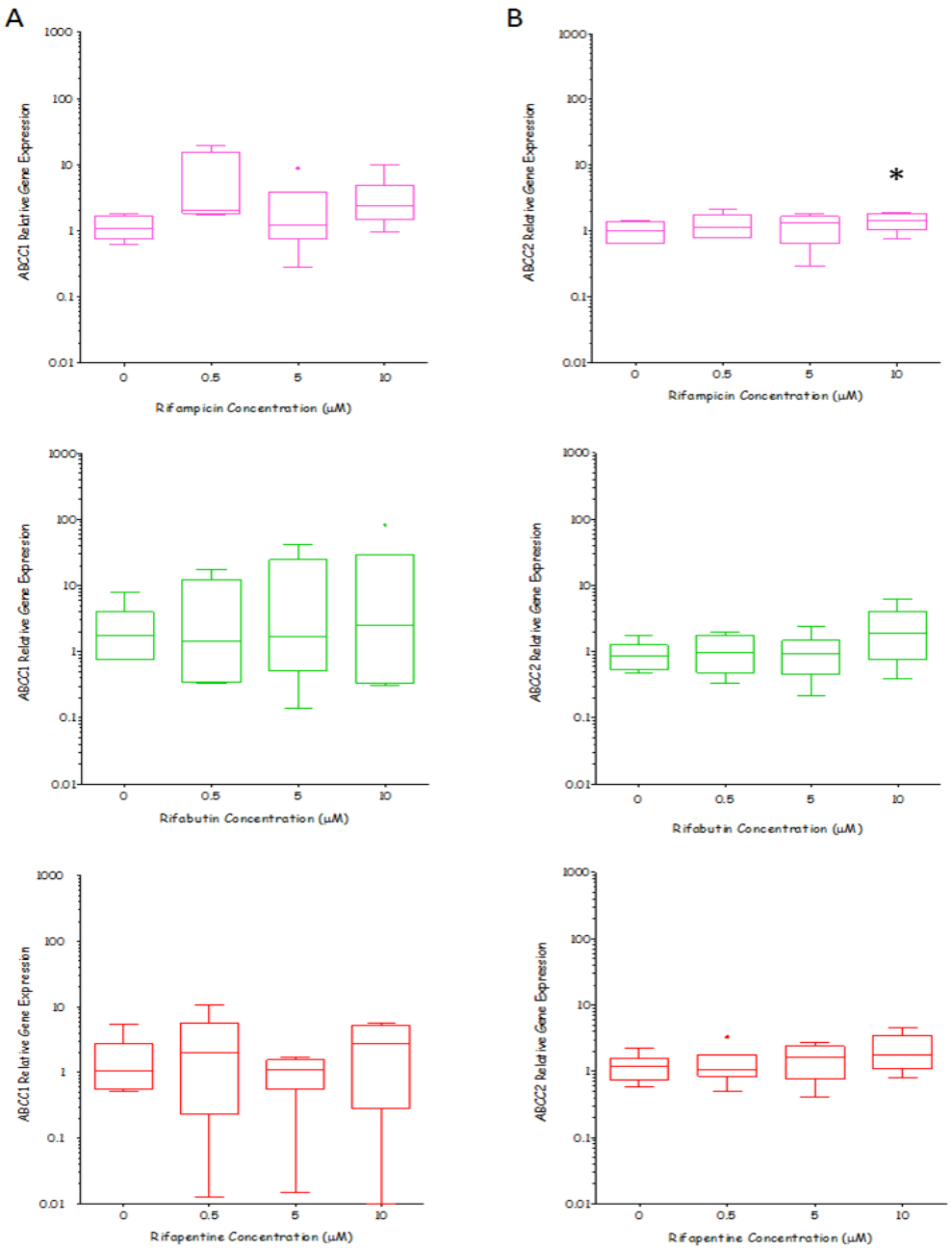

Figure 5.2. Relative gene expression of ABCC1 (A) and ABCC2 (B) in primary hepatocytes when incubated with RIF, RBT or RPT at 0, 0.5, 5 and 10 µM. Data was normalised to GAPDH housekeeping gene and to control primary hepatocytes (0 µM) using the comparative C(t) method ($C(t)=2^{\wedge -ddC(t)}$). Tukey box plot represents the mean of 6 donors completed in triplicate with box showing inter-quartile range (IQR) and whiskers representing <1.5 x IQR. Data outside 1.5 x IQR are labelled as outliers (•).

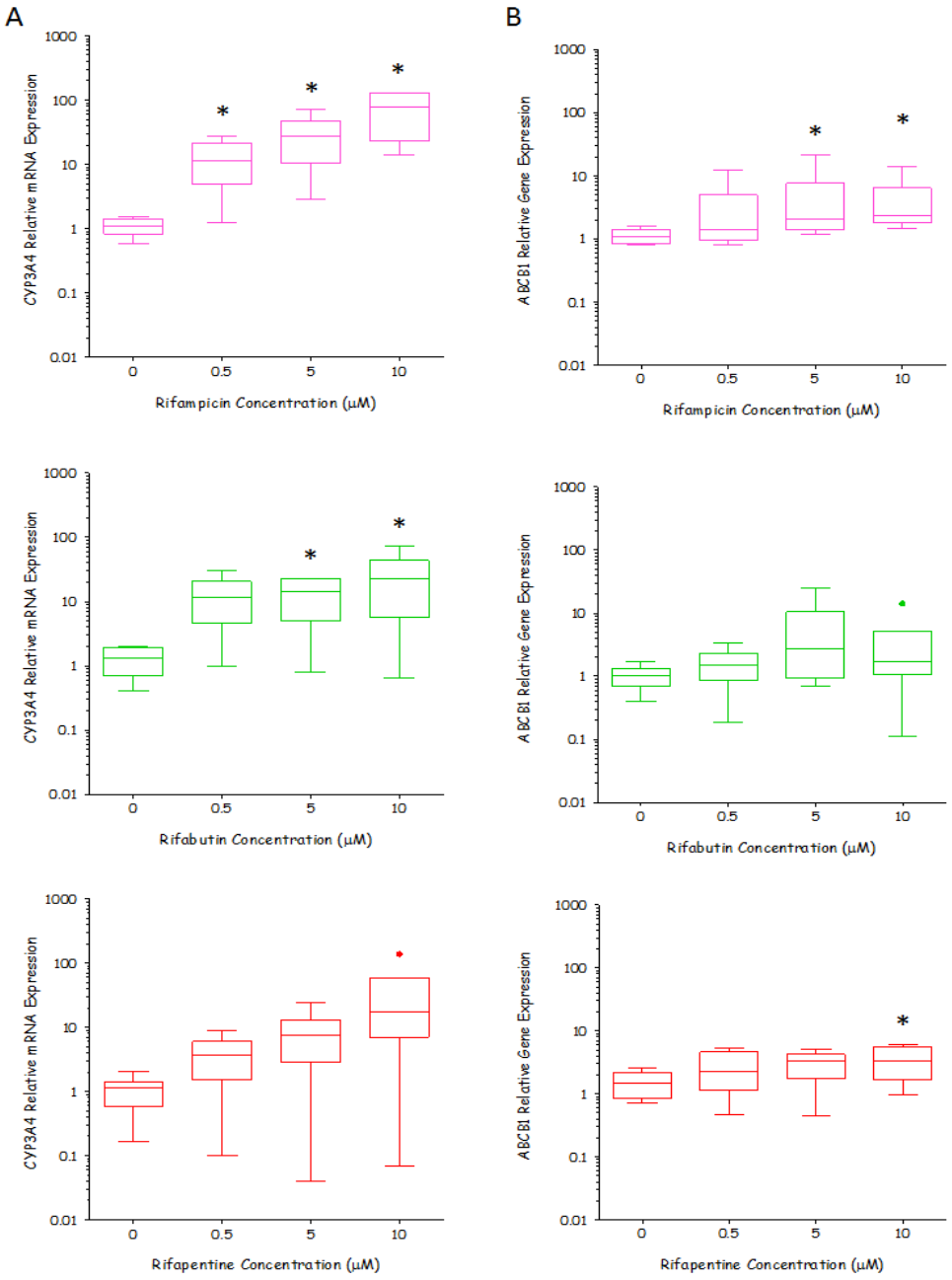

Figure 5.3. Relative gene expression of CYP3A4 (A) and ABCB1 (B) in primary hepatocytes when incubated with RIF, RBT or RPT at 0, 0.5, 5 and 10 µM. Data was normalised to GAPDH housekeeping gene and to control primary hepatocytes (0 µM) using the comparative C(t) method ($C(t)=2^{\wedge -ddC(t)}$). Tukey box plot represents the mean of 6 donors completed in triplicate with box showing inter-quartile range (IQR) and whiskers representing <1.5 x IQR. Data outside 1.5 x IQR are labelled as outliers (•).

5.4 Discussion

This work highlights the extent to which RIF induces CYP3A4-mediated metabolism and the transport of compounds compared to RBT, and RPT as potential alternatives. Consistent with all primary hepatocyte studies, large inter-donor variability was observed (244). However, concentration-dependent responses were seen for most genes (including CYP3A4).

Conversely to RIF and RPT, RBT is metabolised by CYP3A4 and has been shown to induce its own metabolism (369), although as described previously and here, the induction effects are much less profound compared to RIF and RPT (Figure 5.3) (376). *In vitro* analysis has shown RPT is more potent after a 600mg dose once a week compared to a 600mg dose once a day for RIF (380, 381). In comparison, clinical data does not demonstrate the same trend with relapse rates greater for RPT compared to RIF (380). At the same micromolar concentration, larger increases in CYP3A4 mRNA expression were observed when hepatocytes were treated with RIF compared to RBT or RPT. In contrast to data herein, a study with healthy volunteers found the AUC of MDZ was decreased 17% more when coadministered with RPT compared to RIF (380). However, at standard daily doses (10mg/kg), RIF, RBT and RPT average concentrations are approximately 2.3 μM, 0.3 μM and 15.7 μM, respectively (376, 377, 384). Of particular note, plasma concentrations of rifabutin in patients are comparatively low, and this may help rationalise the limited induction seen clinically by rifabutin. Thus, the spectrum of induction by RIF, RBT and RPT are different but the data should be interpreted in the context of differences in plasma concentrations seen clinically. The data should also be interpreted in the context that concentrations in hepatocytes and/or gut may exceed those found in the plasma of

patients. The unbound plasma concentration is often used to estimate clinical drug interactions. However, protein binding can be dependent on health status. For example, rifampicin is 87-91% bound in healthy individuals but 84-88% bound in tuberculosis-infected individuals (372). Nonetheless, it should be noted that previous investigations have shown effects at mRNA level are not always translated to activity (85, 271, 385).

ATP binding cassette transporter (ABC), ABCB1, is a transmembrane efflux protein responsible for the removal of a broad range of bile acids, lipids and xenobiotics out of hepatocytes (see Chapter 1 for more detail) (30). RIF and RPT significantly induced ABCB1; hence an enhanced clearance of co-administered substrates may be predicted. Also, RIF, RPT, ethambutol and isoniazid are all substrates of ABCB1 (85, 386, 387) suggesting a potential role in autoinduction and potential effects between drugs within a TB regimen. Polymorphisms within the *ABCB1* gene may also affect RIF and RPT pharmacokinetics (30) although association studies with ABCB1 SNPs for other drugs have always been contradictory.

The main hepatic influx protein, organic anion transporting polypeptide (OATP) 1B1 mediates the sodium-independent uptake of a broad array of organic amphiphilic compounds (58) (see Chapter 4 for more detail). A significant upregulation of OATP1B1 mRNA was observed with 10 μM RIF. Given that RIF is itself a substrate for OATP1B1 (388) and that polymorphisms within the *SLCO1B1* gene affect RIF pharmacokinetics (389), these data indicate an involvement of OATP1B1 in the reported RIF autoinduction (390).

Many RIF drug interactions arise during HIV treatment (375). Contraindications occur with the concomitant use of RIF with antiretrovirals due to marked PK interactions. For example, the AUC of amprenavir, efavirenz, indinavir, ritonavir and saquinavir is decreased by 82%, 26%, 92%, 35% and 70%, respectively (68, 369, 375, 388, 391, 392). The majority of CYP3A4 substrates overlap with ABCB1 and OATP1B1 resulting in an enhanced pharmacokinetic (PK) shift. Significant induction by RPT was only evident for ABCB1 suggesting contraindications with antiretrovirals may be avoided/reduced with this RIF substitution.

Current clinical trials are investigating high-dose daily RPT (Tuberculosis Trials Consortium Study 29X) and high-dose RIF (PanACEA Consortium) (393) as potential TB treatment shortening regimens. *In vitro* results suggest increasing the concentration of RPT may lead to clinically relevant DDIs mediated through ABCB1. Boeree et al., 2013, found 35mg/kg of RIF daily was safe and well tolerated over 14 days and early bactericidal activity increased with increasing dose, with no apparent plateau (394). Trials are now being planned to assess the activity of high-dose RIF over 8 weeks.

Parallel to optimising the use of rifamycins detailed above, novel innovative approaches utilising immunomodulating compounds to work in concert with bactericidal antibiotics are under investigation (395-397). Understanding and clarification of the human immunological response to *mycobacterium tuberculosis* proves an obstacle for the development of these compounds (373). Nevertheless, 11 candidates for TB vaccination are undergoing trials (398-400).

Data herein suggest that concentration-dependent induction should be considered when interpreting results of ongoing trials of higher-dose RIF and RPT since it cannot be assumed that maximum autoinduction is achieved at standard doses. With the absence of an apparent ceiling as drug exposure increases (394), RIF doses above those used in the clinic today may lead to significant and highly variable DDIs, which is of considerable clinical concern.

CHAPTER 6

Regulation of *CYP3A4*, *ABCB1* and *OATP1B1* gene expression by *VDR* and the effects of *VDR* SNPs

6.1 Introduction

Vitamin D was identified over 90 years ago as an antirachitic substance (103). Humans are exposed to 2 primary sources of vitamin D: diet (mainly cod liver oil and oily fish) and via ultraviolet light (UV-B, 290-315nm) absorption (401). Upon UV-B exposure, 7-dehydrocholesterol is converted into cutaneous previtamin D_3, which is spontaneously thermal isomerised into vitamin D_3. As vitamin D_3 enters the systemic circulation it is hydroxylated into 25-hydroxyvitamin D_3 by cytochrome P450, family 27, subfamily A, polypeptide 1 (CYP27A1) and further converted into 1α,25-dihydroxyvitamin D_3 (1α,25-$(OH)_2D_3$) (active vitamin D) by CYP27B1.

Parathyroid hormone modulation of the *CYP27B1* gene tightly regulates the levels of 1α,25-$(OH)_2D_3$. However, other factors contribute to the circulating levels. For example, individuals located close to the equator maintain high levels of 1α,25-$(OH)_2D_3$ all year round, skin pigmentation determines the amount of UV-B required to produce 1α,25-$(OH)_2D_3$, body surface area, duration spent outside and *VDR* single nucleotide polymorphisms (SNPs) (Table 6.1) can all alter the levels of 1α,25-$(OH)_2D_3$ (218, 402, 403). In contrast, efforts to prevent the incidence of skin cancer through UV-B absorption (e.g. clothing, sun cream) may unintentionally result in vitamin D deficiency (404).

Vitamin D receptor (VDR; *NR1I1*) is a class II steroid nuclear receptor (NR) responsible for mediating 1α,25-$(OH)_2D_3$ effects (405). High affinity binding of 1α,25-$(OH)_2D_3$ to the VDR hydrophobic pocket, induces VDR heterodimerisation binding with retinoid x receptor (RXR) (406). The regulatory region of the target gene possess vitamin D receptor responsive elements (consisting of a direct repeat NR half-

site, separated by 3 nucleotides (DR3)) which the heterodimer binds and transactivates (407), regulating bone mineralisation and resorption, calcium and phosphate homeostasis, parathyroid hormone synthesis and cell growth (408), within vitamin D responsive organs (intestine, parathyroid gland, kidney, bone) (88). To a lesser extent, the liver, pancreas, brain and muscle also express the *VDR* gene, which regulates many biological processes (403, 409, 410).

Recent studies have identified several functioning *cis*-acting response elements for constitutive androstane receptor (CAR), pregnane x receptor (PXR) and VDR on the CYP3A4 gene promoter (an everted repeat, separated by 6 nucleotides in the CYP3A4 proximal promoter and a xenobiotic responsive enhancer module with a functional direct repeat, separated by 3 nucleotides upstream of the CYP3A4 transcription activation site) (411-414). PXR and VDR have been found to synergistically increase *CYP3A4* expression and activity in intestinal cell lines (103, 402). This effect has been observed *in vivo* with seasonal variations (fluctuations in $1\alpha,25\text{-}(OH)_2D_3$ concentrations by UV-B intensity) apparent for CYP3A4 substrate concentrations. Plasma concentrations for tacrolimus and sirolimus differ between summer and winter by 7% and 17%, respectively (415).

Many NRs and transcription factors regulate ATP-binding cassette, subfamily B, member 1 transporter (*ABCB1*) expression (416). VDR exhibits a similar homology to CAR and PXR (417) but only recently has been identified as a regulator of *ABCB1* expression in colon carcinoma cell lines (418-420), which contains vitamin D receptor response elements (421). Treatment with $1\alpha,25\text{-}(OH)_2D_3$ has been shown to double

the expression of *ABCB1* in LS174T cells with the effect further enhanced upon ketoconazole treatment, mediated through *VDR* activation (422).

Under normal physiological conditions, the solute carrier organic anion transporter family member 1B1 (OATP1B1) expression is restricted mainly to the liver but upon inflammation or cancer, expression of the influx transporter is not as firmly restricted (4, 423). For example, OATP1B1 is expressed in colon, pancreatic, ovarian and lung cancer (423). The significant role of OATPs in drug disposition and the occurrence of cancer through altered *VDR* expression, make this transporter and its potential for induction by VDR, of significant pharmacological relevance.

Over 245 polymorphisms have been identified in the *VDR* gene of British Caucasians (424). Many *VDR* single nucleotide polymorphisms (SNPs) (Table 6.1) are associated with the occurrence and prognosis of disease through altered VDR structure and activity, but studies show very contrasting and controversial results (425-428). Hence, the work presented in this chapter focused on *VDR* SNPs that have been found to alter the function or activity of the protein. Transcriptional activity of *VDR* is influenced by a SNP in the 5'-regulatory region (-29649A>G, *Cdx*2, rs11568820), while the stability of *VDR* is affected by SNPs in the 3'-untranslated region (UTR) (IVS8-283G>A, *Bsm*1, rs1544410; 1056C>T, *Taq*1, rs731236; IVS8-49C>A, *Apa*1, rs7975232) and protein function is hindered by the addition of 3 amino acids in the *VDR* translation initiation codon (2T>C, *Fok*1, rs2228570) (429-431).

Studies suggest the conventional and highly researched xenobiotic sensors PXR and CAR are not solely responsible for altered drug pharmacokinetics; fluctuations in

VDR activation by 1α,25-$(OH)_2D_3$ or *VDR* SNPs may also contribute to CYP3A4 and/or ABCB1 substrate concentrations. Although 1α,25-$(OH)_2D_3$ has been shown to benefit human health (403), an upregulation of intestinal CYP3A4 and ABCB1 through VDR activation may have a significant impact on drug-drug interactions, altered drug disposition, efficacy and toxicity. Within the intestine CYP3A4 is a dominant enzyme responsible for 1α,25-$(OH)_2D_3$ catabolism; hence gene induction could also contribute to altered cell homeostasis, calcium absorption and CYP3A4 substrates including ketoconazole (402, 432). A further understanding and clarification of *VDR* expression, *VDR* SNPs and its targets *in vivo* is essential.

The aims of this chapter were two-fold: to confirm the association between *PXR* and *CYP3A4* expression and, *PXR* and *ABCB1* expression in 84 human intestinal donors; and to further characterise any relationship between *VDR* expression and *PXR*, *CYP3A4* and *ABCB1* expression, and determine if *VDR* SNPs (rs2228570, rs11568820, rs731236, rs7975232, rs1544410) have an impact on the expression observed.

SNP	Alleles (ancestral)	Chromosome	Chromosome Position	Strand	Location and characteristics	Effect of SNP	MAF/Minor Allele Count	Population Frequency	Disease Association	PubMed Reference Number
rs7929	A>C/G	12	46522890	-	UTR3	Increased VDR = increased 1α,25-$(OH)_2D_3$ levels	G=0.485/610	European A/A 0.372 A/C 0.398 C/C 0.23 S.S.Africa (Nigerian) A/A 0.372 A/C 0.469 C/C 0.159 S.S.Africa (Kenyan) A/A 0.35 A/C 0.538 C/C 0.112 Asian (Han Chinese) A/A 0.14 A/C 0.326 C/C 0.535 Asian (Japanese) A/A 0.118 A/C 0.459 C/C 0.424	C allele = protective against type 1 diabetes (T1D)	17130574, 19682379, 18593774
rs17878969	(A)13/16/18/19/23/24	12	48236407	-	UTR3	Short tadem repeat Altered mRNA stability	≥18 A-repeats = long (L, major allele), <18 A-repeats = short (S, minor allele)	-	>18 A-repeats = protection against HIV infection (L) <18A repeats = association with VDDR type1	18205531, 19450131, 19052755
rs2228570 FokI	T>A/C/G	12	47070443	+	Non-synonymous Exon 2	Low/medium risk Decreased VDR = decreased 1α,25-(OH)2D3 levels Altered protein structure and capacity Base change eliminates the translation start site in exon 2, encoded protein is shortened by 3 amino acids. The smaller protein exhibits less transcription activity	A=0.266/334	European A/A 0.195 A/G 0.434 G/G 0.372 Asian (Han Cinese) A/A 0.186 A/G 0.512 G/G 0.302 Asian (Japanese) A/A 0.163 A/G 0.326 G/G 0.512 S.S.Africa (Nigerian) A/A0.036 A/G 0.312 G/G 0.655 S.S.Africa (Kenyan) A/A 0.028 A/G 0.352 G/G 0.62	G allele = protection against HIV infection A allele = higher asthma morbidity, low spirometric measures, positive aeroallergen skin test, increased immunoglobulin E levels in A.American, increased breast, ovarian and pancreatic cancer risk, increased risk of type 2 diabetes (T2D)	21693626, 21613960, 19105801, 18205735, 19760020, 19584489, 10707958, 20473893, 19124512, 19450131
rs3847987	C>A	12	47035619	+	UTR3	Increased VDR = increased 1α,25-$(OH)_2D_3$ levels	A=0.149/187	European A/A 0.27 A/C 0.195 C/C 0.779 S.S.Africa (Nigerian) A/C 0.124 C/C 0.876 S.S.Africa (Kenyan) A/A 0.007 A/C 0.105 C/C 0.888 Asian (Han Chinese) A/A 0.116 A/C 0.302 C/C 0.581 Asian (Japanese) A/A 0.047 A/C 0.349 C/C 0.605	A allele = increased risk of COPD onset in men, protective marker against HIV infection C allele = T1D protection	17130574, 19105801, 21610492, 15282199

Table 6.1

SNP	Alleles (ancestral)	Chromosome	Chromosome Position	Strand	Location and characteristics	Effect of SNP	MAF/Minor Allele Count	Population Frequency	Disease Association	PubMed Reference Number
rs1544410 Bsml	G>A	12	47037386	-	Intron 8	Intronic enhancer Low risk Decreased VDR = decreased 1α,25-(OH)2D3 levels	A=0.280/352	European A/A 0.211 A/G 0.434 G/G 0.345 Asian (Han Chinese) A/G 0.047 G/G 0.953 Asian (Japanese) A/G 0.244 G/G 0.756 S.S.Africa (Nigerian) A/A0.071 A/G 0.416 G/G 0.513 S.S.Africa (Kenyan) A/A 0.149 A/G 0.44 G/G 0.411	A/A = 2 fold increase in surgical menopause, association with melanogenesis, T1D, association with rapid progression to AIDS, increase VDR linked to HIV resistance bbaATT and BBAAtt haplotypes associated with increased ovarian cancer risk in Caucasian women	17135034, 21365644, 19734102, 18279374, 20642435, 20361340, 18161000, 18086759 21198767, 18205531
rs7975232 Apal	C>A	12	46525104	+	Intron 8 Anonymous polymorphism	Intronic enhancer Low risk Variation in mRNA stability and protein structure Decreased VDR = decreased 1α,25-(OH)2D3 levels	C=0.482/606	European A/A 0.372 A/C 0.398 C/C 0.23 S.S.Africa (Nigerian) A/A 0.398 A/C 0.478 C/C 0.133 S.S.Africa (Kenyan) A/A 0.448 A/C 0.455 C/C 0.0.98 Asian (Han Chinese) A/A 0.14 A/C 0.326 C/C 0.535 Asian (Japanese) A/A 0.116 A/C 0.453 C/C 0.43	A allele = associated with T1D, increased risk of asthma, protection from follicular carcinoma, development of sporadic pancreatic cancer Chronic periodontitis higher freq of AA in Asians	21548019, 21198767, 19622139, 19499989, 19734102, 18849534
rs731236 TaqI	C>T	12	47036308	-	Cds-synonymous Sense/synonymous; Splicing regulation Exon 9	Medium risk Alters modulation of VDR Decreased VDR = decreased 1α,25-(OH)2D3 levels	G=0.280/352	European C/C 0.221 C/T 0.434 T/T 0.345 S.S.Africa (Kenyan) C/C 0.1 C/T 0.344 T/T 0.556 S.S.Africa (Nigerian) C/C 0.147 C/T 0.573 T/T 0.28 Asian (Han Chinese) C/T 0.024 T/T 0.976 Asian (Japanese) C/T 0.235 T/T 0.765	C allele = association with multiple sclerosis (MS), increase in surgical menopaus, associated with T1D/T2D T allele = protection against MS but an increases chronic periodontitis, risk of pancreatic cancer	21816760, 21664963, 19734102, 19644412, 21168462, 21076051, 17135034, 17130574, 21198767, 19584489
rs11568820 Cdx2	A>G	12	46588812	-	5' UTR Functional effect, transcriptional activity	Decreased VDR = decreased 1α,25-(OH)2D3 levels A to G base substitution (referring to the minus strand) eliminates the Cdx binding site and reduces transcriptional activity of VDR to 70% of the A allele	T=0.461/580	European A/A 0.035 A/G 0.336 G/G 0.628 Asian (Han Chinese) A/A 0.326 A/G 0.442 G/G 0.233 Asian (Japanese) A/A 0.247 A/G 0.435 G/G 0.318 S.S.Africa (Nigerian) A/A 0.995 A/G 0.045 S.S.Africa (Kenyan) A/A 0.601 A/G 0.35 G/G 0.049	G allele = decreased survival in NSCLC, protective against HIV, VDDR type 2A, homozygous require increased calcium for optimal vertebral mass accrual during adolescence A allele –protection against fracture, ovarian and prostate cancer	12968672, 19309297, 14991752, 11450701, 18205531, 18086759 18936471, 18086783

Table 6.1

SNP	Alleles (ancestral)	Chromosome	Chromosome Position	Strand	Location and characteristics	Effect of SNP	MAF/Minor Allele Count	Population Frequency	Disease Association	PubMed Reference Number
rs4516035	C>T	12	47097576	+	Near gene 5 (-)1012 locus of the promoter	Decreased VDR = decreased 1α,25-(OH)2D3 levels	C=0.202/254	European C/C 0.203 C/T 0.508 T/T 0.288 S.S.Africa (Kenyan) C/C 0.007 C/T 0.21 T/T 0.783 S.S.Africa (Nigerian) C/T 0.009 T/T 0.991 Asian (Han Chinese) C/T 0.044 T/T 0.956 Asian (Japanese) C/T 0.012 T/T 0.988	A allele = significant role in melaloma disease progression, risk of cutaneous melanoma, linked with height in europeans G allele = girls require more milk for for optimal vertebral mass accrual, protective against HIV	21365644, 20398755, 19679055, 19615888, 18205531, 20046590, 19309297
rs11574010	G>A	12	48298902	-	Near gene 5 Promoter region	-	A=0.006	Global A/G 0.011 G/G 0.989	G allele = increased risk of MS in low sun exposure	19383647
rs11168287	A>G	12	46571681	+	Intron	-	G=0.452/569	European A/A 0.333 A/G 0.5 G/G 0.167 Asian (Han Chinese) A/A 0.186 A/G 0.465 G/G 0.349 Asian (Japanese) A/A 0.111 A/G 0.533 G/G 0.356 S.S.Africa (Nigerian) A/A 0.55 A/G 0.383 G/G 0.067	A allele = risk of cutaneous melanoma	21365644
rs739837	T>G	12	48238221	+	3 UTR	-	G=0.492/619	European A/A 0.23 A/G 0.398 G/G 0.372 Asian (Han Chinese) A/A 0.535 A/G 0.326 G/G 0.14 Asian (Japanese) A/A 0.43 A/G 0.453 G/G 0.116 S.S.Africa (Nigerian) A/A 0.168 A/G 0.531 G/G 0.306 S.S.Africa (Kenyan) A/A 0.14 A/G 0.448 G/G 0.413	G allele = associated with fair skin A allele = association with increased breast cancer risk A allele = association with non small cell lung carcinoma	19105801

Table 6.1

SNP	Alleles (ancestral)	Chromosome	Chromosome Position	Strand	Location and characteristics	Effect of SNP	MAF/Minor Allele Count	Population Frequency	Disease Association	PubMed Reference Number
rs2238135	G>C	12	48278190	-	Intron 4	-	G=0.243/306	-	C allele = 2 fold increase in pancreatic cancer risk, enhanced BMD of the femoral neck	19753122, 19255064, 17932346, 17130574
rs3782905	C>G	12	48266167	-	Intron 2	-	C=0.241/303	European C/C 0.509 C/G 0.386 G/G 0.105 Asian (Han Chinese) C/C 0.644 C/G 0.311 G/G 0.044 Asian (Japanese) C/C 0.795 C/G 0.205 S.S.Africa (Nigerian) C/C 0.633 C/G 0.3 G/G 0.067	C allele = associated with asthma susceptibility in childhood G allele = recurrence/progression of pancreatic cancer	15282199, 15282200, 20687218, 19956101
rs2239179	A>G	12	47055317	+	Intron 3	-	C=0.335/421	European A/A 0.363 A/G 0.345 G/G 0.298 Asian (Han Chinese) A/A 0.512 A/G 0.419 G/G 0.007 Asian (Japanese) A/A 0.625 A/G 0.302 G/G 0.07 S.S.Africa (Nigerian) A/A 0.331 A/G 0.458 G/G 0.211 S.S.Africa (Kenyan) A/A 0.496 A/G 0.425 G/G 0.08	G allele = associated with lower bronchodilator responsiveness, increased risk of pancreatic cancer	15282200, 15651992, 19753122
rs2239185	C>T	12	47042110	-	Intron 6	Decreased VDR = decreased 1α,25-(OH)2D3 levels	G=0.494/621	S.S.Africa (Nigerian) C/C 0.217 C/T 0.483 T/T 0.3 Asian (Han Chinese) C/C 0.533 C/T 0.333 T/T 0.133 Asian (Japanese) C/C 0.326 C/T 0.558 T/T 0.116	C allele = associated with asthma susceptibility in childhood and adult asthma T allele = fluctuations in serum homocysteine and blood lead concentrations, increased risk of renal cancer	15282199, 15282200, 15282200, 20006704, 19745160, 19622139, 15282199, 19753122

Table 6.1 Selected *VDR* polymorphisms that result in altered levels of $1\alpha,25\text{-}(OH)_2D_3$ and are associated with disease (including gene characteristics and PubMed reference number).

6.2 Materials and Methods

6.2.1 Materials.

Absolute™ QPCR Master Mix (2X), DNA polymerase, $MgCl_2$, dNTPs and buffer were obtained from Thermo Fisher, (Loughborough, UK). Custom assays for VDR (rs11568820A>G, rs2228570A>G, rs1544410G>A, rs7975232C>A, rs731236C>T) allelic discrimination analysis were purchased from Applied Biosystems (Warrington, UK). Isopropyl alcohol and ethanol were obtained from Fisher Scientific (Loughborough, UK). White 96-well PCR plates (Hard-Shell®) and real-time PCR machines (Chromo4™) were obtained from Bio-Rad Laboratories Ltd (Hertfordshire, UK). Absolute™ QPCR clear adhesive plate covers were purchased from ABgene House (Surrey, UK). Genomic DNA extraction kit (QIAmp®) and enzymes were purchased from Qiagen Ltd (West Sussex, UK). All other materials were of highest analytical grade and purchased Sigma-Aldrich Ltd (Dorset, UK).

6.2.2 Donor information

Healthy human volunteers were recruited from the Royal Liverpool University Hospital. Each participant gave informed, written consent for extraction of whole blood and D2 intestinal biopsies and the study was approved by the local research Ethics committee. Gene expression and genotype analysis were completed in all 84 donors. Ethnic origins were as follows; 4 Caucasian European, 75 Caucasian British, 4 African and 1 Cantonese Chinese. Due to the small size of the different ethnic groups, it was not possible to assess the effect of ethnicity on vitamin D gene expression or SNPs. Donor age range was 19 years old to 88 years old with an average age of 60 years old. The cohort included 43 males and 41 females.

6.2.3 mRNA and cDNA Quantification

mRNA was extracted from D2 biopsies using Trizol reagent and reverse transcribed using standard methodology as described in section 2.2.6 and 2.2.7.

6.6.4 Quantitative real time-PCR

A Chromo4™ real time-PCR (LifeTechnologies, UK) was used to determine the gene expression of selected genes (Table 2.2) and conditions were completed as described in section 2.2.8.

6.2.5 Extraction of genomic DNA

Whole blood donor samples were inverted, warmed to room temperature and 200 µl of sample added to 20 µl of Qiagen protease buffer in a sterile eppendorf. Following the addition of 200 µl lysis buffer AL, the samples were pulse-vortexed for 15 sec. Samples were incubated for 10 min at 56 ^{o}C, 200 µl of 100% ethanol added to each sample and again pulse-vortexed for 15 sec. Without touching the rim, the sample solution was transferred to a spin column and centrifuged for 1 min at 6000 x g. The filter was removed to a clean collection tube and filtrate discarded. The sample was washed in 500 µl of wash buffer AW1 and centrifuged for 1 min at 6000 x g. The filter was again removed to a clean collection tube and washed further in 500 µl of wash buffer AW2 and centrifuged at 17000 x g for 3 min to dry the membrane completely. All filtrate was discarded. The filter was transferred to a new sterile eppendorf and 50 µl of elution buffer AE added to the membrane. The membrane was incubated for 3 min at room temperature and centrifuged for 1 min at 6000 x g to elute the genomic DNA (gDNA). The filter was discarded and gDNA spectrophotometrically analysed using a Nanodrop1000 (as per the method described

in section 2.2.6) to determine the concentration and purity. The sample was stored at -20 ^{o}C for future use.

6.2.6 Genotyping of VDR polymorphisms by real time-PCR based allelic discrimination

Real time-PCR reactions were made to a total volume of 25 µl in a 96-well plate, comprising of the following ingredients: 2X Absolute™ QPCR Mix (12.5 µl) containing buffer, $MgCl_2$, dNTPs and DNA polymerase (Thermo-Start™), 9.5 µl protease and nuclease free water, 40X primer/probe custom assay (0.625 µl) and genomic DNA (40 ng/µl) was added (each sample was completed in duplicate). To ensure specific amplification a negative control was included where water was substituted for the gDNA (6 wells). In addition, a positive control was included for all alleles (heterozygote, homozygous common allele and homozygous variant allele) (2 wells/allele). The 96-well plate was covered with an Absolute™ QPCR optically clear adhesive film and centrifuged at 500 x g for 2 min, allowing the components to mix, remove air bubbles and ensure the ingredients had collected at the bottom of the well and to prevent evaporation during the heat cycling.

The real time-QPCR thermal cycling was completed using a Chromo4™ PCR machine to genotype the five *VDR* polymorphisms rs11568820A>G, rs2228570A>G, rs731236C>T, rs1544410G>A, rs7975232C>A (Table 6.2). Thermal cycling conditions consisted of: 15 min at 95 ^{o}C to activate the enzyme, followed by 50 cycles of 15 sec at 95 ^{o}C for enzyme denaturation and 60 sec at 60 ^{o}C for annealing and extension. The Chromo4™ was set to excite FAM and VIC at a wavelength of 488nm and absorbance was read at 518 nm and 552 nm, respectively. The intensity of the

fluorescence for each dye/allele was recorded using Opticon Monitor™ software. Genotypes were determined from fluorescence intensity at endpoint.

Gene	SNP ID	SNP Alleles	Assay ID	Assay Sequence ([VIC/FAM])
VDR	rs2228570	A/G	C__12060045_20	GGAAGTGCTGGCCGCCATTGCCTCC[**A/G**]TCCCTGTA AGAACAGCAAGCAGGCC
VDR	rs7975232	A/C	C__28977635_10	AAGGCACAGGAGCTCTCAGCTGGGC[**A/C**]CCTCACT GCTCAATCCCACCACCCC
VDR	rs731236	A/G	C___2404008_10	TGGACAGGCGGTCCTGGATGGCCTC[**A/G**]ATCAGCG CGGCGTCCTGCACCCCAG
VDR	rs11568820	C/T	C___2880808_10	ACCCATAATAAGAAATAAGTTTTTA[**C/T**]TGTGACCT AGTTTACTCAGGAATAT
VDR	rs1544410	C/T	C___8716062_10	GAGCAGAGCCTGAGTATTGGGAATG[**C/T**]GCAGGCC TGTCTGTGGCCCCAGGAA

Table 6.2 Applied Biosystems Assay ID and sequence of the *VDR* polymorphism for SNP analysis by realtime-PCR.
6-FAM: 6-carboxyfluorescein; VIC: vasoactive intestinal contractor
The bold underlined style represents the site of the variant allele.

6.6.7 Data analysis

Results for categorical data were completed in duplicate for each donor and expressed as the median with interquartile range (IQR) unless stated otherwise. Distribution of the data was determined via Shapiro-Wilk test. Categorical data was compared using the Kruskal Walis or Mann-Whitney test. Univariate and multivariate linear regression analysis was completed (SPSS Statistics Software, Version 21, IBM) and to avoid false positives Bonferroni correction was applied. Pearson's rank or Spearman correlation coefficient was used to assess the correlation of continuous data. Bonferroni correction:

$$\text{Bonferroni correction} = \frac{p \text{ value from multivariate analysis}}{\text{Number of co-variates in the regression}}$$

6.3 Results

6.3.1 Summary of gene expression analysis in D2 biopsies

ABCB1, *CAR* and *OATP1B1* expression were detectable in all samples; *VDR* expression was detectable in 76 out of 84 samples, *PXR* in 80 out of 84 samples and *CYP3A4* in 81 out of 84 samples.

6.3.2 Summary of genotype frequencies in D2 biopsies

Genotype was characterised and achieved for 5 *VDR* SNPs in the D2 biopsies (Table 6.3). Population frequencies were in agreement with published data (see Table 6.1).

***VDR* Polymorphism**	**Population Frequency**
rs11568820	A/A 0.05 A/G 0.36 G/G 0.59
rs731236	C/C 0.14 C/T 0.46 T/T 0.40
rs1544410	A/A 0.15 A/G 0.46 G/G 0.39
rs2228570	T/T 0.11 C/T 0.40 C/C 0.49
rs7975232	A/A 0.10 A/C 0.21 C/C 0.69

Table 6.3 *VDR* genotype frequencies in the donor D2 biopsies

6.3.3 Univariate and multivariate analysis for associations with VDR expression

Univariate linear regression analysis showed no associations with *VDR* expression and donor demographics/physical characteristics such as gender or age. *VDR* expression was correlated with *PXR* and *CAR* expression ($p<0.0000001$ and $p=0.000001$, respectively). Bonferroni corrected multivariate stepwise linear regression analysis confirmed *PXR* expression ($p=0.002$) was independently associated with *VDR* expression. However, CAR did not withstand Bonferroni correction (Table 6.4).

VDR	Univariate		Multivariate		
Covariate	β (95% Confidence Interval)	*P*	β (95% Confidence Interval)	*P*	Bonferroni Corrected *P*
Gender	-0.145 (-1.109 – 0.818)	0.76	-	-	-
Age	0.013 (-0.016 – 0.041)	0.39	-	-	-
PXR	-0.717 (-0.957 - -0.477)	<0.0000001	-0.547 (-0.837 - -0.258)	0.0003	0.002
CAR	-0.975 (-1.298 - -0.625)	0.000001	-0.44 (-0.878 – -0.002)	0.05	-

Table 6.4 Bonferroni corrected, multivariate analysis of *VDR* expression with donor demographics/physical characteristics, gene expression or genotype

6.3.4 Univariate and multivariate analysis for associations of VDR expression with VDR SNPs

The 5 *VDR* SNPs (rs11568820, rs731236, rs1544410, rs2228570, rs7975232) were compared to VDR mRNA expression. rs2228570 and rs7975232 were significantly correlated to lower expression in VDR (p=0.03 and p=0.04, respectively). All other SNPs had no significant effect on VDR expression (Table 6.5).

VDR Polymorphism	Effect on *VDR* expression (*p* value)
rs11568820	0.39
rs731236	0.26
rs1544410	0.25
rs2228570	0.03
rs7975232	0.04

Table 6.5 Effect of *VDR* SNPs on *VDR* gene expression (significance determined using Kruskal Walis test)

Univariate linear regression analysis showed no associations with *VDR* expression and donor demographics/physical characteristics including gender or age. Bonferroni corrected univariate stepwise linear regression analysis confirmed *VDR* expression was correlated to the genotype rs2228570 (p=0.002) (Table 6.6).

VDR	Univariate		
Covariate	β (95% Confidence Interval)	*P*	Bonferroni Corrected P
Age	0.013 (-0.016 – 0.041)	0.39	-
Gender	-0.145 (-1.109 – 0.818)	0.76	-
rs11568820	0.061 (-0.441 – 0.564)	0.81	-
rs731236	0.32 (-0.182 – 0.822)	0.21	-
rs1544410	0.342 (-0.159 – 0.844)	0.18	-
rs2228570	1.185 (0.571 – 1.798)	0.0002	0.002
rs7975232	-0.461 (-1.496 – 0.575)	0.38	-

Table 6.6 Multivariate analysis of *VDR* expression with donor demographics/physical characteristics or genotype

Due to the presence of 2 clear VDR expresser groups, for each *VDR* SNP, the donors were grouped into 2 classes (high and low VDR expressers) and association with VDR expression determined (Table 6.7). A statistically significant association was observed between rs2228570 (T allele) and VDR expression (p=0.024). No association was observed with VDR expression and any other SNP.

VDR Polymorphism	Effect on *VDR* expression (*p* value)
rs11568820	0.84
rs731236	0.10
rs1544410	0.10
rs2228570	0.02
rs7975232	0.08

Table 6.7 Effect of *VDR* SNPs (when grouped as 2 classes; high and low VDR expressers) on *VDR* gene expression (significance determined using Mann-Whitney U test)

The association of rs2228570 and VDR expression as 3 separate alleles or 2 groups (homozygous T allele and homo-/heterozygous C allele) are illustrated in Figure 6.1a and b). There was no significant difference in VDR expression between the C/C or C/T alleles. However, when compared to T/T allele, both C/C and C/T alleles expressed significantly less VDR mRNA ($p<0.0001$) (Figure 6.1a). The T allele impacts on the amino acid sequence, reducing the protein capacity and transcriptional activation (alters the initial AUG) hence the lower CYP3A4 and ABCB1 mRNA expression is to be expected. However, the C allele was associated with significantly lower VDR mRNA expression but more CYP3A4 and ABCB1 mRNA expression when compared to individuals homozygous for the T allele ($p<0.001$) (Figure 6.8, 6.10). The results suggest the longer amino acid sequence has more efficient transcriptional activity (in comparison to the shorter sequence) but hinders the posttranslational activity.

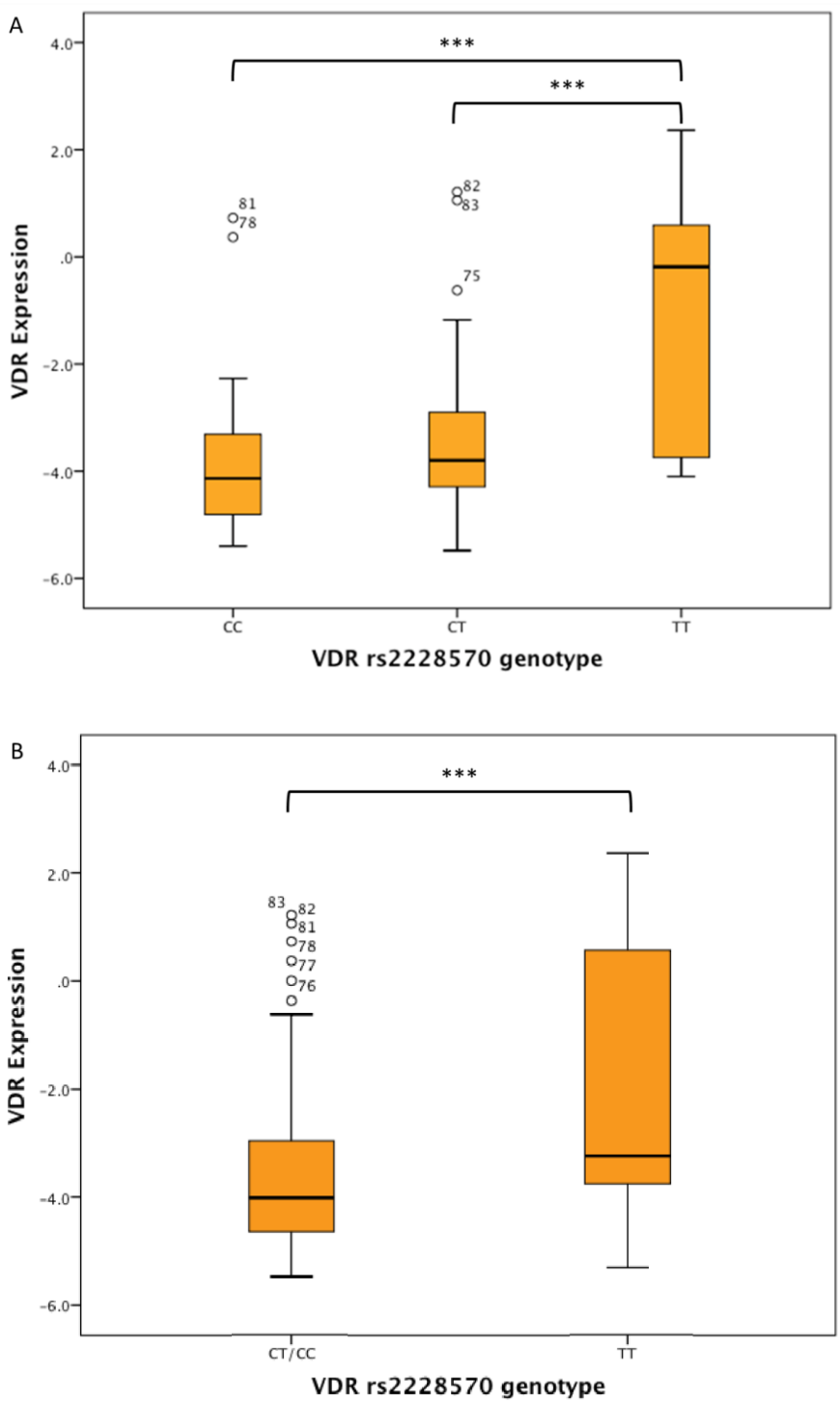

Figure 6.1 Box plots illustrating the association between *VDR* rs2228570 (2T>C) (A) and *VDR* rs2228570 (2T>C) as 2 groups (high and low *VDR* expressers) (B) and VDR expression. Statistical analysis was conducted using a Mann–Whitney U test, *p, 0.05; **p, 0.01; ***p, 0.001. Data is expressed as median values (horizontal line) and IQR (bars) with outliers (donors) numbered

6.3.5 Univariate and multivariate analysis for associations with PXR expression

Univariate linear regression analysis showed no associations with *PXR* expression and donor demographics/physical characteristics including gender or age. *PXR* expression was correlated with *VDR* and *CAR* expression ($p<0.0000001$ and $p<0.0000001$, respectively). Bonferroni corrected multivariate stepwise linear regression analysis confirmed *VDR* expression ($p=0.001$) and *CAR* expression ($p=0.005$) were independently associated with *PXR* expression (Table 6.8).

PXR	Univariate		Multivariate		
Covariate	β (95% Confidence Interval)	*P*	β (95% Confidence Interval)	*P*	Bonferroni Corrected *P*
Gender	0.199 (-0.501 – 0.9)	0.57	-	-	-
Age	0.006 (-0.014 – 0.026)	0.54	-	-	-
VDR	-0.478 (-0.638 - -0.318)	<0.0000001	-0.319 (-0.482 - -0.155)	0.0002	0.001
CAR	0.765 (0.476 – 1.054)	<0.0000001	0.536 (0.23 – 0.842)	0.001	0.005

Table 6.8 Bonferroni corrected multivariate analysis of *PXR* expression with donor demographics/physical characteristics or gene expression

6.3.6 Univariate and multivariate analysis for associations of PXR with VDR SNPs

The 5 *VDR* SNPs (rs11568820, rs731236, rs1544410, rs2228570, rs7975232) were compared to PXR mRNA expression. rs2228570 was significantly correlated to lower expression of PXR ($p=0.03$). All other SNPs had no significant effect on PXR expression (Table 6.9).

VDR Polymorphism	Effect on *PXR* expression (*p* value)
rs11568820	0.53
rs731236	0.61
rs1544410	0.58
rs2228570	0.03
rs7975232	0.79

Table 6.9 Effect of *VDR* SNPs on *PXR* gene expression (significance determined using Kruskal Walis test)

Univariate linear regression analysis showed no associations with *PXR* expression and donor gender or age. *PXR* expression was correlated with the genotype rs2228570 (p=0.002). Bonferroni corrected multivariate stepwise linear regression analysis confirmed the VDR genotype rs2228570 (p=0.01) was independently associated with *PXR* expression (Table 6.10).

PXR	Univariate		Multivariate		
Covariate	β (95% Confidence Interval)	*P*	β (95% Confidence Interval)	*P*	Bonferroni Corrected *P*
Age	0.006 (-0.014 – 0.026)	0.54	-	-	-
Gender	0.199 (-0.501 – 0.900)	0.57	-	-	-
rs11568820	0.003 (-0.365 – 0.371)	0.99	-	-	-
rs731236	-0.008 (-0.376 – 0.359)	0.96	-	-	-
rs1544410	0.007 (-0.363 – 0.378)	0.97	-	-	-
rs2228570	-0.704 (-1.161 - -0.248)	0.003	-0.721 (-1.168 - -0.274)	0.002	0.01
rs7975232	-0.119 (-0.875 – 0.636)	0.75	-	-	-

Table 6.10 Multivariate analysis of *PXR* expression with donor demographics/physical characteristics or *VDR* genotype

6.3.7 Univariate and multivariate analysis for associations with CAR expression

Univariate linear regression analysis showed no associations with *CAR* expression and donor demographics/physical characteristics including gender or age. *CAR* expression was correlated with *VDR* and *PXR* expression (p=0.00001 and p<0.0000001, respectively). Bonferroni corrected multivariate stepwise linear regression analysis confirmed *PXR* expression (p=0.001) was independently associated with *CAR* expression. However, VDR did not withstand Bonferroni correction (Table 6.11).

CAR	Univariate		Multivariate		
Covariate	β (95% Confidence Interval)	*P*	β (95% Confidence Interval)	*P*	Bonferroni Corrected *P*
Gender	0.223 (-0.291 – 0.736)	0.39	-	-	-
Age	0.003 (-0.006 – 0.023)	0.26	-	-	-
VDR	-0.343 (-0.457 - -0.229)	0.000001	-0.129 (-0.257 - -0.001)	0.05	-
PXR	0.353 (0.22 – 0.487)	<0.0000001	0.293 (0.137 – 0.450)	0.0004	0.001

Table 6.11 Bonferroni corrected, multivariate analysis of *CAR* expression with donor demographics/physical characteristics or gene expression

6.3.8 Univariate and multivariate analysis for associations of CAR expression with VDR SNPs

The 5 *VDR* SNPs (rs11568820, rs731236, rs1544410, rs2228570, rs7975232) were compared to CAR mRNA expression. rs2228570 was significantly correlated with a lower expression in CAR (p=0.008). All other SNPs had no significant effect on CAR expression (Table 6.12).

VDR Polymorphism	Effect on *CAR* expression (*p* value)
rs11568820	0.82
rs731236	0.90
rs1544410	0.93
rs2228570	0.008
rs7975232	0.58

Table 6.12 Effect of *VDR* SNPs on *CAR* gene expression (significance determined using Kruskal Walis test)

Univariate linear regression analysis showed no associations with *CAR* expression and donor demographics/physical characteristics including gender or age. *CAR* expression was correlated with the genotype rs2228570 (p=0.02). However, the genotype rs2228570 did not withstand Bonferroni correction (Table 6.13).

CAR	Univariate		
Covariate	β (95% Confid nce Interval)	*P*	Bonferroni Corrected P
Age	0.008 (-0.006 - 0.023)	0.26	-
Gender	0.223 (-0.219 - 0.736)	0.39	-
rs11568820	-0.125 (-0.407 - 0.156)	0.38	-
rs731236	0.013 (-0.254 - 0.317)	0.83	-
rs1544410	0.021 (-0.267 - 0.308)	0.89	-
rs2228570	-0.441 (-0.809 - 0.073)	0.02	-
rs7975232	0.160 (-0.426 - 0.745)	0.59	-

Table 6.13 Multivariate analysis of *CAR* expression with donor demographics/physical characteristics or *VDR* genotype

6.3.9 Univariate and multivariate analysis for associations with CYP3A4 expression

CYP3A4 mRNA expression was positively correlated with PXR and CAR mRNA expression but negatively correlated with VDR mRNA expression. Correlation coefficients, R^2, ranged from 0.68 ($p<0.0000001$), 0.31 ($p<0.0000001$) and 0.38 ($p<0.0000001$), respectively (Figure 6.2a, b, c).

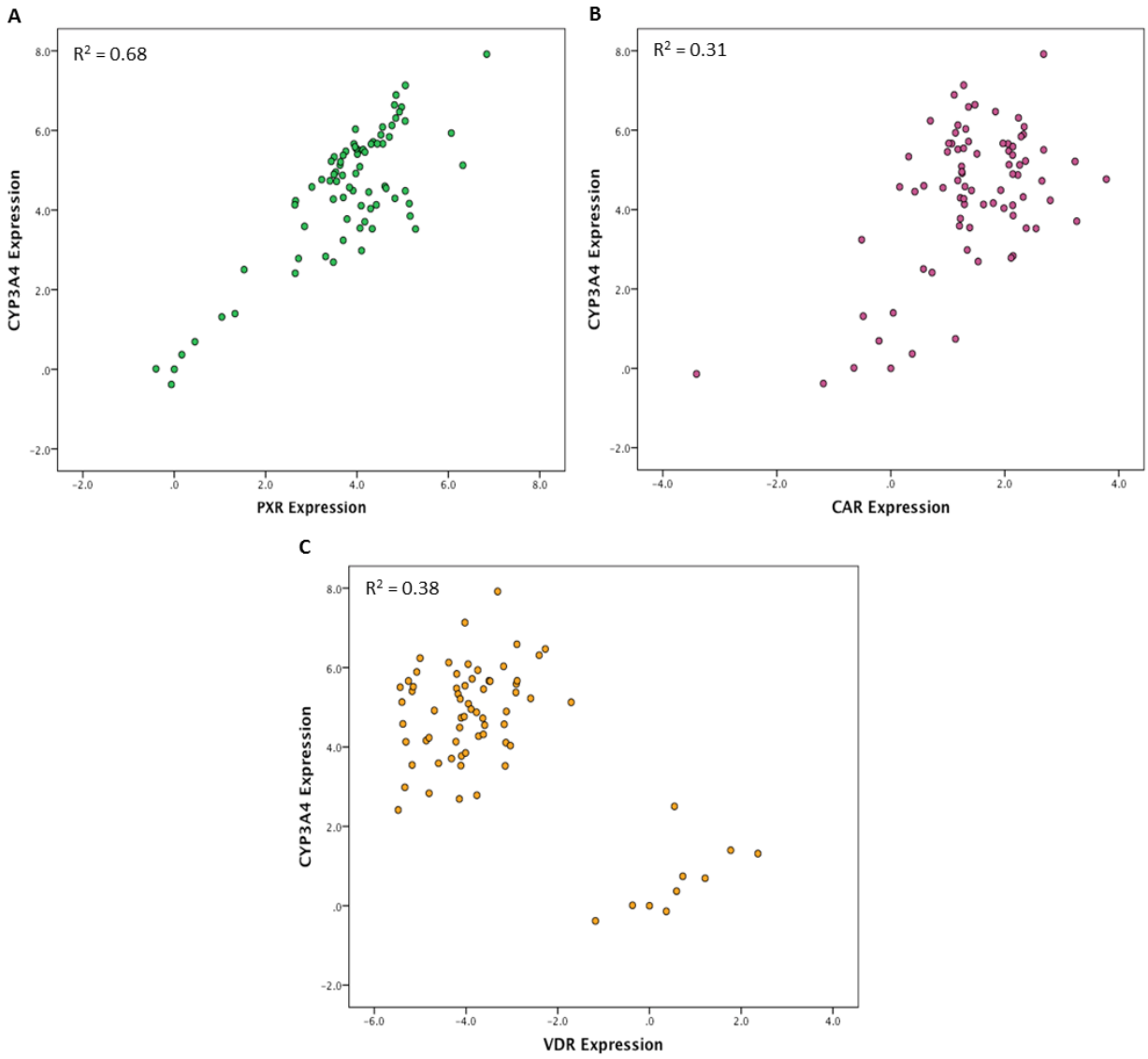

Figure 6.2 Scatter plot representing the correlation between CYP3A4 and PXR (A), CAR (B) and VDR (C) expression in 76 donors.

Univariate linear regression analysis showed no associations with *CYP3A4* expression and donor demographics/physical characteristics including gender or age. *CYP3A4* expression was correlated with *VDR, PXR, CAR, ABCB1* and *OATP1B1* expression ($p<0.0000001$, $p<0.0000001$, $p<0.0000001$, $p=0.000001$ and $p=0.001$, respectively). Bonferroni corrected multivariate stepwise linear regression analysis confirmed *PXR* expression ($p<0.0000005$) was independently associated with *CYP3A4* expression. However, *VDR, CAR, ABCB1* and *OATP1B1* expression were not statistically significant in the multivariate analysis (Table 6.14).

CYP3A4	Univariate		Multivariate		
Covariate	β (95% Confidence Interval)	*P*	β (95% Confidence Interval)	*P*	Bonferroni Corrected *P*
Gender	0.327 (-0.561 – 1.215)	0.47	-	-	-
Age	0.005 (-0.021 – 0.031)	0.69	-	-	-
VDR	-0.613 (-0.802 - -0.424)	<0.0000001	-0.094	0.25	-
PXR	1.013 (0.854 – 1.173)	<0.0000001	1.023 (0.862 – 1.184)	<0.0000001	<0.0000005
CAR	0.931 (0.616 – 1.245)	<0.0000001	0.067	0.41	-
ABCB1	0.772 (0.621 – 0.924)	0.000001	-0.098	0.49	-
OATP1B1	-0.505 (-0.797 – 0.213)	0.001	-0.004	0.96	-

Table 6.14 Bonferroni corrected, multivariate analysis of *CYP3A4* expression with donor demographics/physical characteristics or gene expression

6.3.10 Univariate and multivariate analysis for associations of CYP3A4 expression with VDR SNPs

The 5 *VDR* SNPs (rs11568820, rs731236, rs1544410, rs2228570, rs7975232) were compared with CYP3A4 mRNA expression. rs2228570 was significantly correlated to lower expression of CYP3A4 ($p=0.04$). All other SNPs had no significant effect on CYP3A4 expression (Table 6.15).

VDR Polymorphism	Effect on *CYP3A4* expression (*p* value)
rs11568820	0.35
rs731236	0.64
rs1544410	0.65
rs2228570	0.04
rs7975232	0.78

Table 6.15 Effect of *VDR* SNPs on *CYP3A4* gene expression (significance determined using Kruskal Walis test)

Univariate linear regression analysis showed no associations with *CYP3A4* expression and donor demographics/physical characteristics including gender or age. *CYP3A4* expression was correlated with the genotype rs2228570 (p=0.02). Multivariate analysis was therefore not conducted; the genotype rs2228570 did not withstand Bonferroni correction (Table 6.16).

CYP3A4	Univariate		
Covariate	β (95% Confidence Interval)	*P*	Bonferroni Corrected P
Age	0.005 (-0.021 – 0.031)	0.69	-
Gender	0.327 (-0.561 – 1.215)	0.47	-
rs11568820	-0.307 (-0.777 – 0.163)	0.20	-
rs731236	-0.121 (-0.595 – 0.353)	0.61	-
rs1544410	-0.141 (-0.618 – 0.336)	0.56	-
rs2228570	-0.705 (-1.309 – 0.102)	0.02	-
rs7975232	-0.015 (-0.996 – 0.996)	0.98	-

Table 6.16 Bonferroni corrected univariate analysis of *CYP3A4* expression with donor demographics/physical characteristics or *VDR* genotype

6.3.11 Univariate and multivariate analysis for associations with ABCB1 expression

ABCB1 mRNA expression was positively correlated with PXR and CAR mRNA expression but negatively correlated with VDR mRNA expression. Correlation coefficients, R^2, ranged from 0.78 ($p<0.0000001$), 0.31 ($p=0.000001$) and 0.29 ($p=0.000001$), respectively (Figure 6.3a, b and c).

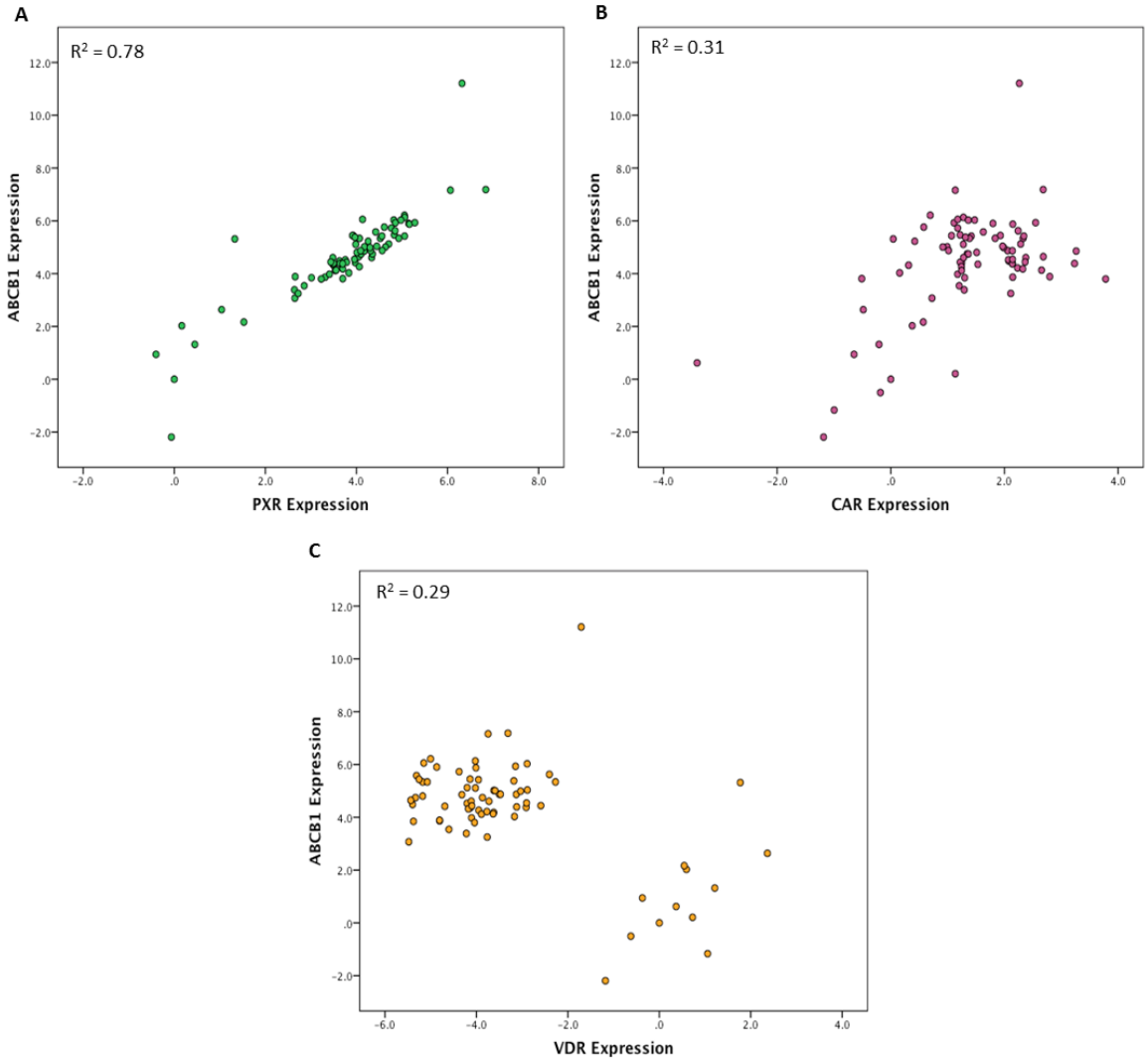

Figure 6.3 Scatter plot representing the correlation between ABCB1 and PXR (A), CAR (B) and VDR (C) expression in 76 donors.

Univariate linear regression analysis showed no associations with *ABCB1* expression and donor demographics/physical characteristics including gender or age. *ABCB1* expression was correlated with *VDR, PXR, CAR, CYP3A4* and *OATP1B1* expression ($p<0.0000001$, $p<0.0000001$, $p=0.000001$, $p=0.00001$ and $p=0.0003$, respectively). Bonferroni corrected multivariate stepwise linear regression analysis confirmed *VDR* and *PXR* expression ($p=0.02$, $p<0.0000005$, respectively) were independently associated with *ABCB1* expression. However, *CAR, CYP3A4* and *OATP1B1* expression were not statistically significant in the multivariate analysis (Table 6.17).

ABCB1	Univariate		Multivariate		
Covariate	β (95% Confidence Interval)	*P*	β (95% Confidence Interval)	*P*	Bonferroni Corrected *P*
Gender	0.446 (-0.489 – 1.39)	0.35	-	-	-
Age	0.008 (-0.02 – 0.036)	0.56	-	-	-
VDR	-0.556 (-0.762 - -0.349)	<0.0000001	0.2 (0.069 – 0.331)	0.003	0.02
PXR	1.057 (0.928 – 1.186)	<0.0000001	1.202 (1.042 – 1.362)	<0.0000001	<0.0000005
CAR	0.962 (0.638 – 1.287)	0.000001	0.02	0.78	-
CYP3A4	0.74 (0.595 – 0.885)	0.00001	-0.032	0.75	-
OATP1B1	-0.576 (-0.877 - -0.276)	0.0003	0.075	0.26	-

Table 6.17 Bonferroni correct multivariate analysis of *ABCB1* expression with donor demographics/physical characteristics or gene expression

6.3.12 Univariate and multivariate analysis for associations of ABCB1 expression with VDR SNPs

The 5 *VDR* SNPs (rs11568820, rs731236, rs1544410, rs2228570, rs7975232) were compared with ABCB1 mRNA expression. No significant effect on ABCB1 expression was observed with any *VDR* SNP (Table 6.18).

VDR Polymorphism	Effect on *ABCB1* expression (*p* value)
rs11568820	0.51
rs731236	0.52
rs1544410	0.55
rs2228570	0.19
rs7975232	0.56

Table 6.18 Effect of *VDR* SNPs on *ABCB1* gene expression (significance determined using Kruskal Walis test)

Univariate linear regression analysis showed no associations with *ABCB1* expression and donor demographics/physical characteristics including gender, age or ethnicity or *VDR* genotype (Table 6.19). Therefore, multivariate analysis was not conducted.

ABCB1	Univariate	
Covariate	β (95% Confidence Interval)	*P*
Age	0.008 (-0.002 – 0.036)	0.56
Gender	0.446 (-0.498 – 1.390)	0.35
rs11568820	0.220 (-0.274 – 0.714)	0.38
rs731236	-0.041 (-0.542 – 0.460)	0.87
rs1544410	-0.020 (-0.525 – 0.484)	0.94
rs2228570	-0.447 (-1.110 – 0.215)	0.18
rs7975232	-0.093 (-1.122 – 0.936)	0.86

Table 6.19 Multivariate analysis of *ABCB1* expression with donor demographics/physical characteristics or *VDR* genotype

6.3.13 Univariate and multivariate analysis for associations with OATP1B1 expression

In contrast to current literature a negative correlation was observed between OATP1B1 mRNA expression and PXR and CAR mRNA expression, with correlation coefficient coefficients ranging from 0.14 (p=0.001) and 0.29 (p=0.0000001), respectively (Figure 6.4a and b). A positive correlation was observed between OATP1B1 mRNA expression and VDR mRNA expression with a correlation coefficient of 0.14 (p=0.001) (Figure 6.4c).

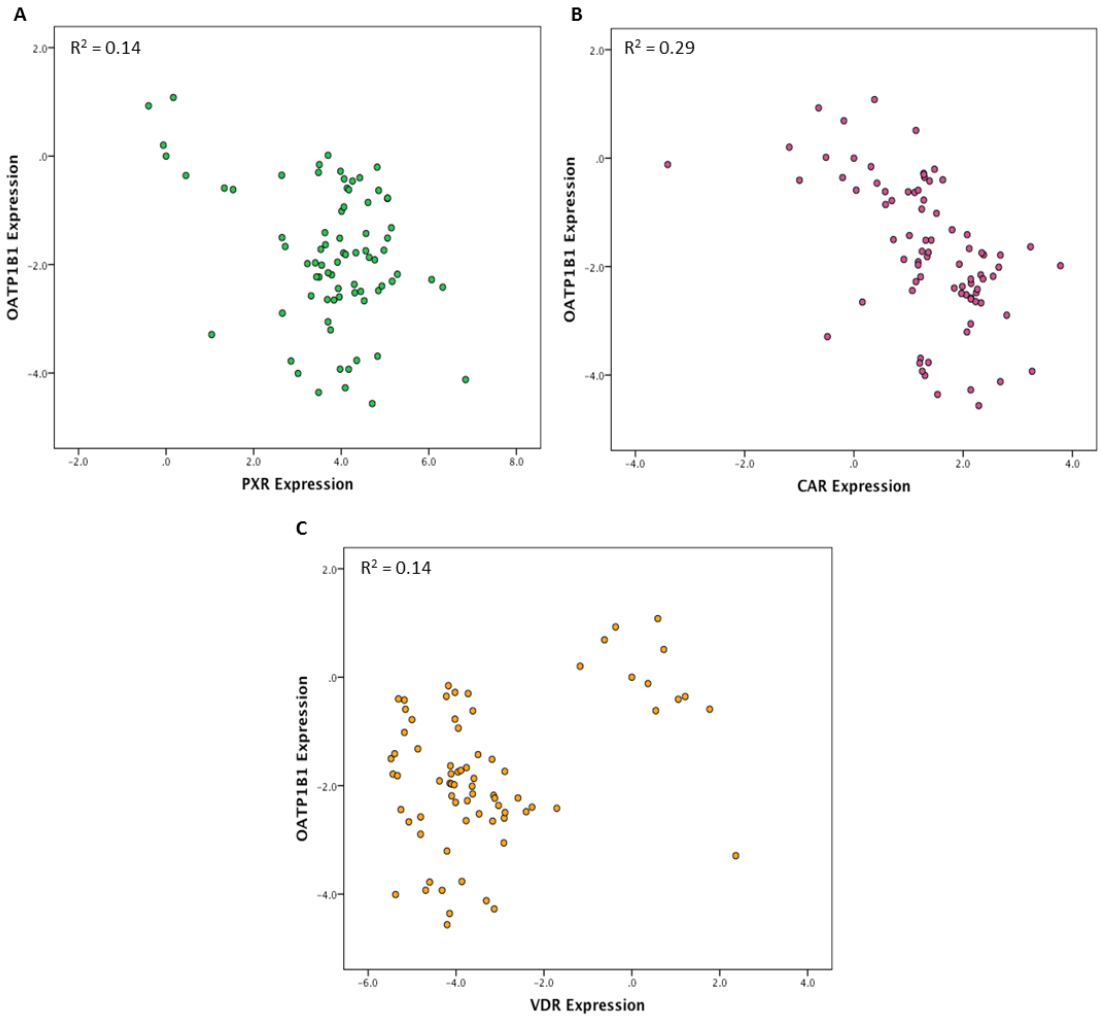

Figure 6.4 Scatter plot representing the correlation between OATP1B1 and PXR (A), CAR (B) and VDR (C) expression in 76 donors.

Univariate linear regression analysis showed no associations with *OATP1B1* expression and donor demographics/physical characteristics including gender. *OATP1B1* expression was correlated with age, *VDR, PXR, CAR, CYP3A4* and *ABCB1* expression (p=0.003, p=0.001, p=0.001, p=0.000001 and p=0.000035, respectively). Bonferroni corrected multivariate stepwise linear regression analysis confirmed age and *CAR* expression (p=0.04 and p=0.0003, respectively) were independently associated with *OATP1B1* expression. However, *VDR, PXR, CYP3A4* and *ABCB1* expression were not statistically significant in the multivariate analysis (Table 6.20).

OATP1B1	Univariate		Multivariate		
Covariate	β (95% Confidence Interval)	*P*	β (95% Confidence Interval)	*P*	Bonferroni Corrected *P*
Gender	0.304 (-0.319 – 0.962)	0.33	-	-	-
Age	-0.027 (-0.044 - -0.01)	0.003	-0.023 (-0.038 - -0.007)	0.005	0.04
VDR	0.262 (0.112 – 0.421)	0.001	0.119	0.35	-
PXR	-0.348 (-0.546 - -0.151)	0.001	-0.2	0.13	-
CAR	-0.638 (-0.864 - -0.431)	0.000001	-0.641 (-0.928 - -0.355)	0.00004	0.0003
CYP3A4	-0.264 (-0.417 - -0.112)	0.001	-0.169	0.18	-
ABCB1	-0.27 (-0.411 - -0.129)	0.00004	-0.062	0.60	-

Table 6.20 Bonferroni corrected multivariate analysis of *OATP1B1* expression with donor demographics/physical characteristics or gene expression

6.3.14 Univariate and multivariate analysis for associations of OATP1B1 expression with VDR SNPs

The 5 *VDR* SNPs (rs11568820, rs731236, rs1544410, rs2228570, rs7975232) were compared with OATP1B1 mRNA expression. No significant effect on OATP1B1 expression was observed with any *VDR* SNP (Table 6.21).

VDR Polymorphism	Effect on *OATP1B1* expression (*p* value)
rs11568820	0.95
rs731236	0.64
rs1544410	0.56
rs2228570	0.37
rs7975232	0.53

Table 6.21 Effect of *VDR* SNPs on *OATP1B1* gene expression (significance determined using Kruskal Walis test)

Univariate linear regression analysis showed no associations with *OATP1B1* expression and donor demographics/physical characteristics including gender or *VDR* genotype. *OATP1B1* expression was correlated with donor age (p=0.003). Multivariate analysis was therefore not conducted. Bonferroni corrected univariate stepwise linear regression analysis confirmed *OATP1B1* expression (p=0.02) was independently associated with age (p=0.02) (Table 6.22).

OATP1B1	Univariate		
Covariate	β (95% Confidence Interval)	*P*	Bonferroni Corrected P
Age	-0.027 (-0.044 to 0.010)	0.003	0.02
Gender	0.304 (-0.319 to 0.926)	0.33	-
rs11568820	-0.027 (-0.353 to 0.298)	0.87	-
rs731236	-0.129 (-0.456 to 0.198)	0.43	-
rs1544410	-0.111 (-0.441 to 0.219)	0.50	-
rs2228570	0.376 (-0.054 to 0.806)	0.09	-
rs7975232	-0.106 (-0.781 to 0.569)	0.76	-

Table 6.22 Multivariate analysis of *OATP1B1* expression with donor demographics/physical characteristics or *VDR* genotype

6.3.15 Exploratory analysis of PXR between high and low VDR expressers

When analysed as a whole group, the expression of VDR was negatively correlated with PXR mRNA expression (Figure 6.5a). However, due to the observation of 2 distinct groups an arbitrary division for VDR expression was applied in subsequent exploratory analysis (VDR high expressers >-1.71). There was a significant difference in PXR mRNA expression between the 2 VDR groups ($p<0.0000001$) (Figure 6.5b). The correlation of PXR mRNA expression with low VDR expressers (Figure 6.5c) and high expressers (Figure 6.5d) was determined. Low and high VDR mRNA levels were positively correlated with mRNA expression of PXR when analysed separately, with correlation coefficients, R^2, ranging from 0.11 ($p=0.008$) and 0.49 ($p=0.03$), respectively (Figure 6.5c and d).

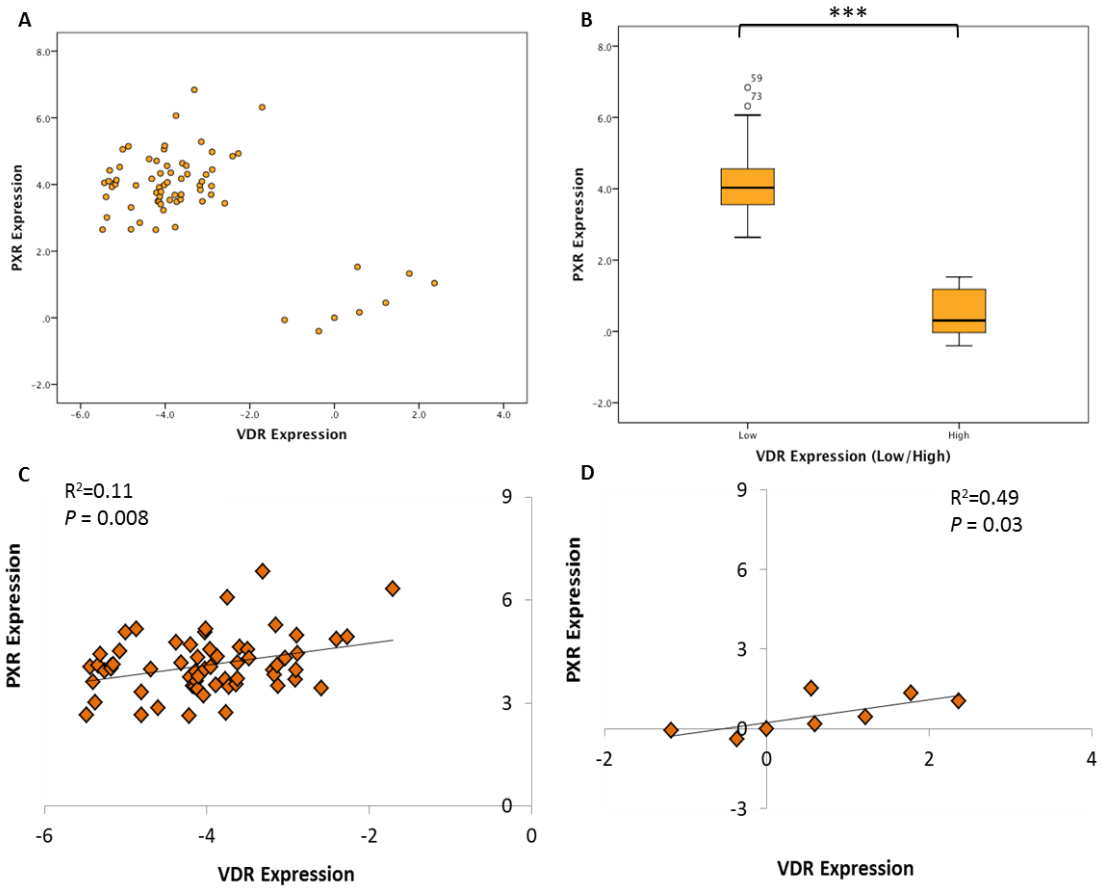

Figure 6.5 Correlations between VDR and PXR expression as a whole group (A), box plot of high and low VDR expressers (median values (horizontal line), IQR

(bars)) (B), scatter plot representing the correlation between low VDR expressers and PXR expression (C) and high VDR expressers and PXR expression (D) (high VDR expression >-1.71).

6.3.16 Exploratory analysis of CAR between high and low VDR expressers

A similar analysis was completed for CAR. There was a significant difference in CAR mRNA expression between the 2 VDR groups ($p<0.00001$) (Figure 6.6b). The correlation of CAR mRNA expression with low VDR expressers (Figure 6.6c) and high expressers (Figure 6.6d) was determined. Low and high VDR mRNA levels were positively correlated with mRNA expression of CAR when analysed separately, with correlation coefficients, R^2, of 0.03 (Figure 6.6c and 6.6d). However, the correlation for each VDR group was not statistically significant.

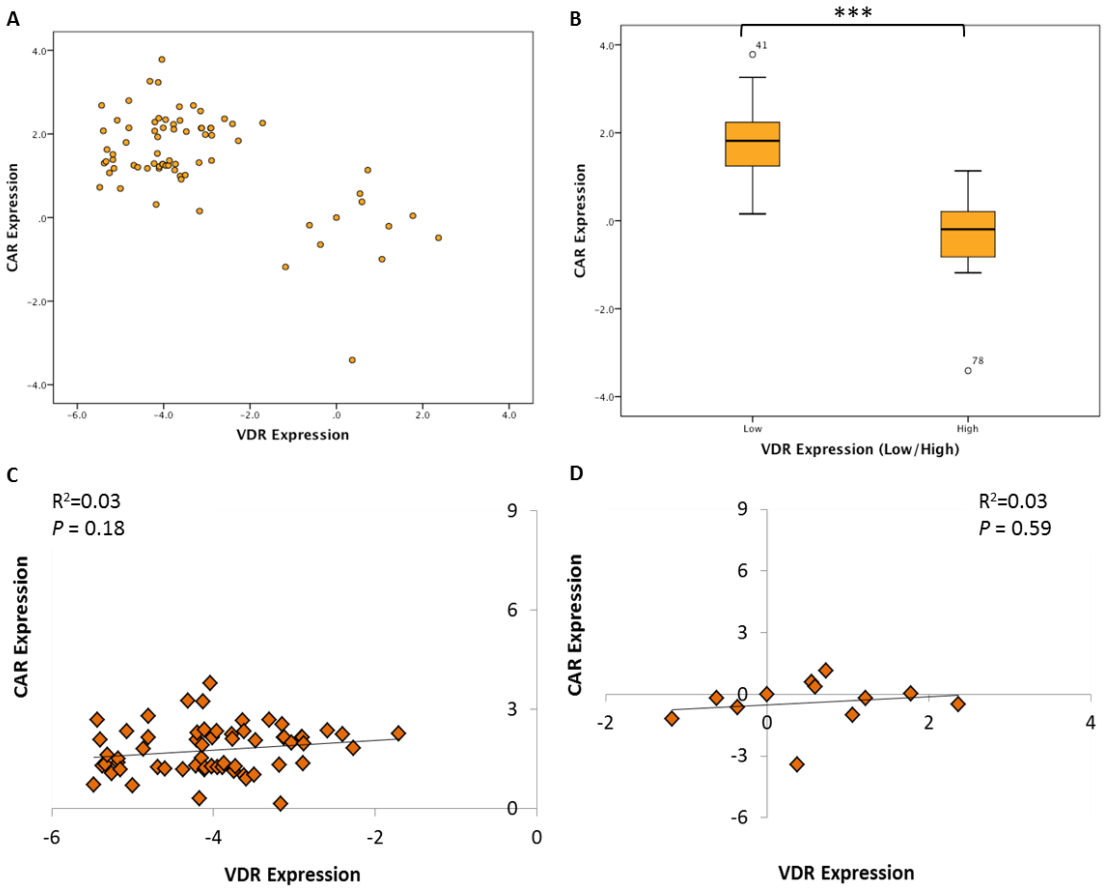

Figure 6.6 Correlations between VDR and CAR expression as a whole group (A),

box plot of high and low VDR expressers (median values (horizontal line), IQR (bars)) (B), scatter plot representing the correlation between low VDR expressers and CAR expression (C) and high VDR expressers and CAR expression (D) (high VDR expression >-1.71).

6.3.17 Exploratory analysis of CYP3A4 between high and low VDR expressers

A similar analysis was completed for CYP3A4. There was a significant difference in CYP3A4 mRNA expression between the 2 VDR groups ($p<0.00001$) (Figure 6.7b). The correlation of CYP3A4 mRNA expression with low VDR expressers (Figure 6.7c) and high expressers (Figure 6.7d) was determined. Low and high VDR mRNA levels were positively correlated with mRNA expression of CYP3A4 when analysed separately, with correlation coefficients, R^2, ranging from 0.09 ($p=0.02$) and 0.4 ($p=0.05$), respectively (Figure 6.7c and d).

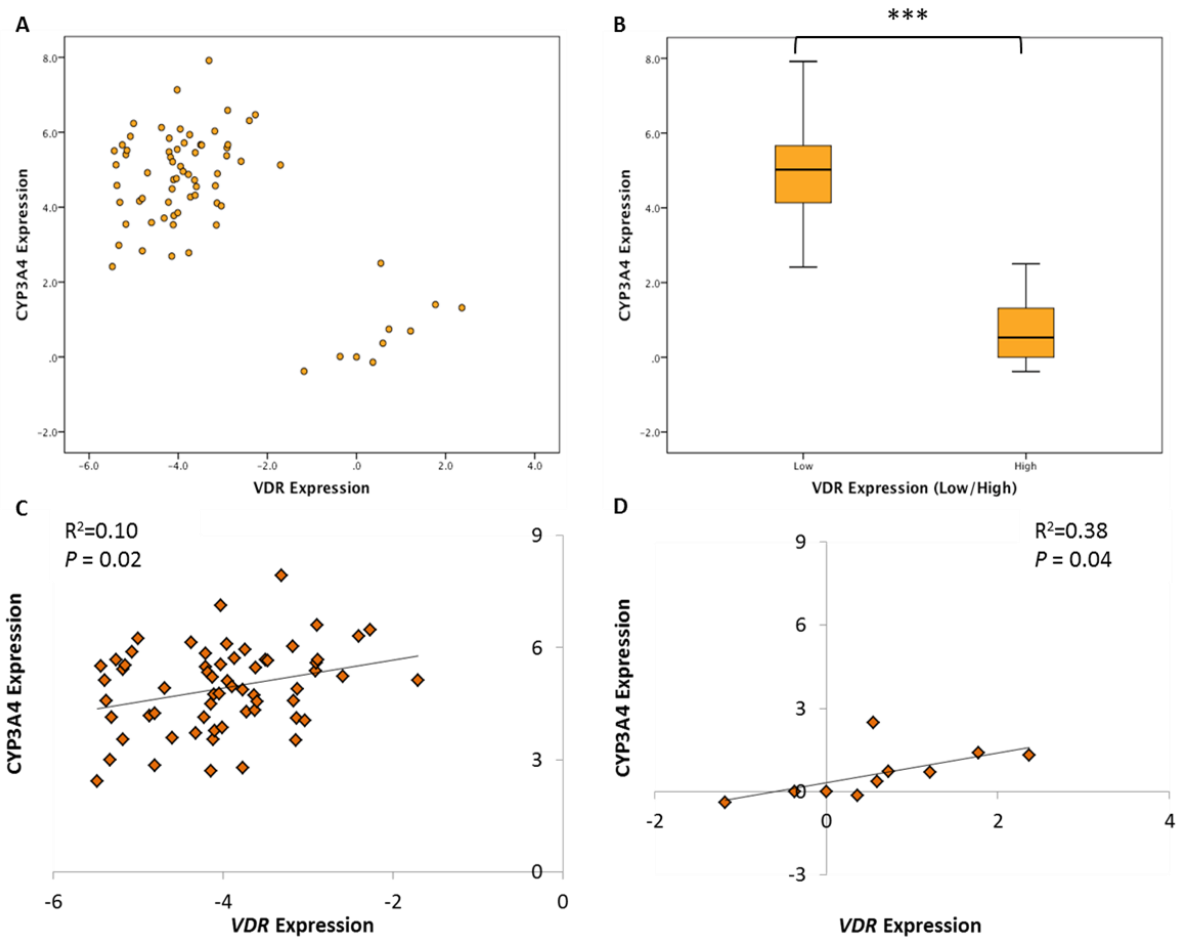

Figure 6.7 Correlations between VDR and CYP3A4 expression as a whole group (A), box plot of high and low VDR expressers (median values (horizontal line), IQR (bars)) (B), scatter plot representing the correlation between low VDR expressers and CYP3A4 expression (C) and high VDR expressers and CYP3A4 expression (D) (high VDR expression >-1.71).

6.3.18 Combined analysis of genotype and gene expression

To determine if the *VDR* SNP rs2228570 contributed to the observation of 2 distinct VDR expressing groups when compared with CYP3A4 expression, bivariate correlation was completed. As observed in Figure 6.8, the C allele was associated with less VDR expression and more CYP3A4 expression.

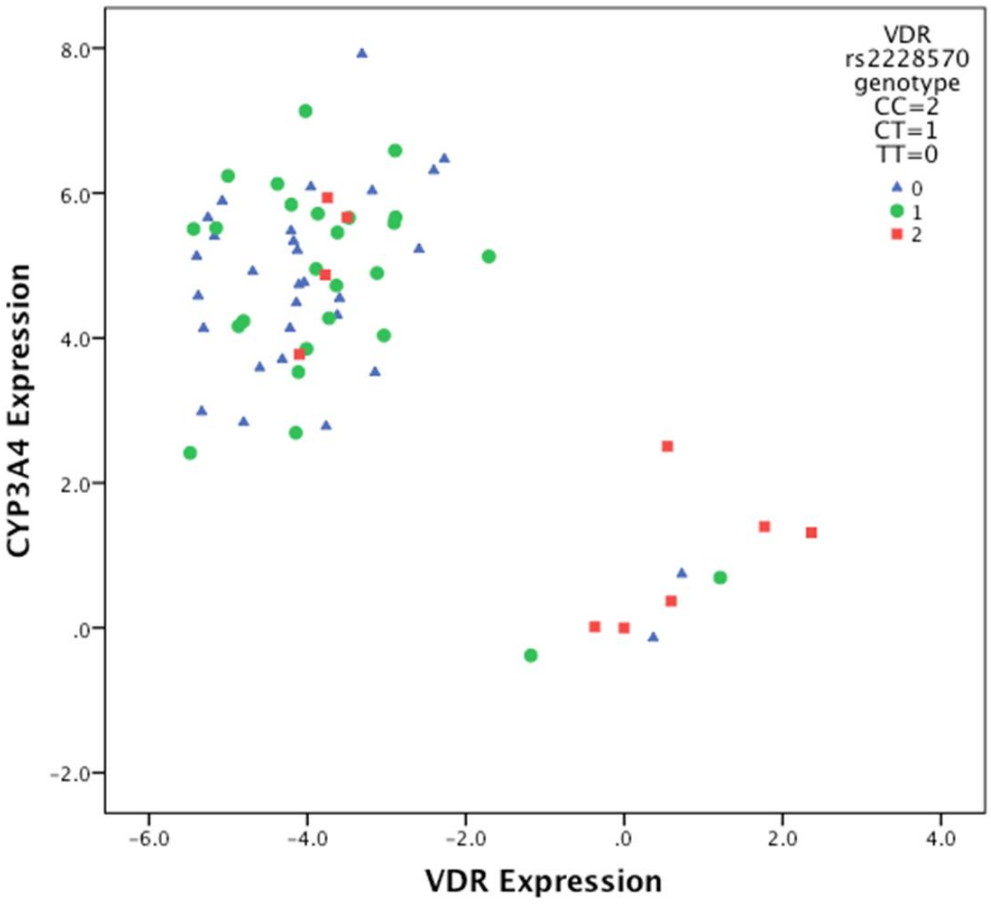

Figure 6.8 Scatter plot representing the correlation between VDR and CYP3A4 expression. Each donor labelled according to their allelic expression of rs2228570 (C/C = 0, C/T = 1, T/T = 2)

6.3.19 Exploratory analysis of ABCB1 between high and low VDR expressers

A similar analysis was completed for ABCB1. There was a significant difference in ABCB1 mRNA expression between the 2 VDR groups ($p<0.00001$) (Figure 6.9b). The correlation of ABCB1 mRNA expression with low VDR expressers (Figure 6.9c) and high expressers (Figure 6.9d) was determined. Low and high VDR mRNA levels were positively correlated with mRNA expression of ABCB1 when analysed separately, with correlation coefficients, R^2, ranging from 0.1 ($p=0.01$) and 0.5 ($p=0.01$), respectively (Figure 6.9c and d).

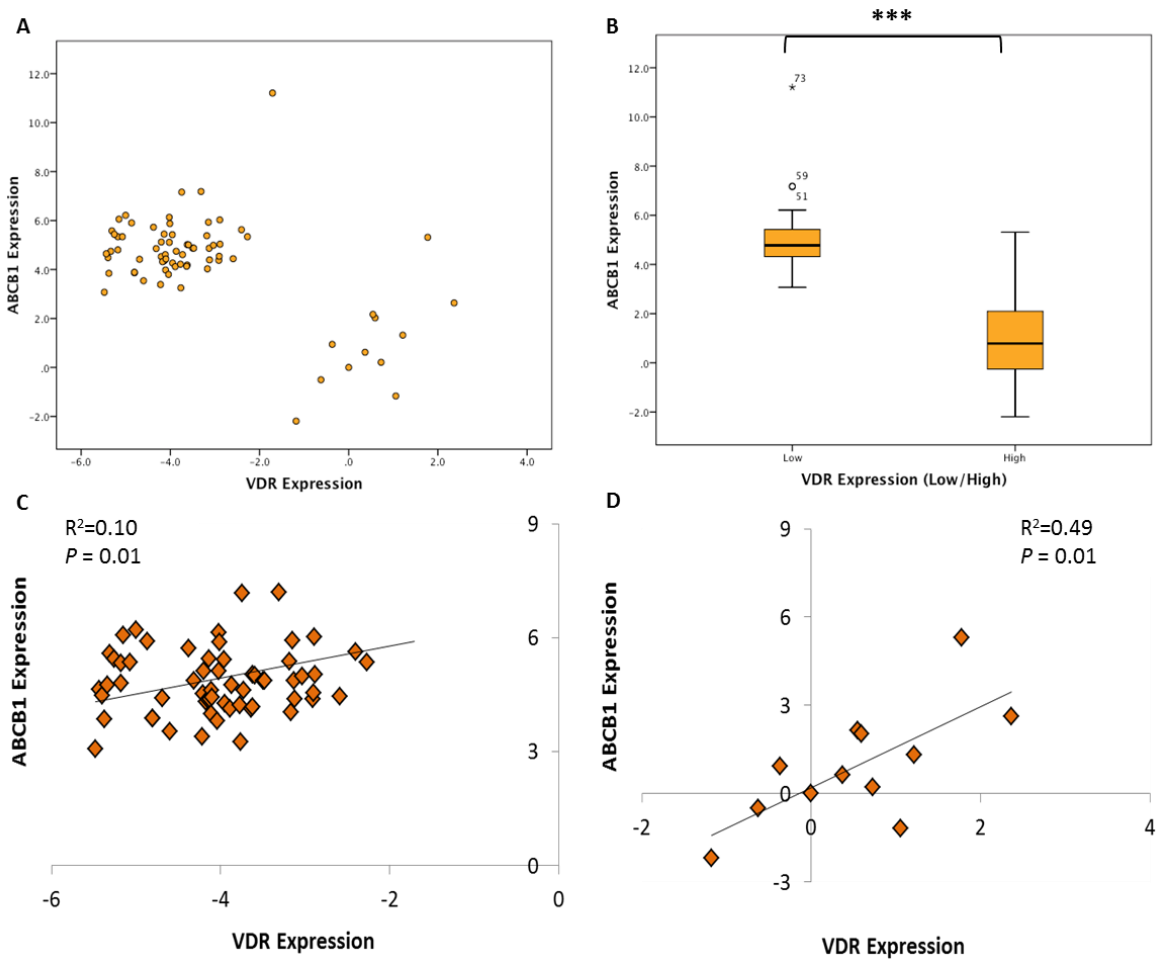

Figure 6.9 Correlations between VDR and ABCB1 expression as a whole group (A), box plot of high and low VDR expressers (median values (horizontal line), IQR (bars)) (B), scatter plot representing the correlation between low VDR expressers and ABCB1 expression (C) and high VDR expressers and ABCB1 expression (D) (high VDR expression >-1.71).

6.3.20 Combined analysis of genotype and gene expression

To determine if the *VDR* SNP rs2228570 contributed to the observation of 2 distinct VDR expressing groups when compared with ABCB1 expression, bivariate correlation was completed. As observed in Figure 6.10, the C allele was associated with less VDR expression and more ABCB1 expression.

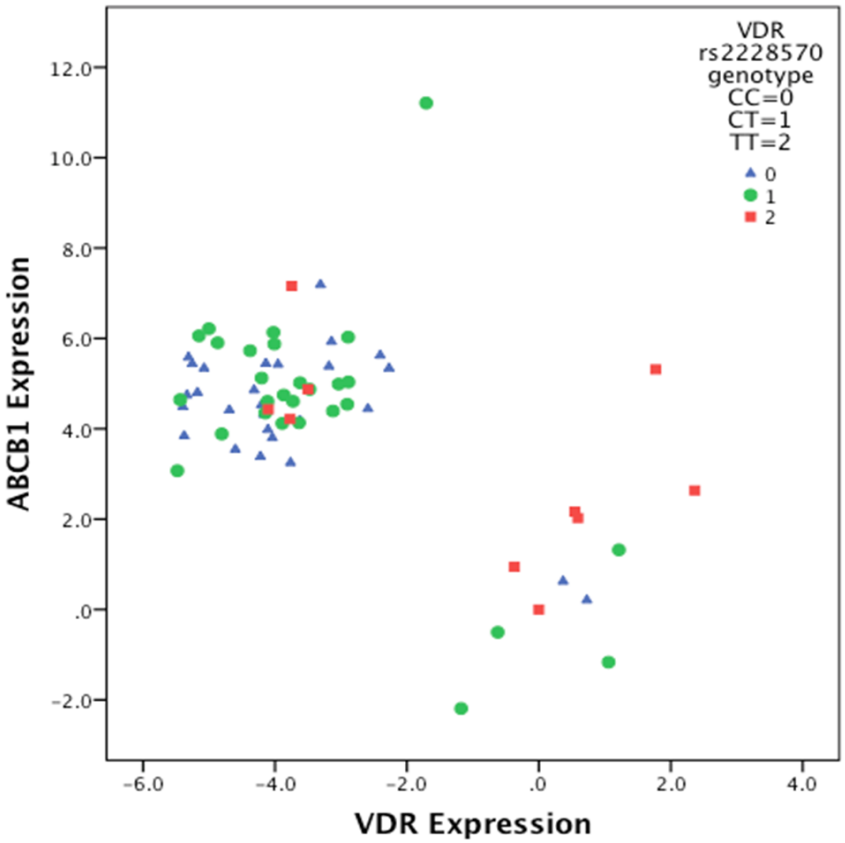

Figure 6.10 Scatter plot representing the correlation between VDR and ABCB1 expression. Each donor labelled according to their allelic expression of rs2228570 (C/C = 0, C/T = 1, T/T = 2)

6.3.21 Exploratory analysis of OATP1B1 between high and low VDR expressers

A similar analysis was completed for OATP1B1. There was a significant difference in OATP1B1 mRNA expression between the 2 VDR groups ($p<0.00001$) (Figure 6.11b). The correlation of OATP1B1 mRNA expression with low VDR expressers (Figure 6.11c) and high expressers (Figure 6.11d) was determined. Low and high VDR mRNA levels were positively correlated with mRNA expression of OATP1B1, with correlation coefficients, R^2, ranging from 0.03 and 0.5 ($p=0.009$), respectively (Figure 6.11c and d). However, the correlation for low VDR expressers was not statistically significant.

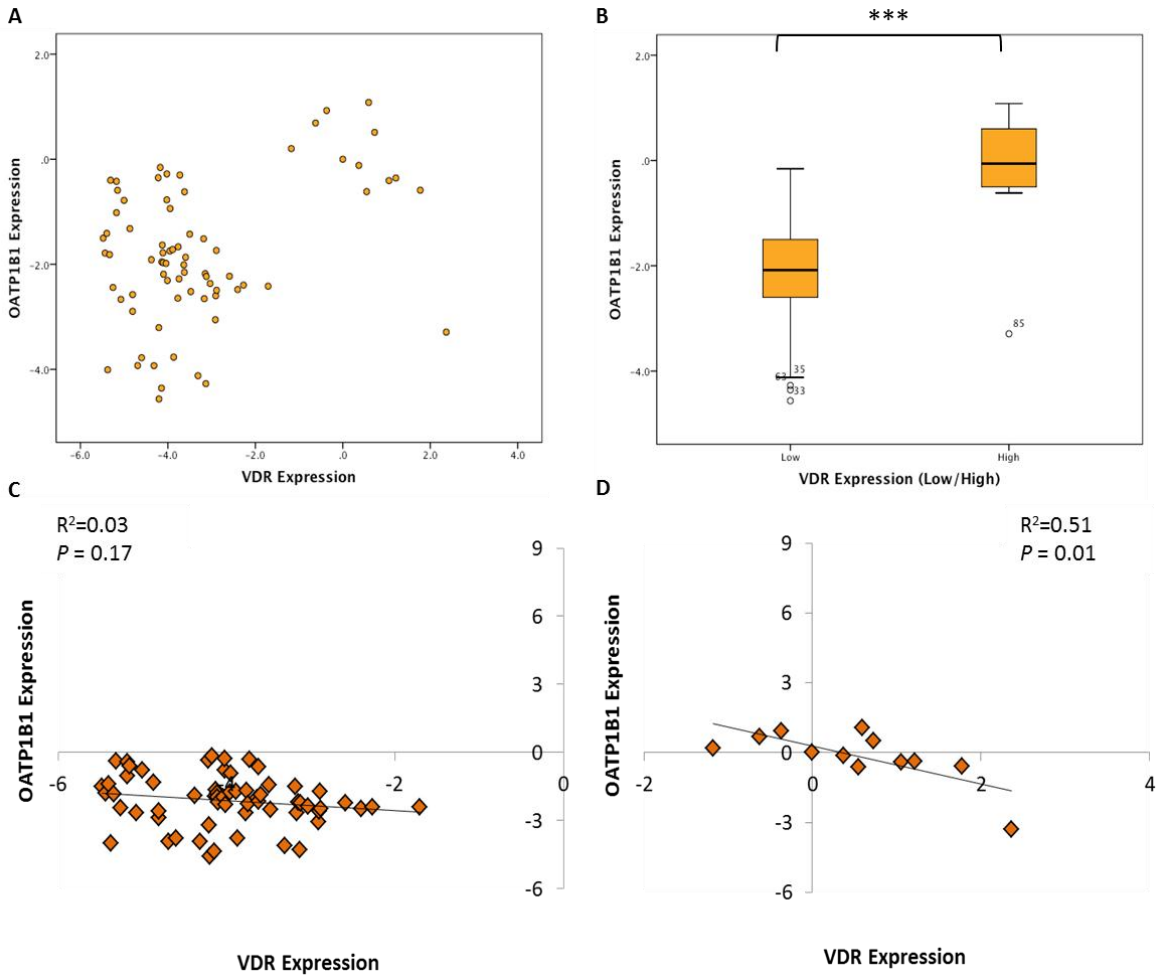

Figure 6.11 Correlations between VDR and OATP1B1 expression as a whole group (A), box plot of high and low VDR expressers (median values (horizontal line), IQR (bars)) (B), scatter plot representing the correlation between low VDR expressers and OATP1B1 expression (C) and high VDR expressers and OATP1B1 expression (D) (high VDR expression >-1.71).

6.3.22 Combined analysis of genotype and gene expression

To determine if the *VDR* SNP rs2228570 contributed to the observation of 2 distinct VDR expressing groups when compared with OATP1B1 expression, bivariate correlation was completed. As observed in Figure 6.12, the C allele was associated with less VDR expression and less OATP1B1 expression.

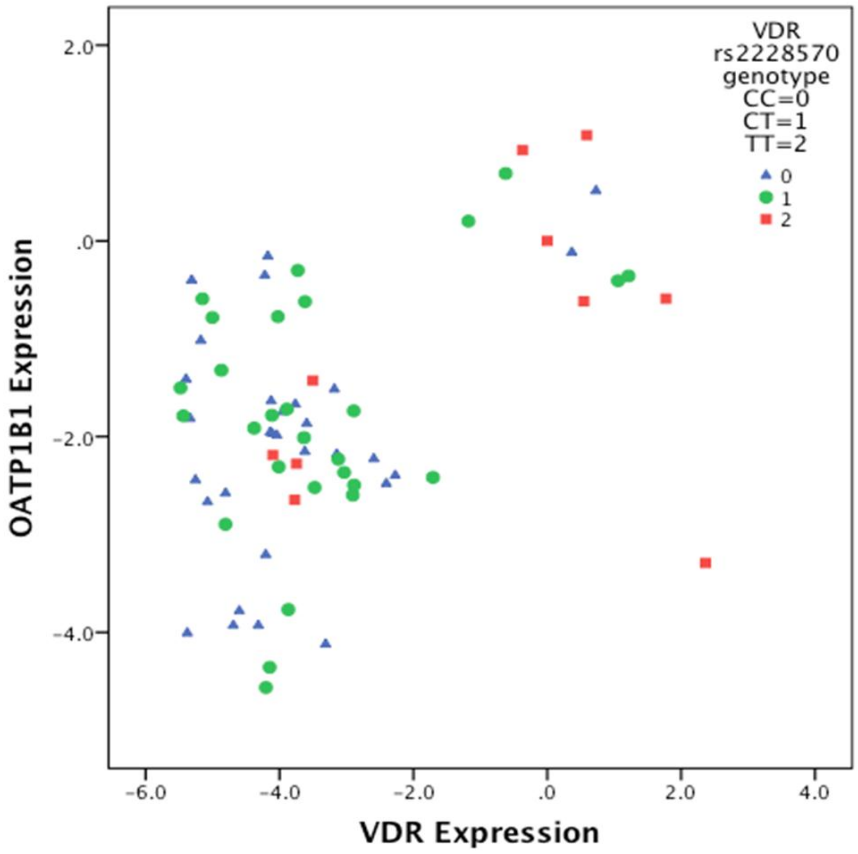

Figure 6.12 Scatter plot representing the correlation between VDR and OATP1B1 expression. Each donor labelled according to their allelic expression of rs2228570 (C/C = 0, C/T = 1, T/T = 2)

6.4 Discussion

Complete functioning of the body's defense mechanisms requires adequate levels of $1\alpha,25\text{-}(OH)_2D_3$ to ensure production of antimicrobicidal proteins (e.g. cathelicidins), chemotaxis of immune cells and regulation of the adaptive and innate immune responses (433, 434). Whilst supplementation with vitamin D improves treatment outcome against conditions such as tuberculosis, psoriasis and vitamin D-dependent rickets (402, 403), alterations of drug pharmacokinetics (PK) may counter-balance the benefits and warrants further studies.

This chapter focused on characterising associations in the human intestine between *VDR* expression and key drug disposition genes including, *PXR, CAR, CYP3A4, ABCB1* and *OATP1B1* in 84 healthy volunteers. In addition, the effects of 5 *VDR* SNPs known to regulate VDR expression were analysed.

Known correlations involving PXR and CAR were analysed to provide confidence in subsequent analysis. In agreement with previous work, *PXR* was positively correlated to *CYP3A4* expression (R^2=0.68, p<0.0000001) (Figure 6.2a) (57, 402) and *ABCB1* expression (R^2=0.78, p<0.0000001) (Figure 6.3a) (54, 435). Whilst OATP1B1 is a liver specific transporter regulated by the nuclear receptor PXR (436), recent studies have established alterations in environment (e.g. inflammation) and cell cycle (e.g. cancer) relax gene expression restrictions (433, 437). Currently there is no described association between PXR and OATP1B1 expression in the human intestine. The correlation between *PXR* and *OATP1B1* reported here suggests that PXR may negatively regulate transcription of this transporter in the intestine (R^2=0.14, p=0.001) (Figure 6.4a). PXR negative regulation of OATP1B1 in the intestine could represent a

novel pharmacological mechanism. Whilst CYP3A4 is induced by PXR the expression of OATP1B1 is reduced, and may thereby enable 'control' of OATP1B1/CYP3A4 substrate transport and metabolism, improving PK parameters. For example, inhibition of OATP1B1 in the hepatic uptake of drugs has lead to positive increases in plasma concentrations (4, 55, 375).

CAR was also positively correlated to *CYP3A4* expression (R^2=0.31, p<0.0000001) (Figure 6.2b) (106) and *ABCB1* expression (R^2=0.31, p=0.00001) (Figure 6.3b) (438) whereas, a negative correlation was also observed between *CAR* and *OATP1B1* expression (R^2=0.29, p=0.001) (Figure 6.4b). This negative association is in contrast to work by Svoboda *et al.,* 2011. However, their work was completed in cell lines and animal models in comparison to the human donors studied here (Figures 6.2-6.4). Further analysis is warranted given OATP1B1 is a major determinant of drug PK (as described in Chapter 4).

No significant associations with donor demographics/physical characteristics, gene expression and genotype were observed for VDR, CAR, CYP3A4 or ABCB1 (Table 6.4, 6.6, 6.11, 6.13, 6.14, 6.16, 6.17 and 6.19). OATP1B1 mRNA expression was significantly associated with donor age (p=0.04) (Table 6.20 and 6.22). A significant independent association with *PXR* expression was observed however it did not withstand Bonferroni correction (Table 6.8). Substantial effects on drug disposition genes are associated with many *PXR* SNPs, which vary between populations (233, 439, 440). However, due to the small cohort and lack of *PXR* SNPs analysed, this association requires further investigation.

Bonferroni corrected multivariate analysis identified VDR to be independently associated with *PXR* and *ABCB1* expression (p=0.001 and p=0.02, respectively) (Table 6.8 and 6.17). However, *VDR* association with *CYP3A4* and *CAR* expression did not withstand Bonferroni correction (Table 6.11 and 6.14). When the correlation coefficient of each gene with *VDR* expression was determined a negative correlation was observed (Figure 6.2-6.4). However, due to the presence of 2 significantly different *VDR* expressing groups ($p<0.001$) (each with their own positive correlation), further analysis compared high *VDR* expressers (>-1.71) and low *VDR* expressers (≤-1.71) with each gene of interest. A positive correlation was observed with high and low *VDR* expressers and *PXR* expression (R^2=0.11, p=0.008 and R^2=0.49, p=0.03, respectively), *CYP3A4* expression (R^2=0.87, p=0.02 and R^2=0.38, p=0.05, respectively) and *ABCB1* expression (R^2=0.1, p=0.01 and R^2=0.49, p=0.01, respectively) (Figure 6.2-6.4). The associations observed are in agreement with previous *in vitro* work utilising intestinal cell lines (416, 418-420). Whilst a positive correlation was observed between high or low *VDR* expressers and *CAR* expression, the association was not statistically significant (Figure 6.6). The converse was found with high or low *VDR* expressers and *OATP1B1* expression. However, this negative correlation was only statistically significant for high *VDR* expressers (R^2=0.51, p=0.008) (Figure 6.11).

Potential drug-drug interactions could be mediated by VDR and this requires further investigation. Recently, ketoconazole and 1α,25-$(OH)_2D_3$ were shown to enhance *ABCB1* expression in the intestine via VDR activation (422). Furthermore, positive correlations have been found with *VDR* expression and *CYP3A4* or *ABCB1* in rat kidney, which resulted in a decreased 1α,25-$(OH)_2D_3$ plasma concentration and half-

life (416). Results herein suggest similar PK alterations and the occurrence of drug resistance could apply or be enhanced within the intestine. In addition, 1α,25-$(OH)_2D_3$ is also metabolised by CYP3A4 (402).

In vitro, 1α,25-$(OH)_2D_3$ induces CYP3A4 from 100 nM – 5 μM (441). In the summer months *in vivo* 1α,25-$(OH)_2D_3$ blood concentrations range from 65 – 100 nM (442-445) suggesting CYP3A4 may not be induced. However, blood concentrations may not be equivalent to levels where induction is observed (e.g. liver or intestine), thus seasonal therapeutic drug monitoring (TDM) may be beneficial, especially for conditions were TDM is rarely completed. 1α,25-$(OH)_2D_3$ has been shown to reduce the plasma concentrations of nifedipine (446). Moreover, the bioavailability of orally administered immunosuppressants and CYP3A4 mRNA expression levels in the intestine have been found to be significantly reduced in the summer months compared to the winter (415, 447). In agreement with previous studies, the strong correlations between *VDR* expression and key drug disposition genes (targets of CAR and PXR) suggest the NR competes with CAR/PXR for the transcription of target genes and VDR regulated genes may also be targets of the CAR/PXR pathways (88).

Five SNPs (Table 6.1) with an impact on *VDR* expression were selected for analysis based on their previous characterisation *in vitro* and *in vivo* (rs11568820, rs2228570, rs731236, rs1544410, rs7975232) (Table 6.1). The *VDR* SNP rs2228570 was the only polymorphism that significantly altered *VDR* gene expression in this cohort (Table 6.5 and Figure 6.1). The 2T>C substitution results in the formation of a variable length VDR that differs in its amino acid chain. If the substitution occurs in the first initiation site, the longer (427 amino acid) inactive VDR is produced (T allele).

However, if the variant translation begins at the second initiation site a short (424 amino acid) VDR is formed (C allele) (448). In contrast to data herein, recent studies have linked rs11568820 and rs1544410 *VDR* SNPs with significantly decreased expression of CYP3A4 in intestinal biopsies (218, 421, 447). Possible reasons for this discrepancy may be due to the small sample size and/or lack of representative ethnic groups. In particular, the A/A genotype of rs1544410 has not been recorded in the Asian (Japanese or Han Chinese) population (Table 6.1). Whilst there is evidence of VDR regulating the drug transporters ABCB1 and OATP1B1 (420) there is no current data describing the effect of *VDR* SNPs on drug transport. The T allele was associated with decreased VDR transactivation capacity but higher mRNA expression (Figure 6.8, 6.10 and 6.12) (448-452). To determine if the high/low *VDR* expressing groups observed throughout were a result of the rs2228570 SNP, the genotype of each donor was labeled in the correlation between *VDR* and *CYP3A4*, *VDR* and *ABCB1*, and *VDR* and *OATP1B1* expression (Figure 6.8, 6.10 and 6.12). 48%, 41% and 52% of the donors in the low VDR expressing groups were found to possess the rs2228570 CC genotype in the correlation with CYP3A4, ABCB1 and OATP1B1, respectively. A further 39%, 34% and 41% possessed the rs2228570 CT genotype. These results further confirm the association of the T allele with decreased VDR protein expression as well as a novel reason for the observation of 2 distinct VDR expressing groups. This SNP may be of significant importance for ABCB1 and CYP3A4 mediated metabolism, therefore, further investigation is required. Multivariate analysis also confirmed *VDR* expression is dependent upon the SNP rs2228570 (Table 6.6). However, it should be noted the effect observed may also be due to the region of the intestine from where the biopsies were taken (data unavailable). Previous investigations have noted varying levels of gene expression throughout the intestine.

For example, as you move along the intestine the expression of intestinal genes reduces which is correlated to a decrease in glucose exposure (glucose acts as a carbon source and polarises the apical membrane) (453).

In conclusion, we have identified associations between *VDR* expression with *CYP3A4, PXR* and *ABCB1* as well as *VDR* rs2228570 polymorphism and *CYP3A4* expression. The results provide an insight into potential reasons for inter- and intra-individual variability in drug disposition and additional complexity in induction mechanisms to those already established. To summarise, this work suggests VDR may be capable of controlling the basal and inducible expression of CYP3A4 and ABCB1. Further studies to investigate the role of VDR and its genetic variants on plasma drug concentrations and drug-drug interactions in the intestine are now warranted.

CHAPTER 7

General Discussion

7.0 Discussion

The efficacy and success of drug regimens results from several interlinking factors between the disease, an individual and their environment. Patient and disease characteristics can vary considerably between individuals hence, treatment can be very unique. One of the most demanding tasks in drug discovery is the accurate prediction of human *in vivo* pharmacokinetics (PK) and drug metabolism. It is of paramount importance that clearance, volume of distribution and half-life are calculated. To achieve this goal suitable *in vitro* models are essential. With the major route of clearance occurring via metabolism in the liver the increased use of primary human hepatocytes, recombinant enzymes or sub-cellular fractions with co-factors over the past 20 years have improved the success of *in vitro* analysis. However, as described in this thesis, the current model systems do not always provide a physiologically-relevant phenotype, and factors such as genotype and inter-individual variability play a substantial role. The findings herein detail important considerations for future study.

The regulatory requirements of scientists to accurately perform *in vitro* analysis is a significant challenge. Production of an organotypic liver model tool will only be achieved through the concerted effort of numerous scientific departments. Though the obstacle is great, the aim to retain the phenotype and configuration of liver specific cell types in perfused conditions is clear. As described in Chapter 1 and 2, increased knowledge of factors influencing hepatic function and structure has been advantageous to allow application of improved culture methods. Understanding the relationships between cell-cells interactions and media/matrix effects on gene expression and cell function has been invaluable, yet duplicating the exact *in vivo*

environment still eludes us. Whilst our knowledge has improved, the increased complexity of new culture systems poses limitations. Incubation of multiple cell types in co-cultures can complicate the definition of drug metabolism and elimination hence, further analysis is required to determine the proportion of activity of the co-incubated cells (237). Maintaining cells within an extracellular matrix sandwich prolongs incubation times however; the cells are not susceptible to transfection, limiting the range of studies that can be completed (240).

The liver as a whole is divided into three zones. Major metabolic differences are evident between zone one (periportal region) and zone three (pericentral region) due to altered levels of enzymes, cell morphology and environment (240). It is key to note, DDIs and hepatotoxicity can be zone specific hence a major disadvantage of using primary human hepatocytes for *in vitro* analysis is their inability to represent the three microenvironments at any one time. Hence, technology is required to engineer a three zone organotypic model that will replicate not only decreasing oxygen levels but also mimic gene expression profiles, liver specific substrates and perfusion rate. Another caveat of using isolated primary human hepatocytes in *in vitro* studies is the inability to define the complex effect of lipids, metabolites and endogenous compounds by the portal vein on the liver as well as blood flow and subsequent xenobiotic metabolism in the liver.

With longer incubation times, the recapitulation of microenvironments as well as the culture of many cell types, 3-dimensional (3-D) organotypic models offer a more representative and high-throughput system for analysing toxicity, metabolism, uptake and DDIs in comparison to current 2-dimensional models. However, cost and delicate

culture conditions currently hinder their use (237). Future possibilities include the combination of 3-D models with stem cells as well as the potential of pluripotent stem cells to provide a renewable source of organotypic cells. Whilst additional improvements are crucial, the advances in cell culture technologies and the potential to improve *in vivo* predictions is particularly encouraging.

The primary focus of this thesis was to investigate nuclear receptor (NR)-mediated control of key hepatic and intestinal drug disposition genes in hepatic cell lines, cryopreserved primary human hepatocytes (Chapter 2 and others) and intestinal biopsies (Chapter 6). Whilst binding of NRs to their response elements governs the expression of cytochrome P450s (CYPs), ATP binding cassette transporters (ABCs) and organic anion transporting polypeptides (OATPs), this regulation is dependent upon the orchestration of NR co-regulators that facilitate NR activation or repression. For example, peroxisome proliferator-activated receptor-gamma co-activator 1-alpha (PGC1α) binds to pregnane x receptor (*PXR*), activating the NR, which then initiates the transcription of CYP3A4 (206, 207, 288, 292). In chapter 3, we demonstrated for the first time that PGC1α and growth arrest and DNA damage inducible 45-beta (Gadd45β) are required for CYP3A4 activity and expression in hepatic cells and manipulation of these NR co-activators allows the production of a more physiologically relevant phenotype. Many drugs have also been shown to induce (to varying amounts) the expression of key drug disposition genes mediated by the activation of PXR or constitutive androstane receptor (CAR) (Chapter 5) (146, 147, 152, 381). Furthermore, the contribution by drug transporters to PK variability is becoming more apparent, with the US Food and Drug Administration (FDA) requiring rigorous *in vitro* transporter assays. Chapter 4 details the significance of

influx transporters in the hepatic uptake of drugs achieved by the optimisation and application of a method in primary human hepatocytes. Additionally, drug transporters and CYPs were analysed in intestinal biopsies to investigate the role of genetic variability and donor demographics, to further outline the importance of all factors and considerations to allow complete definition of PK phenotype (Chapter 6).

Reasons why cell lines display variable phenotypes has been discussed previously, and include the lack of biological stress factors (e.g. xenobiotic insult, inflammatory proteins), absence of hepatic blood flow, artificial media and supplements, artificially high oxygen and unrestricted cell replication but the exact mechanisms are yet to be defined and require further analysis. Marked differences in drug disposition genes between Huh7 and HepG2 cell lines have been outlined previously (67, 89, 101, 105, 246, 261, 274, 418). However, for the first time a comprehensive analysis of NR co-regulator expression has been completed here. The reasons for the differences between the cell lines themselves and primary cells requires further investigation particularly looking at the protein expression of the co-regulators to define if the discrepancy is due to post-transcriptional, post-translational or transcriptional mechanisms. It is interesting to note, previous work has found ABCB1 is induced in transformed cell lines by non-transcriptional mechanisms (454).

NRs act as a regulatory switch for drug disposition target genes that determine PK, though they are also involved in cell growth, differentiation and apoptosis (111). Hence, the low levels observed in hepatoma cell lines were to be expected but the causes, as yet, are to be characterised. The absence of certain CYPs and/or drug transporters could shunt the metabolism/transport of particular substrates into other

CYP/drug transporter pathways and requires further investigation. The hypothesis that alteration of NR co-regulator profiles in hepatoma cell lines may increase NR expression and subsequently improve PK predictions was determined here. This thesis provides novel evidence linking 2 co-activators (PGC1α and Gadd45β) to the activity, expression and inducibility of CYP3A4 in HepG2 cells. Interestingly, concentration-dependent induction was not observed with single transfections. This implies transient transfection with NR co-regulators only partly rectifies the problem when generating a hepatocyte-like cell line. However, when combined into a complex transfection, a strong concentration dependent induction pattern was observed. The slight decrease in CYP3A4 activity but increased induction capability of the complex transfection poses many questions but it is tempting to speculate these differences are mediated through co-activator crosstalk to achieve an optimal effect. To further support this hypothesis, histone deacetylase 1 (HDAC1) mRNA expression was reduced to levels similar of primary human hepatocytes in complex transfected cells. Specific to protein expression, single transfections resulted in an increase of the other co-activator, this may be due to post-translational effects stabilising the protein with no change in mRNA but warrants further investigation and it would be useful to determine if this effect is specific to the co-activators in question. It is exciting to note, CYP3A4 mRNA induction by rifampicin (RIF) in the complex transfected cells was similar to that observed in the primary human hepatocytes in Chapter 5. The generation of a stable cell line would be hugely beneficial but further analysis of the cells should include characterisation of hepatospecific genes (e.g. AldoB, PEPCK, OTC), cell growth, proliferation and effects of nutrition compared to a larger group of hepatocyte donors.

This work focused on co-regulators that have been linked to CYP3A4 activity, but with the significant substrate overlap between CYPs and drug transporters it was notable that the transfections had no effect on drug transporter expression. Following the success of these transfections it would be beneficial to identify co-regulators specific to drug transporters to allow cell line manipulation and the possibility of dual *in vitro* transporter and CYP analysis. The general strategy presented in Chapters 2 and 3 may provide a means to explore such mechanisms in future work.

The role for *OATP1B1* has recently been demonstrated (and further confirmed in this thesis) as a significant factor in the uptake of the protease inhibitor, lopinavir as well as pitavastatin, rosuvastatin, olmesartan and valsartan (49, 50, 53). Early *in vitro* predictions of drug transport could improve the accuracy of PK predictions and success of lead compounds becoming successful therapies. In agreement with previous work (33, 34, 42, 45, 54, 56, 230, 261), the expression of drug transporters varies considerably between individuals and cell type (e.g. hepatic cells, Chapter 5 and intestinal cells, Chapter 6), which is further influenced by drug transporter genetics. The *OATP1B1*15* haplotype results in a 3.1-fold increase in plasma exposure of pitavastatin (328) hence early added detail could allow pre-clinical characterisation of potential DDIs. Application of the assay optimised in Chapter 4 to include a wider range of drug transporters (particularly those required for analysis by the FDA) is likely to have a broad importance in determining relative contribution that individual transporters play in drug disposition. A key strength of this approach is assessment of individual transporter function at physiologically relevant protein density on the backdrop of other relevant proteins, which may be important.

A significant cause of drug failure is DDIs; applications such as those listed above could provide a platform for improved planning of drug regimens. Altering drug regimens may decrease DDIs but understanding the complete PK profile of existing drugs is essential. As previously described and presented in Chapter 5, RIF is a potent CYP3A4 inducer with a relatively short half-life whilst rifapentine (RPT) a potential RIF alternative has lower induction capabilities. However, RPT has a significantly longer half-life therefore any induction could be significantly exacerbated by the longer duration of action. As found in Chapter 5, RIF significantly increases ABCB1, OATP1B1 and CYP3A4 mRNA expression in primary human hepatocytes which *in vivo* would be predicted to correlate to a significantly altered PK profile to those previously predicted. RPT significantly induced ABCB1 suggesting contraindications with this rifamycin may be reduced, but as the drug is also a substrate for the transporter the minimum effective concentration of RPT may not be reached due to extensive efflux. Further analysis of the rifamycins in clinical studies is warranted to allow a complete PK picture to be determined. In addition, protein analysis of the observed *in vitro* induction is essential as well as determining free drug concentrations and the drug concentration at the site of action and/or within the specific metabolic tissue.

Vitamin D can be used in combination with RIF-based tuberculosis treatment. However, as described previously, vitamin D induces CYP3A4 expression and activity (218, 415). Omitting vitamin D from the drug regimen may out weigh the benefits of the additional antimicrobicidal properties due to the additional CYP3A4 induction potential. Similar to the method applied in Chapter 5, it would be interesting to determine the effect on CYP3A4 induction in primary human hepatocytes with and

without vitamin D supplemented RIF, as well as the antimicrobial effects in a clinical setting.

PK is evidently influenced by genetic factors. Rather than concentrating solely on the genotype of ADME genes, the work herein considers polymorphisms in the regulators that mediate these genes (Chapter 6). For example, variability in the gene sequences of *PXR* as well as *CYP3A4*, *OATP1B1* and *ABCB1* have demonstrated the significance of PK variability (e.g. plasma exposure or drug-drug interactions) of HMG-CoA reductase inhibitors and antiretroviral drugs (49, 234, 438). In addition to CAR and PXR, recent studies have found vitamin D receptor (VDR) is significant in altering PK (88, 103, 123, 218, 402, 403, 406, 415, 417-420, 455, 456). VDR has >200 known polymorphisms, 5 of which were analysed in this thesis. A novel pattern for the polymorphism rs2228570 was found herein. The polymorphism produced 2 distinct VDR expressing groups that were significantly correlated to high or low CYP3A4 expression (Chapter 6). This SNP may influence the efficacy of treatment of drug regimens by decreasing CYP3A4 expression in the intestine. This, coupled with a decrease in efflux drug transporter expression may negatively impact drug therapy. For example, a decrease in the expression of efflux proteins (demonstrated in Chapter 6 with ABCB1), may increase the intracellular accumulation, accompanied with reduced metabolism may result in significant toxicity or DDIs. Furthermore, similar correlations were observed when VDR expression was compared to PXR and CAR expression, suggesting VDR SNPs may additionally complicate drug therapy. In contrast, an increase in influx transporters (for example, OATP1B1) with a decrease in CYP3A4 expression may contribute to significant adverse effects. The data presented here highlight the importance of the polymorphic nature of *VDR*. These

data suggest polymorphisms in the co-activators (identified in Chapter 2) should be considered to determine their effect on PXR and CAR expression. In addition, the overlap in target genes between CAR, PXR and VDR suggest the induction by the rifamycins in Chapter 5 may be a concerted effect of all 3 NRs. Genotyping of the 6 primary human hepatocyte donors for *VDR* and *VDR* co-regulator SNPs may provide reasons for the high variability observed, notwithstanding that it is difficult to make meaningful conclusions on genetic analysis in so few individuals.

Here, a positive correlation was observed between *VDR* expression and *PXR* or *ABCB1* expression. In the intestine, drug induced activation (e.g. RIF) of CYP3A4 and CYP24A1 by PXR has been found to decrease the expression of vitamin D_3 and increase the hydroxylation of vitamin D_3, respectively. However, drugs (e.g. RIF) can also induce VDR expression, which activates CYP3A4 expression and activity. Thus, PXR may play a dual role for VDR target genes and vice versa (154). However, this requires further analysis. It would be useful to identify the levels of VDR and VDR specific co-regulators between hepatic cell lines and primary human hepatocytes to determine if the contribution of the NR has a similar significance on drug disposition genes within the liver.

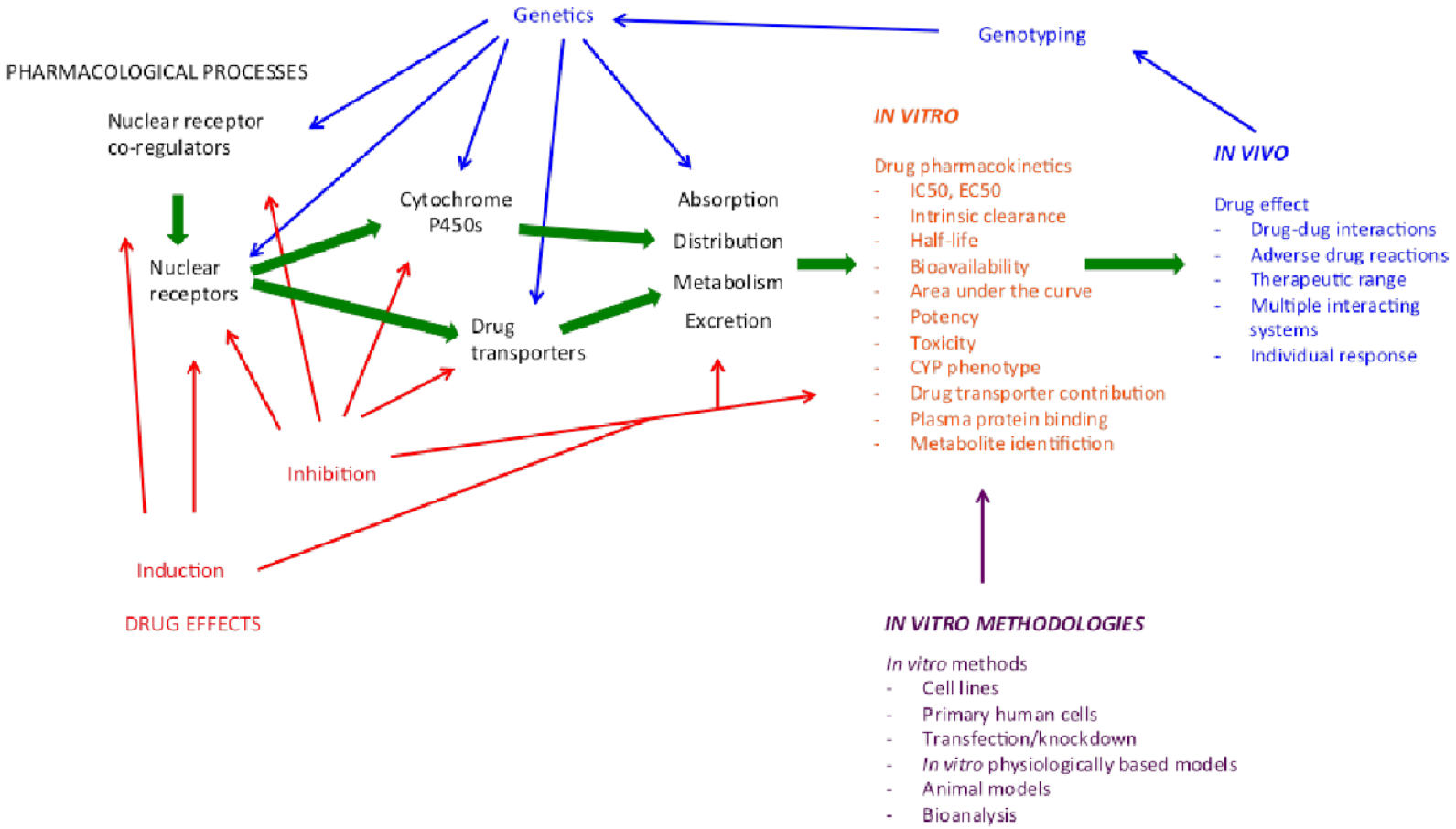

Figure 7.1 Factors and considerations for accurate prediction of *in vivo* drug response from *in vitro* analysis

Figure 7.1 summarises the work completed in this thesis as well as highlighting how each component overlaps to contribute to drug response. Drug metabolism or transport processes may be modulated through induction processes which in turn alter drug pharmacokinetics but as detailed herein a significant lack of key co-regulator genes in *in vitro* cell line assays hinders accurate *in vivo* predictions. Defining the transport of a drug is of crucial importance to reduce DDIs and ADRs in later studies. However, genetic factors may also affect drug disposition by increasing or decreasing the activity of CYPs and transporters. In summary, a complex network of overlapping factors are involved to accurately define treatment response.

In summary, this thesis has focused on specific NR mechanisms and their interrelationship with pharmacological and PK parameters. Mechanisms regulating drug disposition genes have been outlined and further confirmed as fundamental parameters that are central in determining drug-drug interactions and individual PK (Figure 7.1). The bioavailability and absorption of drugs are critically regulated by uptake and efflux transporters that govern the disposition and efficacy profiles of orally administered drugs. During the course of this thesis an assay for determining the relative uptake of drugs by OATP1B1 and a cell line with a physiologically relevant CYP3A4 phenotype were developed to enable simple and relatively high throughput analysis. Novel associations between NR gene expression and polymorphisms were defined and the impact on drug disposition genes was also presented. Generation of the models has allowed many questions to be answered but accordingly many questions have arisen and are yet to be resolved. Nonetheless, a solid platform has been constructed for future studies to further investigate these issues.

Bibliography

1. Xu X, Vugmeyster Y. Challenges and opportunities in absorption, distribution, metabolism, and excretion studies of therapeutic biologics. AAPS J. 2012;14(4):781-91. Epub 2012/08/07. doi: 10.1208/s12248-012-9388-8. PubMed PMID: 22864668; PubMed Central PMCID: PMC3475845.

2. Hukkanen J. Induction of cytochrome P450 enzymes: a view on human in vivo findings. Expert Rev Clin Pharmacol. 2012;5(5):569-85. Epub 2012/11/06. doi: 10.1586/ecp.12.39. PubMed PMID: 23121279.

3. Keppler D. Multidrug resistance proteins (MRPs, ABCCs): importance for pathophysiology and drug therapy. Handb Exp Pharmacol. 2011(201):299-323. Epub 2010/11/26. doi: 10.1007/978-3-642-14541-4_8. PubMed PMID: 21103974.

4. Kalliokoski A, Niemi M. Impact of OATP transporters on pharmacokinetics. Br J Pharmacol. 2009;158(3):693-705. Epub 2009/09/30. doi: 10.1111/j.1476-5381.2009.00430.x. PubMed PMID: 19785645; PubMed Central PMCID: PMC2765590.

5. Sowinski KM. Basic Pharmacokinetics and Pharmacodynamics: An Integrated Textbook and Computer Simulations. The Annals of pharmacotherapy. 2012. Epub 2012/01/26. doi: 10.1345/aph.1Q566. PubMed PMID: 22274143.

6. Grime K, Riley RJ. The impact of in vitro binding on in vitro-in vivo extrapolations, projections of metabolic clearance and clinical drug-drug interactions. Current drug metabolism. 2006;7(3):251-64. PubMed PMID: 16611020.

7. Jones HM, Dickins M, Youdim K, Gosset JR, Attkins NJ, Hay TL, et al. Application of PBPK modelling in drug discovery and development at Pfizer. Xenobiotica; the fate of foreign compounds in biological systems. 2012;42(1):94-106. Epub 2011/11/01. doi: 10.3109/00498254.2011.627477. PubMed PMID: 22035569.

8. Food and Drug Administration UDoH, Human Food Services, Drug Administration Center for Drag Evaluation, Research Center for Biologics Evaluation and Research. AERs reporting by healthcare providers and consumers2010.

9. Singh SS. Preclinical pharmacokinetics: an approach towards safer and efficacious drugs. Current drug metabolism. 2006;7(2):165-82. Epub 2006/02/14. PubMed PMID: 16472106.

10. Joerger M, Huitema AD, Boogerd W, van der Sande JJ, Schellens JH, Beijnen JH. Interactions of serum albumin, valproic acid and carbamazepine with the

pharmacokinetics of phenytoin in cancer patients. Basic & clinical pharmacology & toxicology. 2006;99(2):133-40. Epub 2006/08/22. doi: 10.1111/j.1742-7843.2006.pto_309.x. PubMed PMID: 16918714.

11. Itthipanichpong C, Sirivongs P, Wittayalertpunya S, Chaiyos N. The effect of antacid on aspirin pharmacokinetics in healthy Thai volunteers. Drug Metabol Drug Interact. 1992;10(3):213-28. Epub 1992/01/01. PubMed PMID: 1424642.

12. Yin J, Meng Q. Use of primary rat hepatocytes in the gel entrapment culture to predict in vivo biliary excretion. Xenobiotica; the fate of foreign compounds in biological systems. 2012;42(5):417-28. Epub 2011/11/24. doi: 10.3109/00498254.2011.633716. PubMed PMID: 22106963.

13. Soars MG, Barton P, Ismair M, Jupp R, Riley RJ. The development, characterization, and application of an OATP1B1 inhibition assay in drug discovery. Drug metabolism and disposition: the biological fate of chemicals. 2012;40(8):1641-8. Epub 2012/05/17. doi: 10.1124/dmd.111.042382. PubMed PMID: 22587986.

14. US Department of Health FaDA, Center for Drug Evaluation, Research Center for Biologics Evaluation and Research. Guidance for Industry: Exposure-Response Relationships - Study Design, Data Analysis and Regulatory Applications2003.

15. Teles JS, Fukuda EY, Feder D. Warfarin: pharmacological profile and drug interactions with antidepressants. Einstein (Sao Paulo). 2012;10(1):110-5. Epub 2012/10/11. PubMed PMID: 23045839.

16. Alavijeh MS, Palmer AM. The pivotal role of drug metabolism and pharmacokinetics in the discovery and development of new medicines. IDrugs : the investigational drugs journal. 2004;7(8):755-63. PubMed PMID: 15334309.

17. Wu CY, Benet LZ. Predicting drug disposition via application of BCS: transport/absorption/ elimination interplay and development of a biopharmaceutics drug disposition classification system. Pharmaceutical research. 2005;22(1):11-23. Epub 2005/03/18. PubMed PMID: 15771225.

18. Slordal L, Spigset O. [Basic pharmacokinetics--distribution]. Tidsskr Nor Laegeforen. 2005;125(8):1007-8. Epub 2005/04/27. PubMed PMID: 15852072.

19. Slordal L, Spigset O. [Basic pharmacokinetics--absorption]. Tidsskr Nor Laegeforen. 2005;125(7):886-7. Epub 2005/04/09. PubMed PMID: 15815736.

20. Savic RM, Jonker DM, Kerbusch T, Karlsson MO. Implementation of a transit compartment model for describing drug absorption in pharmacokinetic studies. J

Pharmacokinet Pharmacodyn. 2007;34(5):711-26. Epub 2007/07/27. doi: 10.1007/s10928-007-9066-0. PubMed PMID: 17653836.

21. Yu LX, Amidon GL. A compartmental absorption and transit model for estimating oral drug absorption. Int J Pharm. 1999;186(2):119-25. Epub 1999/09/16. PubMed PMID: 10486429.

22. Fagerholm U. Prediction of human pharmacokinetics--evaluation of methods for prediction of volume of distribution. The Journal of pharmacy and pharmacology. 2007;59(9):1181-90. doi: 10.1211/jpp.59.9.0001. PubMed PMID: 17883888.

23. Amidon GL, Lennernas H, Shah VP, Crison JR. A theoretical basis for a biopharmaceutic drug classification: the correlation of in vitro drug product dissolution and in vivo bioavailability. Pharmaceutical research. 1995;12(3):413-20. Epub 1995/03/01. PubMed PMID: 7617530.

24. Blume HH, McGilveray IJ, Midha KK. BIO-international '94 Conference on Bioavailability, Bioequivalence and Pharmacokinetic Studies and Pre-Conference Satellite on 'In Vivo/In Vitro Correlation'. Munich, Germany, June 14-17, 1994. European journal of drug metabolism and pharmacokinetics. 1995;20(1):3-13. PubMed PMID: 7588991.

25. Morais JA, Lobato Mdo R. The new European Medicines Agency guideline on the investigation of bioequivalence. Basic & clinical pharmacology & toxicology. 2010;106(3):221-5. Epub 2010/01/15. doi: 10.1111/j.1742-7843.2009.00518.x. PubMed PMID: 20070293.

26. Cristofoletti R, Chiann C, Dressman JB, Storpirtis S. A comparative analysis of biopharmaceutics classification system and biopharmaceutics drug disposition classification system: A cross-sectional survey with 500 bioequivalence studies. Journal of pharmaceutical sciences. 2013. doi: 10.1002/jps.23515. PubMed PMID: 23580377.

27. Garcia-Arieta A, Gordon J. Bioequivalence requirements in the European Union: critical discussion. AAPS J. 2012;14(4):738-48. Epub 2012/07/25. doi: 10.1208/s12248-012-9382-1. PubMed PMID: 22826032; PubMed Central PMCID: PMC3475855.

28. Benet LZ, Amidon GL, Barends DM, Lennernas H, Polli JE, Shah VP, et al. The use of BDDCS in classifying the permeability of marketed drugs. Pharmaceutical research. 2008;25(3):483-8. doi: 10.1007/s11095-007-9523-x. PubMed PMID: 18236138; PubMed Central PMCID: PMC3580995.

29. Benet LZ. The role of BCS (biopharmaceutics classification system) and BDDCS (biopharmaceutics drug disposition classification system) in drug development. Journal of pharmaceutical sciences. 2013;102(1):34-42. doi: 10.1002/jps.23359. PubMed PMID: 23147500; PubMed Central PMCID: PMC3684558.

30. Shugarts S, Benet LZ. The role of transporters in the pharmacokinetics of orally administered drugs. Pharmaceutical research. 2009;26(9):2039-54. Epub 2009/07/02. doi: 10.1007/s11095-009-9924-0. PubMed PMID: 19568696; PubMed Central PMCID: PMC2719753.

31. Shirasaka Y, Li Y, Shibue Y, Kuraoka E, Spahn-Langguth H, Kato Y, et al. Concentration-dependent effect of naringin on intestinal absorption of beta(1)-adrenoceptor antagonist talinolol mediated by p-glycoprotein and organic anion transporting polypeptide (Oatp). Pharmaceutical research. 2009;26(3):560-7. Epub 2008/11/13. doi: 10.1007/s11095-008-9771-4. PubMed PMID: 19002566.

32. Food, Drug Administration HHS. Requirements for submission of bioequivalence data; final rule. Final rule. Fed Regist. 2009;74(11):2849-62. Epub 2009/04/24. PubMed PMID: 19385107.

33. Zamek-Gliszczynski MJ, Hoffmaster KA, Tweedie DJ, Giacomini KM, Hillgren KM. Highlights from the International Transporter Consortium second workshop. Clinical pharmacology and therapeutics. 2012;92(5):553-6. Epub 2012/10/23. doi: 10.1038/clpt.2012.126. PubMed PMID: 23085880.

34. Benet LZ. Predicting drug disposition via application of a Biopharmaceutics Drug Disposition Classification System. Basic & clinical pharmacology & toxicology. 2010;106(3):162-7. doi: 10.1111/j.1742-7843.2009.00498.x. PubMed PMID: 20002064; PubMed Central PMCID: PMC3564954.

35. Fagerholm U. The role of permeability in drug ADME/PK, interactions and toxicity--presentation of a permeability-based classification system (PCS) for prediction of ADME/PK in humans. Pharmaceutical research. 2008;25(3):625-38. doi: 10.1007/s11095-007-9397-y. PubMed PMID: 17710514.

36. Fagerholm U. Prediction of human pharmacokinetics--evaluation of methods for prediction of hepatic metabolic clearance. The Journal of pharmacy and pharmacology. 2007;59(6):803-28. doi: 10.1211/jpp.59.6.0007. PubMed PMID: 17637173.

37. Dollery CT. Intracellular drug concentrations. Clinical pharmacology and therapeutics. 2013;93(3):263-6. doi: 10.1038/clpt.2012.240. PubMed PMID: 23361104.

38. Klaassen CD, Slitt AL. Regulation of hepatic transporters by xenobiotic receptors. Current drug metabolism. 2005;6(4):309-28. Epub 2005/08/17. PubMed PMID: 16101571.

39. Gibaldi M. Pharmacogenetics: part II: Perspective. 1992. The Annals of pharmacotherapy. 2007;41(12):2048-54. doi: 10.1345/aph.140072. PubMed PMID: 17986512.

40. Gibaldi M. Pharmacogenetics: part I: Perspective. 1992. The Annals of pharmacotherapy. 2007;41(12):2042-7. doi: 10.1345/aph.140071. PubMed PMID: 17986519.

41. Hagenbuch B, Gui C. Xenobiotic transporters of the human organic anion transporting polypeptides (OATP) family. Xenobiotica; the fate of foreign compounds in biological systems. 2008;38(7-8):778-801. Epub 2008/08/01. doi: 10.1080/00498250801986951. PubMed PMID: 18668430.

42. Hillgren KM, Keppler D, Zur AA, Giacomini KM, Stieger B, Cass CE, et al. Emerging transporters of clinical importance: an update from the international transporter consortium. Clinical pharmacology and therapeutics. 2013;94(1):52-63. Epub 2013/04/17. doi: 10.1038/clpt.2013.74. PubMed PMID: 23588305.

43. Juliano RL, Ling V. A surface glycoprotein modulating drug permeability in Chinese hamster ovary cell mutants. Biochim Biophys Acta. 1976;455(1):152-62. Epub 1976/11/11. PubMed PMID: 990323.

44. Koepsell H, Lips K, Volk C. Polyspecific organic cation transporters: structure, function, physiological roles, and biopharmaceutical implications. Pharmaceutical research. 2007;24(7):1227-51. Epub 2007/05/03. doi: 10.1007/s11095-007-9254-z. PubMed PMID: 17473959.

45. Choudhuri S, Klaassen CD. Structure, function, expression, genomic organization, and single nucleotide polymorphisms of human ABCB1 (MDR1), ABCC (MRP), and ABCG2 (BCRP) efflux transporters. International journal of toxicology. 2006;25(4):231-59. doi: 10.1080/10915810600746023. PubMed PMID: 16815813.

46. Huang SM, Strong JM, Zhang L, Reynolds KS, Nallani S, Temple R, et al. New era in drug interaction evaluation: US Food and Drug Administration update on

CYP enzymes, transporters, and the guidance process. J Clin Pharmacol. 2008;48(6):662-70. Epub 2008/04/02. doi: 10.1177/0091270007312153. PubMed PMID: 18378963.

47. Obaidat A, Roth M, Hagenbuch B. The expression and function of organic anion transporting polypeptides in normal tissues and in cancer. Annu Rev Pharmacol Toxicol. 2012;52:135-51. Epub 2011/08/23. doi: 10.1146/annurev-pharmtox-010510-100556. PubMed PMID: 21854228; PubMed Central PMCID: PMC3257355.

48. Mahagita C, Grassl SM, Piyachaturawat P, Ballatori N. Human organic anion transporter 1B1 and 1B3 function as bidirectional carriers and do not mediate GSH-bile acid cotransport. Am J Physiol Gastrointest Liver Physiol. 2007;293(1):G271-8. Epub 2007/04/07. doi: 10.1152/ajpgi.00075.2007. PubMed PMID: 17412826.

49. Hartkoorn RC, Kwan WS, Shallcross V, Chaikan A, Liptrott N, Egan D, et al. HIV protease inhibitors are substrates for OATP1A2, OATP1B1 and OATP1B3 and lopinavir plasma concentrations are influenced by SLCO1B1 polymorphisms. Pharmacogenetics and genomics. 2010;20(2):112-20. Epub 2010/01/07. doi: 10.1097/FPC.0b013e328335b02d. PubMed PMID: 20051929.

50. Kohlrausch FB, de Cassia Estrela R, Barroso PF, Suarez-Kurtz G. The impact of SLCO1B1 polymorphisms on the plasma concentration of lopinavir and ritonavir in HIV-infected men. Br J Clin Pharmacol. 2010;69(1):95-8. Epub 2010/01/19. doi: 10.1111/j.1365-2125.2009.03551.x. PubMed PMID: 20078617; PubMed Central PMCID: PMC2830602.

51. Li Y, Paxton JW. The effects of flavonoids on the ABC transporters: consequences for the pharmacokinetics of substrate drugs. Expert opinion on drug metabolism & toxicology. 2013;9(3):267-85. Epub 2013/01/08. doi: 10.1517/17425255.2013.749858. PubMed PMID: 23289831.

52. Rees DC, Johnson E, Lewinson O. ABC transporters: the power to change. Nat Rev Mol Cell Biol. 2009;10(3):218-27. Epub 2009/02/24. doi: 10.1038/nrm2646. PubMed PMID: 19234479; PubMed Central PMCID: PMC2830722.

53. Williamson B, Soars AC, Owen A, White P, Riley RJ, Soars MG. Dissecting the relative contribution of OATP1B1-mediated uptake of xenobiotics into human hepatocytes using siRNA. Xenobiotica; the fate of foreign compounds in biological systems. 2013. Epub 2013/03/07. doi: 10.3109/00498254.2013.776194. PubMed PMID: 23461378.

54. Albermann N, Schmitz-Winnenthal FH, Z'Graggen K, Volk C, Hoffmann MM, Haefeli WE, et al. Expression of the drug transporters MDR1/ABCB1, MRP1/ABCC1, MRP2/ABCC2, BCRP/ABCG2, and PXR in peripheral blood mononuclear cells and their relationship with the expression in intestine and liver. Biochemical pharmacology. 2005;70(6):949-58. doi: 10.1016/j.bcp.2005.06.018. PubMed PMID: 16054595.

55. Backman JT, Kajosaari LI, Niemi M, Neuvonen PJ. Cyclosporine A increases plasma concentrations and effects of repaglinide. American journal of transplantation : official journal of the American Society of Transplantation and the American Society of Transplant Surgeons. 2006;6(9):2221-2. doi: 10.1111/j.1600-6143.2006.01456.x. PubMed PMID: 16869799.

56. Camenisch G, Umehara K. Predicting human hepatic clearance from in vitro drug metabolism and transport data: a scientific and pharmaceutical perspective for assessing drug-drug interactions. Biopharmaceutics & drug disposition. 2012;33(4):179-94. doi: 10.1002/bdd.1784. PubMed PMID: 22407504.

57. Christians U, Schmitz V, Haschke M. Functional interactions between P-glycoprotein and CYP3A in drug metabolism. Expert opinion on drug metabolism & toxicology. 2005;1(4):641-54. doi: 10.1517/17425255.1.4.641. PubMed PMID: 16863430.

58. Hagenbuch B, Stieger B. The SLCO (former SLC21) superfamily of transporters. Mol Aspects Med. 2013;34(2-3):396-412. Epub 2013/03/20. doi: 10.1016/j.mam.2012.10.009. PubMed PMID: 23506880; PubMed Central PMCID: PMC3602805.

59. International Transporter C, Giacomini KM, Huang SM, Tweedie DJ, Benet LZ, Brouwer KL, et al. Membrane transporters in drug development. Nature reviews Drug discovery. 2010;9(3):215-36. doi: 10.1038/nrd3028. PubMed PMID: 20190787; PubMed Central PMCID: PMC3326076.

60. Meyer zu Schwabedissen HE, Kim RB. Hepatic OATP1B transporters and nuclear receptors PXR and CAR: interplay, regulation of drug disposition genes, and single nucleotide polymorphisms. Molecular pharmaceutics. 2009;6(6):1644-61. Epub 2009/06/30. doi: 10.1021/mp9000298. PubMed PMID: 19558188.

61. Mottino AD, Catania VA. Hepatic drug transporters and nuclear receptors: regulation by therapeutic agents. World journal of gastroenterology : WJG.

2008;14(46):7068-74. Epub 2008/12/17. PubMed PMID: 19084913; PubMed Central PMCID: PMC2776836.

62. Rigalli JP, Perdomo VG, Luquita MG, Villanueva SS, Arias A, Theile D, et al. Regulation of biotransformation systems and ABC transporters by benznidazole in HepG2 cells: involvement of pregnane X-receptor. PLoS Negl Trop Dis. 2012;6(12):e1951. Epub 2012/12/29. doi: 10.1371/journal.pntd.0001951. PubMed PMID: 23272261; PubMed Central PMCID: PMC3521711.

63. Weiss J, Herzog M, Konig S, Storch CH, Ketabi-Kiyanvash N, Haefeli WE. Induction of multiple drug transporters by efavirenz. J Pharmacol Sci. 2009;109(2):242-50. Epub 2009/02/24. PubMed PMID: 19234366.

64. Tweedie D, Polli JW, Berglund EG, Huang SM, Zhang L, Poirier A, et al. Transporter studies in drug development: experience to date and follow-up on decision trees from the international transporter consortium. Clinical pharmacology and therapeutics. 2013;94(1):113-25. Epub 2013/04/17. doi: 10.1038/clpt.2013.77. PubMed PMID: 23588318.

65. Merrell MD, Augustine LM, Slitt AL, Cherrington NJ. Induction of drug metabolism enzymes and transporters by oltipraz in rats. J Biochem Mol Toxicol. 2008;22(2):128-35. Epub 2008/04/18. doi: 10.1002/jbt.20225. PubMed PMID: 18418891.

66. Williams RT. Detoxication mechanisms in man. Clinical pharmacology and therapeutics. 1963;4:234-54. Epub 1963/03/01. PubMed PMID: 14000932.

67. Castell JV, Jover R, Martinez-Jimenez CP, Gomez-Lechon MJ. Hepatocyte cell lines: their use, scope and limitations in drug metabolism studies. Expert opinion on drug metabolism & toxicology. 2006;2(2):183-212. doi: 10.1517/17425255.2.2.183. PubMed PMID: 16866607.

68. Cheng J, Ma X, Krausz KW, Idle JR, Gonzalez FJ. Rifampicin-activated human pregnane X receptor and CYP3A4 induction enhance acetaminophen-induced toxicity. Drug metabolism and disposition: the biological fate of chemicals. 2009;37(8):1611-21. doi: 10.1124/dmd.109.027565. PubMed PMID: 19460945; PubMed Central PMCID: PMC2712435.

69. Ince I, Knibbe CA, Danhof M, de Wildt SN. Developmental changes in the expression and function of cytochrome P450 3A isoforms: evidence from in vitro and in vivo investigations. Clinical pharmacokinetics. 2013;52(5):333-45. Epub 2013/03/07. doi: 10.1007/s40262-013-0041-1. PubMed PMID: 23463352.

70. Zuber R, Anzenbacherova E, Anzenbacher P. Cytochromes P450 and experimental models of drug metabolism. J Cell Mol Med. 2002;6(2):189-98. Epub 2002/08/10. PubMed PMID: 12169204.

71. Fujino H, Yamada I, Shimada S, Yoneda M, Kojima J. Metabolic fate of pitavastatin, a new inhibitor of HMG-CoA reductase: human UDP-glucuronosyltransferase enzymes involved in lactonization. Xenobiotica; the fate of foreign compounds in biological systems. 2003;33(1):27-41. doi: 10.1080/0049825021000017957. PubMed PMID: 12519692.

72. Wang H, Negishi M. Transcriptional regulation of cytochrome p450 2B genes by nuclear receptors. Current drug metabolism. 2003;4(6):515-25. Epub 2003/12/20. PubMed PMID: 14683479.

73. Lin JH, Lu AY. Inhibition and induction of cytochrome P450 and the clinical implications. Clinical pharmacokinetics. 1998;35(5):361-90. Epub 1998/12/05. PubMed PMID: 9839089.

74. Daily EB, Aquilante CL. Cytochrome P450 2C8 pharmacogenetics: a review of clinical studies. Pharmacogenomics. 2009;10(9):1489-510. doi: 10.2217/pgs.09.82. PubMed PMID: 19761371; PubMed Central PMCID: PMC2778050.

75. Ingelman-Sundberg M. The human genome project and novel aspects of cytochrome P450 research. Toxicology and applied pharmacology. 2005;207(2 Suppl):52-6. Epub 2005/07/05. doi: 10.1016/j.taap.2005.01.030. PubMed PMID: 15993453.

76. Klein K, Zanger UM. Pharmacogenomics of Cytochrome P450 3A4: Recent Progress Toward the "Missing Heritability" Problem. Front Genet. 2013;4:12. Epub 2013/02/28. doi: 10.3389/fgene.2013.00012. PubMed PMID: 23444277; PubMed Central PMCID: PMC3580761.

77. Zanger UM, Fischer J, Raimundo S, Stuven T, Evert BO, Schwab M, et al. Comprehensive analysis of the genetic factors determining expression and function of hepatic CYP2D6. Pharmacogenetics. 2001;11(7):573-85. Epub 2001/10/23. PubMed PMID: 11668217.

78. Lapple F, von Richter O, Fromm MF, Richter T, Thon KP, Wisser H, et al. Differential expression and function of CYP2C isoforms in human intestine and liver. Pharmacogenetics. 2003;13(9):565-75. Epub 2003/09/16. doi: 10.1097/01.fpc.0000054122.14659.1e. PubMed PMID: 12972955.

79. Rowland Yeo K, Jamei M, Yang J, Tucker GT, Rostami-Hodjegan A. Physiologically based mechanistic modelling to predict complex drug-drug interactions involving simultaneous competitive and time-dependent enzyme inhibition by parent compound and its metabolite in both liver and gut - the effect of diltiazem on the time-course of exposure to triazolam. Eur J Pharm Sci. 2010;39(5):298-309. Epub 2009/12/23. doi: 10.1016/j.ejps.2009.12.002. PubMed PMID: 20025966.

80. Reed JR, Brignac-Huber LM, Backes WL. Physical incorporation of NADPH-cytochrome P450 reductase and cytochrome P450 into phospholipid vesicles using glycocholate and Bio-Beads. Drug metabolism and disposition: the biological fate of chemicals. 2008;36(3):582-8. Epub 2007/12/01. doi: 10.1124/dmd.107.018473. PubMed PMID: 18048487; PubMed Central PMCID: PMC2789009.

81. McFadyen MC, Melvin WT, Murray GI. Cytochrome P450 enzymes: novel options for cancer therapeutics. Mol Cancer Ther. 2004;3(3):363-71. Epub 2004/03/18. PubMed PMID: 15026557.

82. Bourrie M, Meunier V, Berger Y, Fabre G. Cytochrome P450 isoform inhibitors as a tool for the investigation of metabolic reactions catalyzed by human liver microsomes. The Journal of pharmacology and experimental therapeutics. 1996;277(1):321-32. PubMed PMID: 8613937.

83. Hu L, Zhuo W, He YJ, Zhou HH, Fan L. Pharmacogenetics of P450 oxidoreductase: implications in drug metabolism and therapy. Pharmacogenetics and genomics. 2012;22(11):812-9. Epub 2012/10/11. doi: 10.1097/FPC.0b013e328358d92b. PubMed PMID: 23047293.

84. Aninat C, Piton A, Glaise D, Le Charpentier T, Langouet S, Morel F, et al. Expression of cytochromes P450, conjugating enzymes and nuclear receptors in human hepatoma HepaRG cells. Drug metabolism and disposition: the biological fate of chemicals. 2006;34(1):75-83. doi: 10.1124/dmd.105.006759. PubMed PMID: 16204462.

85. Baciewicz AM, Chrisman CR, Finch CK, Self TH. Update on rifampin, rifabutin, and rifapentine drug interactions. Current medical research and opinion. 2013;29(1):1-12. Epub 2012/11/10. doi: 10.1185/03007995.2012.747952. PubMed PMID: 23136913.

86. Bort R, Ponsoda X, Carrasco E, Gomez-Lechon MJ, Castell JV. Metabolism of aceclofenac in humans. Drug metabolism and disposition: the biological fate of chemicals. 1996;24(8):834-41. PubMed PMID: 8869816.

87. Dixit V, Hariparsad N, Li F, Desai P, Thummel KE, Unadkat JD. Cytochrome P450 enzymes and transporters induced by anti-human immunodeficiency virus protease inhibitors in human hepatocytes: implications for predicting clinical drug interactions. Drug metabolism and disposition: the biological fate of chemicals. 2007;35(10):1853-9. doi: 10.1124/dmd.107.016089. PubMed PMID: 17639026.

88. Drocourt L, Ourlin JC, Pascussi JM, Maurel P, Vilarem MJ. Expression of CYP3A4, CYP2B6, and CYP2C9 is regulated by the vitamin D receptor pathway in primary human hepatocytes. The Journal of biological chemistry. 2002;277(28):25125-32. doi: 10.1074/jbc.M201323200. PubMed PMID: 11991950.

89. Gerets HH, Tilmant K, Gerin B, Chanteux H, Depelchin BO, Dhalluin S, et al. Characterization of primary human hepatocytes, HepG2 cells, and HepaRG cells at the mRNA level and CYP activity in response to inducers and their predictivity for the detection of human hepatotoxins. Cell biology and toxicology. 2012;28(2):69-87. doi: 10.1007/s10565-011-9208-4. PubMed PMID: 22258563; PubMed Central PMCID: PMC3303072.

90. Handschin C, Meyer UA. Induction of drug metabolism: the role of nuclear receptors. Pharmacological reviews. 2003;55(4):649-73. Epub 2003/12/06. doi: 10.1124/pr.55.4.2. PubMed PMID: 14657421.

91. Istrate MA, Nussler AK, Eichelbaum M, Burk O. Regulation of CYP3A4 by pregnane X receptor: The role of nuclear receptors competing for response element binding. Biochem Biophys Res Commun. 2010;393(4):688-93. Epub 2010/02/23. doi: 10.1016/j.bbrc.2010.02.058. PubMed PMID: 20171174.

92. Jover R, Bort R, Gomez-Lechon MJ, Castell JV. Cytochrome P450 regulation by hepatocyte nuclear factor 4 in human hepatocytes: a study using adenovirus-mediated antisense targeting. Hepatology. 2001;33(3):668-75. Epub 2001/03/07. doi: 10.1053/jhep.2001.22176. PubMed PMID: 11230748.

93. Kaneko A, Kato M, Endo C, Nakano K, Ishigai M, Takeda K. Prediction of clinical CYP3A4 induction using cryopreserved human hepatocytes. Xenobiotica; the fate of foreign compounds in biological systems. 2010;40(12):791-9. Epub 2010/09/25. doi: 10.3109/00498254.2010.517277. PubMed PMID: 20863202.

94. Kublbeck J, Reinisalo M, Mustonen R, Honkakoski P. Up-regulation of CYP expression in hepatoma cells stably transfected by chimeric nuclear receptors. Eur J Pharm Sci. 2010;40(4):263-72. Epub 2010/04/13. doi: 10.1016/j.ejps.2010.03.022. PubMed PMID: 20381613.

95. Li T, Chiang JY. Rifampicin induction of CYP3A4 requires pregnane X receptor cross talk with hepatocyte nuclear factor 4alpha and coactivators, and suppression of small heterodimer partner gene expression. Drug metabolism and disposition: the biological fate of chemicals. 2006;34(5):756-64. Epub 2006/02/04. doi: 10.1124/dmd.105.007575. PubMed PMID: 16455805; PubMed Central PMCID: PMC1524881.

96. Martinez-Jimenez CP, Castell JV, Gomez-Lechon MJ, Jover R. Transcriptional activation of CYP2C9, CYP1A1, and CYP1A2 by hepatocyte nuclear factor 4alpha requires coactivators peroxisomal proliferator activated receptor-gamma coactivator 1alpha and steroid receptor coactivator 1. Molecular pharmacology. 2006;70(5):1681-92. Epub 2006/08/03. doi: 10.1124/mol.106.025403. PubMed PMID: 16882880.

97. Mimura M, Baba T, Yamazaki H, Ohmori S, Inui Y, Gonzalez FJ, et al. Characterization of cytochrome P-450 2B6 in human liver microsomes. Drug metabolism and disposition: the biological fate of chemicals. 1993;21(6):1048-56. Epub 1993/11/01. PubMed PMID: 7905383.

98. Nallani SC, Goodwin B, Maglich JM, Buckley DJ, Buckley AR, Desai PB. Induction of cytochrome P450 3A by paclitaxel in mice: pivotal role of the nuclear xenobiotic receptor, pregnane X receptor. Drug metabolism and disposition: the biological fate of chemicals. 2003;31(5):681-4. Epub 2003/04/16. PubMed PMID: 12695359.

99. Raucy JL. Regulation of CYP3A4 expression in human hepatocytes by pharmaceuticals and natural products. Drug metabolism and disposition: the biological fate of chemicals. 2003;31(5):533-9. Epub 2003/04/16. PubMed PMID: 12695340.

100. Roberts SA. Drug metabolism and pharmacokinetics in drug discovery. Current opinion in drug discovery & development. 2003;6(1):66-80. PubMed PMID: 12613278.

101. Rodriguez-Antona C, Donato MT, Boobis A, Edwards RJ, Watts PS, Castell JV, et al. Cytochrome P450 expression in human hepatocytes and hepatoma cell lines:

molecular mechanisms that determine lower expression in cultured cells. Xenobiotica; the fate of foreign compounds in biological systems. 2002;32(6):505-20. Epub 2002/08/06. doi: 10.1080/00498250210128675. PubMed PMID: 12160483.

102. Schuetz EG. Lessons from the CYP3A4 promoter. Molecular pharmacology. 2004;65(2):279-81. Epub 2004/01/27. doi: 10.1124/mol.65.2.279. PubMed PMID: 14742668.

103. Schuster I. Cytochromes P450 are essential players in the vitamin D signaling system. Biochim Biophys Acta. 2011;1814(1):186-99. Epub 2010/07/14. doi: 10.1016/j.bbapap.2010.06.022. PubMed PMID: 20619365.

104. Shi Y, Li Y, Tang J, Zhang J, Zou Y, Cai B, et al. Influence of CYP3A4, CYP3A5 and MDR-1 polymorphisms on tacrolimus pharmacokinetics and early renal dysfunction in liver transplant recipients. Gene. 2013;512(2):226-31. Epub 2012/10/31. doi: 10.1016/j.gene.2012.10.048. PubMed PMID: 23107770.

105. Sivertsson L, Ek M, Darnell M, Edebert I, Ingelman-Sundberg M, Neve EP. CYP3A4 catalytic activity is induced in confluent Huh7 hepatoma cells. Drug metabolism and disposition: the biological fate of chemicals. 2010;38(6):995-1002. Epub 2010/03/18. doi: 10.1124/dmd.110.032367. PubMed PMID: 20233841.

106. van Waterschoot RA, Rooswinkel RW, Sparidans RW, van Herwaarden AE, Beijnen JH, Schinkel AH. Inhibition and stimulation of intestinal and hepatic CYP3A activity: studies in humanized CYP3A4 transgenic mice using triazolam. Drug metabolism and disposition: the biological fate of chemicals. 2009;37(12):2305-13. Epub 2009/09/16. doi: 10.1124/dmd.109.029397. PubMed PMID: 19752211.

107. Wei P, Zhang J, Egan-Hafley M, Liang S, Moore DD. The nuclear receptor CAR mediates specific xenobiotic induction of drug metabolism. Nature. 2000;407(6806):920-3. Epub 2000/11/01. doi: 10.1038/35038112. PubMed PMID: 11057673.

108. Westlind-Johnsson A, Malmebo S, Johansson A, Otter C, Andersson TB, Johansson I, et al. Comparative analysis of CYP3A expression in human liver suggests only a minor role for CYP3A5 in drug metabolism. Drug metabolism and disposition: the biological fate of chemicals. 2003;31(6):755-61. Epub 2003/05/21. PubMed PMID: 12756208.

109. Wyen C, Hendra H, Siccardi M, Platten M, Jaeger H, Harrer T, et al. Cytochrome P450 2B6 (CYP2B6) and constitutive androstane receptor (CAR) polymorphisms are associated with early discontinuation of efavirenz-containing

regimens. J Antimicrob Chemother. 2011;66(9):2092-8. Epub 2011/07/01. doi: 10.1093/jac/dkr272. PubMed PMID: 21715435.

110. Pavek P, Dvorak Z. Xenobiotic-induced transcriptional regulation of xenobiotic metabolizing enzymes of the cytochrome P450 superfamily in human extrahepatic tissues. Current drug metabolism. 2008;9(2):129-43. Epub 2008/02/22. PubMed PMID: 18288955.

111. Chai X, Zeng S, Xie W. Nuclear receptors PXR and CAR: implications for drug metabolism regulation, pharmacogenomics and beyond. Expert opinion on drug metabolism & toxicology. 2013;9(3):253-66. doi: 10.1517/17425255.2013.754010. PubMed PMID: 23327618.

112. Owen GI, Zelent A. Origins and evolutionary diversification of the nuclear receptor superfamily. Cell Mol Life Sci. 2000;57(5):809-27. Epub 2000/07/13. PubMed PMID: 10892345.

113. Krust A, Green S, Argos P, Kumar V, Walter P, Bornert JM, et al. The chicken oestrogen receptor sequence: homology with v-erbA and the human oestrogen and glucocorticoid receptors. EMBO J. 1986;5(5):891-7. Epub 1986/05/01. PubMed PMID: 3755102; PubMed Central PMCID: PMC1166879.

114. Hwang D, Rhee SH. Receptor-mediated signaling pathways: potential targets of modulation by dietary fatty acids. The American journal of clinical nutrition. 1999;70(4):545-56. Epub 1999/09/29. PubMed PMID: 10500025.

115. Watanabe M, Yanagisawa J, Kitagawa H, Takeyama K, Ogawa S, Arao Y, et al. A subfamily of RNA-binding DEAD-box proteins acts as an estrogen receptor alpha coactivator through the N-terminal activation domain (AF-1) with an RNA coactivator, SRA. EMBO J. 2001;20(6):1341-52. Epub 2001/03/17. doi: 10.1093/emboj/20.6.1341. PubMed PMID: 11250900; PubMed Central PMCID: PMC145523.

116. Freedman LP, Luisi BF. On the mechanism of DNA binding by nuclear hormone receptors: a structural and functional perspective. Journal of cellular biochemistry. 1993;51(2):140-50. doi: 10.1002/jcb.240510205. PubMed PMID: 8440748.

117. Moras D, Gronemeyer H. The nuclear receptor ligand-binding domain: structure and function. Curr Opin Cell Biol. 1998;10(3):384-91. Epub 1998/06/26. PubMed PMID: 9640540.

118. Guiochon-Mantel A, Delabre K, Lescop P, Milgrom E. Nuclear localization signals also mediate the outward movement of proteins from the nucleus. Proceedings of the National Academy of Sciences of the United States of America. 1994;91(15):7179-83. PubMed PMID: 8041765; PubMed Central PMCID: PMC44362.

119. Estebanez-Perpina E, Moore JM, Mar E, Delgado-Rodrigues E, Nguyen P, Baxter JD, et al. The molecular mechanisms of coactivator utilization in ligand-dependent transactivation by the androgen receptor. The Journal of biological chemistry. 2005;280(9):8060-8. doi: 10.1074/jbc.M407046200. PubMed PMID: 15563469.

120. Wurtz JM, Bourguet W, Renaud JP, Vivat V, Chambon P, Moras D, et al. A canonical structure for the ligand-binding domain of nuclear receptors. Nat Struct Biol. 1996;3(2):206. Epub 1996/02/01. PubMed PMID: 8564548.

121. Uppenberg J, Svensson C, Jaki M, Bertilsson G, Jendeberg L, Berkenstam A. Crystal structure of the ligand binding domain of the human nuclear receptor PPARgamma. The Journal of biological chemistry. 1998;273(47):31108-12. Epub 1998/11/13. PubMed PMID: 9813012.

122. Greschik H, Moras D. Structure-activity relationship of nuclear receptor-ligand interactions. Current topics in medicinal chemistry. 2003;3(14):1573-99. PubMed PMID: 14683516.

123. Aranda A, Pascual A. Nuclear hormone receptors and gene expression. Physiological reviews. 2001;81(3):1269-304. PubMed PMID: 11427696.

124. O'Malley BW. A life-long search for the molecular pathways of steroid hormone action. Molecular endocrinology. 2005;19(6):1402-11. Epub 2005/05/26. doi: 10.1210/me.2004-0480. PubMed PMID: 15914709.

125. Shaffer PL, Gewirth DT. Structural basis of VDR-DNA interactions on direct repeat response elements. EMBO J. 2002;21(9):2242-52. Epub 2002/05/01. doi: 10.1093/emboj/21.9.2242. PubMed PMID: 11980721; PubMed Central PMCID: PMC125986.

126. Simoncini T, Hafezi-Moghadam A, Brazil DP, Ley K, Chin WW, Liao JK. Interaction of oestrogen receptor with the regulatory subunit of phosphatidylinositol-3-OH kinase. Nature. 2000;407(6803):538-41. Epub 2000/10/12. doi: 10.1038/35035131. PubMed PMID: 11029009; PubMed Central PMCID: PMC2670482.

127. Beato M, Herrlich P, Schutz G. Steroid hormone receptors: many actors in search of a plot. Cell. 1995;83(6):851-7. PubMed PMID: 8521509.

128. Calkhoven CF, Ab G. Multiple steps in the regulation of transcription-factor level and activity. The Biochemical journal. 1996;317 (Pt 2):329-42. PubMed PMID: 8713055; PubMed Central PMCID: PMC1217492.

129. Zhang XK, Pfahl M. Hetero- and homodimeric receptors in thyroid hormone and vitamin A action. Receptor. 1993;3(3):183-91. Epub 1993/01/01. PubMed PMID: 8167569.

130. Anbalagan M, Huderson B, Murphy L, Rowan BG. Post-translational modifications of nuclear receptors and human disease. Nuclear receptor signaling. 2012;10:e001. doi: 10.1621/nrs.10001. PubMed PMID: 22438791; PubMed Central PMCID: PMC3309075.

131. Berrabah W, Aumercier P, Lefebvre P, Staels B. Control of nuclear receptor activities in metabolism by post-translational modifications. FEBS letters. 2011;585(11):1640-50. doi: 10.1016/j.febslet.2011.03.066. PubMed PMID: 21486568.

132. Urquhart BL, Tirona RG, Kim RB. Nuclear receptors and the regulation of drug-metabolizing enzymes and drug transporters: implications for interindividual variability in response to drugs. J Clin Pharmacol. 2007;47(5):566-78. Epub 2007/04/20. doi: 10.1177/0091270007299930. PubMed PMID: 17442683.

133. Tolson AH, Wang H. Regulation of drug-metabolizing enzymes by xenobiotic receptors: PXR and CAR. Adv Drug Deliv Rev. 2010;62(13):1238-49. Epub 2010/08/24. doi: 10.1016/j.addr.2010.08.006. PubMed PMID: 20727377; PubMed Central PMCID: PMC2991607.

134. Zhou C, Verma S, Blumberg B. The steroid and xenobiotic receptor (SXR), beyond xenobiotic metabolism. Nuclear receptor signaling. 2009;7:e001. Epub 2009/02/26. doi: 10.1621/nrs.07001. PubMed PMID: 19240808; PubMed Central PMCID: PMC2646121.

135. Kliewer SA, Moore JT, Wade L, Staudinger JL, Watson MA, Jones SA, et al. An orphan nuclear receptor activated by pregnanes defines a novel steroid signaling pathway. Cell. 1998;92(1):73-82. Epub 1998/03/07. PubMed PMID: 9489701.

136. Ekins S, Kortagere S, Iyer M, Reschly EJ, Lill MA, Redinbo MR, et al. Challenges predicting ligand-receptor interactions of promiscuous proteins: the nuclear receptor PXR. PLoS computational biology. 2009;5(12):e1000594. doi:

10.1371/journal.pcbi.1000594. PubMed PMID: 20011107; PubMed Central PMCID: PMC2781111.

137. di Masi A, De Marinis E, Ascenzi P, Marino M. Nuclear receptors CAR and PXR: Molecular, functional, and biomedical aspects. Mol Aspects Med. 2009;30(5):297-343. Epub 2009/05/12. doi: 10.1016/j.mam.2009.04.002. PubMed PMID: 19427329.

138. Tirona RG, Leake BF, Podust LM, Kim RB. Identification of amino acids in rat pregnane X receptor that determine species-specific activation. Molecular pharmacology. 2004;65(1):36-44. Epub 2004/01/15. doi: 10.1124/mol.65.1.36. PubMed PMID: 14722235.

139. Ihunnah CA, Jiang M, Xie W. Nuclear receptor PXR, transcriptional circuits and metabolic relevance. Biochim Biophys Acta. 2011;1812(8):956-63. Epub 2011/02/08. doi: 10.1016/j.bbadis.2011.01.014. PubMed PMID: 21295138; PubMed Central PMCID: PMC3111845.

140. Chrencik JE, Orans J, Moore LB, Xue Y, Peng L, Collins JL, et al. Structural disorder in the complex of human pregnane X receptor and the macrolide antibiotic rifampicin. Molecular endocrinology. 2005;19(5):1125-34. doi: 10.1210/me.2004-0346. PubMed PMID: 15705662.

141. Ngan CH, Beglov D, Rudnitskaya AN, Kozakov D, Waxman DJ, Vajda S. The structural basis of pregnane X receptor binding promiscuity. Biochemistry. 2009;48(48):11572-81. Epub 2009/10/28. doi: 10.1021/bi901578n. PubMed PMID: 19856963; PubMed Central PMCID: PMC2789303.

142. Teotico DG, Frazier ML, Ding F, Dokholyan NV, Temple BR, Redinbo MR. Active nuclear receptors exhibit highly correlated AF-2 domain motions. PLoS computational biology. 2008;4(7):e1000111. Epub 2008/07/12. doi: 10.1371/journal.pcbi.1000111. PubMed PMID: 18617990; PubMed Central PMCID: PMC2432469.

143. Li L, Hassan HE, Tolson AH, Ferguson SS, Eddington ND, Wang H. Differential activation of pregnane X receptor and constitutive androstane receptor by buprenorphine in primary human hepatocytes and HepG2 cells. The Journal of pharmacology and experimental therapeutics. 2010;335(3):562-71. Epub 2010/09/11. doi: 10.1124/jpet.110.173187. PubMed PMID: 20829393; PubMed Central PMCID: PMC2993555.

144. Tien ES, Negishi M. Nuclear receptors CAR and PXR in the regulation of hepatic metabolism. Xenobiotica; the fate of foreign compounds in biological systems. 2006;36(10-11):1152-63. Epub 2006/11/23. doi: 10.1080/00498250600861827. PubMed PMID: 17118922; PubMed Central PMCID: PMC1892216.

145. Ma X, Idle JR, Gonzalez FJ. The pregnane X receptor: from bench to bedside. Expert opinion on drug metabolism & toxicology. 2008;4(7):895-908. Epub 2008/07/16. doi: 10.1517/17425255.4.7.895. PubMed PMID: 18624678; PubMed Central PMCID: PMC2535920.

146. Wentworth JM, Agostini M, Love J, Schwabe JW, Chatterjee VK. St John's wort, a herbal antidepressant, activates the steroid X receptor. J Endocrinol. 2000;166(3):R11-6. Epub 2000/09/07. PubMed PMID: 10974665.

147. Watkins RE, Maglich JM, Moore LB, Wisely GB, Noble SM, Davis-Searles PR, et al. 2.1 A crystal structure of human PXR in complex with the St. John's wort compound hyperforin. Biochemistry. 2003;42(6):1430-8. Epub 2003/02/13. doi: 10.1021/bi0268753. PubMed PMID: 12578355.

148. Hariparsad N, Chu X, Yabut J, Labhart P, Hartley DP, Dai X, et al. Identification of pregnane-X receptor target genes and coactivator and corepressor binding to promoter elements in human hepatocytes. Nucleic Acids Res. 2009;37(4):1160-73. Epub 2009/01/09. doi: 10.1093/nar/gkn1047. PubMed PMID: 19129222; PubMed Central PMCID: PMC2651806.

149. Synold TW, Dussault I, Forman BM. The orphan nuclear receptor SXR coordinately regulates drug metabolism and efflux. Nat Med. 2001;7(5):584-90. Epub 2001/05/01. doi: 10.1038/87912. PubMed PMID: 11329060.

150. Uno S, Uraki M, Ito A, Shinozaki Y, Yamada A, Kawase A, et al. Changes in mRNA expression of ABC and SLC transporters in liver and intestines of the adjuvant-induced arthritis rat. Biopharmaceutics & drug disposition. 2009;30(1):49-54. Epub 2009/01/20. doi: 10.1002/bdd.639. PubMed PMID: 19152228.

151. Geick A, Eichelbaum M, Burk O. Nuclear receptor response elements mediate induction of intestinal MDR1 by rifampin. The Journal of biological chemistry. 2001;276(18):14581-7. doi: 10.1074/jbc.M010173200. PubMed PMID: 11297522.

152. Kast HR, Goodwin B, Tarr PT, Jones SA, Anisfeld AM, Stoltz CM, et al. Regulation of multidrug resistance-associated protein 2 (ABCC2) by the nuclear receptors pregnane X receptor, farnesoid X-activated receptor, and constitutive

androstane receptor. The Journal of biological chemistry. 2002;277(4):2908-15. Epub 2001/11/14. doi: 10.1074/jbc.M109326200. PubMed PMID: 11706036.

153. Sonoda J, Xie W, Rosenfeld JM, Barwick JL, Guzelian PS, Evans RM. Regulation of a xenobiotic sulfonation cascade by nuclear pregnane X receptor (PXR). Proceedings of the National Academy of Sciences of the United States of America. 2002;99(21):13801-6. Epub 2002/10/09. doi: 10.1073/pnas.212494599. PubMed PMID: 12370413; PubMed Central PMCID: PMC129778.

154. Xu C, Wang X, Staudinger JL. Regulation of tissue-specific carboxylesterase expression by pregnane x receptor and constitutive androstane receptor. Drug metabolism and disposition: the biological fate of chemicals. 2009;37(7):1539-47. Epub 2009/04/11. doi: 10.1124/dmd.109.026989. PubMed PMID: 19359405; PubMed Central PMCID: PMC2698945.

155. Liu MJ, Takahashi Y, Wada T, He J, Gao J, Tian Y, et al. The aldo-keto reductase Akr1b7 gene is a common transcriptional target of xenobiotic receptors pregnane X receptor and constitutive androstane receptor. Molecular pharmacology. 2009;76(3):604-11. Epub 2009/06/23. doi: 10.1124/mol.109.057455. PubMed PMID: 19542321; PubMed Central PMCID: PMC2730391.

156. Xie W, Yeuh MF, Radominska-Pandya A, Saini SP, Negishi Y, Bottroff BS, et al. Control of steroid, heme, and carcinogen metabolism by nuclear pregnane X receptor and constitutive androstane receptor. Proceedings of the National Academy of Sciences of the United States of America. 2003;100(7):4150-5. Epub 2003/03/20. doi: 10.1073/pnas.0438010100. PubMed PMID: 12644700; PubMed Central PMCID: PMC153063.

157. Baes M, Gulick T, Choi HS, Martinoli MG, Simha D, Moore DD. A new orphan member of the nuclear hormone receptor superfamily that interacts with a subset of retinoic acid response elements. Molecular and cellular biology. 1994;14(3):1544-52. PubMed PMID: 8114692; PubMed Central PMCID: PMC358513.

158. Choi HS, Chung M, Tzameli I, Simha D, Lee YK, Seol W, et al. Differential transactivation by two isoforms of the orphan nuclear hormone receptor CAR. The Journal of biological chemistry. 1997;272(38):23565-71. PubMed PMID: 9295294.

159. Forman BM, Tzameli I, Choi HS, Chen J, Simha D, Seol W, et al. Androstane metabolites bind to and deactivate the nuclear receptor CAR-beta. Nature. 1998;395(6702):612-5. doi: 10.1038/26996. PubMed PMID: 9783588.

160. Honkakoski P, Moore R, Washburn KA, Negishi M. Activation by diverse xenochemicals of the 51-base pair phenobarbital-responsive enhancer module in the CYP2B10 gene. Molecular pharmacology. 1998;53(4):597-601. Epub 1998/05/09. PubMed PMID: 9547348.

161. Qatanani M, Moore DD. CAR, the continuously advancing receptor, in drug metabolism and disease. Current drug metabolism. 2005;6(4):329-39. Epub 2005/08/17. PubMed PMID: 16101572.

162. Shizu R, Shindo S, Yoshida T, Numazawa S. MicroRNA-122 down-regulation is involved in phenobarbital-mediated activation of the constitutive androstane receptor. PLoS One. 2012;7(7):e41291. Epub 2012/07/21. doi: 10.1371/journal.pone.0041291. PubMed PMID: 22815988; PubMed Central PMCID: PMC3399820.

163. Xu RX, Lambert MH, Wisely BB, Warren EN, Weinert EE, Waitt GM, et al. A structural basis for constitutive activity in the human CAR/RXRalpha heterodimer. Mol Cell. 2004;16(6):919-28. Epub 2004/12/22. doi: 10.1016/j.molcel.2004.11.042. PubMed PMID: 15610735.

164. Maglich JM, Parks DJ, Moore LB, Collins JL, Goodwin B, Billin AN, et al. Identification of a novel human constitutive androstane receptor (CAR) agonist and its use in the identification of CAR target genes. The Journal of biological chemistry. 2003;278(19):17277-83. Epub 2003/03/04. doi: 10.1074/jbc.M300138200. PubMed PMID: 12611900.

165. Kobayashi K, Sueyoshi T, Inoue K, Moore R, Negishi M. Cytoplasmic accumulation of the nuclear receptor CAR by a tetratricopeptide repeat protein in HepG2 cells. Molecular pharmacology. 2003;64(5):1069-75. Epub 2003/10/24. doi: 10.1124/mol.64.5.1069. PubMed PMID: 14573755.

166. Chang TK, Bandiera SM, Chen J. Constitutive androstane receptor and pregnane X receptor gene expression in human liver: interindividual variability and correlation with CYP2B6 mRNA levels. Drug metabolism and disposition: the biological fate of chemicals. 2003;31(1):7-10. PubMed PMID: 12485946.

167. Zaher H, Yang TJ, Gelboin HV, Fernandez-Salguero P, Gonzalez FJ. Effect of phenobarbital on hepatic CYP1A1 and CYP1A2 in the Ahr-null mouse. Biochemical pharmacology. 1998;55(2):235-8. Epub 1998/02/04. PubMed PMID: 9448747.

168. Jackson JP, Ferguson SS, Moore R, Negishi M, Goldstein JA. The constitutive active/androstane receptor regulates phenytoin induction of Cyp2c29. Molecular

pharmacology. 2004;65(6):1397-404. Epub 2004/05/25. doi: 10.1124/mol.65.6.1397. PubMed PMID: 15155833.

169. Staudinger JL, Madan A, Carol KM, Parkinson A. Regulation of drug transporter gene expression by nuclear receptors. Drug metabolism and disposition: the biological fate of chemicals. 2003;31(5):523-7. Epub 2003/04/16. PubMed PMID: 12695338.

170. Burk O, Arnold KA, Geick A, Tegude H, Eichelbaum M. A role for constitutive androstane receptor in the regulation of human intestinal MDR1 expression. Biological chemistry. 2005;386(6):503-13. doi: 10.1515/BC.2005.060. PubMed PMID: 16006237.

171. Xiong H, Yoshinari K, Brouwer KL, Negishi M. Role of constitutive androstane receptor in the in vivo induction of Mrp3 and CYP2B1/2 by phenobarbital. Drug metabolism and disposition: the biological fate of chemicals. 2002;30(8):918-23. Epub 2002/07/19. PubMed PMID: 12124310.

172. Cherrington NJ, Hartley DP, Li N, Johnson DR, Klaassen CD. Organ distribution of multidrug resistance proteins 1, 2, and 3 (Mrp1, 2, and 3) mRNA and hepatic induction of Mrp3 by constitutive androstane receptor activators in rats. The Journal of pharmacology and experimental therapeutics. 2002;300(1):97-104. PubMed PMID: 11752103.

173. Ueda A, Hamadeh HK, Webb HK, Yamamoto Y, Sueyoshi T, Afshari CA, et al. Diverse roles of the nuclear orphan receptor CAR in regulating hepatic genes in response to phenobarbital. Molecular pharmacology. 2002;61(1):1-6. Epub 2001/12/26. PubMed PMID: 11752199.

174. Saini SP, Sonoda J, Xu L, Toma D, Uppal H, Mu Y, et al. A novel constitutive androstane receptor-mediated and CYP3A-independent pathway of bile acid detoxification. Molecular pharmacology. 2004;65(2):292-300. Epub 2004/01/27. doi: 10.1124/mol.65.2.292. PubMed PMID: 14742670.

175. Bock KW. Human UDP-glucuronosyltransferases: feedback loops between substrates and ligands of their transcription factors. Biochemical pharmacology. 2012;84(8):1000-6. doi: 10.1016/j.bcp.2012.07.009. PubMed PMID: 22820246.

176. Maglich JM, Stoltz CM, Goodwin B, Hawkins-Brown D, Moore JT, Kliewer SA. Nuclear pregnane x receptor and constitutive androstane receptor regulate overlapping but distinct sets of genes involved in xenobiotic detoxification. Molecular pharmacology. 2002;62(3):638-46. Epub 2002/08/16. PubMed PMID: 12181440.

177. Baskin-Bey ES, Anan A, Isomoto H, Bronk SF, Gores GJ. Constitutive androstane receptor agonist, TCPOBOP, attenuates steatohepatitis in the methionine choline-deficient diet-fed mouse. World journal of gastroenterology : WJG. 2007;13(42):5635-41. PubMed PMID: 17948939.

178. Fiorucci S, Zampella A, Distrutti E. Development of FXR, PXR and CAR agonists and antagonists for treatment of liver disorders. Current topics in medicinal chemistry. 2012;12(6):605-24. PubMed PMID: 22242859.

179. Wang H, Li H, Moore LB, Johnson MD, Maglich JM, Goodwin B, et al. The phytoestrogen coumestrol is a naturally occurring antagonist of the human pregnane X receptor. Molecular endocrinology. 2008;22(4):838-57. Epub 2007/12/22. doi: 10.1210/me.2007-0218. PubMed PMID: 18096694.

180. Baldwin WS, Roling JA. A concentration addition model for the activation of the constitutive androstane receptor by xenobiotic mixtures. Toxicological sciences : an official journal of the Society of Toxicology. 2009;107(1):93-105. doi: 10.1093/toxsci/kfn206. PubMed PMID: 18832183; PubMed Central PMCID: PMC2735418.

181. Lu H, Gonzalez FJ, Klaassen C. Alterations in hepatic mRNA expression of phase II enzymes and xenobiotic transporters after targeted disruption of hepatocyte nuclear factor 4 alpha. Toxicological sciences : an official journal of the Society of Toxicology. 2010;118(2):380-90. Epub 2010/10/12. doi: 10.1093/toxsci/kfq280. PubMed PMID: 20935164; PubMed Central PMCID: PMC2984525.

182. Lonard DM, O'Malley B W. Nuclear receptor coregulators: judges, juries, and executioners of cellular regulation. Mol Cell. 2007;27(5):691-700. Epub 2007/09/07. doi: 10.1016/j.molcel.2007.08.012. PubMed PMID: 17803935.

183. Gronemeyer H, Gustafsson JA, Laudet V. Principles for modulation of the nuclear receptor superfamily. Nature reviews Drug discovery. 2004;3(11):950-64. doi: 10.1038/nrd1551. PubMed PMID: 15520817.

184. Pascussi JM, Gerbal-Chaloin S, Duret C, Daujat-Chavanieu M, Vilarem MJ, Maurel P. The tangle of nuclear receptors that controls xenobiotic metabolism and transport: crosstalk and consequences. Annu Rev Pharmacol Toxicol. 2008;48:1-32. Epub 2007/07/05. doi: 10.1146/annurev.pharmtox.47.120505.105349. PubMed PMID: 17608617.

185. Thomas MC, Chiang CM. The general transcription machinery and general cofactors. Crit Rev Biochem Mol Biol. 2006;41(3):105-78. Epub 2006/07/25. doi: 10.1080/10409230600648736. PubMed PMID: 16858867.

186. Lonard DM, O'Malley BW. The expanding cosmos of nuclear receptor coactivators. Cell. 2006;125(3):411-4. Epub 2006/05/09. doi: 10.1016/j.cell.2006.04.021. PubMed PMID: 16678083.

187. Young JC, Hartl FU. Chaperones and transcriptional regulation by nuclear receptors. Nat Struct Biol. 2002;9(9):640-2. Epub 2002/08/29. doi: 10.1038/nsb0902-640. PubMed PMID: 12198482.

188. Timsit YE, Negishi M. CAR and PXR: the xenobiotic-sensing receptors. Steroids. 2007;72(3):231-46. Epub 2007/02/08. doi: 10.1016/j.steroids.2006.12.006. PubMed PMID: 17284330; PubMed Central PMCID: PMC1950246.

189. Lonard DM, O'Malley BW. Expanding functional diversity of the coactivators. Trends Biochem Sci. 2005;30(3):126-32. Epub 2005/03/09. doi: 10.1016/j.tibs.2005.01.001. PubMed PMID: 15752984.

190. Wada T, Gao J, Xie W. PXR and CAR in energy metabolism. Trends in endocrinology and metabolism: TEM. 2009;20(6):273-9. Epub 2009/07/15. doi: 10.1016/j.tem.2009.03.003. PubMed PMID: 19595610.

191. Nishioka K, Reinberg D. Transcription. Switching partners in a regulatory tango. Science. 2001;294(5551):2497-8. Epub 2001/12/26. doi: 10.1126/science.1067622. PubMed PMID: 11752565.

192. Chen T, Chen Q, Xu Y, Zhou Q, Zhu J, Zhang H, et al. SRC-3 is required for CAR-regulated hepatocyte proliferation and drug metabolism. Journal of hepatology. 2012;56(1):210-7. doi: 10.1016/j.jhep.2011.07.015. PubMed PMID: 21827731; PubMed Central PMCID: PMC3232307.

193. York B, O'Malley BW. Steroid receptor coactivator (SRC) family: masters of systems biology. The Journal of biological chemistry. 2010;285(50):38743-50. Epub 2010/10/20. doi: 10.1074/jbc.R110.193367. PubMed PMID: 20956538; PubMed Central PMCID: PMC2998129.

194. Eckey M, Kraft F, Kob R, Escher N, Asim M, Fischer H, et al. The corepressor activity of Alien is controlled by CREB-binding protein/p300. The FEBS journal. 2013;280(8):1861-8. doi: 10.1111/febs.12211. PubMed PMID: 23441852.

195. Jonas BA, Privalsky ML. SMRT and N-CoR corepressors are regulated by distinct kinase signaling pathways. The Journal of biological chemistry.

2004;279(52):54676-86. Epub 2004/10/20. doi: 10.1074/jbc.M410128200. PubMed PMID: 15491994; PubMed Central PMCID: PMC2653424.

196. Kim YR, Lee BK, Park RY, Nguyen NT, Bae JA, Kwon DD, et al. Differential CARM1 expression in prostate and colorectal cancers. BMC Cancer. 2010;10:197. Epub 2010/05/14. doi: 10.1186/1471-2407-10-197. PubMed PMID: 20462455; PubMed Central PMCID: PMC2881889.

197. Rona-Voros K, Weydt P. The Role of PGC-1alpha in the Pathogenesis of Neurodegenerative Disorders. Curr Drug Targets. 2010. Epub 2010/07/03. PubMed PMID: 20594175.

198. Ju TC, Lin YS, Chern Y. Energy dysfunction in Huntington's disease: insights from PGC-1alpha, AMPK, and CKB. Cell Mol Life Sci. 2012;69(24):4107-20. Epub 2012/05/26. doi: 10.1007/s00018-012-1025-2. PubMed PMID: 22627493.

199. Moreira PI, Oliveira CR. Mitochondria as potential targets in antidiabetic therapy. Handb Exp Pharmacol. 2011(203):331-56. Epub 2011/04/13. doi: 10.1007/978-3-642-17214-4_14. PubMed PMID: 21484578.

200. Fozzatti L, Kim DW, Park JW, Willingham MC, Hollenberg AN, Cheng SY. Nuclear receptor corepressor (NCOR1) regulates in vivo actions of a mutated thyroid hormone receptor alpha. Proceedings of the National Academy of Sciences of the United States of America. 2013;110(19):7850-5. doi: 10.1073/pnas.1222334110. PubMed PMID: 23610395; PubMed Central PMCID: PMC3651436.

201. Gomez-Monterrey I, Sala M, Musella S, Campiglia P. Heat shock protein 90 inhibitors as therapeutic agents. Recent patents on anti-cancer drug discovery. 2012;7(3):313-36. PubMed PMID: 22338602.

202. Tian J, Huang H, Hoffman B, Liebermann DA, Ledda-Columbano GM, Columbano A, et al. Gadd45beta is an inducible coactivator of transcription that facilitates rapid liver growth in mice. J Clin Invest. 2011;121(11):4491-502. Epub 2011/10/04. doi: 10.1172/JCI38760. PubMed PMID: 21965327; PubMed Central PMCID: PMC3204825.

203. Kodama S, Negishi M. Pregnane X receptor PXR activates the GADD45beta gene, eliciting the p38 MAPK signal and cell migration. The Journal of biological chemistry. 2011;286(5):3570-8. Epub 2010/12/04. doi: 10.1074/jbc.M110.179812. PubMed PMID: 21127053; PubMed Central PMCID: PMC3030361.

204. Tojima H, Kakizaki S, Yamazaki Y, Takizawa D, Horiguchi N, Sato K, et al. Ligand dependent hepatic gene expression profiles of nuclear receptors CAR and

PXR. Toxicol Lett. 2012;212(3):288-97. Epub 2012/06/16. doi: 10.1016/j.toxlet.2012.06.001. PubMed PMID: 22698814.

205. Smith DF, Toft DO. Minireview: the intersection of steroid receptors with molecular chaperones: observations and questions. Molecular endocrinology. 2008;22(10):2229-40. Epub 2008/05/03. doi: 10.1210/me.2008-0089. PubMed PMID: 18451092; PubMed Central PMCID: PMC2582531.

206. Takezawa T, Matsunaga T, Aikawa K, Nakamura K, Ohmori S. Lower expression of HNF4alpha and PGC1alpha might impair rifampicin-mediated CYP3A4 induction under conditions where PXR is overexpressed in human fetal liver cells. Drug metabolism and pharmacokinetics. 2012;27(4):430-8. Epub 2012/02/16. PubMed PMID: 22333269.

207. Martinez-Jimenez CP, Gomez-Lechon MJ, Castell JV, Jover R. Underexpressed coactivators PGC1alpha and SRC1 impair hepatocyte nuclear factor 4 alpha function and promote dedifferentiation in human hepatoma cells. The Journal of biological chemistry. 2006;281(40):29840-9. Epub 2006/08/08. doi: 10.1074/jbc.M604046200. PubMed PMID: 16891307.

208. Roth A, Looser R, Kaufmann M, Meyer UA. Sterol regulatory element binding protein 1 interacts with pregnane X receptor and constitutive androstane receptor and represses their target genes. Pharmacogenetics and genomics. 2008;18(4):325-37. Epub 2008/03/13. doi: 10.1097/FPC.0b013e3282f706e0. PubMed PMID: 18334917.

209. Hafner M, Juvan P, Rezen T, Monostory K, Pascussi JM, Rozman D. The human primary hepatocyte transcriptome reveals novel insights into atorvastatin and rosuvastatin action. Pharmacogenetics and genomics. 2011;21(11):741-50. Epub 2011/08/27. doi: 10.1097/FPC.0b013e32834a5585. PubMed PMID: 21869732.

210. Laurenzana EM, Chen T, Kannuswamy M, Sell BE, Strom SC, Li Y, et al. The orphan nuclear receptor DAX-1 functions as a potent corepressor of the constitutive androstane receptor (NR1I3). Molecular pharmacology. 2012;82(5):918-28. Epub 2012/08/17. doi: 10.1124/mol.112.080721. PubMed PMID: 22896671; PubMed Central PMCID: PMC3477224.

211. Lee YK, Moore DD. Dual mechanisms for repression of the monomeric orphan receptor liver receptor homologous protein-1 by the orphan small heterodimer partner. The Journal of biological chemistry. 2002;277(4):2463-7. Epub 2001/10/23. doi: 10.1074/jbc.M105161200. PubMed PMID: 11668176.

212. Xie YB, Nedumaran B, Choi HS. Molecular characterization of SMILE as a novel corepressor of nuclear receptors. Nucleic Acids Res. 2009;37(12):4100-15. Epub 2009/05/12. doi: 10.1093/nar/gkp333. PubMed PMID: 19429690; PubMed Central PMCID: PMC2709580.

213. Persson KP, Ekehed S, Otter C, Lutz ES, McPheat J, Masimirembwa CM, et al. Evaluation of human liver slices and reporter gene assays as systems for predicting the cytochrome p450 induction potential of drugs in vivo in humans. Pharmaceutical research. 2006;23(1):56-69. Epub 2005/12/06. doi: 10.1007/s11095-005-8812-5. PubMed PMID: 16328606.

214. Spears M, Bartlett J. The potential role of estrogen receptors and the SRC family as targets for the treatment of breast cancer. Expert Opin Ther Targets. 2009;13(6):665-74. Epub 2009/05/22. doi: 10.1517/14728220902911509. PubMed PMID: 19456271.

215. Zhou R, Li X, Hu G, Gong AY, Drescher KM, Chen XM. miR-16 targets transcriptional corepressor SMRT and modulates NF-kappaB-regulated transactivation of interleukin-8 gene. PLoS One. 2012;7(1):e30772. Epub 2012/02/01. doi: 10.1371/journal.pone.0030772. PubMed PMID: 22292036; PubMed Central PMCID: PMC3265513.

216. Mahungu TW, Nair D, Smith CJ, Egan D, Youle M, Johnson MA, et al. The relationships of ABCB1 3435C>T and CYP2B6 516G>T with high-density lipoprotein cholesterol in HIV-infected patients receiving Efavirenz. Clinical pharmacology and therapeutics. 2009;86(2):204-11. Epub 2009/05/29. doi: 10.1038/clpt.2009.78. PubMed PMID: 19474786.

217. Lai Y, Varma M, Feng B, Stephens JC, Kimoto E, El-Kattan A, et al. Impact of drug transporter pharmacogenomics on pharmacokinetic and pharmacodynamic variability - considerations for drug development. Expert opinion on drug metabolism & toxicology. 2012;8(6):723-43. Epub 2012/04/19. doi: 10.1517/17425255.2012.678048. PubMed PMID: 22509796.

218. Wang Z, Schuetz EG, Xu Y, Thummel KE. Interplay between vitamin D and the drug metabolizing enzyme CYP3A4. J Steroid Biochem Mol Biol. 2013;136:54-8. Epub 2012/09/19. doi: 10.1016/j.jsbmb.2012.09.012. PubMed PMID: 22985909; PubMed Central PMCID: PMC3549031.

219. Santoro AB, Struchiner CJ, Felipe CR, Tedesco-Silva H, Medina-Pestana JO, Suarez-Kurtz G. CYP3A5 Genotype, but Not CYP3A4*1b, CYP3A4*22, or

Hematocrit, Predicts Tacrolimus Dose Requirements in Brazilian Renal Transplant Patients. Clinical pharmacology and therapeutics. 2013;94(2):201-2. Epub 2013/04/17. doi: 10.1038/clpt.2013.68. PubMed PMID: 23588314.

220. de Jonge H, Kuypers DR. Response to "CYP3A5 Genotype, but Not CYP3A4*1b, CYP3A4*22, or Hematocrit, Predicts Tacrolimus Dose Requirements in Brazilian Renal Transplant Patients". Clinical pharmacology and therapeutics. 2013;94(2):202-3. Epub 2013/05/15. doi: 10.1038/clpt.2013.94. PubMed PMID: 23665867.

221. Elens L, Bouamar R, Hesselink DA, Haufroid V, van der Heiden IP, van Gelder T, et al. A new functional CYP3A4 intron 6 polymorphism significantly affects tacrolimus pharmacokinetics in kidney transplant recipients. Clinical chemistry. 2011;57(11):1574-83. doi: 10.1373/clinchem.2011.165613. PubMed PMID: 21903774.

222. Stockmann C, Fassl B, Gaedigk R, Nkoy F, Uchida DA, Monson S, et al. Fluticasone propionate pharmacogenetics: CYP3A4*22 polymorphism and pediatric asthma control. J Pediatr. 2013;162(6):1222-7, 7 e1-2. Epub 2013/01/08. doi: 10.1016/j.jpeds.2012.11.031. PubMed PMID: 23290512; PubMed Central PMCID: PMC3620714.

223. Pasanen MK, Miettinen TA, Gylling H, Neuvonen PJ, Niemi M. Polymorphism of the hepatic influx transporter organic anion transporting polypeptide 1B1 is associated with increased cholesterol synthesis rate. Pharmacogenetics and genomics. 2008;18(10):921-6. Epub 2008/09/17. doi: 10.1097/FPC.0b013e32830c1b5f. PubMed PMID: 18794729.

224. Kameyama Y, Yamashita K, Kobayashi K, Hosokawa M, Chiba K. Functional characterization of SLCO1B1 (OATP-C) variants, SLCO1B1*5, SLCO1B1*15 and SLCO1B1*15+C1007G, by using transient expression systems of HeLa and HEK293 cells. Pharmacogenetics and genomics. 2005;15(7):513-22. Epub 2005/06/23. PubMed PMID: 15970799.

225. Romaine SP, Bailey KM, Hall AS, Balmforth AJ. The influence of SLCO1B1 (OATP1B1) gene polymorphisms on response to statin therapy. Pharmacogenomics J. 2010;10(1):1-11. Epub 2009/11/04. doi: 10.1038/tpj.2009.54. PubMed PMID: 19884908.

226. Siccardi M, D'Avolio A, Nozza S, Simiele M, Baietto L, Stefani FR, et al. Maraviroc is a substrate for OATP1B1 in vitro and maraviroc plasma concentrations

are influenced by SLCO1B1 521 T>C polymorphism. Pharmacogenetics and genomics. 2010;20(12):759-65. Epub 2011/01/11. doi: 10.1097/FPC.0b013e3283402efb. PubMed PMID: 21217360.

227. Sam WJ, Chamberlain CE, Lee SJ, Goldstein JA, Hale DA, Mannon RB, et al. Associations of ABCB1 3435C>T and IL-10-1082G>A polymorphisms with long-term sirolimus dose requirements in renal transplant patients. Transplantation. 2011;92(12):1342-7. Epub 2011/11/19. doi: 10.1097/TP.0b013e3182384ae2. PubMed PMID: 22094953; PubMed Central PMCID: PMC3237821.

228. Mugusi S, Ngaimisi E, Janabi M, Minzi O, Bakari M, Riedel KD, et al. Liver enzyme abnormalities and associated risk factors in HIV patients on efavirenz-based HAART with or without tuberculosis co-infection in Tanzania. PLoS One. 2012;7(7):e40180. Epub 2012/07/19. doi: 10.1371/journal.pone.0040180. PubMed PMID: 22808112; PubMed Central PMCID: PMC3394799.

229. Haas DW, Smeaton LM, Shafer RW, Robbins GK, Morse GD, Labbe L, et al. Pharmacogenetics of long-term responses to antiretroviral regimens containing Efavirenz and/or Nelfinavir: an Adult Aids Clinical Trials Group Study. The Journal of infectious diseases. 2005;192(11):1931-42. Epub 2005/11/04. doi: 10.1086/497610. PubMed PMID: 16267764.

230. Colombo S, Soranzo N, Rotger M, Sprenger R, Bleiber G, Furrer H, et al. Influence of ABCB1, ABCC1, ABCC2, and ABCG2 haplotypes on the cellular exposure of nelfinavir in vivo. Pharmacogenetics and genomics. 2005;15(9):599-608. PubMed PMID: 16041239.

231. Woods CG, Heuvel JP, Rusyn I. Genomic profiling in nuclear receptor-mediated toxicity. Toxicol Pathol. 2007;35(4):474-94. Epub 2007/06/15. doi: 10.1080/01926230701311351. PubMed PMID: 17562482.

232. Lamba JK. Pharmacogenetics of the constitutive androstane receptor. Pharmacogenomics. 2008;9(1):71-83. Epub 2007/12/25. doi: 10.2217/14622416.9.1.71. PubMed PMID: 18154449.

233. Lamba J, Lamba V, Strom S, Venkataramanan R, Schuetz E. Novel single nucleotide polymorphisms in the promoter and intron 1 of human pregnane X receptor/NR1I2 and their association with CYP3A4 expression. Drug metabolism and disposition: the biological fate of chemicals. 2008;36(1):169-81. Epub 2007/10/11. doi: 10.1124/dmd.107.016600. PubMed PMID: 17925385.

234. Schipani A, Siccardi M, D'Avolio A, Baietto L, Simiele M, Bonora S, et al. Population pharmacokinetic modeling of the association between 63396C->T pregnane X receptor polymorphism and unboosted atazanavir clearance. Antimicrobial agents and chemotherapy. 2010;54(12):5242-50. Epub 2010/10/06. doi: 10.1128/AAC.00781-10. PubMed PMID: 20921307; PubMed Central PMCID: PMC2981241.

235. Cortes CP, Siccardi M, Chaikan A, Owen A, Zhang G, la Porte CJ. Correlates of efavirenz exposure in Chilean patients affected with human immunodeficiency virus reveals a novel association with a polymorphism in the constitutive androstane receptor. Therapeutic drug monitoring. 2013;35(1):78-83. doi: 10.1097/FTD.0b013e318274197e. PubMed PMID: 23172109.

236. Rhodes SP, Otten JN, Hingorani GP, Hartley DP, Franklin RB. Simultaneous assessment of cytochrome P450 activity in cultured human hepatocytes for compound-mediated induction of CYP3A4, CYP2B6, and CYP1A2. J Pharmacol Toxicol Methods. 2011;63(3):223-6. Epub 2010/11/30. doi: 10.1016/j.vascn.2010.11.002. PubMed PMID: 21111054.

237. LeCluyse EL, Witek RP, Andersen ME, Powers MJ. Organotypic liver culture models: meeting current challenges in toxicity testing. Critical reviews in toxicology. 2012;42(6):501-48. doi: 10.3109/10408444.2012.682115. PubMed PMID: 22582993; PubMed Central PMCID: PMC3423873.

238. Olsavsky Goyak KM, Laurenzana EM, Omiecinski CJ. Hepatocyte differentiation. Methods in molecular biology. 2010;640:115-38. doi: 10.1007/978-1-60761-688-7_6. PubMed PMID: 20645049.

239. Olsavsky KM, Page JL, Johnson MC, Zarbl H, Strom SC, Omiecinski CJ. Gene expression profiling and differentiation assessment in primary human hepatocyte cultures, established hepatoma cell lines, and human liver tissues. Toxicology and applied pharmacology. 2007;222(1):42-56. Epub 2007/05/22. doi: 10.1016/j.taap.2007.03.032. PubMed PMID: 17512962; PubMed Central PMCID: PMC2974173.

240. Tong JZ, De Lagausie P, Furlan V, Cresteil T, Bernard O, Alvarez F. Long-term culture of adult rat hepatocyte spheroids. Experimental cell research. 1992;200(2):326-32. PubMed PMID: 1572400.

241. McIntosh MB, Corner SM, Amiot BP, Nyberg SL. Engineering analysis and development of the spheroid reservoir bioartificial liver. Conference proceedings :

Annual International Conference of the IEEE Engineering in Medicine and Biology Society IEEE Engineering in Medicine and Biology Society Conference. 2009;2009:5985-8. doi: 10.1109/IEMBS.2009.5334687. PubMed PMID: 19965068; PubMed Central PMCID: PMC2929141.

242. McGinnity DF, Berry AJ, Kenny JR, Grime K, Riley RJ. Evaluation of time-dependent cytochrome P450 inhibition using cultured human hepatocytes. Drug metabolism and disposition: the biological fate of chemicals. 2006;34(8):1291-300. Epub 2006/05/09. doi: 10.1124/dmd.106.009969. PubMed PMID: 16679385.

243. Griffin SJ, Houston JB. Prediction of in vitro intrinsic clearance from hepatocytes: comparison of suspensions and monolayer cultures. Drug metabolism and disposition: the biological fate of chemicals. 2005;33(1):115-20. doi: 10.1124/dmd.33.1. PubMed PMID: 15608354.

244. Hewitt NJ, Lechon MJ, Houston JB, Hallifax D, Brown HS, Maurel P, et al. Primary hepatocytes: current understanding of the regulation of metabolic enzymes and transporter proteins, and pharmaceutical practice for the use of hepatocytes in metabolism, enzyme induction, transporter, clearance, and hepatotoxicity studies. Drug Metab Rev. 2007;39(1):159-234. Epub 2007/03/17. doi: 10.1080/03602530601093489. PubMed PMID: 17364884.

245. Hamilton GA, Jolley SL, Gilbert D, Coon DJ, Barros S, LeCluyse EL. Regulation of cell morphology and cytochrome P450 expression in human hepatocytes by extracellular matrix and cell-cell interactions. Cell Tissue Res. 2001;306(1):85-99. Epub 2001/10/31. PubMed PMID: 11683185.

246. Donato MT, Lahoz A, Castell JV, Gomez-Lechon MJ. Cell lines: a tool for in vitro drug metabolism studies. Current drug metabolism. 2008;9(1):1-11. PubMed PMID: 18220566.

247. Clement B, Guguen-Guillouzo C, Campion JP, Glaise D, Bourel M, Guillouzo A. Long-term co-cultures of adult human hepatocytes with rat liver epithelial cells: modulation of albumin secretion and accumulation of extracellular material. Hepatology. 1984;4(3):373-80. PubMed PMID: 6373549.

248. Sunman JA, Hawke RL, LeCluyse EL, Kashuba AD. Kupffer cell-mediated IL-2 suppression of CYP3A activity in human hepatocytes. Drug metabolism and disposition: the biological fate of chemicals. 2004;32(3):359-63. doi: 10.1124/dmd.32.3.359. PubMed PMID: 14977871.

249. Guillouzo A, Corlu A, Aninat C, Glaise D, Morel F, Guguen-Guillouzo C. The human hepatoma HepaRG cells: a highly differentiated model for studies of liver metabolism and toxicity of xenobiotics. Chemico-biological interactions. 2007;168(1):66-73. doi: 10.1016/j.cbi.2006.12.003. PubMed PMID: 17241619.

250. Kanebratt KP, Andersson TB. Evaluation of HepaRG cells as an in vitro model for human drug metabolism studies. Drug metabolism and disposition: the biological fate of chemicals. 2008;36(7):1444-52. doi: 10.1124/dmd.107.020016. PubMed PMID: 18385292.

251. Kanebratt KP, Andersson TB. HepaRG cells as an in vitro model for evaluation of cytochrome P450 induction in humans. Drug metabolism and disposition: the biological fate of chemicals. 2008;36(1):137-45. doi: 10.1124/dmd.107.017418. PubMed PMID: 17954527.

252. Shiraki T, Sakai N, Kanaya E, Jingami H. Activation of orphan nuclear constitutive androstane receptor requires subnuclear targeting by peroxisome proliferator-activated receptor gamma coactivator-1 alpha. A possible link between xenobiotic response and nutritional state. The Journal of biological chemistry. 2003;278(13):11344-50. Epub 2003/01/29. doi: 10.1074/jbc.M212859200. PubMed PMID: 12551939.

253. Sullivan GJ, Hay DC, Park IH, Fletcher J, Hannoun Z, Payne CM, et al. Generation of functional human hepatic endoderm from human induced pluripotent stem cells. Hepatology. 2010;51(1):329-35. doi: 10.1002/hep.23335. PubMed PMID: 19877180; PubMed Central PMCID: PMC2799548.

254. Gaudio E, Carpino G, Cardinale V, Franchitto A, Onori P, Alvaro D. New insights into liver stem cells. Digestive and liver disease : official journal of the Italian Society of Gastroenterology and the Italian Association for the Study of the Liver. 2009;41(7):455-62. doi: 10.1016/j.dld.2009.03.009. PubMed PMID: 19403350.

255. Lee PJ, Hung PJ, Lee LP. An artificial liver sinusoid with a microfluidic endothelial-like barrier for primary hepatocyte culture. Biotechnology and bioengineering. 2007;97(5):1340-6. doi: 10.1002/bit.21360. PubMed PMID: 17286266.

256. Khetani SR, Bhatia SN. Microscale culture of human liver cells for drug development. Nature biotechnology. 2008;26(1):120-6. doi: 10.1038/nbt1361. PubMed PMID: 18026090.

257. Chao P, Maguire T, Novik E, Cheng KC, Yarmush ML. Evaluation of a microfluidic based cell culture platform with primary human hepatocytes for the prediction of hepatic clearance in human. Biochemical pharmacology. 2009;78(6):625-32. doi: 10.1016/j.bcp.2009.05.013. PubMed PMID: 19463793.

258. Naughton BA, Sibanda B, Weintraub JP, San Roman J, Kamali V. A stereotypic, transplantable liver tissue-culture system. Applied biochemistry and biotechnology. 1995;54(1-3):65-91. PubMed PMID: 7486986.

259. Domansky K, Inman W, Serdy J, Dash A, Lim MH, Griffith LG. Perfused multiwell plate for 3D liver tissue engineering. Lab on a chip. 2010;10(1):51-8. doi: 10.1039/b913221j. PubMed PMID: 20024050.

260. Grime KH, Barton P, McGinnity DF. Application of in silico, in vitro and preclinical pharmacokinetic data for the effective and efficient prediction of human pharmacokinetics. Molecular pharmaceutics. 2013;10(4):1191-206. doi: 10.1021/mp300476z. PubMed PMID: 23253040.

261. Hilgendorf C, Ahlin G, Seithel A, Artursson P, Ungell AL, Karlsson J. Expression of thirty-six drug transporter genes in human intestine, liver, kidney, and organotypic cell lines. Drug metabolism and disposition: the biological fate of chemicals. 2007;35(8):1333-40. Epub 2007/05/15. doi: 10.1124/dmd.107.014902. PubMed PMID: 17496207.

262. Soars MG, Grime K, Sproston JL, Webborn PJ, Riley RJ. Use of hepatocytes to assess the contribution of hepatic uptake to clearance in vivo. Drug metabolism and disposition: the biological fate of chemicals. 2007;35(6):859-65. Epub 2007/03/09. doi: 10.1124/dmd.106.014464. PubMed PMID: 17344337.

263. Kogure T, Ueno Y, Iwasaki T, Shimosegawa T. The efficacy of the combination therapy of 5-fluorouracil, cisplatin and leucovorin for hepatocellular carcinoma and its predictable factors. Cancer Chemother Pharmacol. 2004;53(4):296-304. Epub 2003/12/23. doi: 10.1007/s00280-003-0725-6. PubMed PMID: 14689231.

264. Gunton JE, Delhanty PJ, Takahashi S, Baxter RC. Metformin rapidly increases insulin receptor activation in human liver and signals preferentially through insulin-receptor substrate-2. The Journal of clinical endocrinology and metabolism. 2003;88(3):1323-32. PubMed PMID: 12629126.

265. Seipp S, Mueller HM, Pfaff E, Stremmel W, Theilmann L, Goeser T. Establishment of persistent hepatitis C virus infection and replication in vitro. J Gen Virol. 1997;78 (Pt 10):2467-76. Epub 1998/02/12. PubMed PMID: 9349466.

266. Page JL, Johnson MC, Olsavsky KM, Strom SC, Zarbl H, Omiecinski CJ. Gene expression profiling of extracellular matrix as an effector of human hepatocyte phenotype in primary cell culture. Toxicological sciences : an official journal of the Society of Toxicology. 2007;97(2):384-97. Epub 2007/03/03. doi: 10.1093/toxsci/kfm034. PubMed PMID: 17329237.

267. Tuschl G, Mueller SO. Effects of cell culture conditions on primary rat hepatocytes-cell morphology and differential gene expression. Toxicology. 2006;218(2-3):205-15. Epub 2005/12/13. doi: 10.1016/j.tox.2005.10.017. PubMed PMID: 16337326.

268. Wilkening S, Stahl F, Bader A. Comparison of primary human hepatocytes and hepatoma cell line Hepg2 with regard to their biotransformation properties. Drug metabolism and disposition: the biological fate of chemicals. 2003;31(8):1035-42. Epub 2003/07/18. doi: 10.1124/dmd.31.8.1035. PubMed PMID: 12867492.

269. Lahoz A, Donato MT, Castell JV, Gomez-Lechon MJ. Strategies to in vitro assessment of major human CYP enzyme activities by using liquid chromatography tandem mass spectrometry. Current drug metabolism. 2008;9(1):12-9. Epub 2008/01/29. PubMed PMID: 18220567.

270. Westerink WM, Schoonen WG. Cytochrome P450 enzyme levels in HepG2 cells and cryopreserved primary human hepatocytes and their induction in HepG2 cells. Toxicol In Vitro. 2007;21(8):1581-91. Epub 2007/07/20. doi: 10.1016/j.tiv.2007.05.014. PubMed PMID: 17637504.

271. Martin P, Riley R, Back DJ, Owen A. Comparison of the induction profile for drug disposition proteins by typical nuclear receptor activators in human hepatic and intestinal cells. Br J Pharmacol. 2008;153(4):805-19. Epub 2007/11/27. doi: 10.1038/sj.bjp.0707601. PubMed PMID: 18037906; PubMed Central PMCID: PMC2259202.

272. Selden C, Shariat A, McCloskey P, Ryder T, Roberts E, Hodgson H. Three-dimensional in vitro cell culture leads to a marked upregulation of cell function in human hepatocyte cell lines--an important tool for the development of a bioartificial liver machine. Ann N Y Acad Sci. 1999;875:353-63. Epub 1999/07/23. PubMed PMID: 10415581.

273. Nakamura T, Sakaeda T, Ohmoto N, Tamura T, Aoyama N, Shirakawa T, et al. Real-time quantitative polymerase chain reaction for MDR1, MRP1, MRP2, and CYP3A-mRNA levels in Caco-2 cell lines, human duodenal enterocytes, normal

colorectal tissues, and colorectal adenocarcinomas. Drug metabolism and disposition: the biological fate of chemicals. 2002;30(1):4-6. Epub 2001/12/18. PubMed PMID: 11744604.

274. Harmsen S, Koster AS, Beijnen JH, Schellens JH, Meijerman I. Comparison of two immortalized human cell lines to study nuclear receptor-mediated CYP3A4 induction. Drug metabolism and disposition: the biological fate of chemicals. 2008;36(6):1166-71. Epub 2008/03/19. doi: 10.1124/dmd.107.017335. PubMed PMID: 18347084.

275. Richert L, Liguori MJ, Abadie C, Heyd B, Mantion G, Halkic N, et al. Gene expression in human hepatocytes in suspension after isolation is similar to the liver of origin, is not affected by hepatocyte cold storage and cryopreservation, but is strongly changed after hepatocyte plating. Drug metabolism and disposition: the biological fate of chemicals. 2006;34(5):870-9. Epub 2006/02/14. doi: 10.1124/dmd.105.007708. PubMed PMID: 16473918.

276. Taipalensuu J, Tavelin S, Lazorova L, Svensson AC, Artursson P. Exploring the quantitative relationship between the level of MDR1 transcript, protein and function using digoxin as a marker of MDR1-dependent drug efflux activity. Eur J Pharm Sci. 2004;21(1):69-75. Epub 2004/01/07. PubMed PMID: 14706813.

277. Helbig AO, Heck AJ, Slijper M. Exploring the membrane proteome--challenges and analytical strategies. J Proteomics. 2010;73(5):868-78. Epub 2010/01/26. doi: 10.1016/j.jprot.2010.01.005. PubMed PMID: 20096812.

278. Soars MG, Webborn PJ, Riley RJ. Impact of hepatic uptake transporters on pharmacokinetics and drug-drug interactions: use of assays and models for decision making in the pharmaceutical industry. Molecular pharmaceutics. 2009;6(6):1662-77. Epub 2009/05/01. doi: 10.1021/mp800246x. PubMed PMID: 19402709.

279. Vos TA, Ros JE, Havinga R, Moshage H, Kuipers F, Jansen PL, et al. Regulation of hepatic transport systems involved in bile secretion during liver regeneration in rats. Hepatology. 1999;29(6):1833-9. Epub 1999/05/29. doi: 10.1002/hep.510290638. PubMed PMID: 10347127.

280. Brandon EF, Raap CD, Meijerman I, Beijnen JH, Schellens JH. An update on in vitro test methods in human hepatic drug biotransformation research: pros and cons. Toxicology and applied pharmacology. 2003;189(3):233-46. PubMed PMID: 12791308.

281. McDonough H, Patterson C. CHIP: a link between the chaperone and proteasome systems. Cell Stress Chaperones. 2003;8(4):303-8. Epub 2004/04/30. PubMed PMID: 15115282; PubMed Central PMCID: PMC514901.

282. Te J, Jia L, Rogers J, Miller A, Hartson SD. Novel subunits of the mammalian Hsp90 signal transduction chaperone. J Proteome Res. 2007;6(5):1963-73. Epub 2007/03/14. doi: 10.1021/pr060595i. PubMed PMID: 17348703.

283. Pratt WB, Galigniana MD, Harrell JM, DeFranco DB. Role of hsp90 and the hsp90-binding immunophilins in signalling protein movement. Cell Signal. 2004;16(8):857-72. Epub 2004/05/26. doi: 10.1016/j.cellsig.2004.02.004. PubMed PMID: 15157665.

284. Beliakoff J, Whitesell L. Hsp90: an emerging target for breast cancer therapy. Anti-cancer drugs. 2004;15(7):651-62. PubMed PMID: 15269596.

285. Kawamoto T, Sueyoshi T, Zelko I, Moore R, Washburn K, Negishi M. Phenobarbital-responsive nuclear translocation of the receptor CAR in induction of the CYP2B gene. Molecular and cellular biology. 1999;19(9):6318-22. Epub 1999/08/24. PubMed PMID: 10454578; PubMed Central PMCID: PMC84602.

286. Grad I, McKee TA, Ludwig SM, Hoyle GW, Ruiz P, Wurst W, et al. The Hsp90 cochaperone p23 is essential for perinatal survival. Molecular and cellular biology. 2006;26(23):8976-83. doi: 10.1128/MCB.00734-06. PubMed PMID: 17000766; PubMed Central PMCID: PMC1636834.

287. Jeong JW, Kwak I, Lee KY, White LD, Wang XP, Brunicardi FC, et al. The genomic analysis of the impact of steroid receptor coactivators ablation on hepatic metabolism. Molecular endocrinology. 2006;20(5):1138-52. Epub 2006/01/21. doi: 10.1210/me.2005-0407. PubMed PMID: 16423883.

288. Novotna A, Doricakova A, Pavek P, Dvorak Z. Construction and characterization of peroxisome proliferator-activated receptor-gamma co-activator 1 alpha (PGC-1alpha over-expressing cell line derived from human hepatocyte carcinoma HepG2 cells). Biomed Pap Med Fac Univ Palacky Olomouc Czech Repub. 2012. Epub 2012/10/18. doi: 10.5507/bp.2012.075. PubMed PMID: 23073537.

289. Calcagno AM, Ludwig JA, Fostel JM, Gottesman MM, Ambudkar SV. Comparison of drug transporter levels in normal colon, colon cancer, and Caco-2 cells: impact on drug disposition and discovery. Molecular pharmaceutics. 2006;3(1):87-93. PubMed PMID: 16686373.

290. Liang H, Ward WF. PGC-1alpha: a key regulator of energy metabolism. Adv Physiol Educ. 2006;30(4):145-51. Epub 2006/11/17. doi: 10.1152/advan.00052.2006. PubMed PMID: 17108241.

291. Herzig S, Long F, Jhala US, Hedrick S, Quinn R, Bauer A, et al. CREB regulates hepatic gluconeogenesis through the coactivator PGC-1. Nature. 2001;413(6852):179-83. Epub 2001/09/15. doi: 10.1038/35093131. PubMed PMID: 11557984.

292. Wallberg AE, Yamamura S, Malik S, Spiegelman BM, Roeder RG. Coordination of p300-mediated chromatin remodeling and TRAP/mediator function through coactivator PGC-1alpha. Mol Cell. 2003;12(5):1137-49. Epub 2003/11/26. PubMed PMID: 14636573.

293. Puigserver P, Adelmant G, Wu Z, Fan M, Xu J, O'Malley B, et al. Activation of PPARgamma coactivator-1 through transcription factor docking. Science. 1999;286(5443):1368-71. Epub 1999/11/13. PubMed PMID: 10558993.

294. Borgius LJ, Steffensen KR, Gustafsson JA, Treuter E. Glucocorticoid signaling is perturbed by the atypical orphan receptor and corepressor SHP. The Journal of biological chemistry. 2002;277(51):49761-6. doi: 10.1074/jbc.M205641200. PubMed PMID: 12324453.

295. Rhee J, Inoue Y, Yoon JC, Puigserver P, Fan M, Gonzalez FJ, et al. Regulation of hepatic fasting response by PPARgamma coactivator-1alpha (PGC-1): requirement for hepatocyte nuclear factor 4alpha in gluconeogenesis. Proceedings of the National Academy of Sciences of the United States of America. 2003;100(7):4012-7. Epub 2003/03/26. doi: 10.1073/pnas.0730870100. PubMed PMID: 12651943; PubMed Central PMCID: PMC153039.

296. Liebermann DA, Hoffman B. Gadd45 in stress signaling. J Mol Signal. 2008;3:15. Epub 2008/09/16. doi: 10.1186/1750-2187-3-15. PubMed PMID: 18789159; PubMed Central PMCID: PMC2563007.

297. Miyake Z, Takekawa M, Ge Q, Saito H. Activation of MTK1/MEKK4 by GADD45 through induced N-C dissociation and dimerization-mediated trans autophosphorylation of the MTK1 kinase domain. Molecular and cellular biology. 2007;27(7):2765-76. Epub 2007/01/24. doi: 10.1128/MCB.01435-06. PubMed PMID: 17242196; PubMed Central PMCID: PMC1899887.

298. Vairapandi M, Balliet AG, Hoffman B, Liebermann DA. GADD45b and GADD45g are cdc2/cyclinB1 kinase inhibitors with a role in S and G2/M cell cycle

checkpoints induced by genotoxic stress. J Cell Physiol. 2002;192(3):327-38. Epub 2002/07/19. doi: 10.1002/jcp.10140. PubMed PMID: 12124778.

299. Chiou SK, Hodges A, Hoa N. Suppression of growth arrest and DNA damage-inducible 45alpha expression confers resistance to sulindac and indomethacin-induced gastric mucosal injury. The Journal of pharmacology and experimental therapeutics. 2010;334(3):693-702. doi: 10.1124/jpet.110.168153. PubMed PMID: 20498252.

300. Yamamoto Y, Moore R, Flavell RA, Lu B, Negishi M. Nuclear receptor CAR represses TNFalpha-induced cell death by interacting with the anti-apoptotic GADD45B. PLoS One. 2010;5(4):e10121. Epub 2010/04/21. doi: 10.1371/journal.pone.0010121. PubMed PMID: 20404936; PubMed Central PMCID: PMC2853562.

301. Qiu W, Zhou B, Chu PG, Luh F, Yen Y. The induction of growth arrest DNA damage-inducible gene 45 beta in human hepatoma cell lines by S-adenosylmethionine. Am J Pathol. 2007;171(1):287-96. Epub 2007/06/27. PubMed PMID: 17591973; PubMed Central PMCID: PMC1941600.

302. Elder DL, Zheng B, White CA, Li D. Stability of midazolam intranasal formula for the treatment of status epileptus in dogs. International journal of pharmaceutical compounding. 2011;15(1):74-7. PubMed PMID: 23696049.

303. Liu Y, Jiao J, Zhang C, Lou J. A simplified method to determine five cytochrome p450 probe drugs by HPLC in a single run. Biol Pharm Bull. 2009;32(4):717-20. Epub 2009/04/02. PubMed PMID: 19336911.

304. Kaartama R, Jarho P, Savolainen J, Kokki H, Lehtonen M. Determination of midazolam and 1-hydroxymidazolam from plasma by gas chromatography coupled to methane negative chemical ionization mass spectrometry after sublingual administration of midazolam. Journal of chromatography B, Analytical technologies in the biomedical and life sciences. 2011;879(19):1668-76. Epub 2011/05/03. doi: 10.1016/j.jchromb.2011.04.009. PubMed PMID: 21531182.

305. Dostalek M, Macwan JS, Chitnis SD, Ionita IA, Akhlaghi F. Development and validation of a rapid and sensitive assay for simultaneous quantification of midazolam, 1'-hydroxymidazolam, and 4-hydroxymidazolam by liquid chromatography coupled to tandem mass-spectrometry. Journal of chromatography B, Analytical technologies in the biomedical and life sciences. 2010;878(19):1629-33. doi: 10.1016/j.jchromb.2010.04.001. PubMed PMID: 20434409.

306. Aldrich S. Rifampicin Product Information (R3501).

307. McGinnity DF, Zhang G, Kenny JR, Hamilton GA, Otmani S, Stams KR, et al. Evaluation of multiple in vitro systems for assessment of CYP3A4 induction in drug discovery: human hepatocytes, pregnane X receptor reporter gene, and Fa2N-4 and HepaRG cells. Drug metabolism and disposition: the biological fate of chemicals. 2009;37(6):1259-68. Epub 2009/03/25. doi: 10.1124/dmd.109.026526. PubMed PMID: 19307295.

308. Donato MT, Hallifax D, Picazo L, Castell JV, Houston JB, Gomez-Lechon MJ, et al. Metabolite formation kinetics and intrinsic clearance of phenacetin, tolbutamide, alprazolam, and midazolam in adenoviral cytochrome P450-transfected HepG2 cells and comparison with hepatocytes and in vivo. Drug metabolism and disposition: the biological fate of chemicals. 2010;38(9):1449-55. doi: 10.1124/dmd.110.033605. PubMed PMID: 20501911.

309. Maruyama M, Matsunaga T, Harada E, Ohmori S. Comparison of basal gene expression and induction of CYP3As in HepG2 and human fetal liver cells. Biol Pharm Bull. 2007;30(11):2091-7. Epub 2007/11/06. PubMed PMID: 17978482.

310. Guo GL, Moffit JS, Nicol CJ, Ward JM, Aleksunes LA, Slitt AL, et al. Enhanced acetaminophen toxicity by activation of the pregnane X receptor. Toxicological sciences : an official journal of the Society of Toxicology. 2004;82(2):374-80. doi: 10.1093/toxsci/kfh286. PubMed PMID: 15456926.

311. Spiegelman BM, Heinrich R. Biological control through regulated transcriptional coactivators. Cell. 2004;119(2):157-67. Epub 2004/10/14. doi: 10.1016/j.cell.2004.09.037. PubMed PMID: 15479634.

312. Knutti D, Kralli A. PGC-1, a versatile coactivator. Trends in endocrinology and metabolism: TEM. 2001;12(8):360-5. Epub 2001/09/12. PubMed PMID: 11551810.

313. Knutti D, Kressler D, Kralli A. Regulation of the transcriptional coactivator PGC-1 via MAPK-sensitive interaction with a repressor. Proceedings of the National Academy of Sciences of the United States of America. 2001;98(17):9713-8. Epub 2001/08/02. doi: 10.1073/pnas.171184698. PubMed PMID: 11481440; PubMed Central PMCID: PMC55518.

314. Yoon JC, Puigserver P, Chen G, Donovan J, Wu Z, Rhee J, et al. Control of hepatic gluconeogenesis through the transcriptional coactivator PGC-1. Nature. 2001;413(6852):131-8. Epub 2001/09/15. doi: 10.1038/35093050. PubMed PMID: 11557972.

315. Daitoku H, Yamagata K, Matsuzaki H, Hatta M, Fukamizu A. Regulation of PGC-1 promoter activity by protein kinase B and the forkhead transcription factor FKHR. Diabetes. 2003;52(3):642-9. PubMed PMID: 12606503.

316. Ou DL, Shen YC, Yu SL, Chen KF, Yeh PY, Fan HH, et al. Induction of DNA damage-inducible gene GADD45beta contributes to sorafenib-induced apoptosis in hepatocellular carcinoma cells. Cancer Res. 2010;70(22):9309-18. Epub 2010/11/11. doi: 10.1158/0008-5472.CAN-10-1033. PubMed PMID: 21062976.

317. Yoo J, Ghiassi M, Jirmanova L, Balliet AG, Hoffman B, Fornace AJ, Jr., et al. Transforming growth factor-beta-induced apoptosis is mediated by Smad-dependent expression of GADD45b through p38 activation. The Journal of biological chemistry. 2003;278(44):43001-7. Epub 2003/08/23. doi: 10.1074/jbc.M307869200. PubMed PMID: 12933797.

318. Arpiainen S, Jarvenpaa SM, Manninen A, Viitala P, Lang MA, Pelkonen O, et al. Coactivator PGC-1alpha regulates the fasting inducible xenobiotic-metabolizing enzyme CYP2A5 in mouse primary hepatocytes. Toxicology and applied pharmacology. 2008;232(1):135-41. doi: 10.1016/j.taap.2008.06.001. PubMed PMID: 18602936.

319. Yamagata K, Furuta H, Oda N, Kaisaki PJ, Menzel S, Cox NJ, et al. Mutations in the hepatocyte nuclear factor-4alpha gene in maturity-onset diabetes of the young (MODY1). Nature. 1996;384(6608):458-60. Epub 1996/12/05. doi: 10.1038/384458a0. PubMed PMID: 8945471.

320. Maire P, Wuarin J, Schibler U. The role of cis-acting promoter elements in tissue-specific albumin gene expression. Science. 1989;244(4902):343-6. Epub 1989/04/21. PubMed PMID: 2711183.

321. Tronche F, Ringeisen F, Blumenfeld M, Yaniv M, Pontoglio M. Analysis of the distribution of binding sites for a tissue-specific transcription factor in the vertebrate genome. J Mol Biol. 1997;266(2):231-45. Epub 1997/02/21. doi: 10.1006/jmbi.1996.0760. PubMed PMID: 9047360.

322. Riley RJ. The potential pharmacological and toxicological impact of P450 screening. Current opinion in drug discovery & development. 2001;4(1):45-54. Epub 2001/12/01. PubMed PMID: 11727322.

323. Asberg A, Hartmann A, Fjeldsa E, Bergan S, Holdaas H. Bilateral pharmacokinetic interaction between cyclosporine A and atorvastatin in renal transplant recipients. American journal of transplantation : official journal of the

American Society of Transplantation and the American Society of Transplant Surgeons. 2001;1(4):382-6. Epub 2002/07/09. PubMed PMID: 12099384.

324. Olbricht C, Wanner C, Eisenhauer T, Kliem V, Doll R, Boddaert M, et al. Accumulation of lovastatin, but not pravastatin, in the blood of cyclosporine-treated kidney graft patients after multiple doses. Clinical pharmacology and therapeutics. 1997;62(3):311-21. Epub 1997/10/23. doi: 10.1016/S0009-9236(97)90034-5. PubMed PMID: 9333107.

325. Hedman M, Neuvonen PJ, Neuvonen M, Holmberg C, Antikainen M. Pharmacokinetics and pharmacodynamics of pravastatin in pediatric and adolescent cardiac transplant recipients on a regimen of triple immunosuppression. Clinical pharmacology and therapeutics. 2004;75(1):101-9. Epub 2004/01/30. doi: 10.1016/j.clpt.2003.09.011. PubMed PMID: 14749696.

326. Regazzi MB, Iacona I, Campana C, Raddato V, Lesi C, Perani G, et al. Altered disposition of pravastatin following concomitant drug therapy with cyclosporin A in transplant recipients. Transplantation proceedings. 1993;25(4):2732-4. Epub 1993/08/01. PubMed PMID: 8356729.

327. Simonson SG, Raza A, Martin PD, Mitchell PD, Jarcho JA, Brown CD, et al. Rosuvastatin pharmacokinetics in heart transplant recipients administered an antirejection regimen including cyclosporine. Clinical pharmacology and therapeutics. 2004;76(2):167-77. Epub 2004/08/04. doi: 10.1016/j.clpt.2004.03.010. PubMed PMID: 15289793.

328. Ieiri I, Suwannakul S, Maeda K, Uchimaru H, Hashimoto K, Kimura M, et al. SLCO1B1 (OATP1B1, an uptake transporter) and ABCG2 (BCRP, an efflux transporter) variant alleles and pharmacokinetics of pitavastatin in healthy volunteers. Clinical pharmacology and therapeutics. 2007;82(5):541-7. doi: 10.1038/sj.clpt.6100190. PubMed PMID: 17460607.

329. Neuvonen PJ, Niemi M, Backman JT. Drug interactions with lipid-lowering drugs: mechanisms and clinical relevance. Clinical pharmacology and therapeutics. 2006;80(6):565-81. Epub 2006/12/21. doi: 10.1016/j.clpt.2006.09.003. PubMed PMID: 17178259.

330. Hirano M, Maeda K, Shitara Y, Sugiyama Y. Drug-drug interaction between pitavastatin and various drugs via OATP1B1. Drug metabolism and disposition: the biological fate of chemicals. 2006;34(7):1229-36. Epub 2006/04/06. doi: 10.1124/dmd.106.009290. PubMed PMID: 16595711.

331. Karlgren M, Vildhede A, Norinder U, Wisniewski JR, Kimoto E, Lai Y, et al. Classification of inhibitors of hepatic organic anion transporting polypeptides (OATPs): influence of protein expression on drug-drug interactions. Journal of medicinal chemistry. 2012;55(10):4740-63. Epub 2012/05/01. doi: 10.1021/jm300212s. PubMed PMID: 22541068; PubMed Central PMCID: PMC3361267.

332. Noe J, Portmann R, Brun ME, Funk C. Substrate-dependent drug-drug interactions between gemfibrozil, fluvastatin and other organic anion-transporting peptide (OATP) substrates on OATP1B1, OATP2B1, and OATP1B3. Drug metabolism and disposition: the biological fate of chemicals. 2007;35(8):1308-14. Epub 2007/05/02. doi: 10.1124/dmd.106.012930. PubMed PMID: 17470528.

333. Shitara Y, Horie T, Sugiyama Y. Transporters as a determinant of drug clearance and tissue distribution. European journal of pharmaceutical sciences : official journal of the European Federation for Pharmaceutical Sciences. 2006;27(5):425-46. Epub 2006/02/21. doi: 10.1016/j.ejps.2005.12.003. PubMed PMID: 16488580.

334. Miyagawa M, Maeda K, Aoyama A, Sugiyama Y. The eighth and ninth transmembrane domains in organic anion transporting polypeptide 1B1 affect the transport kinetics of estrone-3-sulfate and estradiol-17beta-D-glucuronide. The Journal of pharmacology and experimental therapeutics. 2009;329(2):551-7. Epub 2009/02/27. doi: 10.1124/jpet.108.148411. PubMed PMID: 19244099.

335. Degorter MK, Ho RH, Leake BF, Tirona RG, Kim RB. Interaction of three regiospecific amino acid residues is required for OATP1B1 gain of OATP1B3 substrate specificity. Molecular pharmaceutics. 2012;9(4):986-95. Epub 2012/02/23. doi: 10.1021/mp200629s. PubMed PMID: 22352740; PubMed Central PMCID: PMC3319192.

336. Soars MG, McGinnity DF, Grime K, Riley RJ. The pivotal role of hepatocytes in drug discovery. Chemico-biological interactions. 2007;168(1):2-15. Epub 2007/01/09. doi: 10.1016/j.cbi.2006.11.002. PubMed PMID: 17208208.

337. Watanabe T, Kusuhara H, Debori Y, Maeda K, Kondo T, Nakayama H, et al. Prediction of the overall renal tubular secretion and hepatic clearance of anionic drugs and a renal drug-drug interaction involving organic anion transporter 3 in humans by in vitro uptake experiments. Drug metabolism and disposition: the biological fate of

chemicals. 2011;39(6):1031-8. Epub 2011/03/09. doi: 10.1124/dmd.110.036129. PubMed PMID: 21383204.

338. Watanabe T, Kusuhara H, Maeda K, Kanamaru H, Saito Y, Hu Z, et al. Investigation of the rate-determining process in the hepatic elimination of HMG-CoA reductase inhibitors in rats and humans. Drug metabolism and disposition: the biological fate of chemicals. 2010;38(2):215-22. Epub 2009/10/31. doi: 10.1124/dmd.109.030254. PubMed PMID: 19875501.

339. Yabe Y, Galetin A, Houston JB. Kinetic characterization of rat hepatic uptake of 16 actively transported drugs. Drug metabolism and disposition: the biological fate of chemicals. 2011;39(10):1808-14. Epub 2011/07/07. doi: 10.1124/dmd.111.040477. PubMed PMID: 21730030.

340. Paine SW, Parker AJ, Gardiner P, Webborn PJ, Riley RJ. Prediction of the pharmacokinetics of atorvastatin, cerivastatin, and indomethacin using kinetic models applied to isolated rat hepatocytes. Drug metabolism and disposition: the biological fate of chemicals. 2008;36(7):1365-74. Epub 2008/04/23. doi: 10.1124/dmd.107.019455. PubMed PMID: 18426955.

341. Poirier A, Cascais AC, Funk C, Lave T. Prediction of pharmacokinetic profile of valsartan in human based on in vitro uptake transport data. Journal of pharmacokinetics and pharmacodynamics. 2009;36(6):585-611. Epub 2009/11/26. doi: 10.1007/s10928-009-9139-3. PubMed PMID: 19936896.

342. Venkatakrishnan K, von Moltke LL, Greenblatt DJ. Relative quantities of catalytically active CYP 2C9 and 2C19 in human liver microsomes: application of the relative activity factor approach. Journal of pharmaceutical sciences. 1998;87(7):845-53. Epub 1998/07/02. doi: 10.1021/js970435t. PubMed PMID: 9649353.

343. de Fougerolles A, Vornlocher HP, Maraganore J, Lieberman J. Interfering with disease: a progress report on siRNA-based therapeutics. Nature reviews Drug discovery. 2007;6(6):443-53. Epub 2007/06/02. doi: 10.1038/nrd2310. PubMed PMID: 17541417.

344. Vaishnaw AK, Gollob J, Gamba-Vitalo C, Hutabarat R, Sah D, Meyers R, et al. A status report on RNAi therapeutics. Silence. 2010;1(1):14. Epub 2010/07/10. doi: 10.1186/1758-907X-1-14. PubMed PMID: 20615220; PubMed Central PMCID: PMC2908561.

345. Yu AM. Small interfering RNA in drug metabolism and transport. Current drug metabolism. 2007;8(7):700-8. Epub 2007/11/06. PubMed PMID: 17979658.

346. Yue W, Abe K, Brouwer KL. Knocking down breast cancer resistance protein (Bcrp) by adenoviral vector-mediated RNA interference (RNAi) in sandwich-cultured rat hepatocytes: a novel tool to assess the contribution of Bcrp to drug biliary excretion. Molecular pharmaceutics. 2009;6(1):134-43. Epub 2008/12/25. doi: 10.1021/mp800100e. PubMed PMID: 19105722; PubMed Central PMCID: PMC3135650.

347. Liao M, Raczynski AR, Chen M, Chuang BC, Zhu Q, Shipman R, et al. Inhibition of hepatic organic anion-transporting polypeptide by RNA interference in sandwich-cultured human hepatocytes: an in vitro model to assess transporter-mediated drug-drug interactions. Drug metabolism and disposition: the biological fate of chemicals. 2010;38(9):1612-22. Epub 2010/06/03. doi: 10.1124/dmd.110.032995. PubMed PMID: 20516252.

348. Aleku M, Fisch G, Mopert K, Keil O, Arnold W, Kaufmann J, et al. Intracellular localization of lipoplexed siRNA in vascular endothelial cells of different mouse tissues. Microvascular research. 2008;76(1):31-41. doi: 10.1016/j.mvr.2008.02.004. PubMed PMID: 18455200.

349. Santel A, Aleku M, Keil O, Endruschat J, Esche V, Durieux B, et al. RNA interference in the mouse vascular endothelium by systemic administration of siRNA-lipoplexes for cancer therapy. Gene therapy. 2006;13(18):1360-70. doi: 10.1038/sj.gt.3302778. PubMed PMID: 16625242.

350. Santel A, Aleku M, Keil O, Endruschat J, Esche V, Fisch G, et al. A novel siRNA-lipoplex technology for RNA interference in the mouse vascular endothelium. Gene therapy. 2006;13(16):1222-34. doi: 10.1038/sj.gt.3302777. PubMed PMID: 16625243.

351. Kullak-Ublick GA, Ismair MG, Stieger B, Landmann L, Huber R, Pizzagalli F, et al. Organic anion-transporting polypeptide B (OATP-B) and its functional comparison with three other OATPs of human liver. Gastroenterology. 2001;120(2):525-33. Epub 2001/02/13. PubMed PMID: 11159893.

352. Hirano M, Maeda K, Shitara Y, Sugiyama Y. Contribution of OATP2 (OATP1B1) and OATP8 (OATP1B3) to the hepatic uptake of pitavastatin in humans. The Journal of pharmacology and experimental therapeutics. 2004;311(1):139-46. Epub 2004/05/26. doi: 10.1124/jpet.104.068056. PubMed PMID: 15159445.

353. Cui Y, Konig J, Leier I, Buchholz U, Keppler D. Hepatic uptake of bilirubin and its conjugates by the human organic anion transporter SLC21A6. The Journal of

biological chemistry. 2001;276(13):9626-30. Epub 2001/01/13. doi: 10.1074/jbc.M004968200. PubMed PMID: 11134001.

354. Poirier A, Lave T, Portmann R, Brun ME, Senner F, Kansy M, et al. Design, data analysis, and simulation of in vitro drug transport kinetic experiments using a mechanistic in vitro model. Drug metabolism and disposition: the biological fate of chemicals. 2008;36(12):2434-44. Epub 2008/09/24. doi: 10.1124/dmd.108.020750. PubMed PMID: 18809732.

355. Kotani N, Maeda K, Watanabe T, Hiramatsu M, Gong LK, Bi YA, et al. Culture period-dependent changes in the uptake of transporter substrates in sandwich-cultured rat and human hepatocytes. Drug metabolism and disposition: the biological fate of chemicals. 2011;39(9):1503-10. Epub 2011/06/16. doi: 10.1124/dmd.111.038968. PubMed PMID: 21673128.

356. Hirano M, Maeda K, Shitara Y, Sugiyama Y. Contribution of OATP2 (OATP1B1) and OATP8 (OATP1B3) to the hepatic uptake of pitavastatin in humans. J Pharmacol Exp Ther. 2004;311(1):139-46. Epub 2004/05/26. doi: 10.1124/jpet.104.068056. PubMed PMID: 15159445.

357. Niemi M, Pasanen MK, Neuvonen PJ. Organic anion transporting polypeptide 1B1: a genetically polymorphic transporter of major importance for hepatic drug uptake. Pharmacological reviews. 2011;63(1):157-81. Epub 2011/01/20. doi: 10.1124/pr.110.002857. PubMed PMID: 21245207.

358. Brown HS, Ito K, Galetin A, Houston JB. Prediction of in vivo drug-drug interactions from in vitro data: impact of incorporating parallel pathways of drug elimination and inhibitor absorption rate constant. British journal of clinical pharmacology. 2005;60(5):508-18. Epub 2005/10/21. doi: 10.1111/j.1365-2125.2005.02483.x. PubMed PMID: 16236041; PubMed Central PMCID: PMC1884945.

359. Pasanen MK, Fredrikson H, Neuvonen PJ, Niemi M. Different effects of SLCO1B1 polymorphism on the pharmacokinetics of atorvastatin and rosuvastatin. Clinical pharmacology and therapeutics. 2007;82(6):726-33. Epub 2007/05/03. doi: 10.1038/sj.clpt.6100220. PubMed PMID: 17473846.

360. Suwannakul S, Ieiri I, Kimura M, Kawabata K, Kusuhara H, Hirota T, et al. Pharmacokinetic interaction between pravastatin and olmesartan in relation to SLCO1B1 polymorphism. Journal of human genetics. 2008;53(10):899-904. Epub 2008/07/22. doi: 10.1007/s10038-008-0324-9. PubMed PMID: 18641915.

361. Raviglione MC. The Global Plan to Stop TB, 2006-2015. Int J Tuberc Lung Dis. 2006;10(3):238-9. Epub 2006/03/28. PubMed PMID: 16562699.

362. Squire SB, Obasi A, Nhlema-Simwaka B. The Global Plan to Stop TB: a unique opportunity to address poverty and the Millennium Development Goals. Lancet. 2006;367(9514):955-7. Epub 2006/03/21. doi: 10.1016/S0140-6736(06)68393-1. PubMed PMID: 16546551.

363. WHO. World Health Organisation. *Global Tuberculosis Control.* WHO Report 2012. WHO Press, Geneva, Switzerland, 2012 2012. Report No.

364. World Health O. WHO global tuberculosis control report 2010. Summary. Cent Eur J Public Health. 2010;18(4):237. Epub 2011/03/03. PubMed PMID: 21361110.

365. Organisation WH. Global Tuberculosis Control2012.

366. Person AK, Sterling TR. Treatment of latent tuberculosis infection in HIV: shorter or longer? Curr HIV/AIDS Rep. 2012;9(3):259-66. Epub 2012/05/15. doi: 10.1007/s11904-012-0120-1. PubMed PMID: 22581360; PubMed Central PMCID: PMC3410968.

367. Stop TBP. The Global Plan to Stop TB, 2006-2015. actions for life: towards a world free of tuberculosis. Int J Tuberc Lung Dis. 2006;10(3):240-1. Epub 2006/03/28. PubMed PMID: 16562700.

368. Rosenthal IM, Tasneen R, Peloquin CA, Zhang M, Almeida D, Mdluli KE, et al. Dose-ranging comparison of rifampin and rifapentine in two pathologically distinct murine models of tuberculosis. Antimicrobial agents and chemotherapy. 2012;56(8):4331-40. Epub 2012/06/06. doi: 10.1128/AAC.00912-12. PubMed PMID: 22664964; PubMed Central PMCID: PMC3421552.

369. Aristoff PA, Garcia GA, Kirchhoff PD, Hollis Showalter HD. Rifamycins--obstacles and opportunities. Tuberculosis. 2010;90(2):94-118. doi: 10.1016/j.tube.2010.02.001. PubMed PMID: 20236863.

370. Artsimovitch I, Vassylyeva MN, Svetlov D, Svetlov V, Perederina A, Igarashi N, et al. Allosteric modulation of the RNA polymerase catalytic reaction is an essential component of transcription control by rifamycins. Cell. 2005;122(3):351-63. doi: 10.1016/j.cell.2005.07.014. PubMed PMID: 16096056.

371. Ma Z, Lienhardt C, McIlleron H, Nunn AJ, Wang X. Global tuberculosis drug development pipeline: the need and the reality. Lancet. 2010;375(9731):2100-9. Epub 2010/05/22. doi: 10.1016/S0140-6736(10)60359-9. PubMed PMID: 20488518.

372. Boman G, Ringberger VA. Binding of rifampicin by human plasma proteins. European journal of clinical pharmacology. 1974;7(5):369-73. PubMed PMID: 4138537.

373. Ginsberg AM. Drugs in development for tuberculosis. Drugs. 2010;70(17):2201-14. doi: 10.2165/11538170-000000000-00000. PubMed PMID: 21080738.

374. Zhang Y, Yew WW. Mechanisms of drug resistance in Mycobacterium tuberculosis. Int J Tuberc Lung Dis. 2009;13(11):1320-30. Epub 2009/10/29. PubMed PMID: 19861002.

375. Niemi M, Backman JT, Fromm MF, Neuvonen PJ, Kivisto KT. Pharmacokinetic interactions with rifampicin : clinical relevance. Clinical pharmacokinetics. 2003;42(9):819-50. Epub 2003/07/29. PubMed PMID: 12882588.

376. Burman WJ, Gallicano K, Peloquin C. Comparative pharmacokinetics and pharmacodynamics of the rifamycin antibacterials. Clinical pharmacokinetics. 2001;40(5):327-41. Epub 2001/07/04. PubMed PMID: 11432536.

377. Skinner MH, Blaschke TF. Clinical pharmacokinetics of rifabutin. Clinical pharmacokinetics. 1995;28(2):115-25. Epub 1995/02/01. PubMed PMID: 7736687.

378. Li AP, Reith MK, Rasmussen A, Gorski JC, Hall SD, Xu L, et al. Primary human hepatocytes as a tool for the evaluation of structure-activity relationship in cytochrome P450 induction potential of xenobiotics: evaluation of rifampin, rifapentine and rifabutin. Chemico-biological interactions. 1997;107(1-2):17-30. Epub 1997/12/24. PubMed PMID: 9402947.

379. Tam CM, Chan SL, Kam KM, Sim E, Staples D, Sole KM, et al. Rifapentine and isoniazid in the continuation phase of a 6-month regimen. Interim report: no activity of isoniazid in the continuation phase. Int J Tuberc Lung Dis. 2000;4(3):262-7. Epub 2000/04/06. PubMed PMID: 10751074.

380. Dooley KE, Bliven-Sizemore EE, Weiner M, Lu Y, Nuermberger EL, Hubbard WC, et al. Safety and pharmacokinetics of escalating daily doses of the antituberculosis drug rifapentine in healthy volunteers. Clinical pharmacology and therapeutics. 2012;91(5):881-8. Epub 2012/04/05. doi: 10.1038/clpt.2011.323. PubMed PMID: 22472995.

381. Dooley K, Flexner C, Hackman J, Peloquin CA, Nuermberger E, Chaisson RE, et al. Repeated administration of high-dose intermittent rifapentine reduces rifapentine and moxifloxacin plasma concentrations. Antimicrobial agents and

chemotherapy. 2008;52(11):4037-42. Epub 2008/09/04. doi: 10.1128/AAC.00554-08. PubMed PMID: 18765687; PubMed Central PMCID: PMC2573112.

382. Rosenthal IM, Zhang M, Williams KN, Peloquin CA, Tyagi S, Vernon AA, et al. Daily dosing of rifapentine cures tuberculosis in three months or less in the murine model. PLoS Med. 2007;4(12):e344. Epub 2007/12/21. doi: 10.1371/journal.pmed.0040344. PubMed PMID: 18092886; PubMed Central PMCID: PMC2140085.

383. Sterling TR, Villarino ME, Borisov AS, Shang N, Gordin F, Bliven-Sizemore E, et al. Three months of rifapentine and isoniazid for latent tuberculosis infection. N Engl J Med. 2011;365(23):2155-66. Epub 2011/12/14. doi: 10.1056/NEJMoa1104875. PubMed PMID: 22150035.

384. Acocella G. Clinical pharmacokinetics of rifampicin. Clinical pharmacokinetics. 1978;3(2):108-27. PubMed PMID: 346286.

385. Ohtsuki S, Schaefer O, Kawakami H, Inoue T, Liehner S, Saito A, et al. Simultaneous absolute protein quantification of transporters, cytochromes P450, and UDP-glucuronosyltransferases as a novel approach for the characterization of individual human liver: comparison with mRNA levels and activities. Drug metabolism and disposition: the biological fate of chemicals. 2012;40(1):83-92. doi: 10.1124/dmd.111.042259. PubMed PMID: 21994437.

386. Yimer G, Ueda N, Habtewold A, Amogne W, Suda A, Riedel KD, et al. Pharmacogenetic & pharmacokinetic biomarker for efavirenz based ARV and rifampicin based anti-TB drug induced liver injury in TB-HIV infected patients. PLoS One. 2011;6(12):e27810. Epub 2011/12/14. doi: 10.1371/journal.pone.0027810. PubMed PMID: 22162992; PubMed Central PMCID: PMC3232196.

387. Crews KR, Hicks JK, Pui CH, Relling MV, Evans WE. Pharmacogenomics and individualized medicine: translating science into practice. Clinical pharmacology and therapeutics. 2012;92(4):467-75. doi: 10.1038/clpt.2012.120. PubMed PMID: 22948889; PubMed Central PMCID: PMC3589526.

388. Choi MK, Jin QR, Choi YL, Ahn SH, Bae MA, Song IS. Inhibitory effects of ketoconazole and rifampin on OAT1 and OATP1B1 transport activities: considerations on drug-drug interactions. Biopharmaceutics & drug disposition. 2011;32(3):175-84. doi: 10.1002/bdd.749. PubMed PMID: 21456052.

389. Chigutsa E, Visser ME, Swart EC, Denti P, Pushpakom S, Egan D, et al. The SLCO1B1 rs4149032 polymorphism is highly prevalent in South Africans and is

associated with reduced rifampin concentrations: dosing implications. Antimicrobial agents and chemotherapy. 2011;55(9):4122-7. doi: 10.1128/AAC.01833-10. PubMed PMID: 21709081; PubMed Central PMCID: PMC3165308.

390. Smythe W, Khandelwal A, Merle C, Rustomjee R, Gninafon M, Bocar Lo M, et al. A semimechanistic pharmacokinetic-enzyme turnover model for rifampin autoinduction in adult tuberculosis patients. Antimicrobial agents and chemotherapy. 2012;56(4):2091-8. Epub 2012/01/19. doi: 10.1128/AAC.05792-11. PubMed PMID: 22252827; PubMed Central PMCID: PMC3318330.

391. Polk RE, Brophy DF, Israel DS, Patron R, Sadler BM, Chittick GE, et al. Pharmacokinetic Interaction between amprenavir and rifabutin or rifampin in healthy males. Antimicrobial agents and chemotherapy. 2001;45(2):502-8. Epub 2001/02/13. doi: 10.1128/AAC.45.2.502-508.2001. PubMed PMID: 11158747; PubMed Central PMCID: PMC90319.

392. Ferry JJ, Herman BD, Carel BJ, Carlson GF, Batts DH. Pharmacokinetic drug-drug interaction study of delavirdine and indinavir in healthy volunteers. Journal of acquired immune deficiency syndromes and human retrovirology : official publication of the International Retrovirology Association. 1998;18(3):252-9. PubMed PMID: 9665503.

393. Amira Jindani HH, S Charalambous, S Mungofa, S Zizhou, J van Dijk, J Sheperd, P Phillips, A J Nunn, D A Mitchison. A multicenter randomized clinical trial to evaluate high-dose rifapentine with a quinolone for treatment of pulmonary TB: The RIFAQUIN Trail. 20th Conference on Retrovirus and Opportunisitic Infections; 3-6 March 2013; Atlanta, Georgia, USA. 2013.

394. M Boeree AD, R Dawson, A Venter, J du Bois, K Narunsky, M Hoelscher, S Gillespie, P Phillips, R Aarnoutse. What Is the “Right” Dose of Rifampin? 20th Conference on Retrovirus and Opportunistic Infections; 3-6th March, 2013; Atlanta, Georgia, USA. 2013.

395. Rivero-Lezcano OM. Cytokines as immunomodulators in tuberculosis therapy. Recent Pat Antiinfect Drug Discov. 2008;3(3):168-76. Epub 2008/11/11. PubMed PMID: 18991799.

396. Zaitzeva SI, Matveeva SL, Gerasimova TG, Pashkov YN, Butov DA, Pylypchuk VS, et al. Treatment of cavitary and infiltrating pulmonary tuberculosis with and without the immunomodulator Dzherelo. Clin Microbiol Infect.

2009;15(12):1154-62. Epub 2009/05/22. doi: 10.1111/j.1469-0691.2009.02760.x. PubMed PMID: 19456829.

397. Vilaplana C, Montane E, Pinto S, Barriocanal AM, Domenech G, Torres F, et al. Double-blind, randomized, placebo-controlled Phase I Clinical Trial of the therapeutical antituberculous vaccine RUTI. Vaccine. 2010;28(4):1106-16. Epub 2009/10/27. doi: 10.1016/j.vaccine.2009.09.134. PubMed PMID: 19853680.

398. Kaufmann SH, Hussey G, Lambert PH. New vaccines for tuberculosis. Lancet. 2010;375(9731):2110-9. Epub 2010/05/22. doi: 10.1016/S0140-6736(10)60393-5. PubMed PMID: 20488515.

399. Parida SK, Kaufmann SH. Novel tuberculosis vaccines on the horizon. Curr Opin Immunol. 2010;22(3):374-84. Epub 2010/05/18. doi: 10.1016/j.coi.2010.04.006. PubMed PMID: 20471231.

400. Lambert PH, Hawkridge T, Hanekom WA. New vaccines against tuberculosis. Clin Chest Med. 2009;30(4):811-26, x. Epub 2009/11/21. doi: 10.1016/j.ccm.2009.08.014. PubMed PMID: 19925969.

401. Lips P. Worldwide status of vitamin D nutrition. J Steroid Biochem Mol Biol. 2010;121(1-2):297-300. Epub 2010/03/04. doi: 10.1016/j.jsbmb.2010.02.021. PubMed PMID: 20197091.

402. Zheng XE, Wang Z, Liao MZ, Lin YS, Shuhart MC, Schuetz EG, et al. Human PXR-mediated induction of intestinal CYP3A4 attenuates 1alpha,25-dihydroxyvitamin D(3) function in human colon adenocarcinoma LS180 cells. Biochemical pharmacology. 2012;84(3):391-401. Epub 2012/05/09. doi: 10.1016/j.bcp.2012.04.019. PubMed PMID: 22562045; PubMed Central PMCID: PMC3372629.

403. Khoo AL, Chai L, Koenen H, Joosten I, Netea M, van der Ven A. Translating the role of vitamin D3 in infectious diseases. Crit Rev Microbiol. 2012;38(2):122-35. Epub 2012/02/07. doi: 10.3109/1040841X.2011.622716. PubMed PMID: 22304022.

404. Holick MF. Vitamin D deficiency. N Engl J Med. 2007;357(3):266-81. Epub 2007/07/20. doi: 10.1056/NEJMra070553. PubMed PMID: 17634462.

405. Carlberg C. Mechanisms of nuclear signalling by vitamin D3. Interplay with retinoid and thyroid hormone signalling. European journal of biochemistry / FEBS. 1995;231(3):517-27. PubMed PMID: 7649150.

406. Carlberg C. The concept of multiple vitamin D signaling pathways. The journal of investigative dermatology Symposium proceedings / the Society for

Investigative Dermatology, Inc [and] European Society for Dermatological Research. 1996;1(1):10-4. PubMed PMID: 9627685.

407. Kato S. The function of vitamin D receptor in vitamin D action. J Biochem. 2000;127(5):717-22. Epub 2000/05/02. PubMed PMID: 10788778.

408. Brown AJ. Regulation of vitamin D action. Nephrology, dialysis, transplantation : official publication of the European Dialysis and Transplant Association - European Renal Association. 1999;14(1):11-6. PubMed PMID: 10052463.

409. Miyaguchi S, Watanabe T. The role of vitamin D3 receptor mRNA in the proliferation of hepatocellular carcinoma. Hepatogastroenterology. 2000;47(32):468-72. Epub 2000/05/03. PubMed PMID: 10791215.

410. Shany S, Levy Y, Lahav-Cohen M. The effects of 1alpha,24(S)-dihydroxyvitamin D(2) analog on cancer cell proliferation and cytokine expression. Steroids. 2001;66(3-5):319-25. Epub 2001/02/17. PubMed PMID: 11179740.

411. Bertilsson G, Heidrich J, Svensson K, Asman M, Jendeberg L, Sydow-Backman M, et al. Identification of a human nuclear receptor defines a new signaling pathway for CYP3A induction. Proceedings of the National Academy of Sciences of the United States of America. 1998;95(21):12208-13. PubMed PMID: 9770465; PubMed Central PMCID: PMC22810.

412. Pavek P, Pospechova K, Svecova L, Syrova Z, Stejskalova L, Blazkova J, et al. Intestinal cell-specific vitamin D receptor (VDR)-mediated transcriptional regulation of CYP3A4 gene. Biochemical pharmacology. 2010;79(2):277-87. Epub 2009/08/29. doi: 10.1016/j.bcp.2009.08.017. PubMed PMID: 19712670.

413. Goodwin B, Hodgson E, Liddle C. The orphan human pregnane X receptor mediates the transcriptional activation of CYP3A4 by rifampicin through a distal enhancer module. Molecular pharmacology. 1999;56(6):1329-39. PubMed PMID: 10570062.

414. Makishima M, Lu TT, Xie W, Whitfield GK, Domoto H, Evans RM, et al. Vitamin D receptor as an intestinal bile acid sensor. Science. 2002;296(5571):1313-6. Epub 2002/05/23. doi: 10.1126/science.1070477. PubMed PMID: 12016314.

415. Lindh JD, Andersson ML, Eliasson E, Bjorkhem-Bergman L. Seasonal variation in blood drug concentrations and a potential relationship to vitamin D. Drug metabolism and disposition: the biological fate of chemicals. 2011;39(5):933-7. Epub 2011/02/26. doi: 10.1124/dmd.111.038125. PubMed PMID: 21349923.

416. Chow EC, Sondervan M, Jin C, Groothuis GM, Pang KS. Comparative effects of doxercalciferol (1alpha-hydroxyvitamin D(2)) versus calcitriol (1alpha,25-dihydroxyvitamin D(3)) on the expression of transporters and enzymes in the rat in vivo. Journal of pharmaceutical sciences. 2010. doi: 10.1002/jps.22366. PubMed PMID: 20967888.

417. Reschly EJ, Krasowski MD. Evolution and function of the NR1I nuclear hormone receptor subfamily (VDR, PXR, and CAR) with respect to metabolism of xenobiotics and endogenous compounds. Current drug metabolism. 2006;7(4):349-65. Epub 2006/05/27. PubMed PMID: 16724925; PubMed Central PMCID: PMC2231810.

418. Aiba T, Susa M, Fukumori S, Hashimoto Y. The effects of culture conditions on CYP3A4 and MDR1 mRNA induction by 1alpha,25-dihydroxyvitamin D(3) in human intestinal cell lines, Caco-2 and LS180. Drug metabolism and pharmacokinetics. 2005;20(4):268-74. PubMed PMID: 16141606.

419. Fan J, Liu S, Du Y, Morrison J, Shipman R, Pang KS. Up-regulation of transporters and enzymes by the vitamin D receptor ligands, 1alpha,25-dihydroxyvitamin D3 and vitamin D analogs, in the Caco-2 cell monolayer. The Journal of pharmacology and experimental therapeutics. 2009;330(2):389-402. doi: 10.1124/jpet.108.149815. PubMed PMID: 19414624.

420. Tachibana S, Yoshinari K, Chikada T, Toriyabe T, Nagata K, Yamazoe Y. Involvement of Vitamin D receptor in the intestinal induction of human ABCB1. Drug metabolism and disposition: the biological fate of chemicals. 2009;37(8):1604-10. Epub 2009/05/23. doi: 10.1124/dmd.109.027219. PubMed PMID: 19460946.

421. Saeki M, Kurose K, Tohkin M, Hasegawa R. Identification of the functional vitamin D response elements in the human MDR1 gene. Biochemical pharmacology. 2008;76(4):531-42. Epub 2008/07/08. doi: 10.1016/j.bcp.2008.05.030. PubMed PMID: 18602086.

422. Kota BP, Allen JD, Roufogalis BD. The effect of vitamin D3 and ketoconazole combination on VDR-mediated P-gp expression and function in human colon adenocarcinoma cells: implications in drug disposition and resistance. Basic & clinical pharmacology & toxicology. 2011;109(2):97-102. Epub 2011/03/09. doi: 10.1111/j.1742-7843.2011.00693.x. PubMed PMID: 21382175.

423. Ogura M, Nishida S, Ishizawa M, Sakurai K, Shimizu M, Matsuo S, et al. Vitamin D3 modulates the expression of bile acid regulatory genes and represses

inflammation in bile duct-ligated mice. The Journal of pharmacology and experimental therapeutics. 2009;328(2):564-70. Epub 2008/11/08. doi: 10.1124/jpet.108.145987. PubMed PMID: 18988769.

424. Nejentsev S, Godfrey L, Snook H, Rance H, Nutland S, Walker NM, et al. Comparative high-resolution analysis of linkage disequilibrium and tag single nucleotide polymorphisms between populations in the vitamin D receptor gene. Human molecular genetics. 2004;13(15):1633-9. doi: 10.1093/hmg/ddh169. PubMed PMID: 15175274.

425. White JH. Vitamin D signaling, infectious diseases, and regulation of innate immunity. Infect Immun. 2008;76(9):3837-43. Epub 2008/05/29. doi: 10.1128/IAI.00353-08. PubMed PMID: 18505808; PubMed Central PMCID: PMC2519414.

426. Alagarasu K, Selvaraj P, Swaminathan S, Narendran G, Narayanan PR. 5' regulatory and 3' untranslated region polymorphisms of vitamin D receptor gene in south Indian HIV and HIV-TB patients. Journal of clinical immunology. 2009;29(2):196-204. doi: 10.1007/s10875-008-9234-z. PubMed PMID: 18712587.

427. de la Torre MS, Torres C, Nieto G, Vergara S, Carrero AJ, Macias J, et al. Vitamin D receptor gene haplotypes and susceptibility to HIV-1 infection in injection drug users. The Journal of infectious diseases. 2008;197(3):405-10. Epub 2008/01/22. doi: 10.1086/525043. PubMed PMID: 18205531.

428. Kostner K, Denzer N, Muller CS, Klein R, Tilgen W, Reichrath J. The relevance of vitamin D receptor (VDR) gene polymorphisms for cancer: a review of the literature. Anticancer Res. 2009;29(9):3511-36. Epub 2009/08/12. PubMed PMID: 19667145.

429. Ukaji M, Saito Y, Fukushima-Uesaka H, Maekawa K, Katori N, Kaniwa N, et al. Genetic variations of VDR/NR1I1 encoding vitamin D receptor in a Japanese population. Drug metabolism and pharmacokinetics. 2007;22(6):462-7. Epub 2007/12/27. PubMed PMID: 18159135.

430. Selvaraj P, Prabhu Anand S, Harishankar M, Alagarasu K. Plasma 1,25 dihydroxy vitamin D3 level and expression of vitamin d receptor and cathelicidin in pulmonary tuberculosis. Journal of clinical immunology. 2009;29(4):470-8. Epub 2009/02/17. doi: 10.1007/s10875-009-9277-9. PubMed PMID: 19219539.

431. Ochs-Balcom HM, Cicek MS, Thompson CL, Tucker TC, Elston RC, S JP, et al. Association of vitamin D receptor gene variants, adiposity and colon cancer.

Carcinogenesis. 2008;29(9):1788-93. Epub 2008/07/17. doi: 10.1093/carcin/bgn166. PubMed PMID: 18628249; PubMed Central PMCID: PMC2722851.

432. Zhou C, Assem M, Tay JC, Watkins PB, Blumberg B, Schuetz EG, et al. Steroid and xenobiotic receptor and vitamin D receptor crosstalk mediates CYP24 expression and drug-induced osteomalacia. J Clin Invest. 2006;116(6):1703-12. Epub 2006/05/13. doi: 10.1172/JCI27793. PubMed PMID: 16691293; PubMed Central PMCID: PMC1459072.

433. Nies AT, Niemi M, Burk O, Winter S, Zanger UM, Stieger B, et al. Genetics is a major determinant of expression of the human hepatic uptake transporter OATP1B1, but not of OATP1B3 and OATP2B1. Genome Med. 2013;5(1):1. Epub 2013/01/15. doi: 10.1186/gm405. PubMed PMID: 23311897; PubMed Central PMCID: PMC3706890.

434. Barbeiro DF, Barbeiro HV, Zampieri FG, Cesar Machado MC, Torggler Filho F, Gomes Cunha DM, et al. Cathelicidin LL-37 bloodstream surveillance is down regulated during septic shock. Microbes and infection / Institut Pasteur. 2013;15(5):342-6. doi: 10.1016/j.micinf.2013.01.001. PubMed PMID: 23328115.

435. Sandanaraj E, Lal S, Selvarajan V, Ooi LL, Wong ZW, Wong NS, et al. PXR pharmacogenetics: association of haplotypes with hepatic CYP3A4 and ABCB1 messenger RNA expression and doxorubicin clearance in Asian breast cancer patients. Clin Cancer Res. 2008;14(21):7116-26. Epub 2008/11/05. doi: 10.1158/1078-0432.CCR-08-0411. PubMed PMID: 18981011.

436. Maeda K, Sugiyama Y. Transporter biology in drug approval: regulatory aspects. Mol Aspects Med. 2013;34(2-3):711-8. Epub 2013/03/20. doi: 10.1016/j.mam.2012.10.012. PubMed PMID: 23506904.

437. Svoboda M, Wlcek K, Taferner B, Hering S, Stieger B, Tong D, et al. Expression of organic anion-transporting polypeptides 1B1 and 1B3 in ovarian cancer cells: relevance for paclitaxel transport. Biomed Pharmacother. 2011;65(6):417-26. Epub 2011/07/02. doi: 10.1016/j.biopha.2011.04.031. PubMed PMID: 21719246.

438. Niemi M, Schaeffeler E, Lang T, Fromm MF, Neuvonen M, Kyrklund C, et al. High plasma pravastatin concentrations are associated with single nucleotide polymorphisms and haplotypes of organic anion transporting polypeptide-C (OATP-C, SLCO1B1). Pharmacogenetics. 2004;14(7):429-40. Epub 2004/07/01. PubMed PMID: 15226675.

439. Hustert E, Zibat A, Presecan-Siedel E, Eiselt R, Mueller R, Fuss C, et al. Natural protein variants of pregnane X receptor with altered transactivation activity toward CYP3A4. Drug metabolism and disposition: the biological fate of chemicals. 2001;29(11):1454-9. Epub 2001/10/17. PubMed PMID: 11602521.

440. Swart M, Whitehorn H, Ren Y, Smith P, Ramesar RS, Dandara C. PXR and CAR single nucleotide polymorphisms influence plasma efavirenz levels in South African HIV/AIDS patients. BMC Med Genet. 2012;13:112. Epub 2012/11/24. doi: 10.1186/1471-2350-13-112. PubMed PMID: 23173844; PubMed Central PMCID: PMC3523080.

441. Schmiedlin-Ren P, Thummel KE, Fisher JM, Paine MF, Lown KS, Watkins PB. Expression of enzymatically active CYP3A4 by Caco-2 cells grown on extracellular matrix-coated permeable supports in the presence of 1alpha,25-dihydroxyvitamin D3. Molecular pharmacology. 1997;51(5):741-54. Epub 1997/05/01. PubMed PMID: 9145912.

442. Lund RJ, Andress DL, Amdahl M, Williams LA, Heaney RP. Differential effects of paricalcitol and calcitriol on intestinal calcium absorption in hemodialysis patients. Am J Nephrol. 2010;31(2):165-70. Epub 2009/12/18. doi: 10.1159/000266204. PubMed PMID: 20016142.

443. Burgaz A, Akesson A, Oster A, Michaelsson K, Wolk A. Associations of diet, supplement use, and ultraviolet B radiation exposure with vitamin D status in Swedish women during winter. The American journal of clinical nutrition. 2007;86(5):1399-404. PubMed PMID: 17991652.

444. Jorgensen SP, Agnholt J, Glerup H, Lyhne S, Villadsen GE, Hvas CL, et al. Clinical trial: vitamin D3 treatment in Crohn's disease - a randomized double-blind placebo-controlled study. Aliment Pharmacol Ther. 2010;32(3):377-83. Epub 2010/05/25. doi: 10.1111/j.1365-2036.2010.04355.x. PubMed PMID: 20491740.

445. Virtanen JK, Nurmi T, Voutilainen S, Mursu J, Tuomainen TP. Association of serum 25-hydroxyvitamin D with the risk of death in a general older population in Finland. Eur J Nutr. 2011;50(5):305-12. Epub 2010/10/27. doi: 10.1007/s00394-010-0138-3. PubMed PMID: 20976461.

446. Negoro S, Izumi S, Furukubo T, Satoh M, Matsunaga C, Yamakawa T, et al. Interaction between activated VD3 and Ca channel blockers in patients undergoing hemodialysis. Int J Clin Pharmacol Ther. 2007;45(3):186-7. Epub 2007/04/10. PubMed PMID: 17416114.

447. Thirumaran RK, Lamba JK, Kim RB, Urquhart BL, Gregor JC, Chande N, et al. Intestinal CYP3A4 and midazolam disposition in vivo associate with VDR polymorphisms and show seasonal variation. Biochemical pharmacology. 2012;84(1):104-12. doi: 10.1016/j.bcp.2012.03.017. PubMed PMID: 22484315.

448. Swapna N, Vamsi UM, Usha G, Padma T. Risk conferred by FokI polymorphism of vitamin D receptor (VDR) gene for essential hypertension. Indian J Hum Genet. 2011;17(3):201-6. Epub 2012/02/22. doi: 10.4103/0971-6866.92104. PubMed PMID: 22345993; PubMed Central PMCID: PMC3276990.

449. Renne C, Benz AH, Hansmann ML. Vitamin D3 receptor is highly expressed in Hodgkin's lymphoma. BMC Cancer. 2012;12:215. Epub 2012/06/08. doi: 10.1186/1471-2407-12-215. PubMed PMID: 22672495; PubMed Central PMCID: PMC3488550.

450. Annamaneni S, Bindu CH, Reddy KP, Vishnupriya S. Association of vitamin D receptor gene start codon (Fok1) polymorphism with high myopia. Oman journal of ophthalmology. 2011;4(2):57-62. doi: 10.4103/0974-620X.83654. PubMed PMID: 21897619; PubMed Central PMCID: PMC3160070.

451. Vaidya A, Sun B, Forman JP, Hopkins PN, Brown NJ, Kolatkar NS, et al. The Fok1 vitamin D receptor gene polymorphism is associated with plasma renin activity in Caucasians. Clin Endocrinol (Oxf). 2011;74(6):783-90. Epub 2011/04/28. doi: 10.1111/j.1365-2265.2011.03991.x. PubMed PMID: 21521263; PubMed Central PMCID: PMC3089671.

452. Arjumand W, Ahmad ST, Seth A, Saini AK, Sultana S. Vitamin D receptor FokI and BsmI gene polymorphism and its association with grade and stage of renal cell carcinoma in North Indian population. Tumour biology : the journal of the International Society for Oncodevelopmental Biology and Medicine. 2012;33(1):23-31. doi: 10.1007/s13277-011-0236-8. PubMed PMID: 21931993.

453. Rubin DC, Ong DE, Gordon JI. Cellular differentiation in the emerging fetal rat small intestinal epithelium: mosaic patterns of gene expression. Proceedings of the National Academy of Sciences of the United States of America. 1989;86(4):1278-82. PubMed PMID: 2645578; PubMed Central PMCID: PMC286671.

454. Yague E, Armesilla AL, Harrison G, Elliott J, Sardini A, Higgins CF, et al. P-glycoprotein (MDR1) expression in leukemic cells is regulated at two distinct steps, mRNA stabilization and translational initiation. The Journal of biological chemistry. 2003;278(12):10344-52. doi: 10.1074/jbc.M211093200. PubMed PMID: 12525496.

455. Amacher DE. The effects of cytochrome P450 induction by xenobiotics on endobiotic metabolism in pre-clinical safety studies. Toxicology mechanisms and methods. 2010;20(4):159-66. doi: 10.3109/15376511003690307. PubMed PMID: 20218941.

456. Kota BP, Abdul MI, Allen JD, Kalagara M, Roufogalis BD. Effect of vitamin D3 supplementation on the pharmacokinetics of digoxin--a pilot study. Fundam Clin Pharmacol. 2012;26(4):543-8. Epub 2011/04/12. doi: 10.1111/j.1472-8206.2011.00944.x. PubMed PMID: 21477267.